To the Graduate Council:

I am submitting herewith a dissertation written by Robert Allen LeMaster entitled "Finite Deformation--Finite Element Formulations for Elastic-Viscoplastic Materials." I have examined the final copy of this dissertation for form and content and recommend that it be accepted in partial fulfillment of the requirements for the degree of Doctor of Philosophy, with a major in Engineering Science.

Maurice A. Wright

Maurice A. Wright, Major Professor

We have read this dissertation and recommend its acceptance:

Laurence E. Malvern

Jerry E. Stoneking

JC Reddy

Dennis Keefer

Accepted for the Council:

L Evans Roth

Vice Chancellor
Graduate Studies and Research

FINITE DEFORMATION--FINITE ELEMENT FORMULATIONS FOR ELASTIC-VISCOPLASTIC MATERIALS

A Dissertation

Presented for the

Doctor of Philosophy

Degree

The University of Tennessee, Knoxville

Robert Allen LeMaster

June 1983

DEDICATION

This dissertation is dedicated to my wife, Debbie, who has made many sacrifices over the last nine years in order that I may pursue my formal education.

ACKNOWLEDGEMENTS

The author would like to express his appreciation to the members of his committee for their time and effort spent in reviewing this dissertation. Also, the author expresses his appreciation to The University of Tennessee Space Institute for arranging to have Dr. Malvern of the University of Florida on the doctoral committee. Dr. Malvern provided many helpful comments.

The author expresses his gratitude to Sverdrup Technology, Inc., for providing the computer facilities and computer time required to develop the programs and perform the numerical computations contained in this dissertation. The author is grateful to Sverdrup Technology, Inc., and the United States Air Force at Arnold Engineering Development Center for the financial support provided to take the courses in the doctoral program.

ABSTRACT

Three fundamentally different finite strain constitutive formulations for describing elastic-viscoplastic materials are considered. These are classified as: (1) hyperelastic-viscoplastic, (2) hypolastic-viscoplastic, and (3) updated hyperelastic-viscoplastic. The formulations differ primarily in the kinetic and kinematic quantities used to characterize the material constitutive equations. Objectives are to: (1) establish the theoretical bases of the three constitutive formulations; (2) evaluate the relative numerical efficiency of the material models; (3) determine under what conditions the various descriptions yield comparable results; and (4) develop a computer program which can be used to study finite strain, elastic-viscoplastic constitutive equations in low, intermediate, and high strain rate environments.

The three material models are based on the Perzyna generalization of the Malvern and Sokolovsky viscoplastic over-stress constitutive equations. Although an over-stress model is used, other state-variable constitutive equations may be described using the three constitutive formulations.

The implementation of the three constitutive formulations into a finite element computer program is discussed, and both explicit and implicit methods for integrating the

equations of motion and constitutive equations are presented.

Two problems are considered which deal with dynamic plasticity and finite strains. The first problem involves a right circular cylinder impacting a rigid wall (Taylor's cylinder problem), and is dominated by finite dilatational strains while the rotations are small. The second problem is a cantilever beam loaded at its free-end by a triangular-shaped impulse, and involves finite rotations with small dilatational strains.

The results indicate that when the dilatational strains are finite, the hyperelastic-viscoplastic constitutive equation may yield numerical results which differ significantly from those obtained from the hypoelastic-viscoplastic and updated hyperelastic-viscoplastic constitutive equations. When the dilatational strains are small, the three constitutive formulations yield similar numerical results.

TABLE OF CONTENTS

LIST OF FIGURES

FIGURE PAGE

CHAPTER I

INTRODUCTION

In recent years, a number of elastic-viscoplastic constitutive equations have been developed which appear to be capable of reproducing certain types of inelastic material behavior [1-6].[1] In particular, the fundamentally different phenomena of rate sensitivity to dynamic loading, and the combined plastic-creep response at elevated temperatures can be simulated using elastic-viscoplastic constitutive theories. In addition, several state variable elastic-viscoplastic constitutive theories are based on microstructure or dislocation movement phenomena [4,5]. This coupling of microstructure physics with continuum-based constitutive equations represents an important trend which should lead to constitutive equations which treat in a consistent manner the interaction between the physical phenomena currently referred to as elastic, anelastic, plastic, and creep.

The rate form of the inelastic strain and state-variable evolution equations make elastic-viscoplastic constitutive equations very attractive numerically. Numerical implementation of elastic-plastic constitutive equations requires a mechanism for ensuring that the

---

[1] Numbers in brackets refer to similarly numbered references in the Bibliography.

equilibrium stress in a computed configuration lies on the current yield surface. This is not a problem with elastic-viscoplastic constitutive equations since the stress may be outside the static yield surface. Some state-variable, elastic-viscoplastic constitutive equations do not rely on the concept of a yield surface.

Elastic-viscoplastic, state-variable constitutive equations offer a convenient mathematical structure for formulating or extending constitutive theories. Because of experimental constraints, much of the experimental data used to develop constitutive descriptions is limited to small strains and is usually uniaxial in nature. Therefore, the extension of these theories to finite strain environments relies heavily on mathematics and invariance principles. Unfortunately, it is possible to obtain a large number of finite strain constitutive equations, all of which reduce to the same small strain and rotation constitutive theory.

This investigation is concerned with the development and numerical implementation of finite strain, elastic-viscoplastic constitutive equations. Specifically, three fundamentally different finite strain constitutive formulations for elastic-viscoplastic materials are considered. These are classified as: (1) hyperelastic-viscoplastic, (2) hypoelastic-viscoplastic, and (3) updated hyperelastic-viscoplastic. The three classes of proposed constitutive formulations differ primarily in their respective kinetic and kinematic variables. They represent general classifications which are not limited to a specific elastic-viscoplastic constitutive equation. However, for the purpose of this investigation, only a Perzyna-type elastic-viscoplastic constitutive equation is used.

Since the three constitutive formulations reduce to the same infinitesimal strain and rotation equations, it is important to: (1) establish the theoretical basis of the three constitutive formulations, (2) determine when the descriptions yield similar numerical results, (3) determine the relative numerical efficiency of the different constitutive formulations, and (4) determine how well the computed results obtained using the different constitutive formulations agree with experimental data. Results from this investigation will provide important information to researchers working to develop general elastic-viscoplastic constitutive equations. To the author's knowledge, the literature covering this field does not contain the above information.

Although elastic-viscoplastic constitutive equations have several attractive features, their implementation into computer programs has been very limited. The few computer programs which do utilize elastic-viscoplastic constitutive equations are limited to infinitesimal strain or geometrically nonlinear environments, and may treat only one-dimensional problems. A few other programs utilize methods which enable them to account for the strain rate sensitivity of the yield stress, without using elastic-viscoplastic constitutive equations. For example, the finite element computer program HONDO [7] uses a hypo-elastic-plastic constitutive equation, and accounts for strain rate sensitivity effects by increasing the static yield stress. This type of procedure is in general limited to a specific phenomenon, and cannot be used to obtain general constitutive equations capable of describing the interaction of several phenomena. HONDO is also limited to "wave propagation"-type problems, and is not suited to quasi-static problems. "Hydro-codes" such as EPIC [8] also suffer from the same limitations as HONDO. Therefore, to accomplish the goals of this investigation, it was necessary to develop the required computer programs.

The three finite strain, elastic-viscoplastic constitutive equations were implemented into a new finite element computer program. The computer program is applicable to two-dimensional and axisymmetric solid continua, and treats geometric and material nonlinear problems involving finite strains. Static, quasi-static, and dynamic load environments may be considered, and the equations of motion may be solved using either implicit or explicit time integration schemes. Pre- and post-processing graphics programs were written to assist in handling the large quantities of data inherent in nonlinear finite element analysis.

An important feature of the finite element computer program written during this investigation is its ability to handle problems covering a wide range of load application rates. It may be used to efficiently obtain solutions to problems involving static, quasi-static, and low- and high-frequency dynamic load application rates. Most finite element computer programs are limited to only a small range of load application rates. Since elastic-viscoplastic constitutive equations are capable of reproducing the inelastic behavior of materials over a wide range of load application rates, this finite element program will permit elastic-viscoplastic constitutive equations to be studied over the complete spectrum of load application rates using a single program.

In summary, this investigation has two specific goals: (1) the development of a finite element computer program which can be used to study elastic-viscoplastic materials experiencing finite strains over a wide range of load application rates, and (2) to perform a theoretical and numerical comparison of three proposed finite strain, elastic-viscoplastic constitutive formulations for a Perzyna-type material description.

In Chapter II, the general structure of elastic-viscoplastic constitutive equations is discussed, and then specialized to a Perzyna over-stress model. The kinetic and kinematic variables used to describe a general continuum undergoing finite deformations are presented in Chapter III, and then used in Chapter IV to describe the behavior of elastic-viscoplastic materials experiencing finite strains.

In Chapter V, procedures for solving the governing equations of motion and constitutive equations using the finite element method are presented. Since elastic-viscoplastic constitutive equations are capable of describing inelastic response over a wide range of application rates, both implicit and explicit schemes for integrating the equations of motion and constitutive equations are presented. A description of the computer program used to solve the equations is given in Chapter VI.

In Chapter VII, numerical results are presented for a right circular cylinder impacting a rigid wall (Taylor's cylinder), and a cantilever beam loaded transversely at its free-end by a triangular pulse. Chapter VIII contains a summary of the work performed during this investigation, and Chapter IX presents conclusions and recommendations for future research.

CHAPTER II

ELASTIC-VISCOPLASTIC CONSTITUTIVE EQUATIONS

One of the most well-known features of the stress-strain curve for a crystalline solid is the characteristic knee signifying the start of plastic deformation. The stress at which the plastic deformation begins is called the yield stress, and serves as an upper limit in many failure criteria. In many situations, however, it is necessary to consider the load and deformation capacity of the material after the yield stress (strain) has been exceeded. The development of constitutive equations describing this nonlinear material response is the basic problems addressed by plasticity theories.

Classical plasticity theory is based on three important ingredients; (1) a yield function which determines the onset of plastic deformation, (2) a flow rule which governs the evolution of plastic strains, and (3) a hardening rule which describes subsequent yield functions after plastic deformation has occurred. For example, the initial and subsequent yield condition for isothermal kinematic or isotropic hardening is

$$f(\underset{\sim}{\sigma},\underset{\sim}{\alpha},\eta) = 0 \,, \qquad (2.1)$$

where $\underset{\sim}{\sigma}$ is the stress tensor defined with respect to the current configuration of the material, $\underset{\sim}{\alpha}$ is a symmetric tensor whose components locate the center of the yield surface in nine-dimensional stress space and, η is a parameter defining the size of the yield surface, which increases during plastic deformation and is usually assumed to be a function of either the plastic work or of an equivalent plastic strain measure. For kinematic hardening, the parameter η is taken to be zero; for isotropic hardening, the components of $\underset{\sim}{\alpha}$ are taken to be zero. The evolution of the plastic strain components after the onset of yielding is governed by a flow rule,

$$\dot{\varepsilon}_{ij}^{(p)} = \dot{\lambda} \frac{\partial f}{\partial \sigma_{ij}} , \qquad (2.2)$$

where $\dot{\lambda}$ is a scalar function, and $\dot{\varepsilon}_{ij}^{(p)}$ are the components of the plastic strain rate tensor. Since the yield condition is a function of the current values of $\underset{\sim}{\sigma}$, $\underset{\sim}{\alpha}$, and η, it is history-dependent. However, it is not rate-dependent, and plastic deformation will not occur without an increase in the applied stress.

It is well known that metal plasticity is time-dependent. The manifestation of the time-dependent nature of inelastic deformation is controlled by the microstructure of the particular material, temperature, age, and load application rate. The time lag between the application of loads and the movement of molecular dislocations appears to be responsible for the phenomenon of strain rate sensitivity.

Strain rate effects usually result in a decrease of the inelastic deformation at high load application rates. Materials having abrupt transitions between the elastic and inelastic regimes usually demonstrate a more pronounced strain rate sensitivity than those making a gradual transition. For example, the yield stress of mild steel at a strain rate of 10^2 in./in./sec is reported to be 2.5 times its static value, as shown in Figure 2.1.

Depending on the particular material, strain rate effects may be of importance at rates of strain having magnitudes greater than 1 in./in./sec. A normal tensile test is conducted at approximately 10^{-3} in./in./sec. Strain rates greater than 1 in./in./sec are not uncommon during dynamic load environments, and for metal forming processes, explosive environments, or impact conditions strain rates of 10^6 in./in./sec are not uncommon. Figure 2.2 shows strain rates and time scales associated with different load rate environments.

Temperature also has a significant effect on the strain rate sensitivity of metallic materials. Figure 2.3 shows the effect of temperature and strain rate on the stress-strain curve of aluminum alloy 6061-T6.

At high temperatures, inelastic deformation occurs under constant stress, and is properly referred to as creep or relaxation. The creep phenomenon is a result of a thermally activated diffusion of the molecular dislocations

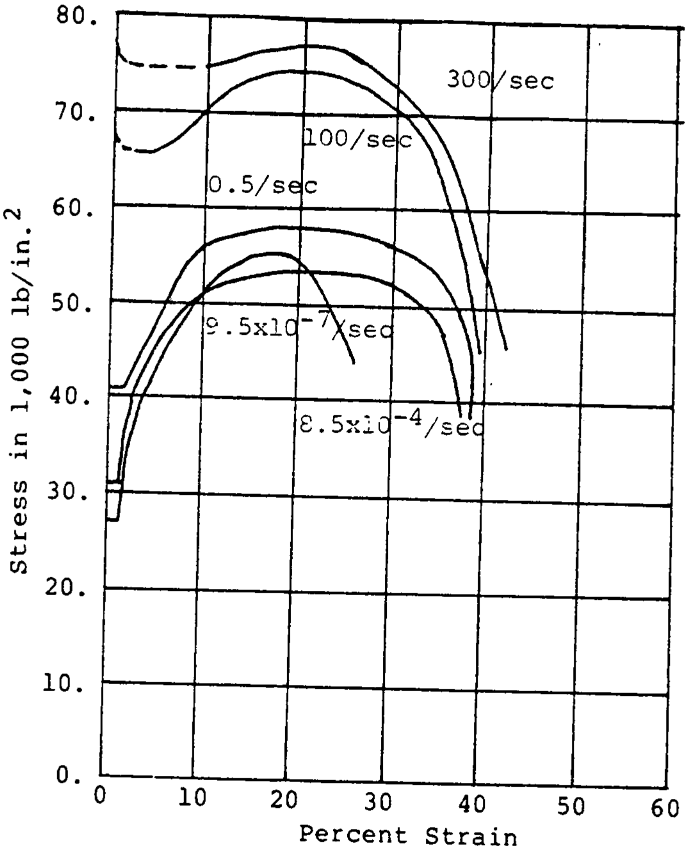

Figure 2.1. Stress-Strain Curves for Mild Steel at Room Temperatures at Various Rates of Strain [9].

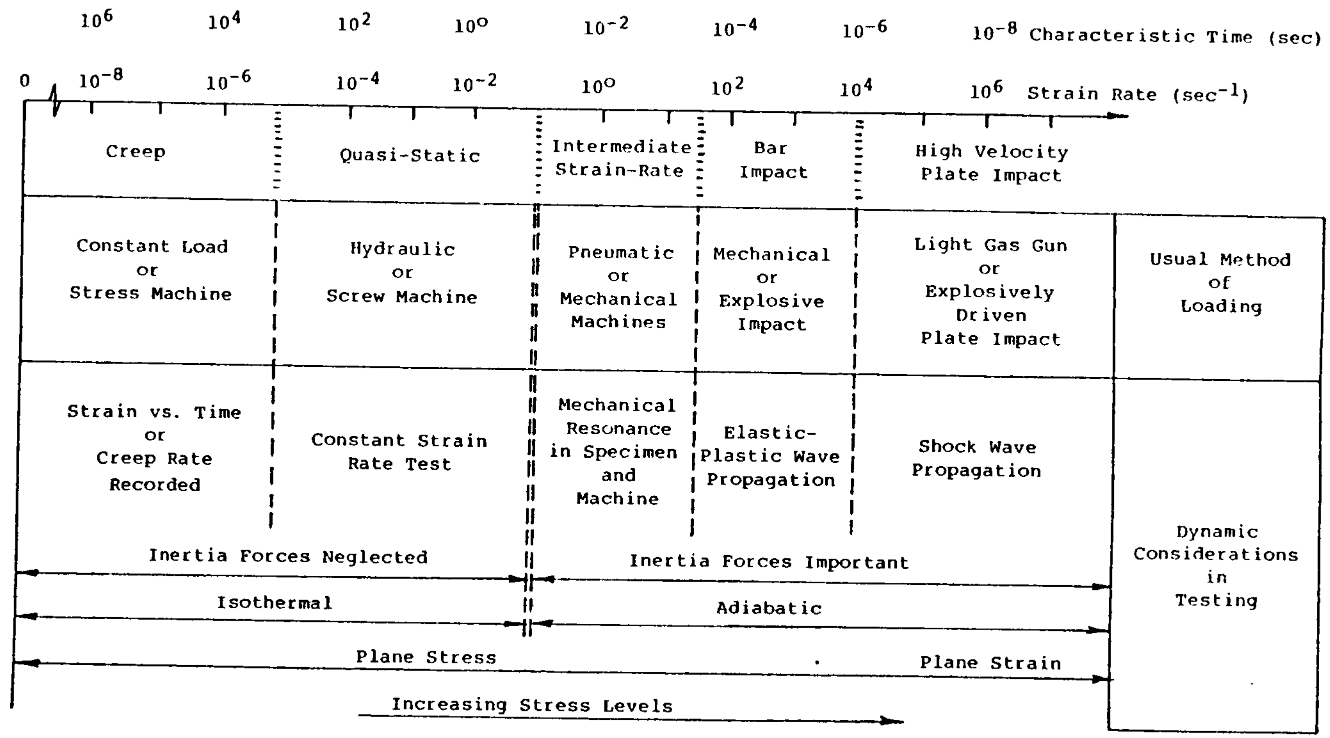

Figure 2.2. Time Scales Associated with Load Rate Environments [10].

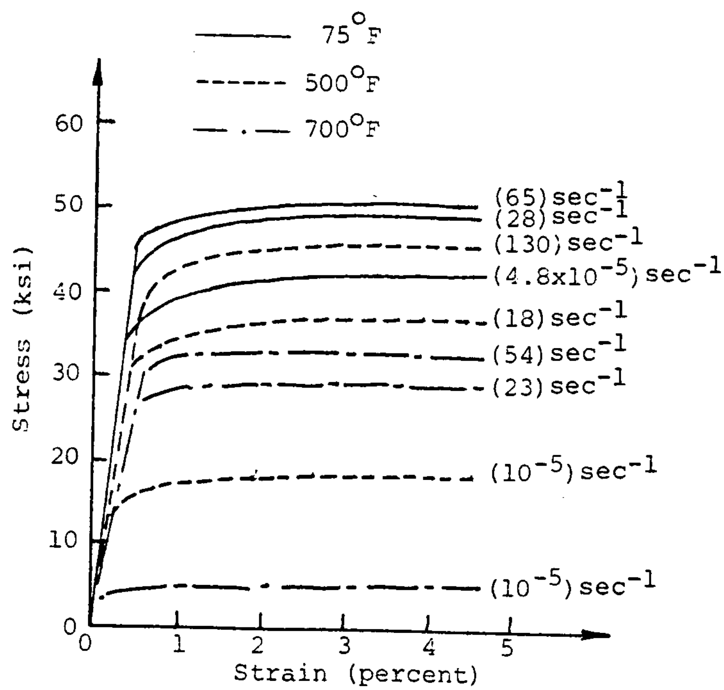

Figure 2.3. Effect of Strain Rate and Temperature on Stress-Strain Curves for 6061-T6 Aluminum [11].

in the material. In addition, recent experiments performed on several different materials (using servo-controlled load application machines) have shown a definite strain rate effect at room temperatures [12].

As evidenced by the different mechanisms and environments controlling the time-dependent nature of metal plasticity, constitutive equations describing inelastic deformation should be capable of predicting a wide range of mechanical and thermal responses. Elastic-viscoplastic constitutive descriptions have been developed to account for rate-dependent phenomena occurring in metal plasticity.

In general, the mathematical structure of elastic-viscoplastic constitutive equations can be summarized by the following equations [13],

$$\dot{\varepsilon}_{ij} = \dot{\varepsilon}_{ij}^{(e)} + \dot{\varepsilon}_{ij}^{(n)} + \dot{\varepsilon}_{ij}^{(T)} , \qquad (2.3)$$

$$\dot{\varepsilon}_{ij}^{(n)} = f_{ij}(\sigma_{ij}, q_{ij}^{(k)}, T) , \qquad (2.4)$$

$$\dot{q}_{ij}^{(k)} = g_{ij}(\sigma_{ij}, q_{ij}^{(k)}, T) , \qquad (2.5)$$

where $\dot{\varepsilon}_{ij}^{(e)}$, $\dot{\varepsilon}_{ij}^{(n)}$, and $\dot{\varepsilon}_{ij}^{(T)}$ are the elastic, inelastic, and thermal strain rates, respectively; σ_{ij} is the stress tensor; T is the temperature; and $q_{ij}^{(k)}$ are state variables. The number of state variables varies in the different models and they can be scalars or tensors. These state variables are assumed to completely characterize the present deformation state of the material, and the history-dependence of the rate of inelastic strain up to the current time is assumed to be completely taken into account by their current values. It is important to note that the rates of the inelastic strain and state variables at any time depend only on the current values of the stress, state variables, and temperature. This fact plays a key role in the computational technique using a rate formulation.

Overstress constitutive models represent a particular class of elastic-viscoplastic constitutive equations used to describe the strain rate sensitivity of the inelastic deformation of metals. In this investigation, the Perzyna [3] generalization of the Malvern [1] and Sokolovsky [6] overstress constitutive model is used, where the evolution of the viscoplastic strain rate components are controlled by the flow rule

$$\dot{\varepsilon}_{ij}^{(vp)} = \gamma \langle \Phi(F) \rangle \frac{\partial f}{\partial \sigma^{ij}} . \tag{2.6}$$

The overstress F is defined as

$$F = \frac{f}{\phi(\bar{\varepsilon}^{(vp)})} - 1 , \tag{2.7}$$

where $\phi(\bar{\varepsilon}^{(vp)})$ is the value of the static stress-plastic strain curve at the current value, $\bar{\varepsilon}^{(vp)}$, of the integral of the equivalent viscoplastic strain rate. The integral of the equivalent viscoplastic strain rate is given by

$$\bar{\varepsilon}^{(vp)} = \int_0^t \sqrt{\frac{2}{3}\,\dot{\varepsilon}_{ij}^{(vp)}\,\dot{\varepsilon}^{ij\,(vp)}}\;dt \ , \tag{2.8}$$

when a Von-Mises yield function is used; that is,

$$f = \sqrt{\frac{3}{2}\,\sigma'^{ij}\,\sigma'_{ij}} \ , \tag{2.9}$$

where σ'^{ij} and σ'_{ij} are the contravariant and covariant components of the deviatoric stress tensor $\underset{\sim}{\sigma}'$. The brackets $< >$ represent the function defined as

$$<\Phi(F)> = \begin{cases} 0 & \text{for} \quad F < 0 \\ \Phi(F) & \text{for} \quad F \geq 0 \end{cases} . \tag{2.10}$$

The overstress function, Φ, and strain rate sensitivity parameter, γ, are chosen to match experimental data. In this constitutive model, the integral of the equivalent viscoplastic strain rate serves as the state variable. Also, the overstress F given by Eq. (2.7) provides a measure of how much the yield function f exceeds the static stress-strain curve. The rate of viscoplastic deformation increases as F increases, provided it is greater than zero.

Also, viscoplastic deformation will continue until the overstress F decreases to zero.

Important characteristics of most elastic-viscoplastic state-variable constitutive models can be summarized by the following statements:

1. The inelastic deformation is postulatd to be incompressible, which yields a deviatoric-type flow rule.
2. The onset of inelastic deformation is controlled by the concept of a yield stress.
3. The rate of inelastic deformation is a function of the difference between the current stress and the "static stress" at the same strain, which relies on the concept of a static stress-strain curve.
4. The process of inelastic deformation is postulated to be isothermal.

CHAPTER III

THE KINETIC AND KINEMATIC VARIABLES OF FINITE DEFORMATION

The study of finite deformation phenomena requires that special care be taken in the definition of the kinetic (stress) and kinematic (deformation) quantities used in the formulation of the governing field equations. In this chapter, the kinetic and kinematic quantities used in the description of finite deformation motion will be developed. Some of the concepts and definitions used in this chapter are not found in texts on continuum mechanics, and had to be gleaned from the literature pertaining to this field. During a review of this literature, the investigator observed some confusion with respect to the terminology used to describe some of the quantities. It is not uncommon to find different authors referring to the same quantity by terminology which is associated with another completely different quantity. The intent of this chapter is to bring together in one place the kinetic and kinematic variables used in the constitutive equations to be presented in Chapter IV.

3.1. Kinematics of Finite Deformation Motion

Consider a body, B, with surface area ∂B which occupies a finite region of Euclidean space. The geometry or configuration of the particles of B at a reference point in time, t_o, is defined as the reference configuration. In the reference configuration (Figure 3.1), the particles are identified by the coordinates X^{α}, which are called material coordinates.[1] The relationship between the particles and material coordinates does not change in time. Associated with the material coordinates are the covariant base vectors $\underset{\sim}{G}_{\alpha}$, the contravariant base vectors $\underset{\sim}{G}^{\alpha}$, the metric tensor $G_{\alpha\beta}$, and its dual $G^{\alpha\beta}$.

When subjected to prescribed body forces and surface tractions, the body B moves to a new position in space referred to as the current configuration. In the current configuration, the locations which the material particles occupy are identified by the coordinates x^i, which are called spatial coordinates. Associated with the spatial coordinates are the covariant base vectors $\underset{\sim}{g}_i$, the contravariant base vectors $\underset{\sim}{g}^i$, the metric tensor g_{ij}, and its dual g^{ij}. It is often desirable to choose a common coordinate system for describing both the reference and current configurations.

---

[1]Standard tensor notation is used in this investigation where superscripted indices denote contravariant components, and subscripted indices denote covariant components. Greek indices denote components referred to the reference configuration base vectors. Capital Roman indices denote components referred to the convected configuration base vectors. Lower-case Roman indices denote components referred to the current configuration base vectors.

The spatial coordinates are related to the material coordinates through the relationship,

$$x^i = \chi^i(X^\alpha, t) \ . \tag{3.1}$$

The functions χ^i define the motion of the particles X^α as a function of time. Therefore, χ^i are sought to completely describe the deformation history of the body B to the prescribed loads.

In addition to the material and spatial coordinates, convected coordinates defined by the material coordinates as they deform and move with the body are often used. The convected coordinates are denoted by X^I. Associated with the convected coordinates are the covariant base vectors $\underset{\sim}{a}_I$, the contravariant base vectors $\underset{\sim}{a}^I$, and the metric tensor a_{IJ}, and its dual a^{IJ}. The base vectors $\underset{\sim}{a}_I$ are obtained from the relationship[2]

$$\underset{\sim}{a}_I = x^i{}_{,I}\, \underset{\sim}{g}_i \ . \tag{3.2}$$

A fundamental, yet rarely seen, relationship between the spatial, material, and convected coordinates is [14]:

$$x^i = \chi^i(X^\alpha, t) = \chi^i(X^I, t) \ . \tag{3.3}$$

---

[2]The subscripted comma denotes partial differentiation. For example, $x^i{}_{,I} = \partial x^i / \partial X^I$.

Equation (3.3) states that the functions χ^i relating the material and spatial coordinates, also relate the convected and spatial coordinates. The relationship between the material coordinates and the convected coordinates is given by

$$X^\alpha = \delta^\alpha_{\ I}\, X^I \ , \tag{3.4}$$

where $\delta^\alpha_{\ I}$ is the mixed Kronecker delta function. Note that although the material and convected coordinates are related by the simple expression given by Eq. (3.4), the length of the convected coordinate system base vectors has been altered due to the deformation of the body.

To characterize the intensity or severity of the deformation defined by Eqs. (3.1) and alternatively by Eqs. (3.3), different measures of the stretching or elongation of the material have been developed. The most commonly used deformation measures are based on the change in squared length of a material line element.

Consider an infinitesimal line element connecting the point $P(X^\alpha)$ to $P'(X^\alpha + dX^\alpha)$, defined with respect to the reference configuration (Figure 3.1). The squared length of this line element is given by

$$(dS_o)^2 = dX^\alpha\, dX^\beta\, G_{\alpha\beta} \ . \tag{3.5}$$

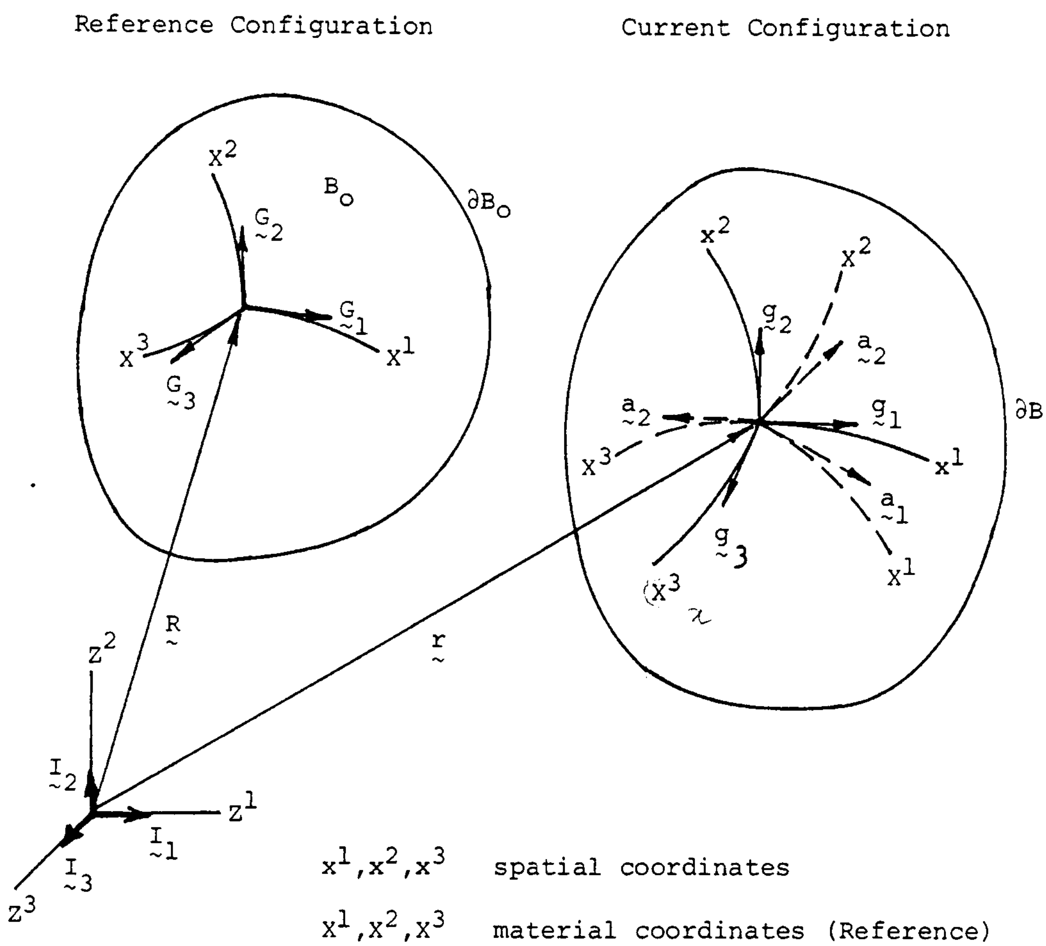

x^1, x^2, x^3 spatial coordinates

X^1, X^2, X^3 material coordinates (Reference)
convected coordinates (Current)

z^1, z^2, z^3 basic Cartesian coordinates

Figure 3.1. Configurations of General Continua Undergoing Finite Deformations.

As a result of the motion χ^i, the point P has moved to the spatial point $Q(x^i)$ and P' to the point $Q'(x^i + dx^i)$. In the spatial coordinates, the new squared length is given by

$$(ds)^2 = dx^i \, dx^j \, g_{ij} \; . \tag{3.6}$$

The change in squared length is given by

$$(ds)^2 - (dS_o)^2 = dx^i \, dx^j \, g_{ij} - dX^\alpha \, dX^\beta \, G_{\alpha\beta} \; . \tag{3.7}$$

The components of the differential line element in the spatial configuration are related to the components in the reference configuration by the relationship,

$$dx^i = x^i{}_{,\alpha} \, dX^\alpha \; , \tag{3.8}$$

where the $x^i{}_{,\alpha}$ are the components of the deformation gradient tensor. The components of the inverse deformation gradient tensor are defined by

$$dX^\alpha = X^\alpha{}_{,i} \, dx^i \; , \tag{3.9}$$

and relate the components of a line element in the spatial configuration to its components when it occupied the reference configuration.

Substituting Eqs. (3.8) into (3.7) yields

$$(ds)^2 - (dS_o)^2 = \left(x^i{}_{,\alpha} \, x^j{}_{,\beta} \, g_{ij} - G_{\alpha\beta} \right) dX^\alpha \, dX^\beta \; . \tag{3.10}$$

Equation (3.10) may be written in an alternate form as

$$(dS)^2 - (dS_o)^2 = (C_{\alpha\beta} - G_{\alpha\beta})dX^\alpha\, dX^\beta \tag{3.11a}$$

$$= 2E_{\alpha\beta}\, dX^\alpha\, dX^\beta\ , \tag{3.11b}$$

where

$$C_{\alpha\beta} = x^i{}_{,\alpha}\, x^j{}_{,\beta}\, g_{ij}\ , \tag{3.11c}$$

and $E_{\alpha\beta}$ are the covariant components of the well-known Green's strain tensor $\underset{\sim}{E}$; $C_{\alpha\beta}$ are covariant components of the right Cauchy-Green tensor $\underset{\sim}{C}$ [15, page 158]. It is important to note that the covariant components of Green's strain tensor are referred to the reference configuration contravariant base vectors;

$$\underset{\sim}{E} = E_{\alpha\beta}\, \underset{\sim}{G}^\alpha\, \underset{\sim}{G}^\beta\ . \tag{3.12}$$

A different, yet seldom used, deformation measure is the Almansi strain tensor, which may be obtained from Eq. (3.7) and the inverse deformation gradient tensor. The covariant components of the Almansi strain, $\underset{\sim}{A}$, are defined by the following equations,

$$(dS)^2 - (dS_o)^2 = (g_{ij} - c_{ij})dx^i\, dx^j \tag{3.13a}$$

$$= 2A_{ij}\, dx^i\, dx^j\ , \tag{3.13b}$$

where

$$c_{ij} = G_{\alpha\beta}\, X^\alpha{}_{,i}\, X^\beta{}_{,j}\ . \tag{3.13c}$$

The covariant components of the Almansi strain are associated with the current configuration contravariant base vectors,

$$\underset{\sim}{A} = A_{ij}\, \underset{\sim}{g}^i\, \underset{\sim}{g}^j\ . \tag{3.14}$$

In Eq. (3.13c), c_{ij} are the covariant components of the left Cauchy-Green tensor $\underset{\sim}{C}$ [15, page 158].

It is often convenient to deal with the rate at which the deformation is occurring. The velocity field expressed in terms of the spatial coordinates is,

$$v_k = \nu_k(x^i, t) \quad . \tag{3.15}$$

The relative velocity between the ends of the infinitesimal material element currently occupying the spatial point x^i is given by,[3]

$$dv_k = v_k|_i \; dx^i. \tag{3.16}$$

The velocity gradient, $v_k|_i$, may be separated into symmetric and antisymmetric components,

$$v_k|_i = D_{ki} + \omega_{ki} \; , \tag{3.17}$$

where D_{ki} are the components of symmetric rate of deformation tensor $\underset{\sim}{D}$, and the ω_{ki} are the components of the skew-symmetric spin or vorticity tensor $\underset{\sim}{\omega}$. The covariant components of the rate of deformation tensor are given by,

$$D_{ki} = \frac{1}{2}(v_k|_i + v_i|_k) \; , \tag{3.18}$$

and the covariant components of the vorticity tensor by,

$$\omega_{ki} = \frac{1}{2}(v_k|_i - v_i|_k) \; . \tag{3.19}$$

---

[3] The symbol | is used to denote covariant differentiation.

The rate of deformation and vorticity tensors are used extensively in the field of fluid mechanics, but also play an important role in finite deformation theories in solid mechanics. Physically, the rate of deformation is the rate of change of the squared length of the infinitesimal material element instantaneously occupying the spatial point under consideration [15]; that is, $\frac{d}{dt}[(dS)^2] = 2D_{ki}\, dx^k\, dx^i$.

The covariant components of the rate of deformation are associated with the current configuration contravariant base vectors,

$$\underset{\sim}{D} = D_{ij}\, \underset{\sim}{g}^i\, \underset{\sim}{g}^j \ . \tag{3.20}$$

The rate of deformation may alternatively be expressed in terms of the convected base vectors by

$$\underset{\sim}{D} = D_{AB}\, \underset{\sim}{a}^A\, \underset{\sim}{a}^B \ , \tag{3.21}$$

where,

$$D_{AB} = D_{ij}\, x^i{}_{,A}\, x^j{}_{,B} \ . \tag{3.22}$$

Note that Eq. (3.22) represents a second-order tensor transformation between two coordinate systems defined in the current configuration.

The rate of change of the squared length of a material line element may also be found from Eq. (3.11b);

$$\frac{d}{dt}[(dS)^2] = 2\dot{E}_{\alpha\beta}\, dX^\alpha dX^\beta \tag{3.23a}$$

$$= 2\dot{E}_{\alpha\beta}\, X^\alpha{}_{,i}\, X^\beta{}_{,j}\, dx^i\, dx^j \tag{3.23b}$$

$$= 2D_{ij}\, dx^i\, dx^j \ . \tag{3.23c}$$

Therefore, the components of the rate of deformation tensor are related to the components of the rate of Green's strain tensor through the expression,

$$D_{ij} = \dot{E}_{\alpha\beta}\, X^\alpha{}_{,i}\, X^\beta{}_{,j} \tag{3.24a}$$

or,

$$\dot{E}_{\alpha\beta} = D_{ij}\, x^i{}_{,\alpha}\, x^j{}_{,\beta} \ . \tag{3.24b}$$

Using Eqs. (3.4), (3.22), and (3.24a), the following relationship between the convected coordinate components of the rate of deformation and the components of the rate of Green's strain tensor may be obtained:

$$D_{AB} = \delta^\alpha{}_A\, \delta^\beta{}_B\, \dot{E}_{\alpha\beta} \ . \tag{3.25}$$

Note that the relationship (Eq. (3.24b)) appears at first glance to be simply a coordinate transformation for a second-order tensor; it is actually quite different. Equation (3.22) represents a transformation of the rate of deformation from one coordinate system to another. However, the coordinate axes are both defined with respect to the same configuration. Equation (3.24b) represents a transformation of a quantity defined in the current configuration back to a quantity defined in the reference configuration. As pointed out by Key et al. [14], the deformation gradient tensor is the mechanism by which a quantity in the current configuration is related to the reference configuration. In Eqs. (3.8) and (3.9), the components of the deformation gradient and inverse deformation gradient tensors are seen to relate the components of a differential line element in one configuration to the components of the same differential line element in a different configuration.

3.2. Kinetics of Finite Deformation Motion

In the preceding section, a framework was developed within which the motion experienced by a body undergoing finite deformations could be examined. However, no attention was given to the forces required to initiate and maintain the motion. In this section, several kinetic or force-related quantities will be discussed, with emphasis placed on the physical significance of the various terms.

Consider a differential area, da, on the surface ∂B of the body B in the current configuration. The unit outward normal $\underset{\sim}{n}$ to da may be expressed in terms of the current configuration contravariant base vectors as,

$$\underset{\sim}{n} = n_i \, \underset{\sim}{g}^i \ . \tag{3.26}$$

Let $d\underset{\sim}{f} = df^i \underset{\sim}{g}_i$ be the force vector acting on da from outside B, then the surface traction per unit current area is given by,

$$\underset{\sim}{t} = t^i \underset{\sim}{g}_i = (df^i/da)\underset{\sim}{g}_i \ . \qquad (3.27)$$

The Cauchy stress tensor $\underset{\sim}{\sigma} = \sigma^{ij} \underset{\sim}{g}_i \underset{\sim}{g}_j$ is related to the surface tractions through the equations,

$$t^i = \sigma^{ij} n_j \ . \qquad (3.28)$$

The components of the Cauchy stress tensor may be transformed to local coordinate axes by following the rules for second-order tensor transformations. For the particular case of the convected coordinate system, the Cauchy stress becomes,

$$\underset{\sim}{\sigma} = \sigma^{ij} \underset{\sim}{g}_i \underset{\sim}{g}_j = \sigma^{IJ} \underset{\sim}{a}_I \underset{\sim}{a}_J \ , \qquad (3.29)$$

where,

$$\sigma^{IJ} = \sigma^{ij} X^I{}_{,i} X^J{}_{,j} \ . \qquad (3.30)$$

The Kirchhoff stress tensor [16] is another stress tensor defined with respect to the current configuration. It is related to the Cauchy stress through the relationship,

$$\underset{\sim}{\tau} = \frac{\rho_0}{\rho} \underset{\sim}{\sigma} \ . \qquad (3.31)$$

With respect to the convected base vectors the components of the Kirchhoff stress tensor are given by,

$$\tau^{IJ} = \frac{\rho_o}{\rho} \sigma^{ij} X^I{}_{,i} X^J{}_{,j} . \tag{3.32}$$

In the previous section, it was possible to relate the rate of deformation (current configuration) to the rate of Green's strain (reference configuration) through an equation involving the deformation gradient. It is also possible to relate the kinetic quantities in the current configuration to quantities in the reference configuration; the deformation gradient will again play a prominent role.

As mentioned previously, the force acting on an element of surface area may be written in terms of the Cauchy stress as,

$$df^i = \sigma^{ij} n_j da . \tag{3.33}$$

An element of area with unit normal in the current configuration is related to the same element of area with unit normal in the reference configuration through the expression (Malvern [15], page 222),

$$n_i da = \frac{\rho_o}{\rho} N_\alpha X^\alpha{}_{,i} da_o . \tag{3.34}$$

Substituting Eq. (3.34) into Eq. (3.33) yields,

$$df^i = T^{i\alpha} N_\alpha da_o , \tag{3.35}$$

where,

$$T^{i\alpha} = \frac{\rho_o}{\rho} \sigma^{ij} X^\alpha{}_{,j} \tag{3.36}$$

is the first Piola stress tensor. Physically, the first Piola stress tensor relates the reference configuration unit normal and element of area to the force vector acting at the same point in the current configuration. In general, the inverse deformation gradient tensor is not symmetric, and Eq. (3.36) renders the first Piola stress tensor non-symmetric.

A symmetric stress tensor may be obtained by relating the surface force in the current configuration to a surface force in the reference configuration by using the deformation gradient; that is

$$df^i = x^i{}_{,\beta} \, d\tilde{f}^\beta . \tag{3.37}$$

Combining Eqs. (3.35), (3.36), and (3.37) yields,

$$d\tilde{f}^\beta = \tilde{T}^{\beta\alpha} N_\alpha da_o , \tag{3.38}$$

where,

$$\tilde{T}^{\beta\alpha} = X^\beta{}_{,i} T^{i\alpha} = \frac{\rho_o}{\rho} \sigma^{ij} X^\alpha{}_{,i} X^\beta{}_{,j} \tag{3.39}$$

is the second Piola stress tensor. The second Piola stress tensor is symmetric when the Cauchy stress tensor is symmetric, and relates the surface traction $d\tilde{f}^{\beta} = X^{\beta}{}_{,i}\, df^{i}$ (df^{i} defined with respect to the current configuration) to the unit area and unit normal of the same point in the reference configuration. Note that the contravariant components of the second Piola stress tensor are related to the reference configuration covariant base vectors; hence,

$$\underset{\sim}{\tilde{T}} = \tilde{T}^{\alpha\beta}\, \underset{\sim}{G}_{\alpha}\, \underset{\sim}{G}_{\beta} \;. \tag{3.40}$$

It is of interest to compare the convected coordinate components of the Kirchhoff stress, Eq. (3.32), and the components of the second Piola stress tensor, Eq. (3.39);

$$\tau^{IJ} = \frac{\rho_o}{\rho}\, \sigma^{ij}\, X^{I}{}_{,i}\, X^{J}{}_{,j} \;, \tag{3.41}$$

$$\tilde{T}^{\beta\alpha} = \frac{\rho_o}{\rho}\, \sigma^{ij}\, X^{\beta}{}_{,i}\, X^{\alpha}{}_{,j} \;. \tag{3.42}$$

Since, $X^{\alpha}{}_{,i} = X^{I}{}_{,i}\, \delta^{\alpha}{}_{I}$ (Eq. (3.4)), the convected coordinate components of the Kirchhoff stress are numerically equal to the components of the second Piola stress. However, the physical significance of the two stress tensors are quite different; they are defined with respect to two different configurations and associated with different sets of base vectors. As pointed out by Key et al. [14], this seemingly obvious distinction has been overlooked by many authors.

Elastic-plastic and elastic-viscoplastic constitutive equations are expressed in terms of stress rates or increments. "If the time rate of change of stress is to affect the dynamics of the substance, it must do so only in a way which is invariant under rigid motions" (Truesdell, [17]). Therefore, stress rates used in elastic-plastic and elastic-viscoplastic constitutive equations must be invariant to rigid body translations and rotations.

The material derivative of the Cauchy stress tensor may be considered as a candidate for the Cauchy stress rate used in constitutive equations. Equation (3.28) gives an expression which defines the components of the Cauchy stress tensor in terms of the surface traction vector, unit outward normal and element of area. The components of the Cauchy stress tensor will change if any of the quantities df^i, n_j, or da changes. Therefore, the components of the Cauchy stress are affected by changes in applied load, surface geometry and orientation with respect to a fixed coordinate system. Hence, the material derivative of the Cauchy stress is not invariant to rigid body rotations, and will yield a stress change without any deformation of the material. Consequently, the material derivative of the components of the Cauchy stress tensor should not be used in constitutive equations.

Although the components of the Cauchy stress tensor in a fixed coordinate system are not invariant to rigid body rotations, the second Piola stress tensor behaves differently. Consider Eq. (3.36), which can be written as,

$$d\tilde{f}^{\beta} = X^{\beta}{}_{,i}\, df^{i} \; . \tag{3.43}$$

The current configuration surface force vector components are related to the convected components through the expression,

$$df^{i} = x^{i}{}_{,I}\, df^{I} \; . \tag{3.44}$$

The combination of Eqs. (3.43) and (3.44) yield,

$$d\tilde{f}^{\beta} = X^{\beta}{}_{,i}\, x^{i}{}_{,I}\, df^{I} \; . \tag{3.45}$$

If the body experiences a rigid body rotation, the convected surface force components do not change, and Eq. (3.45) becomes,

$$d\tilde{f}^{\beta} = \delta^{\beta}{}_{I}\, df^{I} \; . \tag{3.46}$$

Therefore, the components of the pseudosurface force vector $d\tilde{\underset{\sim}{f}}$ in a fixed coordinate system are invariant with respect to rigid body rotations. Since the components of the second Piola stress tensor are referred to a fixed configuration, the element of area and the components of its outward unit normal do not change. Hence, the components in a fixed coordinate system of the material derivative of the second Piola stress tensor are invariant with respect to rigid body translations and rotations.

A stress rate which is invariant to rigid body rotations and is written in terms of the components of the Cauchy stress tensor may be obtained by taking the material derivative of Eqs. (3.42) [18],

$$\dot{\tilde{T}}^{\beta\alpha} = \frac{d}{dt}\left(\frac{\rho_o}{\rho}\right)\sigma^{ij}\, X^{\alpha}{}_{,i}\, X^{\beta}{}_{,j} + \frac{\rho_o}{\rho}\,\dot{\sigma}^{ij}\, X^{\alpha}{}_{,i}\, X^{\beta}{}_{,j}$$

$$+ \frac{\rho_o}{\rho}\,\sigma^{ij}\,\dot{X}^{\alpha}{}_{,i}\, X^{\beta}{}_{,j} + \frac{\rho_o}{\rho}\,\sigma^{ij}\, X^{\alpha}{}_{,i}\,\dot{X}^{\beta}{}_{,j}\ . \qquad (3.47)$$

If the current and reference configuration are taken to be instantaneously coincident, then,

$$\dot{\tilde{T}}^{ij} = \dot{\sigma}^{ij} + v^c|_c\,\sigma^{ij} - v^i|_c\,\sigma^{cj} - v^j|_c\,\sigma^{ci}\ . \qquad (3.48)$$

To obtain Eq. (3.48), the identities $\rho_o/\rho = 1$, $\frac{d}{dt}(\rho_o/\rho) = v^c|_c$, and $\dot{X}^{\alpha}|_i = -X^{\alpha}|_c\, v^c|_i$ were used. The right-hand side of Eq. (3.48) is frequently referred to as the Truesdell rate of the Cauchy stress tensor [19]. Equation (3.48) can be written alternatively as,

$$\dot{\tilde{T}}^{ij} = \dot{\sigma}^{ij} + g^{cd}\, v_d|_c\,\sigma^{ij} - g^{id}\, v_d|_c\,\sigma^{cj}$$

$$- g^{jd}\, v_d|_c\,\sigma^{ci}\ , \qquad (3.49a)$$

or

$$\overset{\circ}{T}{}^{ij} = \dot{\sigma}^{ij} + g^{cd}(D_{dc}+\omega_{dc})\sigma^{ij}$$

$$- g^{id}(D_{dc}+\omega_{dc})\sigma^{cj} - g^{jd}(D_{dc}+\omega_{dc})\sigma^{ci} \ . \quad (3.49b)$$

Equations (3.48), (3.49a), and (3.49b) represent the rate of change of the second Piola stress tensor referred to the current configuration geometry and base vectors. Since $\tau^{ij} = \rho_0/\rho\ \sigma^{ij}$ by Eq. (3.31), $\dot{\tau}^{ij} = \frac{d}{dt}(\rho_0/\rho)\sigma^{ij}+\rho_0/\rho\ \dot{\sigma}^{ij}$. When the current configuration is the reference configuration, this reduces to $\dot{\tau}^{ij} = v^c|_c\ \sigma^{ij} + \dot{\sigma}^{ij}$, and Eq. (3.48) becomes

$$\overset{\circ}{T}{}^{ij} = \dot{\tau}^{ij} - v^i|_c\ \tau^{cj} - v^j|_c\ \tau^{ci} \ , \quad (3.50)$$

when the Kirchhoff stress (Eq. (3.31)) is used instead of the Cauchy stress.

Other stress rates which are invariant to rigid body motions may be obtained by considering the convected coordinates which move and deform with the body. Consider the case where the convected and current configurations are instantaneously coincident at time t, and this configuration is taken as the reference configuration for a time step δt. Then a material line element,

$$d\underset{\sim}{x}(t) = dx^i(t)\ \underset{\sim}{g}_i = dX^I(t)\ \underset{\sim}{a}_I(t) \ , \quad (3.51)$$

will have components

$$d\underset{\sim}{x}(t+\delta t) = dx^i(t+\delta t)\, \underset{\sim}{g}_i = dX^I(t+\delta t)\, \underset{\sim}{a}_I(t+\delta t) \qquad (3.52a)$$

$$= dX^I(t)\, \underset{\sim}{a}_I(t+\delta t) \qquad (3.52b)$$

at time $t+\delta t$, where δt represents an infinitesimal increment in time. (Note that for a given material element $dX^I(t+\delta t) = dX^I(t)$.) Also,

$$dx^i(t+\delta t) = dx^i(t) + \delta t\, v^i{}_c\, dx^c(t) \qquad (3.53a)$$

$$= [\, \delta^i{}_c + \delta t\, v^i|_c\,]\, \delta^c{}_I\, dX^I(t+\delta t) \ . \qquad (s.53b)$$

Hence,

$$dX^I(t+\delta t) = \delta^I{}_c\, [\, \delta^c{}_i - \delta t\, v^c|_i\,]\, dx^i(t+\delta t) \qquad (3.54a)$$

and, at $t+\delta t$,

$$X^I{}_{,i} = \delta^I{}_c\, [\, \delta^c{}_i - \delta t\, v^c|_i\,] \ . \qquad (3.54b)$$

The Cauchy stress tensor at time $t+\delta t$ has the components,

$$\sigma^{ij}(t+\delta t) = \sigma^{ij}(t) + \dot{\sigma}^{ij}(t)\delta t \ , \qquad (3.55)$$

which may be transformed to the convected coordinates using Eqs. (3.30) and (3.54b). Hence,

$$\sigma^{IJ}(t+\delta t) = \delta^I{}_c\, [\, \delta^c{}_i - \delta t\, v^c|_i\,]\, \delta^J{}_d\, [\, \delta^d{}_j - \delta t\, v^d|_j\,]$$
$$[\, \sigma^{ij}(t) + \dot{\sigma}^{ij}(t)\delta t\,] \ , \qquad (3.56)$$

which can be written in the form,

$$\sigma^{IJ}(t+\delta t) = \delta^I{}_c\, \delta^J{}_d \{ \delta^c{}_i\, \delta^d{}_j\, \sigma^{ij}(t)$$

$$+ [\delta^c{}_i\, \delta^d{}_j\, \dot{\sigma}^{ij}(t) - v^c|_i\, \delta^d{}_j\, \sigma^{ij}$$

$$- v^d|_j\, \delta^c{}_i\, \sigma^{ij}]\, \delta t \} + O[(\delta t)^2] \ . \quad (3.57)$$

The convected derivative is the rate of change of the Cauchy stress as seen from a coordinate system which deforms and moves with the body. Therefore, for contravariant components

$$\overset{\circ}{\sigma}{}^{cd} = \dot{\sigma}^{cd} - v^c|_i\, \sigma^{id} - v^d|_j\, \sigma^{jc} \ , \quad (3.58)$$

where the superscript ° represents a convected derivative. The reader is referred to Malvern [15, page 403] for a definition of the convected derivative of the covariant components of the Cauchy stress. Equation (3.58) can be written in the following equivalent forms,

$$\overset{\circ}{\sigma}{}^{cd} = \dot{\sigma}^{cd} - g^{cn}\, v_n|_i\, \sigma^{id} - g^{dn}\, v_n|_j\, \sigma^{jc} \quad (3.59a)$$

and

$$\overset{\circ}{\sigma}{}^{cd} = \dot{\sigma}^{cd} - g^{cn}(D_{ni} + \omega_{ni})\sigma^{id}$$

$$- g^{dn}(D_{nj} + \omega_{nj})\sigma^{jc} \ . \quad (3.59b)$$

Comparing Eqs. (3.58), (3.59a), and (3.59b) to Eqs. (3.48), (3.49a), and (3.49b) reveals that the components of the convected derivative of the Cauchy stress tensor differ from the components of the Truesdell rate by the term $v^c|_c \, \sigma^{ij}$, which involves the dilatational components of the velocity gradient tensor. It should be emphasized, however, that the Truesdell rate of the Cauchy stress is equal to the rate of change of the second Piola stress referred to the current configuration,

$$^{t+\delta t}\tilde{T}^{mn} = {}^{t}\tilde{T}^{mn} + \dot{\tilde{T}}^{mn}\delta t \ . \tag{3.60}$$

The convected derivative is the rate of change of the Cauchy stress as seen from a coordinate system which deforms and moves with the body. Therefore,

$$^{t+\delta t}\sigma^{IJ} = \delta^I{}_i \, \delta^J{}_j \left[{}^{t}\sigma^{ij} + \overset{\circ}{\sigma}{}^{ij} \, \delta t\right] \ . \tag{3.61}$$

Note that $^{t+\delta t}\sigma^{IJ}$ in Eq. (3.61) is defined with respect to the current configuration and convected base vectors at t+δt; $^{t+\delta t}\tilde{T}^{mn}$ in Eq. (3.60) is referred to the configuration and base vectors of the current configuration at time t. Therefore, although the convected and Truesdell rates are similar in appearance, they represent two physically different quantities.

The Jaumann rate is often encountered, and represents the rate of change of a quantity as observed from a coordinate system which rotates with the body, but does not deform. The Jaumann rate of the Cauchy stress tensor is derived in a manner similar to that used in obtaining an expression for the convected rate of the Cauchy stress tensor. The Jaumann rate of the Cauchy stress is given by,

$$\overset{\nabla}{\sigma}{}^{ij} = \dot{\sigma}^{ij} - g^{in}\,\omega_{nd}\,\sigma^{dj} - g^{jn}\,\omega_{nd}\,\sigma^{di} , \qquad (3.62)$$

and is related to the convected derivative through

$$\overset{\nabla}{\sigma}{}^{ij} = \overset{\circ}{\sigma}{}^{ij} + g^{in}\,D_{nd}\,\sigma^{dj} + g^{jn}\,D_{nd}\,\sigma^{di} , \qquad (3.63)$$

where the symbol ∇ represents the Jaumann (co-rotational) derivative.

3.3. Work Conjugate Stress and Strain Quantities

In the previous sections of this chapter, several different tensor quantities and their respective rates were discussed. However, the kinetic and kinematic quantities were developed independently, and it may not be obvious which quantities should be used together in constitutive equations. Considerable insight may be obtained by considering the rate at which work is being done on the body B with surface ∂B. In terms of the current configuration surface tractions and body forces, the work rate is given by

$$\dot{W} = \int_{\partial B} t^i\, v_i\, d(\partial B) + \int_{B} \rho b^i\, v_i\, dB . \qquad (3.64)$$

Through the use of the divergence theorem and Eq. (3.28), Eq. (3.64) may be written as,

$$\dot{W} = \int_B \left[v_i \left(\sigma^{ij}|_j + \rho b^i \right) + \sigma^{ij} v_i|_j \right] dB \ . \qquad (3.65)$$

Since $\sigma^{ij}|_j + \rho b^i$ is equal to the rate of change of the momentum, Eq. (3.65) becomes,

$$\dot{W} = \frac{D}{Dt} \int_B \frac{1}{2} \rho \, v_i \, v_i \, dB + \int_B \sigma^{ij} \, v_i|_j \, dB \ . \qquad (3.66)$$

The first term is the rate of change of the kinetic energy; the second term is referred to as the stress power.

The stress power may alternatively be written as,

$$\int_B \sigma^{ij} \, v_i|_j \, dB = \int_B \sigma^{ij} \, D_{ij} \, dB \ , \qquad (3.67)$$

since,

$$v_i|_j = D_{ij} + \omega_{ij} \ . \qquad (3.68)$$

The stress power in the reference configuration may be obtained by substituting Eqs. (3.24a) and (3.29) into (3.67) to yield,

$$\int_B \sigma^{ij} \, D_{ij} \, dB = \int_{B_o} \tilde{T}^{\alpha\beta} \, \dot{E}_{\alpha\beta} \, dB_o \ . \qquad (3.69)$$

In Eq. (3.69) the stress and deformation combinations $\sigma^{ij} D_{ij}$ and $\tilde{T}^{\alpha\beta} \dot{E}_{\alpha\beta}$ yield work conjugate stress and strain measures.

The Cauchy stress and rate of deformation tensors are conjugate variables and are referred to the current configuration. The second Piola stress and Green's strain tensors are conjugate variables and are referred to the reference configuration. Using Eq. (3.31) and Eq. (3.69), the work conjugate deformation measure associated with the contravariant components of the Kirchhoff stress is seen to be $\frac{\rho}{\rho_o} D_{ij}$.

CHAPTER IV

FINITE STRAIN, ELASTIC-VISCOPLASTIC CONSTITUTIVE EQUATIONS

In Chapter II the mathematical structure of elastic-viscoplastic constitutive equations was considered. Subsequently, the kinematic and kinetic variables used to describe finite deformation motion were discussed in Chapter III. In the present chapter, three fundamentally different finite strain constitutive formulations for elastic-viscoplastic materials are considered. These are classified as: (1) hyperelastic-viscoplastic, (2) hypoelastic-viscoplastic, and (3) updated hyperelastic-viscoplastic.

In many practical problems involving finite inelastic deformations, the finite inelastic strains are confined to localized regions. In other cases, the strains and/or rotations may be of an intermediate magnitude, where possibly more than one set of constitutive equations provides a satisfactory material description. Additionally, the constitutive equations should be amenable to numerical implementation. Therefore, it is important to: (1) establish the theoretical and experimental bases of the various material models, (2) determine under what conditions the different descriptions yield comparable results, and (3) evaluate the relative numerical efficiency of the different descriptions with respect to accuracy versus computing time.

As a specific application, the Perzyna [3] generalization of the Malvern [1] and Sokolovsky [6] viscoplastic constitutive equations will be considered. Although the Perzyna over-stress viscoplastic description is considered, the developments are also applicable to other state-variable models.

4.1. Hyperelastic-Viscoplastic Constitutive Equations

The hyperelastic-viscoplastic constitutive theory has been proposed by Kanchi et al. [20] and Nagarajan and Popov [21] to treat problems where rotational or "geometric" effects are important. The appropriate kinetic and kinematic variables employed in the hyperelastic-viscoplastic constitutive equations are the second Piola stress tensor, $\tilde{\underset{\sim}{T}}$, and Green's strain tensor, $\underset{\sim}{E}$. Following Green and Naghdi [22,23], it is postulated that the total Green's strain may be separated into elastic and inelastic contributions,

$$\underset{\sim}{E} = \underset{\sim}{E}^{(e)} + \underset{\sim}{E}^{(vp)} \quad . \tag{4.1}$$

In Eq. (4.1), only the total Green's strain is given a kinematic interpretation, and the elastic and inelastic components are obtained from constitutive postulates. For a hyperelastic material, the second Piola stress tensor is related to the components of the Green's strain through the expression,

$$\tilde{\underset{\sim}{T}} = \rho_o \frac{\partial \psi}{\partial \underset{\sim}{E}} , \tag{4.2}$$

where ρ_o is the density in the undeformed configuration, and ψ is the strain energy function. For a linear, isotropic material, the strain energy function is given by

$$\psi = \frac{1}{2} [\lambda G^{\alpha\beta} E_{\alpha\beta} G^{\zeta\eta} E_{\zeta\eta} + 2\mu G^{\alpha\zeta} G^{\beta\eta} E_{\alpha\beta} E_{\zeta\eta}] , \tag{4.3}$$

where λ and μ are Lame's isotropic material coefficients. To obtain a hyperelastic-viscoplastic material description, Eq. (4.2) is used to relate the second Piola stress tensor to the elastic components of the Green's strain tensor appearing in Eq. (4.1),

$$\tilde{\underset{\sim}{T}} = \rho_o \frac{\partial \psi}{\partial E^{(e)}} . \tag{4.4}$$

With regard to the present constitutive development, it is desirable to express the constitutive variables in terms of rates, and Eq. (4.1) is written as

$$\dot{\underset{\sim}{E}} = \dot{\underset{\sim}{E}}^{(e)} + \dot{\underset{\sim}{E}}^{(vp)} . \tag{4.5}$$

The rate form of Eq. (4.4) may be written as

$$\dot{\tilde{T}}^{\alpha\beta} = D^{\alpha\beta\zeta\eta}\, \dot{E}^{(e)}_{\zeta\eta} \ , \tag{4.6}$$

where

$$D^{\alpha\beta\zeta\eta} = \rho_o \frac{\partial^2\psi}{\partial E^{(e)}_{\alpha\beta}\ \partial E^{(e)}_{\zeta\eta}} \tag{4.7a}$$

$$= \rho_o\, [\, \lambda G^{\alpha\beta}\, G^{\zeta\eta} + 2\mu G^{\alpha\zeta}\, G^{\beta\eta}\,] \ . \tag{4.7b}$$

The combination of Eqs. (4.5) and (4.6) may be written in component form as

$$\dot{\tilde{T}}^{\alpha\beta} = D^{\alpha\beta\zeta\eta}\, (\, \dot{E}_{\zeta\eta} - \dot{E}^{(vp)}_{\zeta\eta}\,) \ . \tag{4.8}$$

The viscoplastic rate of Green's strain is found by replacing the kinetic and kinematic quantities in Eq. (2.6) by the second Piola stress and Green's strain,

$$\dot{E}_{\zeta\eta} = \gamma \langle \Phi(F) \rangle \frac{\partial f(\tilde{T})}{\partial \tilde{T}^{\zeta\eta}} \ . \tag{4.9}$$

The over-stress in Eq. (4.9) is given by

$$F = \frac{f(\tilde{T})}{\phi\, (\, \bar{E}^{(vp)})} - 1 \ , \tag{4.10}$$

where the symbol < > denotes the function defined as

$$\langle\Phi(F)\rangle = \begin{cases} \Phi(F) & \text{for} \quad F \geq 0 \\ 0. & \text{for} \quad F < 0 \end{cases} . \tag{4.11}$$

Several observations concerning the material behavior described by Eqs. (4.7), (4.9), and (4.10) should now be considered. First, the equivalent dynamic stress, $f(\tilde{T})$, is expressed in terms of the components of the second Piola stress tensor, which are defined per unit area of the reference configuration. This is theoretically inconsistent, since a mathematical change in the reference configuration will alter the viscoplastic strain rate [18]. This statement has no significance when a state-variable constitutive equation is used which does not rely on the concept of a yield function.

Furthermore, the viscoplastic material description should be consistent with classical inviscid plasticity, which is correctly expressed in terms of kinetic and kinematic quantities referred to the current configuration. In particular, invariance of the loading and unloading elastic moduli requires that the stress and strain measures be referred to the current configuration. Hill [24] is very distinct about referring the stress and strain measures used in his book to the current configuration. An excellent discussion of the experimental observation underlying incremental plasticity theories is given by Lee [25].

4.2. Hypoelastic-Viscoplastic Material Descriptions

The second constitutive model may be described as a hypoelastic-viscoplastic material description which utilizes the rate of deformation, $\underset{\sim}{D}$, as the appropriate kinematic variable. Two formulations will be presented; the first uses the Cauchy stress, $\underset{\sim}{\sigma}$, while the other uses the Kirchhoff stress, $\underset{\sim}{\tau}$. Depending on the type of numerical integration procedure employed, one of the formulations may be more desirable than the other. Hypoelastic-plastic constitutive equations have been presented by Hutchinson [26], Key et al. [14], Hibbitt et al. [27], and McMeeking and Rice [28]. However, little theoretical or numerical work appears in the literature for hypoelastic-viscoplastic materials.

The first formulation to be considered will utilize the Cauchy stress tensor. The basic hypothesis is that of an additive decomposition of $\underset{\sim}{D}$ into elastic and viscoplastic components,

$$\underset{\sim}{D} = \underset{\sim}{D}^{(e)} + \underset{\sim}{D}^{(vp)} \quad . \tag{4.12}$$

Note that Eq. (4.12) does not involve any limitations as to the magnitude of the instantaneous velocity.

For a hypoelastic description, the elastic contribution to the rate of deformation is expressed in terms of the Jaumann rate of the Cauchy stress tensor by the expression

$$\overset{\nabla}{\sigma}{}^{ij} = C^{ijkl}\, D^{(e)}_{kl} \quad , \tag{4.13}$$

where,

$$\overset{\nabla}{\sigma}{}^{ij} = \dot{\sigma}^{ij} - g^{im}\, \omega_{mn}\, \sigma^{nj} - g^{jm}\, \omega_{mn}\, \sigma^{ni} \quad , \tag{4.14}$$

and

$$C^{ijkl} = g^{ij}\, g^{kl}\, \lambda + 2\mu g^{ik}\, g^{jl} \quad . \tag{4.15}$$

In Eq. (4.13), the superscripted dot signifies a material time derivative, g^{mn} is the contravariant metric tensor for the fixed coordinate system to which the current configuration is referred, and ω_{mn} is the vorticity or spin tensor. Combining Eqs. (4.12) and (4.13) yields,

$$\overset{\nabla}{\sigma}{}^{ij} = C^{ijkl} \left(D_{kl} - D^{(vp)}_{kl} \right) . \tag{4.16}$$

For a Perzyna-type material, the viscoplastic component of the rate of deformation is obtained by replacing the kinetic and kinematic quantities in Eq. (2.6) by the Cauchy stress and the viscoplastic component of the rate of deformation,

$$D^{(vp)}_{kl} = \gamma \langle \Phi(F) \rangle \frac{\partial f(\underset{\sim}{\sigma})}{\partial \sigma^{kl}} \quad . \tag{4.17}$$

The over-stress function in Eq. (4.17) is given by

$$F = \frac{f(\underset{\sim}{\sigma})}{\phi(\bar{\varepsilon}^{(vp)})} - 1 \; . \qquad (4.18)$$

The material derivative of the Cauchy stress obtained from Eqs. (4.14), (4.16), and (4.17) is

$$\dot{\sigma}^{ij} = C^{ijkl} D_{kl} - C^{ijkl} \gamma \langle \Phi(F) \rangle \frac{\partial f(\underset{\sim}{\sigma})}{\partial \sigma^{kl}}$$

$$+ g^{im} \omega_{mn} \sigma^{nj} + g^{jm} \omega_{mn} \sigma^{ni} \; . \qquad (4.19)$$

It will be shown in Chapter V that Eq. (4.19) is ideally suited for use in a finite element program employing an explicit time integration scheme. Also, it will be shown that a constitutive equation employing the material derivative of the second Piola stress tensor is required when an implicit time integration scheme is employed. Recall that the Truesdell rate of the Cauchy stress tensor represents the rate of change of the second Piola stress tensor referred to the current configuration geometry and base vectors. The Truesdell rate of the Cauchy stress may be written in terms of the Jaumann rate of the Cauchy stress as

$$\dot{\tilde{T}}^{ij} = \overset{\nabla}{\sigma}{}^{ij} + g^{cd} D_{dc} \sigma^{ij} - g^{id} D_{dc} \sigma^{cj}$$

$$- g^{jd} D_{dc} \sigma^{ci} \; . \qquad (4.20)$$

Combining Eqs. (4.16), (4.17), and (4.20) yields

$$\dot{\tilde{T}}^{ij} = \{ C^{ijkl} + g^{kl}\,\sigma^{ij} - g^{ik}\,\sigma^{lj} - g^{jk}\,\sigma^{li} \} D_{kl} - C^{ijkl}\,\gamma\langle\Phi(F)\rangle \frac{\partial f(\underset{\sim}{\sigma})}{\partial \sigma^{kl}} . \tag{4.21}$$

When referenced to the original configuration, Eq. (4.21) may be written as

$$\dot{\tilde{T}}^{\alpha\beta} = X^{\alpha}{}_{,i}\, X^{\beta}{}_{,j}\, X^{\Gamma}{}_{,k}\, X^{\phi}{}_{,l} \{ C^{ijkl} + g^{kl}\,\sigma^{ij} - g^{ik}\,\sigma^{lj} - g^{jk}\,\sigma^{li} \} \dot{E}_{\Gamma\phi} - X^{\alpha}{}_{,i}\, X^{\beta}{}_{,j}\, C^{ijkl}\,\gamma\langle\Phi(F)\rangle \frac{\partial f(\underset{\sim}{\sigma})}{\partial \sigma^{kl}} . \tag{4.22}$$

A hypoelastic-plastic equation similar to Eq. (4.22) has been presented by Hibbit, Marcal, and Rice [27]. Although Eqs. (4.19) and (4.22) represent suitable constitutive equations for use in conjunction with updated Lagrangian and total Lagrangian implicit finite element procedures, they will result in an unsymmetric stiffness matrix. It can easily be shown that the term $g^{kl}\,\sigma^{ij}$ in Eqs. (4.19) and (4.22) give rise to an unsymmetric matrix relating the components of rate of stress and strain written in vector form; that is,

$$\begin{Bmatrix} \dot{\tilde{T}}^{11} \\ \dot{\tilde{T}}^{22} \\ \dot{\tilde{T}}^{33} \\ \dot{\tilde{T}}^{12} \\ \dot{\tilde{T}}^{23} \\ \dot{\tilde{T}}^{13} \end{Bmatrix} = \begin{bmatrix} \text{unsymmetric} \\ \text{material} \\ \text{coefficient} \\ \text{matrix} \end{bmatrix} \begin{Bmatrix} \dot{E}_{11} \\ \dot{E}_{22} \\ \dot{E}_{33} \\ \dot{E}_{12} \\ \dot{E}_{23} \\ \dot{E}_{13} \end{Bmatrix} . \tag{4.23}$$

It has been pointed out by Hutchinson [26], that if the Kirchhoff stress tensor, $\underset{\sim}{\tau}$, is chosen as the kinetic quantity used in the constitutive equation, then a symmetric coefficient matrix can be obtained. Recall that the Kirchhoff stress is defined through the relationship,

$$\underset{\sim}{\tau} = \frac{\rho_o}{\rho} \underset{\sim}{\sigma} . \tag{4.24}$$

Note that the material derivative of the Kirchhoff stress is related to the material derivative of the Cauchy stress through the relationship,

$$\dot{\underset{\sim}{\tau}} = \frac{d}{dt}\left(\frac{\rho_o}{\rho}\right) \underset{\sim}{\sigma} + \frac{\rho_o}{\rho} \dot{\underset{\sim}{\sigma}} . \tag{4.25}$$

Combining Eqs. (3.47) and (4.25), and letting the reference and current configurations be instantaneously coincident yields a relationship between the rate of the Kirchhoff stress and the material derivative of the second Piola stress referenced to the current configuration;

$$\dot{\tilde{T}}^{ij} = \tau^{ij} - V^{i}|_{c}\, \tau^{cj} - V^{j}|_{c}\, \tau^{ci} \; . \qquad (4.26)$$

Equation (4.26) was given previously as Eq. (3.50), and can be written in terms of the Jaumann rate of the Kirchhoff stress as

$$\dot{\tilde{T}}^{ij} = \overset{\nabla}{\tau}{}^{ij} - g^{in}\, D_{nm}\, \tau^{mj} - g^{jn}\, D_{nm}\, \tau^{mi} \; . \qquad (4.27)$$

Therefore, if the elastic rate of deformation is related to the Jaumann rate of the Kirchhoff stress, and the viscoplastic rate of deformation is written in terms of the Kirchhoff stress, a second hypoelastic-viscoplastic constitutive equation is obtained;

$$\dot{\tilde{T}}^{ij} = \{ B^{ijkl} - g^{ik}\, \tau^{lj} - g^{jk}\, \tau^{li} \}\, D_{kl}$$

$$- B^{ijkl}\, \gamma \langle \Phi(F) \rangle \frac{\partial f(\tilde{\tau})}{\partial \tau^{kl}} \; , \qquad (4.28)$$

where

$$B^{ijkl} = \frac{\rho}{\rho_o}\, C^{ijkl} \; . \qquad (4.29)$$

When referenced to the original configuration, Eq. (4.28) may be written as

$$\dot{\tilde{T}}^{\alpha\beta} = X^{\alpha}{}_{,i}\; X^{\beta}{}_{,j}\; X^{\Gamma}{}_{,k}\; X^{\phi}{}_{,l}\; \{ B^{ijkl} - g^{ik}\, \tau^{lj}$$

$$- g^{jk}\, \tau^{li} \}\, \dot{E}_{\Gamma\phi} - X^{\alpha}{}_{,i}\; X^{\beta}{}_{,j}\; B^{ijkl}\; \gamma \langle \Phi(F) \rangle \frac{\partial f(\tau)}{\partial \tau^{kl}} \quad (4.30)$$

Note that Eqs. (4.28) and (4.30) do not contain a term similar to $g^{kl}\ \sigma^{ij}$ in Eqs. (4.19) and (4.22). Therefore, this constitutive equation will yield a symmetric stiffness matrix when used in conjunction with an implicit time integration scheme.

It should be pointed out, that the transformations required by Eqs. (4.22) and (4.30) are expensive to carry out numerically, and Eqs. (4.21) and (4.28) are preferable and require an updated Lagrangian implementation. Recall that the primary reason for choosing the Kirchhoff stress over the Cauchy stress is the numerical advantage obtained from working with a symmetric stiffness matrix versus an unsymmetric stiffness. If the Cauchy stress is chosen, an additional term involving the dilatational components of the rate of deformation is encountered, which results in an unsymmetric stiffness matrix. It can be argued that when the hydrostatic stresses are small, the differences between the two formulations will be small.

Within the last decade, a kinematic theory for finite strain, elastic-plastic deformation has been developed based on the work of Lee [29]. In this theory, the total deformation gradient is given by

$$\underset{\sim}{F} = \underset{\sim}{F}^{(e)} \underset{\sim}{F}^{(p)} , \tag{4.31}$$

where $\underset{\sim}{F}^{(e)}$ is the deformation gradient obtained in going from a stress-free intermediate configuration to the current configuration, and $\underset{\sim}{F}^{(p)}$ is the deformation gradient obtained in going from the reference configuration to the intermediate stress-free configuration.

Significant to the current development, when the elastic strains remain small, the kinematic postulate (Eq. (4.31)) is equivalent to the additive composition of the rate of deformation into elastic and plastic components (Lee, [25]). For metals, not exposed to high hydrostatic stresses, the elastic strains are bounded by plastic yielding to magnitudes of the order 10^{-3}. Therefore, for elastic-plastic materials, Eq. (4.12) represents a good approximation to the kinematic postulate (Eq. (4.31)). For elastic-viscoplastic materials, the stresses are permitted to exceed the static yield surfaces, and the decomposition of the rate of deformation into elastic and viscoplastic components may not be as good an approximation to the kinematic postulate of Eq. (4.31).

Since the kinetic and kinematic variables in the hypoelastic-viscoplastic constitutive equations are referred to the current configuration, they are believed to more closely represent the behavior of real materials experiencing finite strains than do the hyperelastic-viscoplastic constitutive equations.

4.3. Updated Hyperelastic-Viscoplastic Material Description

The third material model is classified as an updated hyperelastic-viscoplastic material description. A similar constitutive development for elastic-plastic materials has been presented by Bathe et al. [30]. This material description is based on the updated Lagrangian analysis procedure in which the reference configuration is taken to be the current configuration, and is updated at each time interval during the analysis. This updating procedure yields the "updated Lagrangian" form of the incremental equations of motion. The rate of Green's strain referred to the current configuration is separated into its elastic and viscoplastic contributions

$$ {}^{t}_{t}\dot{\varepsilon}_{kl} = {}^{t}_{t}\dot{\varepsilon}^{(e)}_{kl} + {}^{t}_{t}\dot{\varepsilon}^{(vp)}_{kl} \; , \tag{4.32} $$

where the left superscript identifies the time at which the quantity is known, and the left subscript identifies the configuration to which the quantity is referenced. For example, ${}^{t}_{t}\dot{\underset{\sim}{\varepsilon}}$ is the rate of Green's strain at time t, referenced to the configuration at time t. Assuming the existence of a hyperelastic-type constitutive expression, applicable in the neighborhood of the current configuration, one obtains,

$$ {}^{t}_{t}\tilde{T}^{ij} = C^{ijkl}\ {}^{t}_{t}\varepsilon^{(e)}_{kl} \ . \tag{4.33} $$

Using Eqs. (4.32) and (4.33) the material derivative of the second Piola stress referenced to the current configuration is given as

$$ {}^{t}_{t}\dot{\tilde{T}}^{ij} = C^{ijkl}\left({}^{t}_{t}\dot{\varepsilon}_{kl} - {}^{t}_{t}\dot{\varepsilon}^{(vp)}_{kl}\right) . \tag{4.34} $$

In Eq. (4.34), the viscoplastic component of the rate of Green's strain referenced to the current configuration is

$$ {}^{t}_{t}\dot{\varepsilon}^{(vp)}_{kl} = \gamma\langle\Phi(F)\rangle \frac{\partial f(\tilde{\sigma})}{\partial\sigma^{kl}} \ . \tag{4.35} $$

The second Piola stress at time $t+\Delta t$ may be obtained by integrating Eq. (4.34). For a simple Euler-type integration

$$ {}^{t+\Delta t}_{t}\tilde{T}^{ij} = {}^{t}_{t}\tilde{T}^{ij} + {}^{t}_{t}\dot{\tilde{T}}^{ij}\Delta t \ , \tag{4.36} $$

where Δt is the integration time step.

The components of the Cauchy stress at time $t+\Delta t$ are obtained from the relationship

$$ {}^{t+\Delta t}\sigma^{ij} = \frac{{}^{t+\Delta t}\rho}{{}^{t}\rho}\; {}^{t+\Delta t}_{\;\;t}(x^{i}{}_{,\alpha})\; {}^{t+\Delta t}_{\;\;t}(x^{j}{}_{,\beta})\; {}^{t+\Delta t}_{\;\;t}\tilde{T}^{\alpha\beta} \;. \tag{4.37} $$

Note that no left subscript is used with the Cauchy stress, since by definition, the Cauchy stress is always referenced to the current configuration. Also note the following relationship between the Cauchy stress and the second Piola stress referenced to the current configuration,

$$ {}^{t}_{t}\tilde{T} = {}^{t}\underset{\sim}{\sigma} \;. \tag{4.38} $$

The updated hyperelastic-viscoplastic constitutive description is similar to the hypoelastic-viscoplastic constitutive equations presented previously. One difference between the two models appears in the elastic coefficients, which differ by a factor of ρ_o/ρ when the Kirchhoff stress is used;

$$ C^{ijkl} = \frac{\rho_o}{\rho} B^{ijkl} \;. \tag{4.39} $$

Since the Cauchy stress is used in the Von-Mises yield function instead of the Kirchhoff stress, the viscoplastic strain rates given by Eqs. (4.17) and (4.28) will also differ by approximately a factor of ρ_o/ρ. For incompressible inelastic deformation of metals, the ratio ρ_o/ρ is approximately equal to one, and the effects of the density change should be small.

The main difference between the hypoelelastic-viscoplastic and updated hyperelastic-viscoplastic constitutive equations is in the choice of the stress rate appearing in the constitutive equations. For the hypoelastic description, the elastic coefficients must be modified to account for rigid body rotations. The distinction between the two descriptions arises purely from the choice of the kinetic and kinematic variables selected for use in the constitutive equations.

4.4. Comments on the Multiplicative Decomposition of the Deformation Gradient

The majority of the constitutive equations used to describe the inelastic deformation of crystalline solids utilize the concept that the total strain increment may be divided into elastic and plastic components. Hence, it is maintained that the physical phenomena controlling the evolution of the elastic and plastic components of the total strain increments are basically uncoupled. Elastic response is controlled by distortions of the crystal lattice which do not result in permanent changes in the microstructure of the material. According to Lee [25]:

> Plastic deformation is that remaining when the stress in a body subjected to elastic-plastic deformation is reduced to zero and thus also is the elastic strain. Physically, plastic strain is caused by the migration of dislocations and other defects through the crystal lattice.

The above definitions of elastic and plastic deformations may be illustrated by considering the results of a tensile test, as shown in Figure 4.1. As the tensile specimen is loaded, the initial response may be characterized by the line segment from point O to A. Subsequent unloading of the tensile specimen from point A will result in a response along the same line $\overline{OA}$ obtained during loading, and the unloaded specimen will return to its original stress-free configuration. If the tensile specimen is reloaded to a stress σ_B, the stress-strain curve will become nonlinear, as shown by curve $\overline{OAB}$ of Figure 4.1. Subsequent unloading from σ_B will be along the line $\overline{BC}$. The total strain, ε, at point B is seen to be comprised of a recoverable component, $\varepsilon^{(e)}$ (elastic), and nonrecoverable component, $\varepsilon^{(p)}$ (plastic). It is important to note that the configuration at point C used to define the plastic strain has zero stress and zero elastic strain. If the configuration at point C is used as the reference configuration, subsequent reloading from C to B will follow the line $\overline{CB}$, and will have the same slope as $\overline{OA}$. Therefore, if the kinetic and kinematic quantities are expressed in terms of the current stress-free configuration, the elastic properties are not affected strongly by prior plastic deformation [31].

Although rather concise definitions for the elastic and plastic components can be obtained from an examination

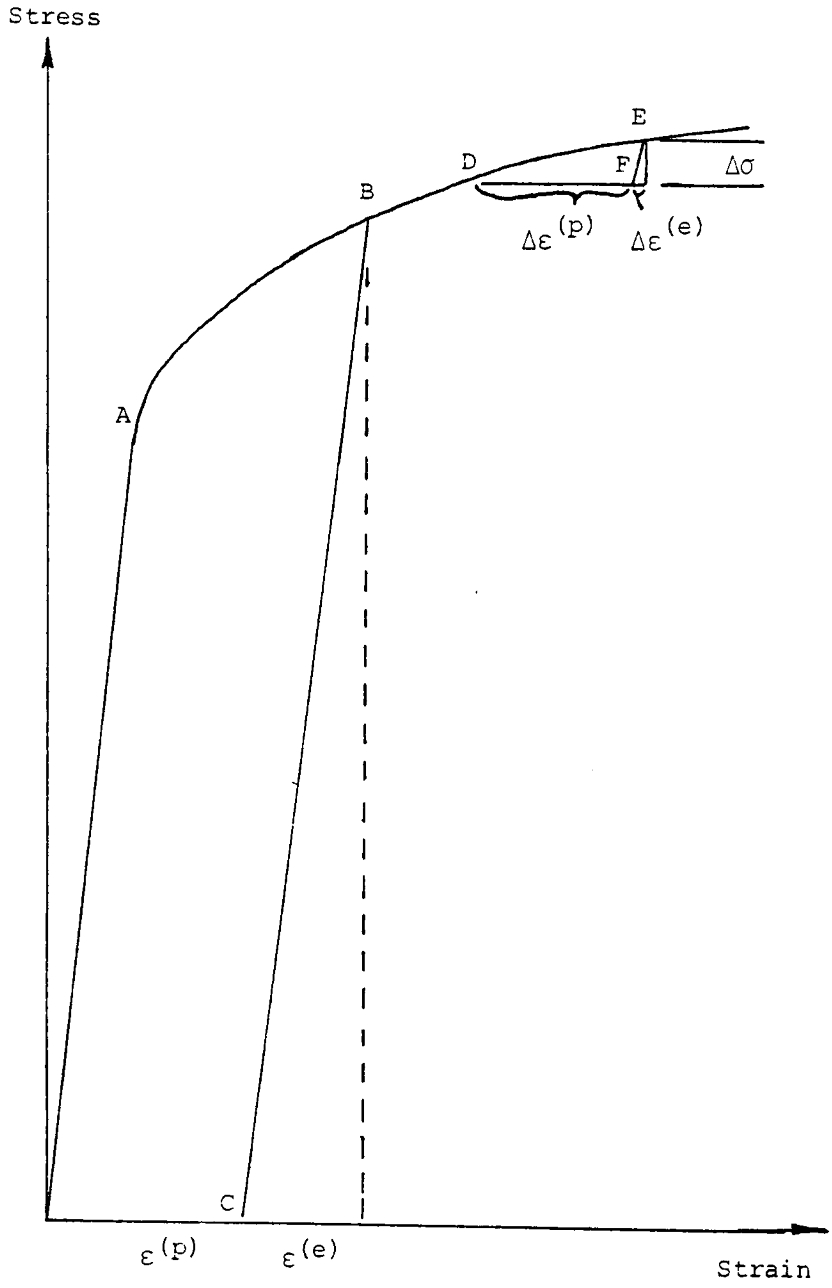

Figure 4.1. Elastic and Plastic Strain Increments.

of Figure 4.1, it is not always desirable to load and unload the specimen to determine the plastic strain component. For two- and three-dimensional stress fields it is seldom possible to obtain a stress-free configuration in which no stress or elastic strains exist. Therefore, it is desirable to consider increments in the elastic and plastic strain components, which may be integrated to yield the total elastic and plastic strain components.

Increments in the elastic and plastic strain components may be obtained by loading the specimen along the curve DE in Figure 4.1, through application of the stress increment $\Delta\sigma$. Upon unloading back to the stress σ_D, increments in the recoverable (elastic) and inelastic (plastic) strain components are obtained. Clearly, from Figure 4.1, it is seen that both the elastic and plastic strain increments can be functions of the current stress, stress increment, total elastic strain, and total plastic strain:

$$\Delta\varepsilon^{(e)} = \Delta\varepsilon^{(e)}\left(\sigma,\Delta\sigma,\varepsilon^{(e)},\varepsilon^{(p)}\right), \tag{4.40}$$

$$\Delta\varepsilon^{(p)} = \Delta\varepsilon^{(p)}\left(\sigma,\Delta\sigma,\varepsilon^{(e)},\varepsilon^{(p)}\right). \tag{4.41}$$

In accordance with the previous discussion, the elastic and plastic strains are generally maintained to be uncoupled. Hence, it is natural to assume that the elastic and plastic strain increments are not coupled to the total elastic and plastic strains, and Eqs. (4.40) and (4.41) may be written as,

$$\Delta\varepsilon^{(e)} = \Delta\varepsilon^{(e)}\left(\sigma,\Delta\sigma,\varepsilon^{(e)} \right), \tag{4.42}$$

$$\Delta\varepsilon^{(p)} = \Delta\varepsilon^{(p)}\left(\sigma,\Delta\sigma,\varepsilon^{(p)} \right). \tag{4.43}$$

Assuming a linear elastic response, Eq. (4.42) may be further simplified to,

$$\Delta\varepsilon^{(e)} = \Delta\varepsilon^{(e)}(\Delta\sigma) \; . \tag{4.44}$$

Therefore, the total strain increment may be written as,

$$\Delta\varepsilon = \Delta\varepsilon^{(e)}(\Delta\sigma) + \Delta\varepsilon^{(p)}\left(\sigma,\Delta\sigma,\varepsilon^{(p)} \right). \tag{4.45}$$

Equation (4.45) serves as a starting point for most incremental plasticity theories, and utilizes the current configuration as the appropriate reference configuration.

It has been suggested by Lee [29], that the elastic strain may distort the plastic strain increment to the extent that the accumulated increments obtained by Eq. (4.45) do not reflect the elastic and plastic strains defined with respect to a stress-free configuration. To accommodate this interaction, Lee proposed a finite strain theory based on the multiplicative decomposition of the deformation gradient into elastic and plastic components,

$$\underset{\sim}{F} = \underset{\sim}{F}^{(e)} \, \underset{\sim}{F}^{(p)} \, , \tag{4.46}$$

where $\underset{\sim}{F}$ is the deformation gradient, $\underset{\sim}{F}^{(e)}$ is the elastic contribution, and $\underset{\sim}{F}^{(p)}$ is the plastic contribution.

Since the introduction of Lee's kinematic description for elastic-plastic deformation, a significant amount of research has been directed toward developing a consistent theory based on the kinematic postulate, and interpreting it in light of previously established theories. In the remainder of this section, certain aspects of Lee's kinematic postulate will be developed and discussed with respect to the finite strain, elastic-viscoplastic constitutive equations presented in the first three sections of this chapter.

Consider an initially stress-free configuration, in which the particles of the body are identified by the material coordinates X^{α}. While undergoing elastic-plastic deformation, the particles are moved to a new configuration where the material particles occupy the spatial points having coordinates x^{i}. The components of a material line element in the deformed configuration are related to the components of the same line element in the initial configuration through the deformation gradient $\underset{\sim}{F}$, where,

$$dx^{i} = F^{i}{}_{\alpha} \, dX^{\alpha} \tag{4.47}$$

and

$$F_{i\alpha} = \frac{\partial x^i}{\partial X^\alpha} \; . \tag{4.48}$$

Suppose that the stress in the spatial configuration is removed so that the body goes along a reversible path to a new stress-free state. The particles in the new stress-free state are identified by the coordinates p^I. The configurations of the body corresponding to $\underset{\sim}{X}$, $\underset{\sim}{p}$, and $\underset{\sim}{x}$ are called the initial, intermediate, and deformed configurations, and are illustrated in Figure 4.2.

The intermediate configuration reflects the permanent deformation remaining after a plastically deformed body has been unloaded to a state of zero stress, and is consistent with the definition of plastic strain given earlier in this section. The initial and intermediate configurations are related through the deformation gradient $\underset{\sim}{F}^{(p)}$, where,

$$dp^I = F^{(p)I}{}_{\alpha} \, dX \quad . \tag{4.49}$$

Similarly, the reversible de-stressing from the deformed configuration to the intermediate configuration corresponds to the elastic unloading of the tensile specimen previously considered. The deformed and intermediate configurations are related through the deformation gradient $\underset{\sim}{F}^{(e)}$, where,

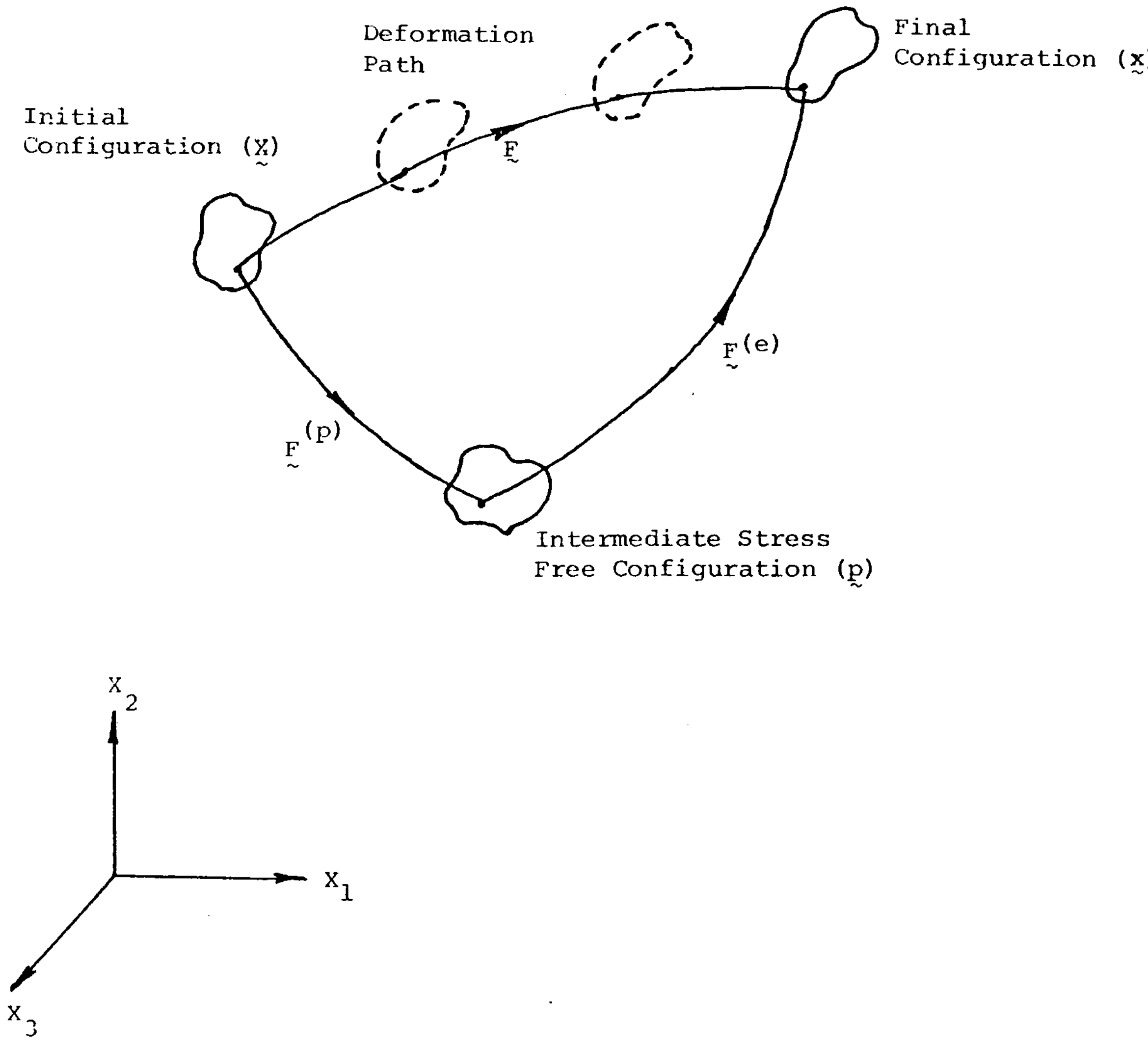

Figure 4.2. Configurations Used in the Multiplicative Decomposition of the Deformation Gradient.

$$dx^i = F^{(e)i}{}_I \, dp^I \ . \qquad (4.50)$$

In general, the deformation gradients $\underset{\sim}{F}^{(p)}$ and $\underset{\sim}{F}^{(e)}$ defined respectively by Eqs. (4.49) and (4.50) are point functions, and in general are not the partial derivatives $\partial \underset{\sim}{p}/\partial \underset{\sim}{X}$ and $\partial \underset{\sim}{x}/\partial \underset{\sim}{p}$ [29].

The composite elastic-plastic motion is thus described by the multiplicative decomposition of the total deformation gradient into its elastic and plastic components,

$$\underset{\sim}{F} = \underset{\sim}{F}^{(e)} \ \underset{\sim}{F}^{(p)} \ . \qquad (4.51)$$

Green's strain may be written as,

$$2\underset{\sim}{E} = \underset{\sim}{F}^T \ \underset{\sim}{F} - \underset{\sim}{I} \ , \qquad (4.52)$$

where in Cartesian coordinates, $\underset{\sim}{I}$ has one's on the diagonals and is zero elsewhere; otherwise, $\underset{\sim}{I}$ is the appropriate metric tensor. Yaghmai [32] introduced Eq. (4.51) into Eq. (4.52) to obtain the expression,

$$2\underset{\sim}{E} = \underset{\sim}{F}^{(p)T}(\underset{\sim}{F}^{(e)T} \ \underset{\sim}{F}^{(e)}-\underset{\sim}{I})\underset{\sim}{F}^{(p)}+(\underset{\sim}{F}^{(p)T} \ \underset{\sim}{F}^{(p)}-\underset{\sim}{I}) \ , \qquad (4.53)$$

and concluded that if the first term on the right is defined as the elastic strain and the second term as the plastic strain, that Eq. (4.53) is in agreement with Eq. (4.1) presented by Green and Naghdi [22]. Argyris [33] made the same observation, and used the three-configuration concept of Lee to develop a finite strain, "natural strain" finite element theory.

Although Eq. (4.53) may be obtained using consistent mathematics, it does not address the physical phenomenon which concerned Lee. That is, it does not show the interaction between the elastic strain field, and the plastic strain increments. Eq. (4.53) basically states that if the total Green's strain is divided into elastic and plastic components, the usual kinematic interpretation cannot be attached to the elastic and plastic components. Thus, it is in agreement with Green and Naghdi, but neither proves or disproves their basic hypothesis.

The velocity gradient in the deformed configuration can be written as

$$v^i|_j = v^i|_\alpha \, X^\alpha|_j \tag{4.54}$$

or

$$\underset{\sim}{L} = \dot{\underset{\sim}{F}} \, \underset{\sim}{F}^{-1} \, . \tag{4.55}$$

The velocity gradient $\underset{\sim}{L}$ may be written in terms of its symmetric and antisymmetric components as

$$\underset{\sim}{L} = \underset{\sim}{D} + \underset{\sim}{\omega} \, , \tag{4.56}$$

where $\underset{\sim}{D}$ is the rate of deformation tensor, and $\underset{\sim}{\omega}$ is the vorticity tensor. Substituting Eq. (4.51) into Eq. (4.55) yields

$$\underset{\sim}{L} = \dot{\underset{\sim}{F}}^{(e)} \underset{\sim}{F}^{(e)-1} + \underset{\sim}{F}^{(e)} \dot{\underset{\sim}{F}}^{(p)} F^{(p)-1} F^{(e)-1} \qquad (4.57a)$$

$$= L^{(e)} + F^{(e)} L^{(p)} F^{(e)-1} , \qquad (4.57b)$$

where $\underset{\sim}{L}^{(e)}$ corresponds to the velocity gradient associated with the purely elastic deformation, and $\underset{\sim}{L}^{(p)}$ corresponds to the velocity gradient associated with the purely plastic deformation. Hence, Eq. (4.57b) shows that if the kinematic hypothesis of Eq. (4.51) is accepted, the elastic deformation gradient will influence the plastic rate of deformation, or ultimately, the plastic strain increment.

Lubarda and Lee [34] have developed an elastic-plastic rate constitutive equation which includes the coupling between the elastic deformation field and plastic rate of deformation, as represented by Eq. (4.59a). An important premise in their work states that the elastic de-stressing occurs without rotation. Wang [35] utilizes the same premise in another elastic-plastic constitutive development based on Eq. (4.57a). Based on rotation-free de-stressing in conjunction with Eq. (4.57a), Lubarda and Lee showed that for infinitesimal elastic strains, the elastic coupling with the plastic rate of deformation is reduced to the order of the elastic strains. Hence, the multiplicative decomposition of the deformation gradient into elastic and plastic components is equivalent to the additive decomposition of the current configuration rate of deformation into elastic and plastic components under the conditions of small elastic strains. For most metals not exposed to high hydrostatic pressures, the elastic strains are limited by the plastic yield surfaces to the order 10^{-3}.

It is interesting to note the similarity between the approaches used by Green and Nadghi [22] and Lubarda and Lee [34] to develop elastic-plastic constitutive equations based on completely different kinematic hypotheses. In both developments, only the total Green's strain, or rate of deformation, are given a true kinematic interpretation. The elastic and plastic components in both theories are obtained from the same constitutive postulates applicable to either elastic or plastic material behavior. Thus, the seemingly different theories have some ground of commonality.

4.5. Hypoelastic-Plastic Constitutive Equation

This section presents a hypoelastic-plastic constitutive equation which was implemented during this investigation to provide a comparison between the inviscid and viscous theories. The hypoelastic-plastic constitutive equation is an extension of the small-deformation equations presented by Tanaka [36], and can be used to describe both combined isotropic and Ziegler's modified kinematic hardening. Following Prager's [37] kinematic hardening theory, the stress state of a body undergoing elastic-plastic deformation must lie on the yield surface defined by

$$\frac{3}{2}\left(\overset{\prime}{\sigma}{}^{ij} - \overset{\prime}{\alpha}{}^{ij}\right)\left(\overset{\prime}{\sigma}_{ij} - \overset{\prime}{\alpha}_{ij}\right) = \left(\sigma_o(\eta)\right)^2 , \tag{4.58}$$

where $\overset{\prime}{\sigma}{}^{ij}$ is the deviatoric Cauchy stress tensor; $\overset{\prime}{\alpha}{}^{ij}$ is the deviatoric component of α^{ij} which denotes the center of the yield surface; and $\sigma_o(\eta)$ denotes the instantaneous yield stress; η is the equivalent plastic strain defined by

$$\eta = \int_0^t \sqrt{\frac{2}{3} D_{ij}^{(p)} \, g^{im} \, g^{jn} \, D_{mn}^{(p)}} \, dt . \tag{4.59}$$

It is convenient to define the quantities

$$S^{ij} = \sigma^{ij} - \alpha^{ij} \tag{4.60}$$

and

$$\overset{\prime}{S}{}^{ij} = \overset{\prime}{\sigma}{}^{ij} - \overset{\prime}{\alpha}{}^{ij} . \tag{4.61}$$

Then Eq. (4.58) can be written as

$$\frac{3}{2} \overset{\prime}{S}{}^{ij} \overset{\prime}{S}_{ij} = (\sigma_o(\eta))^2 . \tag{4.62}$$

The total rate of deformation is decomposed into elastic and plastic components,

$$D_{kl} = D_{kl}^{(e)} + D_{kl}^{(p)} \ . \tag{4.63}$$

The elastic component of the rate of deformation is related to the Jaumann rate of the Cauchy stress through the linear hypoelastic relationship,

$$\overset{\nabla}{\sigma}{}^{ij} = C^{ijkl} \ D_{kl}^{(e)} \ . \tag{4.64}$$

The plastic component of the rate of deformation is defined by the flow rule,

$$D_{kl}^{(p)} = \dot{\lambda} \ S'_{kl} \ . \tag{4.65}$$

To determine the unknown scalar function $\dot{\lambda}$ in Eq. (4.65), another relationship between the stress and rate of deformation is required. Consider the true stress-logarithmic strain curve for uniaxial tension or compression as shown in Figure 4.3. The hatched area $BB'C$ of Figure 4.3 represents the specific plastic work increment due to strain hardening which is consumed while the stress varies from σ^{11} to $\sigma^{11} + d\sigma^{11}$, and the plastic strain from $\varepsilon_{11}^{(p)}$ to $\varepsilon_{11}^{(p)} + d\varepsilon_{11}^{(p)}$. From Figure 4.3, the following uniaxial relationship is obtained:

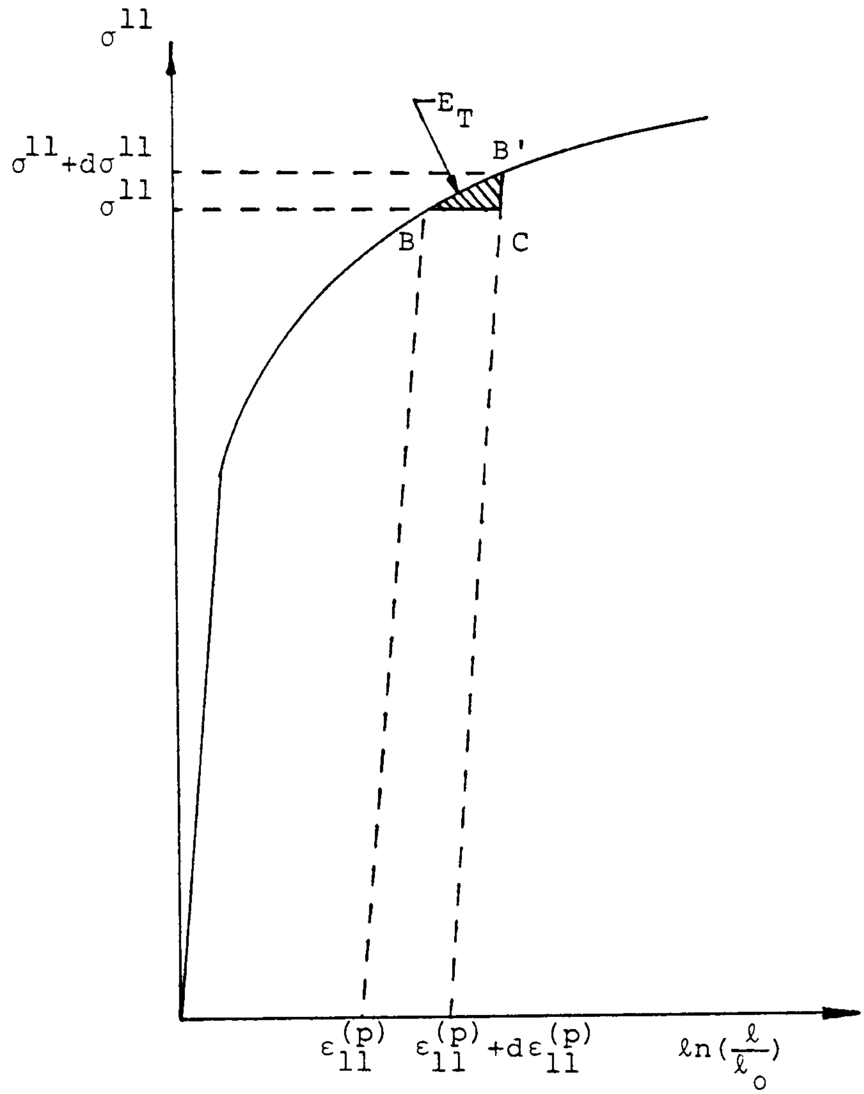

Figure 4.3. Specific Plastic Work Increment.

$$d\sigma^{11} = E_T \, d\varepsilon_{11} \ , \tag{4.66}$$

or, in rate form

$$\dot{\sigma}^{11} = E_T \, D_{11} \ , \tag{4.67}$$

where E_T is the current slope of the stress-strain curve. Using the uniaxial case of Eq. (4.63), Eq. (4.67) may be written as

$$\dot{\sigma}^{11} = E_T \, D_{11}^{(e)} + E_T \, D_{11}^{(p)} \ . \tag{4.68}$$

From the uniaxial case of Eq. (4.64)

$$\dot{\sigma}^{11} = E \, D_{11}^{(e)} \ , \tag{4.69}$$

where E is Young's modulus.

Combining Eqs. (4.68) and (4.69) yields the expression

$$\dot{\sigma}^{11} = H \, D_{11}^{(p)} \ , \tag{4.70}$$

where

$$H = \frac{E_T \, E}{E - E_T} \tag{4.71}$$

The specific plastic work increment represented by the hatched area in Figure 4.3 then becomes

$$d\sigma^{11}\, d\varepsilon_{11}^{(p)} = H\, d\varepsilon_{11}^{(p)}\, d\varepsilon_{11}^{(p)} \,. \tag{4.72}$$

By analogy with Eq. (4.72), it is assumed that in multiaxial stress fields the following relationship holds:

$$d\sigma^{ij}\, d\varepsilon_{ij}^{(p)} = K\, d\varepsilon_{ij}^{(p)}\, g^{ik}\, g^{jl}\, d\varepsilon_{kl}^{(p)} \,. \tag{4.73}$$

The constant K is chosen so that Eqs. (4.72) and (4.73) do not contradict. Therefore,

$$K = \frac{2}{3} H \tag{4.74}$$

and Eq. (4.73) becomes

$$d\sigma^{ij}\, d\varepsilon_{ij}^{(p)} = \frac{2}{3} H\, d\varepsilon_{ij}^{(p)}\, g^{ik}\, g^{jl}\, d\varepsilon_{kl}^{(p)} \,. \tag{4.75}$$

In rate form, Eq. (4.75) may be written as

$$\overset{\nabla}{\sigma}{}^{ij}\, D_{ij}^{(p)} = \frac{2}{3} H\, D_{ij}^{(p)}\, g^{ik}\, g^{jl}\, D_{kl}^{(p)} \,. \tag{4.76}$$

The combination of Eqs. (4.62), (4.71), and (4.76) may be written as

$$\dot{\lambda}\left(\frac{4}{9}\right)H(\sigma_o(\eta))^2 = \dot{S}'_{ij}\, \overset{\nabla}{\sigma}{}^{ij} \,. \tag{4.77}$$

Also, Eqs. (4.63) and (4.64) may be combined and written as

$$\overset{\nabla}{\sigma}{}^{ij} = C^{ijkl}\left(D_{kl} - D_{kl}^{(p)}\right). \tag{4.78}$$

Combining Eqs. (4.65), (4.77), (4.78), and solving for $\dot{\lambda}$ yields

$$\dot{\lambda} = \frac{\overset{\nabla}{S}'_{ij}\, C^{ijkl} D_{kl}}{\frac{4}{9}\, H(\sigma_o(\eta))^2 + \overset{\nabla}{S}'_{mn}\, C^{mnrs}\, \overset{\nabla}{S}'_{rs}} \ . \tag{4.79}$$

Combining Eqs. (4.64), (4.65), and (4.79) yields

$$\overset{\nabla}{\sigma}{}^{mn} = \left[C^{mnrs} - \frac{C^{mnkl}\, \overset{\nabla}{S}'_{kl}\, \overset{\nabla}{S}'_{ij}\, C^{ijrs}}{\frac{4}{9}\, H(\sigma_o(\eta))^2 + \overset{\nabla}{S}'_{xy}\, C^{xyuv}\, \overset{\nabla}{S}'_{uv}} \right] D_{rs} \ . \tag{4.80}$$

To complete the constitutive equation, it is necessary to obtain evolution laws for the location of the center of the yield surface in stress space, and the instantaneous value of the yield criteria. Consistent with Ziegler's [38] modification of Prager's kinematic hardening theory, it is assumed that the yield surface translates in stress space along the direction from its center to the stress point; that is,

$$\overset{\nabla}{\alpha}{}^{ij} = \dot{\mu}\,(\sigma^{ij} - \alpha^{ij}) \ . \tag{4.81}$$

From Eq. (4.60) one can write

$$\overset{\nabla}{\sigma}{}^{ij}\, D^{(p)}_{ij} = \overset{\nabla}{\alpha}{}^{ij}\, D^{(p)}_{ij} + \overset{\nabla}{S}{}^{ij}\, D^{(p)}_{ij} \ . \tag{4.82}$$

It is now expedient to introduce a new parameter β, defined such that

$$\overset{\nabla}{\alpha}{}^{ij} D_{ij}^{(p)} = (1-\beta) \overset{\nabla}{\sigma}{}^{ij} D_{ij}^{(p)} \tag{4.83}$$

and

$$\overset{\nabla}{S}{}^{ij} D_{ij}^{(p)} = \beta \overset{\nabla}{\sigma}{}^{ij} D_{ij}^{(p)} . \tag{4.84}$$

An investigation of Eqs. (4.83) and (4.84) shows that Eq. (4.82) is always satisfied. Combining Eqs. (4.65), (4.81), and (4.83), yields

$$\dot{\mu} = \frac{3}{2}(1-\beta) \overset{'}{S}_{ij} \overset{\nabla}{\sigma}{}^{ij}/(\sigma_o(\eta))^2 . \tag{4.85}$$

Therefore,

$$\overset{\nabla}{\alpha}{}^{ij} = \frac{3}{2} (1-\beta) \overset{'}{S}{}^{ij} \overset{'}{S}_{mn} \overset{\nabla}{\sigma}{}^{mn}/(\sigma_o(\eta))^2 . \tag{4.86}$$

Considering the fact that the stress must stay on the yield surface, the following consistency relationship must hold during elastic-plastic deformation,

$$\frac{\partial f}{\partial \underset{\sim}{S}} \underset{\sim}{\overset{\nabla}{S}} - \dot{\sigma}_o(\eta) = 0 . \tag{4.87}$$

where

$$f = \sqrt{3J_2} , \tag{4.88}$$

$$J_2 = \frac{S'_{ij}\, S'^{ij}}{2} \,, \tag{4.89}$$

and

$$S'^{ij} = \sigma'^{ij} - \alpha'^{ij} \,. \tag{4.90}$$

In component form, Eq. (4.87) may be written as

$$\dot{\sigma}_o(\eta) = \frac{3}{2}\, \frac{S'_{ij}\, \overset{\nabla}{S}{}'^{ij}}{\sigma_o(\eta)} \,, \tag{4.91}$$

or

$$\dot{\sigma}_o(\eta) = \frac{3}{2}\, \frac{S'_{ij}}{\sigma_o(\eta)} \left(\overset{\nabla}{\sigma}{}^{ij} - \overset{\nabla}{\alpha}{}^{ij}\right) \,. \tag{4.92}$$

Substituting Eq. (4.86) into Eq. (4.92), and using Eq. (4.62), the following expression is obtained

$$\dot{\sigma}_o(\eta) = \frac{2}{3}\, \dot{\lambda}\; H\; \beta\; \sigma_o(\eta) \,. \tag{4.93}$$

Using Eqs. (4.65) and (4.59), the scalar function $\dot{\lambda}$ may be written in an alternative form as

$$\dot{\lambda} = \frac{3}{2}\, \dot{\eta}/\sigma_o(\eta) \,. \tag{4.94}$$

Substituting Eq. (4.94) into Eq. (4.93) yields the relationship

$$\dot{\sigma}_o(\eta) = H\; \beta\; \dot{\eta} \,. \tag{4.95}$$

Equations (4.80), (4.86), and (4.95) represent the complete set of hypoelastic-plastic constitutive equations. These equations may be integrated in time to obtain the stress history in the elastic-plastic body undergoing finite deformations. It can be shown that if β is taken to be 1.0, that these equations reduce to those for isotropic hardening. For $\beta = 0.0$, they reduce to Ziegler's modified kinematic hardening. For $0. < \beta < 1.$ they represent combined modified kinematic and isotropic hardening.

Note that the elastic-plastic material tensor of Eq. (4.80) does not depend explicitly on time (compare this to Eq. (5.12), page 85). Also, it is required that a small enough time step be used to insure that the computed stresses remain on the yield surface during elastic-plastic motion. This is not always easily achieved numerically, and much literature exists describing techniques for satisfying this condition. In this investigation an initial strain method similar to that described by Bathe [39] was employed. This technique is similar to the adaptive method used to integrate the implicit viscoplastic constitutive equations described later in Section 5.1.

CHAPTER V

INTEGRATION OF EQUATIONS OF MOTION AND CONSTITUTIVE EQUATIONS

In general, the governing field equations of solid mechanics are highly nonlinear. The nonlinearities in the governing equations may arise from either kinematic or material considerations. Fortunately, for many practical problems, the equations may be linearized by noting that the strains and rotations are infinitesimal, and that the material constitutive equations are basically linear. Classical elasticity theory is based on the linearized Green's strain and Hooke's law.

Although the concepts and equations surrounding solid mechanics have been in existence for a long time, attempts to solve the fully nonlinear equations have been limited to approximately the last 25 years. The rapid development of digital computers and peripheral hardware has made it possible to obtain approximate solutions to many highly nonlinear problems. Within recent years, the finite element method has received considerable attention, and represents a general technique for obtaining discrete equations which yield approximate solutions to the governing field equations.

In this chapter, techniques for the numerical implementation of finite strain, elastic-viscoplastic constitutive equations will be developed. Since the constitutive equations are expressed in rate form, it is necessary to investigate both the integration of the constitutive equations and the equations of motion of the body. The integration of the finite strain, elastic-viscoplastic constitutive equations will be considered first.

5.1. Integration of Finite Strain, Elastic-Viscoplastic Constitutive Equations

In 1972, Zienkiewicz and Cormeau [40] presented a finite element formulation for the quasi-static response of elastic-viscoplastic materials. The basic feature of their formulation involved the additive decomposition of the total strain tensor into elastic and viscoplastic components. The viscoplastic strain increment during the time interval was obtained as

$$\Delta \underset{\sim}{\varepsilon}^{(vp)} = \dot{\underset{\sim}{\varepsilon}}^{(vp)} \Delta t \ , \tag{5.1}$$

the current viscoplastic strain rate times the time increment Δt. Zienkiewicz's formulation considered only infinitesimal strains and rotations, and is particularly useful in describing creep phenomena where inertia effects are not important. To obtain the viscoplastic strain rate, a power law specialization of Perzyna's material description was employed. Equation (5.1) represents an explicit Euler-type integration.

The stability of the quasi-static solution algorithm was subsequently studied by Cormeau [41] in 1975, and by Hughes and Taylor in 1978 [42]. For quasi-static problems using the simple Euler integration scheme, Cormeau demonstrated that the solution was stable if the integration time increment was kept below a critical time increment of

$$\gamma \Delta t_c \leq \frac{4(1+\nu)F_o}{3E} \tag{5.2}$$

where ν is Poisson's ratio, E is Young's modulus, γ is the strain rate sensitivity parameter, and Δt_c is the critical time increment. Equation (5.2) was derived using a von Mises yield function.

In 1974, Nagarajan and Popov [21] and subsequently, Kanchi et al. [20], extended the work of Zienkiewicz and Cormeau to include geometrically nonlinear effects. Their formulation included dynamic effects, and was based on an additive decomposition of the rate of Green's strain into elastic and viscoplastic components,

$$\dot{\underset{\sim}{E}} = \dot{\underset{\sim}{E}}^{(e)} + \dot{\underset{\sim}{E}}^{(vp)} \; . \tag{5.3}$$

As a direct extension of Perzyna's material description, the viscoplastic rate of Green's strain was expressed directly in terms of the second Piola-Kirchhoff stress tensor. This results in the hyperelastic-viscoplastic constitutive equations discussed in Chapter IV, Section 4.1.

Nagarajan and Popov included inertia effects, and supplemented the Euler-type, quasi-static scheme of Zienkiewicz and Cormeau, with a conditionally stable implicit integration scheme for the equations of motion to solve a number of problems.

In 1974, Zienkiewicz [43] presented an implicit "mid-interval time stepping scheme" for integrating the rate evolution laws encountered with creep and viscoplastic constitutive equations. The time stepping procedure is more accurate than the Euler explicit scheme and almost unconditional stability can be achieved. In later paragraphs, this method will be presented in more detail to obtain an implicit integration scheme for finite strain, elastic-viscoplastic materials.

In the period from 1978 to 1980, Argyris et al. [44,45,46] developed a finite strain, elastic-plastic and elastic- viscoplastic theory based on an additive decomposition of the "natural strain" into elastic and inelastic components. The theory involves the identification of three configurations used to describe plastic deformation, and attempts to embody the concepts associated with Lee's kinematic postulate. Argyris's interpretation of the multiplicative decomposition of the deformation gradient into elastic and plastic components is discussed in Section 4.4. Argyris employs a somewhat unconventional technique known as the "natural approach," and builds his theory around a particular element, the equivalent of a constant strain triangle.

In the following paragraphs, Zienkiewicz's "mid-interval time stepping scheme" for integrating the constitutive equations will be applied to obtain an implicit constitutive equation for a hypoelastic-viscoplastic material. The technique can be applied to the other finite strain, constitutive equations in a similar manner. The Jaumann rate of the Cauchy stress may be related to the total and viscoplastic component of the rate of deformation through the equation,

$$\overset{\nabla}{\sigma}{}^{ij} = C^{ijkl}\left(D_{kl} - D_{kl}^{(vp)}\right), \tag{5.4}$$

where,

$$D_{kl}^{(vp)} = \gamma\langle\Phi(F)\rangle \ \frac{\partial f}{\partial \sigma^{kl}} \ . \tag{5.5}$$

The viscoplastic component of the rate of deformation at any point between two instances in time may be approximated by

$$D_{kl}^{(vp)} = (1-\zeta)\ {}^{t}D_{kl}^{(vp)} + \zeta\ {}^{t+\Delta t}D_{kl}^{(vp)}\ , \tag{5.6}$$

where ζ is a time parameter normalized to one over the time interval Δt; i.e., $\zeta=0$ at time t, and $\zeta=1.0$ at time $t+\Delta t$.

The viscoplastic component of the rate of deformation at time $t+\Delta t$ may be approximated by

$$^{t+\Delta t}D_{kl}^{(vp)} = {}^{t}D_{kl}^{(vp)} + \Delta t\ \frac{\partial\ {}^{t}D_{kl}^{(vp)}}{\partial \sigma^{mn}}\ \overset{\nabla}{\sigma}{}^{mn}\ . \tag{5.7}$$

Combining Eqs. (5.6) and (5.7) yields

$$D_{kl}^{(vp)} = {}^{t}D_{kl}^{(vp)} + \zeta\Delta t\ \frac{\partial\ {}^{t}D_{kl}^{(vp)}}{\partial \sigma^{mn}}\ \sigma^{mn}\ . \tag{5.8}$$

Equations (5.4) and (5.8) can then be written as

$$\overset{\nabla}{\sigma}{}^{ij} + \zeta\Delta t\ C^{ijkl}\ \frac{\partial\ {}^{t}D_{kl}^{(vp)}}{\partial \sigma^{mn}}\ \overset{\nabla}{\sigma}{}^{mn} = C^{ijkl}\ (D_{kl} - {}^{t}D_{kl}^{(vp)})\ . \tag{5.9}$$

After some manipulation, Eq. (5.9) can be written as

$$\overset{\nabla}{\sigma}{}^{mn} = K^{mn}{}_{ij}\ C^{ijkl}\ (D_{kl} - {}^{t}D_{kl}^{(vp)})\ , \tag{5.10}$$

where $K^{mn}{}_{ij}$ is the inverse of the relationship

$$K^{ij}{}_{mn} = \delta^{i}{}_{m}\ \delta^{j}{}_{n} + \zeta\Delta t\ C^{ijrs}\ \frac{\partial\ {}^{t}D_{rs}^{(vp)}}{\partial \sigma^{mn}}\ . \tag{5.11}$$

Equation (5.10) may alternatively be written as

$$\dot{\sigma}^{mn} = K^{mn}{}_{ij}\, C^{ijkl}(D_{kl} - {}^{t}D^{(vp)}_{kl}) + g^{mk}\, \omega_{kl}\, \sigma^{ln} + g^{nk}\, \omega_{kl}\, \sigma^{lm} . \tag{5.12}$$

Zienkiewicz has shown that this type of constitutive equation integration demonstrates excellent stability if $\zeta \geq 1/2$. If ζ is taken to be 1/2, Eq. (5.12) amounts to obtaining the stress rate at the mid-point in the time interval using information at the beginning of the time interval. This represents an extremely interesting concept.

To implement Eq. (5.12), it is necessary to evaluate the partial derivative,

$$\frac{\partial\ {}^{t}D^{(vp)}_{rs}}{\partial\sigma^{mn}} = \frac{\partial}{\partial\sigma^{mn}}\left(\gamma\langle\Phi(F)\rangle\ \frac{\partial f(\underset{\sim}{\sigma})}{\partial\sigma^{rs}}\right). \tag{5.13}$$

For a power law overstress function $\Phi(F) = F^n$, and von Mises yield function $f = \sqrt{3J_2}$, Eq. (5.13) may be written as

$$\frac{\partial\ {}^{t}D^{(vp)}_{rs}}{\partial\sigma^{mn}} = \frac{\partial}{\partial\sigma^{mn}}\left(\gamma F^n\ \frac{3}{2}\ \frac{\sigma'_{rs}}{\sqrt{3J_2}}\right), \tag{5.14}$$

where the bracket function notation $\langle F^n\rangle$ has been omitted for brevity.

It is easily verified that Eq. (5.14) yields

$$\frac{\partial \; {}^{t}D^{(vp)}_{rs}}{\partial \sigma^{mn}} = \frac{3}{4J_2} \gamma F^n \left\{ \frac{n}{F\phi(\bar{\varepsilon})} - \frac{1}{\sqrt{3J_2}} \right\} \sigma'_{rs} \, \sigma'_{mn}$$

$$+ \gamma F^n \frac{3}{2} \frac{1}{\sqrt{3J_2}} \left(\delta_{rm} \, \delta_{sn} - \frac{1}{3} \delta_{rs} \, \delta_{mn} \right) , \qquad (5.15)$$

where $\underset{\sim}{\sigma'}$ is the deviatoric Cauchy stress tensor.

In Eq. (5.12) it is necessary to obtain the inverse of $K^{ij}{}_{mn}$ defined by Eq. (5.11). The inverse is computed on the element Gauss point level, and for a two-dimensional finite element, requires a 4 x 4 matrix to be inverted (see Section 6.10.4). When compared to the time step advantage obtained, the inversion operation is only a minor consideration. Also, note that Eq. (5.12) depends explicitly on the time step interval.

The accuracy of the computed stress can be improved by dividing the time interval into subintervals and using Eq. (5.12) to compute the stress rate at the mid-interval of each subinterval. In this investigation, an adaptive technique was programmed which limited the subinterval time increment according to the following criteria:

$$\sqrt{3\dot{J}_2} \; \Delta t_c \leq 0.1 \sqrt{3J_2} \; . \qquad (5.16)$$

These criteria limited the stress increments during a subinterval to 10% of the current stresses. During the course of this investigation, Eq. (5.12) in conjunction with the subinterval selection criteria always gave a stable solution, even when the viscoplastic components of the rate of deformation were very large. Figure 5.1 illustrates the concepts involved in the adaptive subinterval computations.

In this section, explicit and implicit methods for the numerical integration of finite strain, elastic-viscoplastic constitutive equations have been presented. In the following sections, the finite element equations required for the solution of the equations of motion describing the elastic-viscoplastic medium will be presented. These equations are used as a basis for the numerical implementation of the three finite strain, elastic-viscoplastic constitutive theories presented in Chapter IV. The finite element equations are general and may be used with other constitutive equations.

5.2. Eulerian and Lagrangian Statements of the Rate of Virtual Work

Equilibrium of the tractions and body forces at a spatial point in the current configuration is given by

$$\sigma^{ij}|_j + f^i = 0 \ , \qquad (5.17)$$

where σ^{ij} is the Cauchy stress tensor, and f^i is the body force per unit of the current volume. The traction vector acting on an element of area having unit normal $\underset{\sim}{n}$, is given

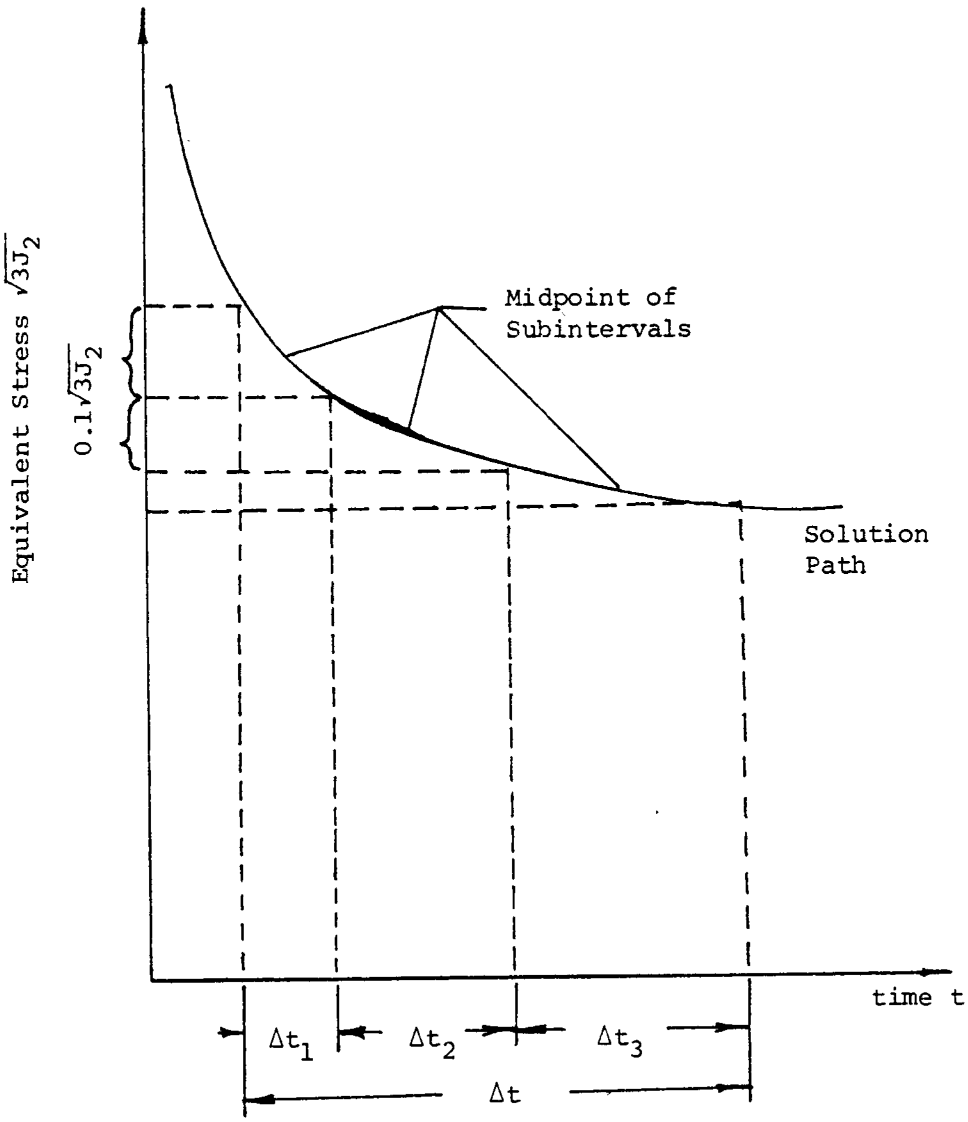

Figure 5.1. Illustration of Subintervals Used in Constitutive Equation Integration.

by Eq. (3.28) as

$$t^i = \sigma^{ij} n_j \ . \tag{5.18}$$

Multiplying Eq. (5.17) by a virtual velocity δv, and integrating over the current volume yields

$$\int_B \left(\sigma^{ij}|_j \ \delta v_i + f^i \ \delta v_i\right) dB = 0 \ . \tag{5.19}$$

The restrictions placed on the virtual velocity field are that it satisfy the kinematic constraints imposed on B, and does not vary with time (i.e., $(\dot{\delta v}) = 0$, where the superscripted dot signifies temporal differentiation). The Eulerian statement of the rate of virtual work is obtained by rearranging Eq. (5.19) to the form

$$\int_B \sigma^{ij} \ \delta v_i|_j \ dB = \int_{\partial B} t^i \ \delta v_i \ d(\partial B) + \int_B f^i \ \delta v_i \ dB \ . \tag{5.20}$$

A more useful form of the Eulerian statement of the rate of virtual work may be obtained by substituting Eq. (3.17) into Eq. (5.20), which yields

$$\int_B \sigma^{ij} \ \delta D_{ij} \ dB = \int_{\partial B} t^i \ \delta v_i \ d(\partial B) + \int_B f^i \ \delta v_i \ dB \ . \tag{5.21}$$

The application of Eq. (5.21) requires that the volume and surface geometry of B be known at the time at which the integration is being performed. In general, this is not known since it is the deformation history of the body which is being evaluated. One way of using Eq. (5.21) is to consider a volume fixed in space, with the material flowing continuously through it. This may be considered a control volume-type approach and could be applied in the context of fluid flow phenomena.

In the inelastic deformation of solids, where initial anisotropy and anisotropy resulting from the deformation history influences the material behavior, it is more desirable to follow the deformation and orientation of a particular material particle through its complete motion. In this context, Key [47] has used Eq. (5.21) in conjunction with an explicit central difference scheme, by updating the geometry at the end of each time step.

When implicit solution schemes are employed, or the constitutive equations are written in terms of Lagrangian variables, it is often more desirable to use a statement of the rate of virtual work based on a Lagrangian frame of reference.

A Lagrangian statement of the rate of virtual work may be obtained by substituting Eqs. (3.24a) and (3.39) into Eq. (5.21) to yield

$$\int_{B_o} \tilde{T}^{\alpha\beta}\, \delta\dot{E}_{\alpha\beta}\, dB_o = \int_{\partial B} t^i\, \delta v_i\, d(\partial B) + \int_{B} f^i\, \delta v_i\, dB \; . \quad (5.22)$$

If the current configuration is described with the same base vectors as the reference configuration, $\delta v_i = \delta v_\alpha$ and Eq. (5.22) may be written as

$$\int_{B_o} \tilde{T}^{\alpha\beta}\ \delta\dot{E}_{\alpha\beta}\ dB_o = \int_{\partial B_o} t_o^\alpha\ \delta v_\alpha\ d(\partial B_o) + \int_{B_o} f_o^\alpha\ \delta v_\alpha\ dB_o\ , \quad (5.23)$$

where t_o^α and f_o^α are based on the surface area and volume of the reference configuration.

Equation (5.23) is the Lagrangian statement of the rate of virtual work, in which all variables are defined with respect to the reference configuration. The integrations in Eq. (5.23) may now be carried out since the geometry of the reference configuration is presumed to be known. Note that no reference to the material behavior was made during the derivation of the rate of virtual work expression. Therefore, the rate of virtual work may be used in conjunction with any consistent constitutive formulation.

Inertia terms may be introduced into the rate of virtual work expression (Eq. (5.23)) using D'Alembert's principle. Hence, a body force $\underset{\sim}{f}_{(d)} = -\rho_o \ddot{\underset{\sim}{x}}$ is substituted into Eq. (5.23) to yield

$$\int_{B_o} \rho_o \ddot{x}^{\alpha} \, \delta v_{\alpha} \, dB_o + \int_{B_o} \tilde{T}^{\alpha\beta} \, \delta \dot{E}_{\alpha\beta} \, dB_o$$

$$= \int_{\partial B_o} t_o^{\alpha} \, \delta v \, d(\partial B_o) + \int_{B_o} f_o^{\alpha} \, \delta v_{\alpha} \, dB_o \, . \qquad (5.24)$$

Equation (5.24) is basically an integral statement of equilibrium, and will serve as a basis for the numerical implementation of elastic-viscoplastic constitutive equations.

In the following sections, two different techniques for the numerical implementation of the rate of virtual work will be considered. The first technique is an explicit central difference scheme; the second technique is based on an incremental form of Eq. (5.24). To provide a coherent and readable document, only the basic equations will be given in the text of the following sections.

5.3. Explicit Integration of the Rate of Virtual Work

Explicit time integration schemes have been used extensively in finite difference computer codes for a number of years. However, explicit integration schemes have been used only recently with the finite element method. In 1974, Key [47] utilized an explicit time integration scheme in conjunction with a finite element, spatial discretization of the Eulerian statement of the rate of virtual work (Eq. (5.21)). Although the Eulerian or current configuration statement of the rate of virtual work is used by Key, the overall procedure relies on an updating of the geometry at the end of each time step. Integration of the stress tensor was based on the rigid-convected (Jaumann) stress rate.

In 1975, Belytschko [48] considered several techniques for removing the spurious oscillations inherent to explicit time integration schemes, and compared the computing times with an implicit algorithm. The explicit procedure utilized by Belytschko was essentially the same as that employed by Key.

In 1979, Bathe [49] presented results from calculations performed using an explicit time integration scheme in conjunction with the Lagrangian statement of the rate of virtual work (Eq. (5.24)). For an updated Lagrangian procedure, there is little difference between Bathe's and Key's respective formulations.

In this investigation, the Lagrangian statement of the rate of virtual work was employed in conjunction with an explicit central difference time integration scheme. The Lagrangian statement was chosen since it provided the most flexibility. Specifically, it was possible to employ much of the same software in both explicit and implicit time integration schemes, since the implicit scheme (to be presented later) also utilizes the Lagrangian statement of the rate of virtual work.

Consistent with standard finite element techniques, the displacements and geometry of an element may be expressed in terms of its node point values. Therefore, the particle accelerations within an element may be written as

$$\ddot{x}^i = N^i{}_j \, \bar{\ddot{x}}^j \, , \tag{5.25}$$

where $N^i{}_j$ are a set of interpolation[1] or shape functions which relate the internal element parameters to the j node point values. Throughout the remainder of this study, barred (—) quantities will refer to node point values.

Substituting Eq. (5.25) into (5.24) and rearranging the terms yields

$$\int_{{}^tB_o} \rho_o \, N^\alpha{}_\beta \, \delta v_\alpha \, d\,{}^tB_o \, \bar{\ddot{x}}^\beta$$

$$= \int_{\partial {}^tB_o} t^\alpha_o \, \delta v_\alpha \, d(\partial\,{}^tB_o) + \int_{{}^tB_o} f^\alpha_o \, \delta v_\alpha \, d\,{}^tB_o$$

$$- \int_{{}^tB_o} \tilde{T}^{\alpha\beta} \, \delta\,{}^t\dot{E}_{\alpha\beta} \, d\,{}^tB_o \, . \tag{5.26}$$

[1]The interpolation functions are not tensor quantities; however, it is convenient to retain the inner product subscript convention.

In Eq. (5.26), the left superscripted "t" signifies that the parameters are evaluated at time t (i.e., ${}^{t}B_{o}$ denotes the reference volume at time t).

The virtual velocity expressed in terms of the interpolation functions may be written as

$$\delta v_{\alpha} = N_{\alpha}{}^{\phi}\ \delta \overline{v}_{\phi}\ . \tag{5.27}$$

Combining Eq. (5.26) and Eq. (5.27) yields

$$\int_{{}^{t}B_{o}}^{t} \rho_{o}\ N^{\alpha}{}_{\beta}\ N_{\alpha}{}^{\phi}\ d\,{}^{t}B_{o}\ \ddot{\overline{x}}^{\beta}\ \delta \overline{v}_{\phi}$$

$$= \left[\int_{\partial {}^{t}B_{o}}^{t} t_{o}^{\alpha}\ N_{\alpha}{}^{\phi}\ d(\,{}^{t}B_{o}) + \int_{{}^{t}B_{o}}^{t} f_{o}^{\alpha}\ N_{\alpha}{}^{\phi}\ d\,{}^{t}B_{o} \right] \delta \overline{v}_{\phi}$$

$$- \int_{{}^{t}B_{o}}^{t} \tilde{T}^{\alpha\beta}\ \delta \dot{E}_{\alpha\beta}\ d\,{}^{t}B_{o}\ . \tag{5.28}$$

The virtual rate of Green's strain may be written as

$$\delta \dot{E}_{\alpha\beta} = L_{\alpha\beta}^{\phi}\ \delta \overline{v}_{\phi}\ , \tag{5.29}$$

where $L_{\alpha\beta}^{\phi}$ is discussed in Section 6.8. Combining Eqs. (5.28) and (5.29) yields, since the $\delta \overline{v}_{\phi}$ are arbitrary,

$$\int_{{}^tB_o}^{t} \rho_o \, N^{\alpha}{}_{\beta} \, N_{\alpha}{}^{\phi} \, d\,{}^tB_o \, \ddot{x}^{\beta} = \int_{\partial {}^tB_o}^{t} t_o^{\alpha} \, N_{\alpha}{}^{\phi} \, d(\partial {}^tB_o)$$

$$+ \int_{{}^tB_o}^{t} f_o^{\alpha} \, N_{\alpha}{}^{\phi} \, d\,{}^tB_o - \int_{{}^tB_o}^{t} \tilde{T}^{\alpha\beta} \, L^{\phi}{}_{\alpha\beta} \, d\,{}^tB_o \; . \tag{5.30}$$

In matrix notation, Eq. (5.30) may be written as

$$[M]\{\ddot{\bar{x}}\} = \{E\} - \{I\} \; , \tag{5.31}$$

where

$$[M] = \int_{{}^tB_o}^{t} \rho_o \, N^{\alpha}{}_{\beta} \, N_{\alpha}{}^{\phi} \, d\,{}^tB_o \; , \tag{5.32a}$$

$$\{E\} = \int_{\partial {}^tB_o}^{t} t_o^{\alpha} \, N_{\alpha}{}^{\phi} \, d(\partial {}^tB_o) + \int_{{}^tB_o}^{t} f_o^{\alpha} \, N_{\alpha}{}^{\phi} \, d\,{}^tB_o \; , \tag{5.32b}$$

$$\{I\} = \int_{{}^tB_o}^{t} \tilde{T}^{\alpha\beta} \, L^{\phi}{}_{\alpha\beta} \, d\,{}^tB_o \; . \tag{5.32c}$$

The node point accelerations may be obtained from Eq. (5.31) as

$$\{\ddot{\bar{x}}\} = [M]^{-1}(\{E\} - \{I\}) \; . \tag{5.33}$$

The well-known central difference time integration equations are

$$^{t}\ddot{\bar{x}}^{\beta} = \frac{^{t+\Delta t}\bar{x}^{\beta} - 2\ ^{t}\bar{x}^{\beta} + {}^{t-\Delta t}\bar{x}^{\beta}}{\Delta t^{2}} \quad . \tag{5.34}$$

Solving Eq. (5.33) and Eq. (5.34) for the node point coordinates at time $t+\Delta t$ yields

$$^{t+\Delta t}\{\bar{x}^{\beta}\} = \Delta t^{2}[M]^{-1}({}^{t}\{E\}-{}^{t}\{I\})+2\,{}^{t}\{\bar{x}^{\beta}\}-{}^{t-\Delta t}\{\bar{x}^{\beta}\} \quad . \tag{5.35}$$

Equation (5.35) may be used to advance the solution in time based on the information available from the previous two time steps. Since constraints on the solution at time $t+\Delta t$ are not used to advance the solution, the recursive relationship of Eq. (5.35) is an explicit expression.

To evaluate the integral in Eq. (5.32c), the components of the second Piola stress tensor at time t are required. The stress components are obtained by integrating rate constitutive equations through time. In general,

$$^{t}\tilde{T}^{\alpha\beta} = {}^{t-\Delta t}\tilde{T}^{\alpha\beta} + \Delta t\ {}^{t}\dot{\tilde{T}}^{\alpha\beta} \quad . \tag{5.36}$$

If the reference configuration is updated, the second Piola stress tensor must be referenced to the new configuration using the inverse of Eq. (3.39),

$$\sigma^{ij} = \tilde{T}^{ij} = \frac{\rho}{\rho_{0}}\,\tilde{T}^{\alpha\beta}\,x^{i}{}_{,\alpha}\,x^{j}{}_{,\beta} \quad . \tag{5.37}$$

The stability of the central difference time integration scheme described by Eq. (5.34) has been studied by many authors. For linear problems the time step must be kept below the critical time step,

$$\Delta t_{cr} = \frac{\pi}{\lambda_{max}} , \tag{5.38}$$

where λ_{max} is the maximum eigenvalue of the computational mesh. This may be estimated as the time required for a uniaxial wave to travel across the minimum length, δ_{min}, associated with a particular element. Therefore, Eq. (5.38) may alternatively be written as

$$\Delta t_{cr} = \frac{\delta_{min}}{c} , \tag{5.39}$$

where c is the bar wave speed for the material.

For nonlinear problems in which the material properties change and/or the mesh changes, it is necessary to use a variable time step. It is easily shown that for a variable time, Eq. (5.35) can be written as

$$\begin{aligned} {}^{t+\Delta t_2}\{\bar{x}^{\beta}\} &= {}^{t}\{\bar{x}^{\beta}\} + \frac{\Delta t_2}{\Delta t_1}\left[{}^{t}\{\bar{x}^{\beta}\} - {}^{t-\Delta t_1}\{\bar{x}^{\beta}\}\right] \\ &\quad + \frac{1}{2}(\Delta t_2 + \Delta t_1)\Delta t_2 [M]^{-1}({}^{t}\{E\} - {}^{t}\{I\}) \ . \end{aligned} \tag{5.40}$$

A characteristic of high amplitude wave propagation in solids is the presence of shock waves. Shock waves may arise from the initial boundary conditions or from nonlinear materials. In addition, numerical shocks may develop due to changing mesh size. One approach to handling both physical and numerical shock waves is to model them as mathematical discontinuities located along element boundaries. Since the waves propagate through the body, it would be extremely difficult to program a floating boundary which depends on the solution. To handle physical and numerical shock waves and to smooth the solution obtained for hyperbolic problems, it is customary to introduce an artificial viscosity into the solution. The form of the artificial viscosity used in this investigation is taken from Bertholf and Benzley [50]. The technique is based on the work of Richtmeyer and Morton [51], and has been used successfully by Key [47]. The artificial viscosity is used to generate a viscous pressure given by

$$\begin{aligned} P &= \rho\sqrt{A}\left(\frac{1}{\rho}\frac{\partial\rho}{\partial t}\right)\left[(B_1)^2\sqrt{A}\left|\frac{1}{\rho}\frac{\partial\rho}{\partial t}\right| + B_2 c\right] && \text{for } \frac{1}{\rho}\frac{\partial\rho}{\partial t} > 0 \\ &= 0 && \text{for } \frac{1}{\rho}\frac{\partial\rho}{\partial t} \le 0 \, , \end{aligned} \tag{5.41}$$

where c is the bar wave speed; A is the area of the element; and B_1 and B_2 are nondimensional constants designed to spread the shock over a fixed number of elements. The viscous pressure is added directly to the total stresses at the particular instance in time under consideration.

To account for artificial viscosity in the computation of the critical time step, Bertholf and Benzley suggest the following equation:

$$\Delta t_{crit} = \frac{\delta}{B_2 c + (B_1)^2 \delta \left|\frac{1}{\rho}\frac{\partial \rho}{\partial t}\right| + \sqrt{\left[B_2 c + (B_1)^2 \delta \left|\frac{1}{\rho}\frac{\partial \rho}{\partial t}\right|\right]^2 + c^2}} \ . \tag{5.42}$$

Figure 5.2 shows the effects of artificial viscosity on the numerical solution for a long rod impacting a rigid barrier. As seen in this figure, the artificial viscosity tends to smooth the solution in the areas where steep gradients exist. For more detailed treatments on artificial viscosity, the reader is referred to Zukas [52] and Wilkins [53].

Due to the small time step requirements displayed by the central difference scheme, it is most commonly used only for wave propagation problems. For dynamic problems where the structure or shape of the stress waves are not important, implicit time integration schemes are normally used.

5.4. Implicit Integration of the Rate of Virtual Work

To understand the basic concepts associated with implicit methods used to obtain solutions to the Lagrangian statement of rate of virtual work, it is instructive to

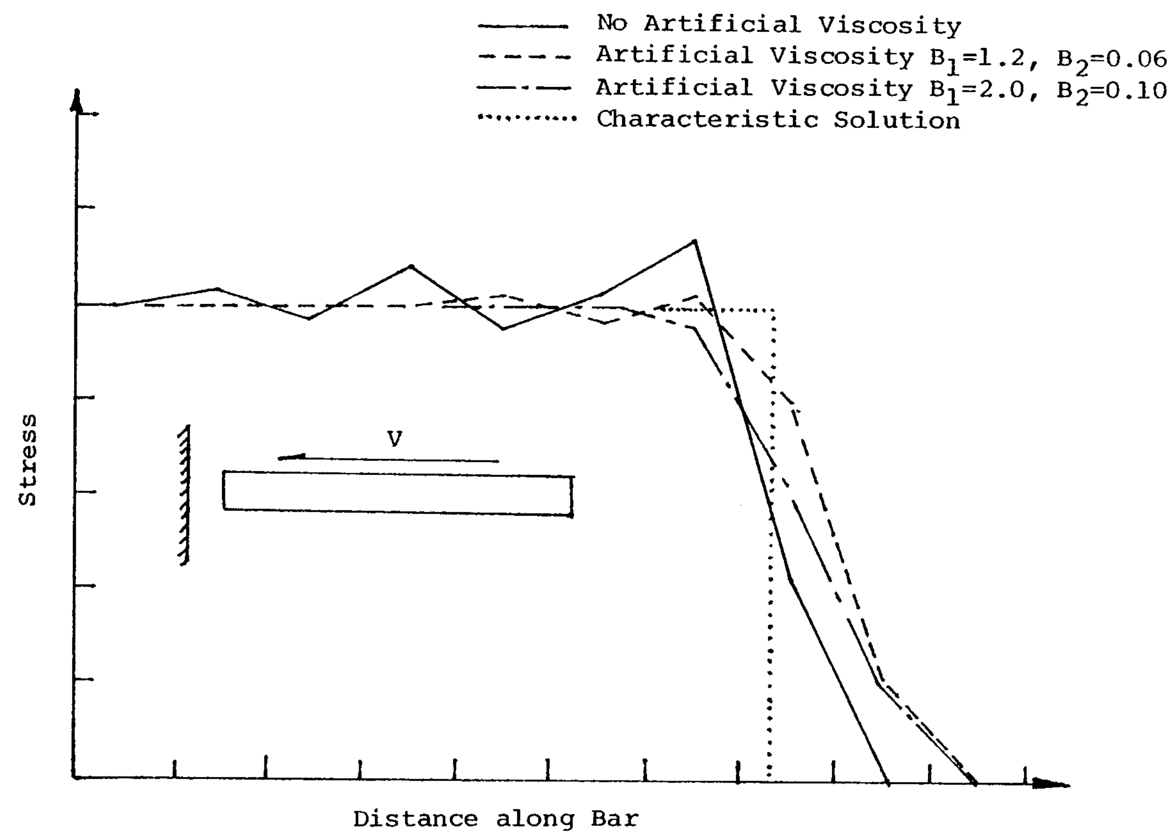

Figure 5.2. Effects of Artificial Viscosity on the Solution for Rod Impact.

consider Eq. (5.24) without the inertia terms:

$$\int_{B_o} \tilde{T}^{\alpha\beta} \, \delta\dot{E}_{\alpha\beta} \, dB_o = \int_{\partial B_o} t_o^{\alpha} \, \delta v_{\alpha} \, d(\partial B_o) + \int_{B_o} f_o^{\alpha} \, \delta v_{\alpha} \, dB_o . \quad (5.43)$$

To develop an implicit strategy for the solution of Eq. (5.43), a constitutive equation relating the components of the second Piola stress tensor to an appropriate kinematic variable must be known. If the material can be classified as a linear hyperelastic material, then

$$T^{\alpha\beta} = B^{\alpha\beta\Gamma\phi} \, E_{\Gamma\phi} \, , \quad (5.44)$$

and Eq. (5.43) becomes

$$\int_{B_o} B^{\alpha\beta\Gamma\phi} \, E_{\Gamma\phi} \, \delta\dot{E}_{\alpha\beta} \, dB_o = \int_{\partial B_o} t_o^{\alpha} \, \delta v_{\alpha} \, d(\partial B_o) + \int_{B_o} f_o^{\alpha} \, \delta v_{\alpha} \, dB_o \, . \quad (5.45)$$

It can be shown that the solution of Eq. (5.45) using a finite element spatial discretization yields a system of nonlinear equations in which the node point displacements are the unknowns.

For elastic-viscoplastic or elastic-plastic materials, the constitutive equations are expressed in rate form. Since the material response is history-dependent, the constitutive variables are not analytic and a potential function relating the stress and deformation variables does not exist. The history dependence of the material suggests that a solution strategy which allows the loads to be applied in small increments while following the solution path is required.

Equation (5.43) states that the rate of virtual work performed by the internal stresses must equal the rate of virtual work performed by the externally applied loads. Symbolically,

$$\delta \dot{W}_I = \delta \dot{W}_E \ , \tag{5.46a}$$

or alternatively,

$$\delta \dot{W}_I - \delta \dot{W}_E = 0 \ . \tag{5.46b}$$

As mentioned previously, Eq. (5.46b) represents an integral statement of equilibrium. If equilibrium between the surface tractions and internal stresses is not satisfied, then Eq. (5.46b) is not equal to zero. Consider a Taylor's series of expansion of Eq. (5.46b) about a state which is not in equilibrium, then

$$\begin{aligned} {}^2(\delta \dot{W}_I - \delta \dot{W}_E) &= {}^1(\delta \dot{W}_I - \delta \dot{W}_E) \\ &+ \frac{\partial}{\partial \underset{\sim}{u}} \, {}^1(\delta \dot{W}_I - \delta \dot{W}_E) d\underset{\sim}{u} + 0(d\underset{\sim}{u})^2 \ , \end{aligned} \tag{5.47}$$

where the left superscripted number 1 or 2 denotes the configuration (note that configuration 1 is considered not to be in equilibrium). If configuration 2 in Eq. (5.47) is chosen to be a configuration which is in equilibrium, then

$$^{2}(\delta\dot{W}_I - \delta\dot{W}_E) = 0 \ , \tag{5.48}$$

and Eq. (5.48) becomes

$$\frac{\partial}{\partial u} \, ^{1}(\delta\dot{W}_I - \delta\dot{W}_E)du = {}^{1}(\delta\dot{W}_E - \delta\dot{W}_I) \ . \tag{5.49}$$

The right side of Eq. (5.49) represents the amount by which configuration 1 is out of equilibrium, and can be considered an unbalanced force. As will be shown later, the left-hand side of Eq. (5.49) represents a system of equations with unknown displacement increments $d\underset{\sim}{u}$. The displacement increments $d\underset{\sim}{u}$ are the displacements required to bring the unbalanced forces into equilibrium. The expression $\partial/\partial u \ ^{1}(\delta\dot{W}_I - \delta\dot{W}_E)$ will be used in Section 5.5 to obtain the coefficient matrix for a set of linear incremental equations. The coefficient matrix is commonly referred to as the tangent stiffness matrix, and is denoted by $K_T(^{1}\underset{\sim}{\tilde{T}} \ , \ ^{1}\underset{\sim}{u})$. Note that the tangent stiffness matrix is a function of the stresses and displacements in configuration 1.

In 1960, Turner et al. [54] used an equation similar to Eq. (5.49) to investigate geometrically nonlinear structural problems. Turner's equations may be written symbolically as

$$K_T({}^1\underset{\sim}{\tilde{T}} \; , \; {}^1\underset{\sim}{u})\Delta\underset{\sim}{u} = \Delta\underset{\sim}{F} \; , \tag{5.50}$$

where $\Delta\underset{\sim}{F}$ represents an increment in the applied loads, and can be considered as the unbalanced load of Eq. (5.49). The displacements in configuration 2 are obtained as

$${}^2\underset{\sim}{u} = {}^1\underset{\sim}{u} + \Delta\underset{\sim}{u} \; . \tag{5.51}$$

Since Eq. (5.49) and equivalently, Eq. (5.50), were obtained from a truncated Taylor's series expansion, the displacement increments obtained by Eq. (5.50) are not exactly those required to bring configuration 1 into equilibrium. In general, the displacement solution will tend to drift away from the true solution, as shown in Figure 5.3.

In 1970, Haisler [55] and Hofmeister, Greenbaum, and Evenson [56] recognized the significance of the unbalanced force term of Eq. (5.49). If the unbalanced force term of Eq. (5.49) is taken to be

$$\delta({}^2\dot{W}_E - {}^1\dot{W}_I) \; , \tag{5.52}$$

then the incremental solution scheme tends to be self-correcting. Theoretically, Eq. (5.52) will tend to correct the drift encountered with Eq. (5.50). This is shown graphically in Figure 5.4.

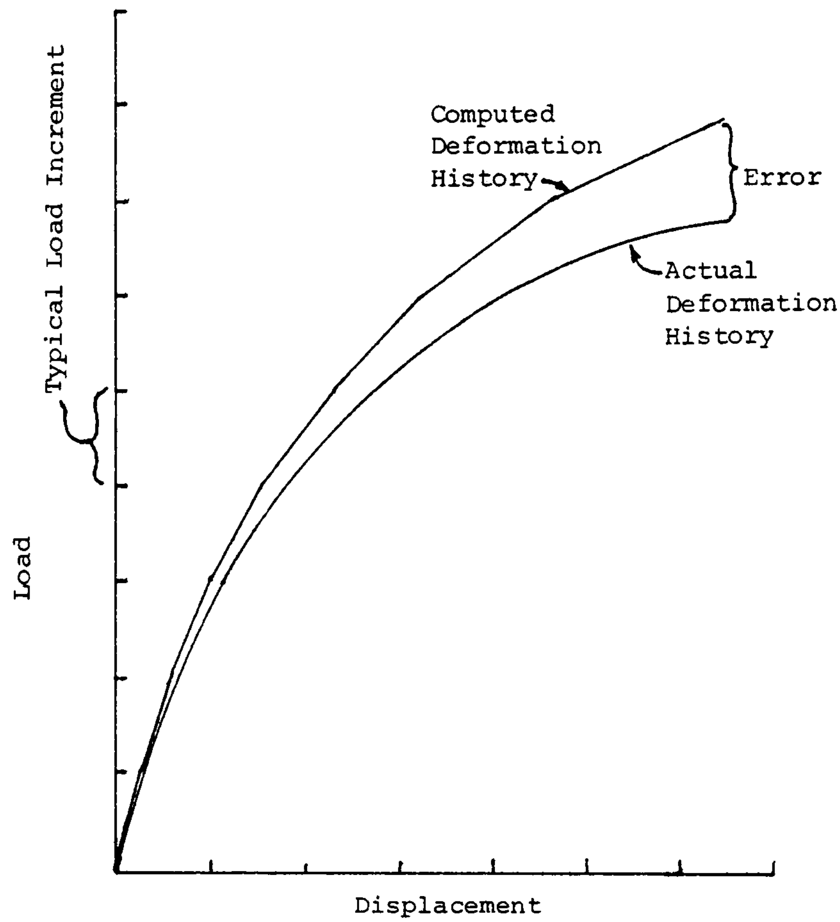

Figure 5.3. Drift Associated with Incremental Solution Strategy.

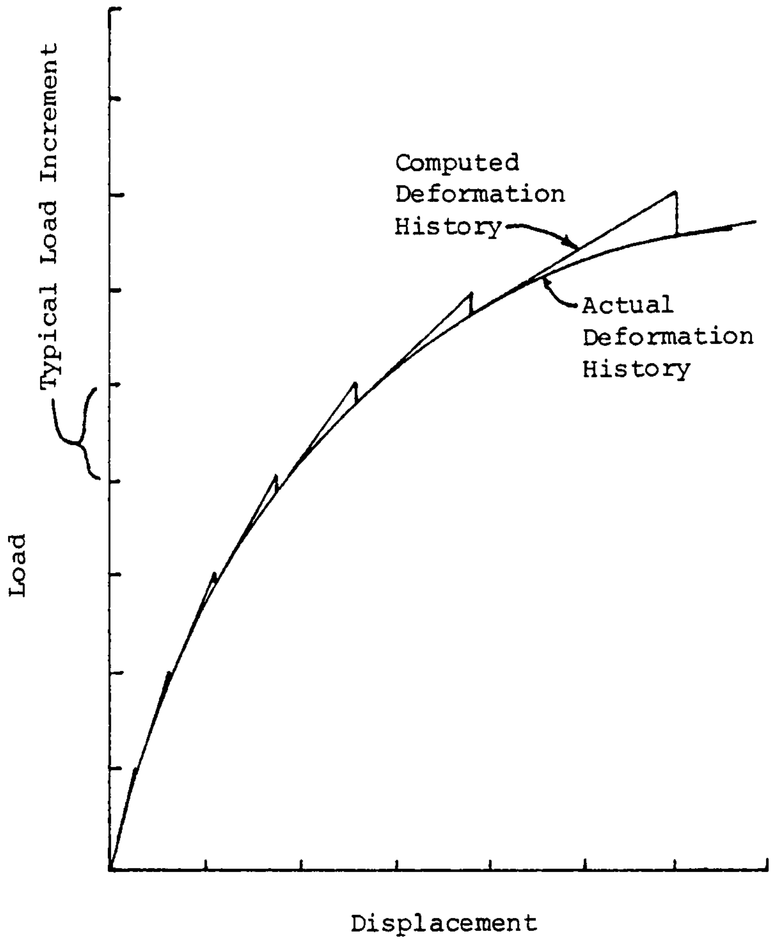

Figure 5.4. Correction of Solution Drift Resulting from Unbalanced Load Vector.

It is now recognized that Eq. (5.49) can be generalized to yield a general Newton-Raphson-type solution scheme in which iterations are performed to ensure equilibrium;

$$\frac{\partial}{\partial \underset{\sim}{u}} \, {}^{j}(\delta \dot{W}_I - \delta \dot{W}_E)^{i}(d\underset{\sim}{u}) = \delta({}^{2}\dot{W}_E - {}^{i}\dot{W}_I) \ , \qquad (5.53)$$

where the superscript j denotes the configuration used to evaluate the tangent stiffness matrix. The superscript i denotes the number of the equilibrium iteration. The improved displacement after i equilibrium iterations is obtained as

$${}^{i+1}\underset{\sim}{u} = {}^{i}\underset{\sim}{u} + {}^{i}d\underset{\sim}{u} \ . \qquad (5.54)$$

The incremental solution scheme with equilibrium iteration is shown graphically in Figure 5.5. By selecting different configurations for the superscript j in Eq. (5.53), a variety of solution strategies may be obtained. Figure 5.6 shows three of the more common approaches; these are: (1) constant tangent with iteration, (2) modified Newton-Raphson with iteration, and (3) full Newton-Raphson with iteration. In the constant tangent technique, the load is applied in multiple increments, but the tangent stiffness matrix is assembled only once. Convergence is achieved at the expense of a large number of equilibrium

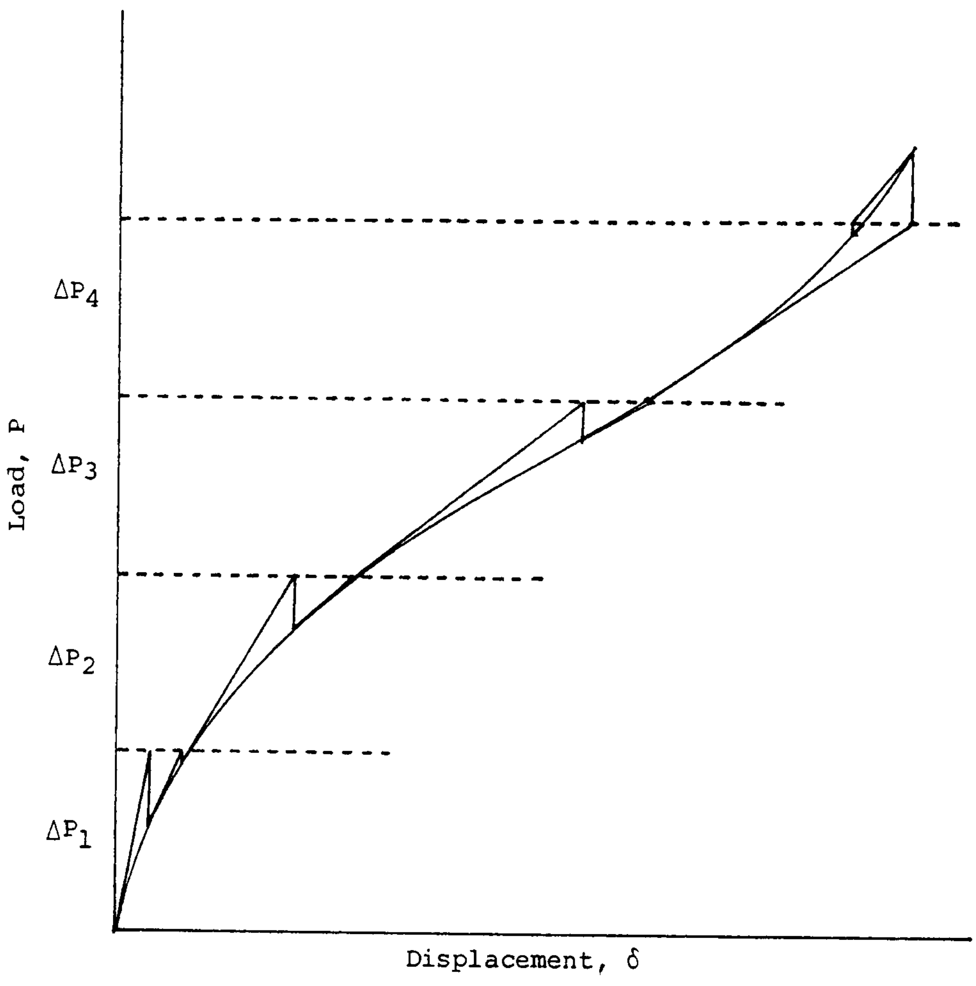

Figure 5.5. Incremental Solution Scheme with Equilibrium Iterations.

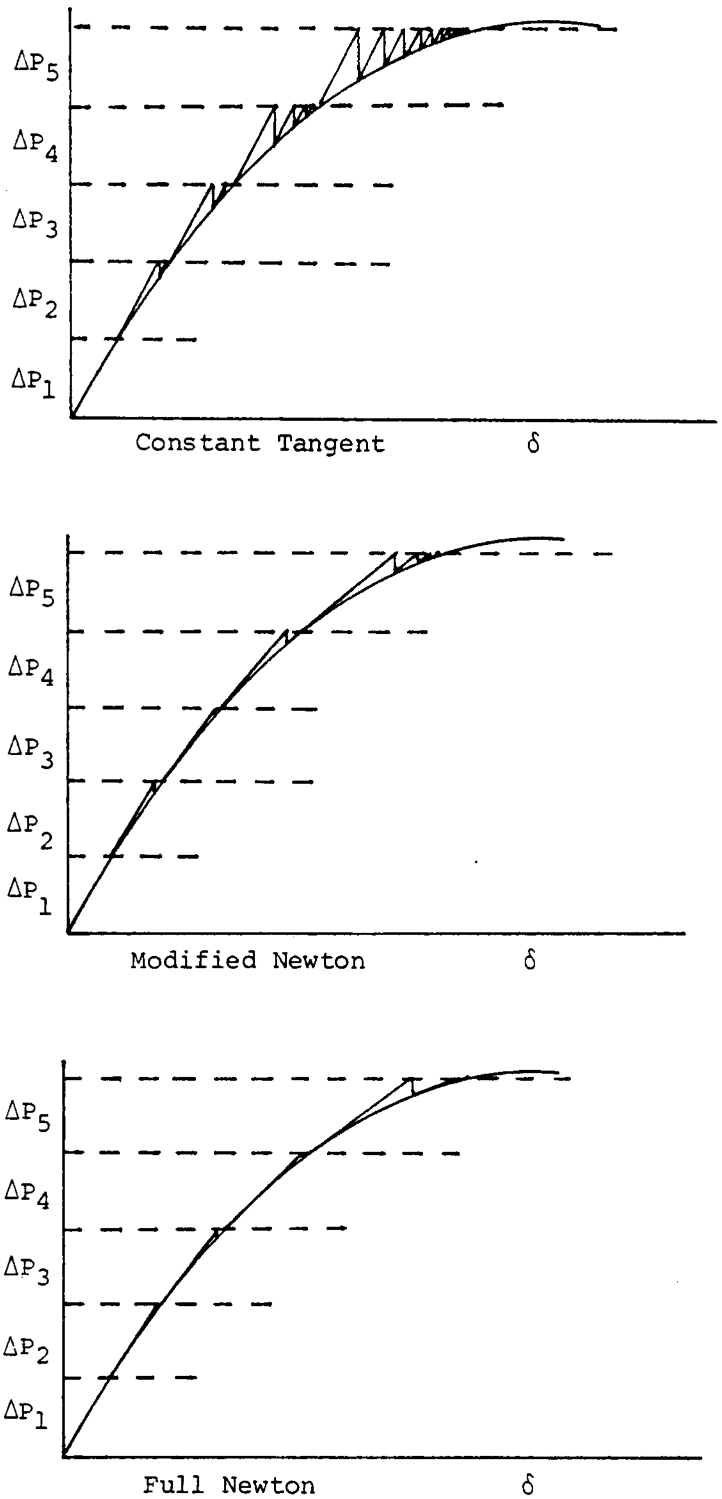

Figure 5.6. Solution Strategies Available Using Load Incrementation with Equilibrium Iteration.

iterations. This approach will not always converge, and should be used with care.

The modified Newton-Raphson method also applies the load in several increments. At the beginning of each increment, the new tangent stiffness matrix is found. Therefore, the computed solution is tangent to the actual response curve at the beginning of each new load increment. Convergence is achieved through the application of equilibrium iterations which use the same tangent stiffness matrix obtained at the beginning of the load step.

In the full Newton-Raphson method, a new tangent stiffness matrix is found at the beginning of each equilibrium iteration. The full Newton-Raphson method should require fewer equilibrium iterations than the modified Newton-Raphson method. However, the smaller number of iterations are obtained at the expense of having to recompute and factor a new tangent stiffness matrix. The most efficient solution strategy is usually problem-dependent; for highly nonlinear problems a combination of methods may be required.

In 1974, Bathe et al. [30] generalized Eq. (5.53) to include inertial and viscous damping terms. It can be shown that the incremental equations of motion may be written in matrix form as

$$[K_T]\{\Delta u\} = {}^{t+\Delta t}\{R\} - {}^{t}\{F\} - [M]\,{}^{t+\Delta t}\{\ddot{u}\} - [C]\,{}^{t+\Delta t}\{\dot{u}\}\,, \quad (5.55)$$

where ${}^{t+\Delta t}\{R\}$ is the applied load vector at time $t+\Delta t$, $\{\ddot{u}\}$ and $\{\dot{u}\}$ are the acceleration and velocity vectors, $[M]$ and $[C]$ are the mass and damping matrices, respectively. Equation (5.55) may be written in the alternative form,

$$[M]\ {}^{t+\Delta t}\{\ddot{u}\} + [C]\ {}^{t+\Delta t}\{\dot{u}\} + [K_T]\{\Delta u\}$$

$$= {}^{t+\Delta t}\{R\} - {}^{t}\{F\}\ . \qquad (5.56)$$

A variety of numerical time integration schemes could be used to solve Eq. (5.56). In this investigation, the Newmark-β method [57] is used. Newmark's equations may be written as

$${}^{t+\Delta t}\underset{\sim}{\dot{u}} = {}^{t}\underset{\sim}{\dot{u}} + \left[(1-\delta)\,{}^{t}\underset{\sim}{\ddot{u}} + \delta\ {}^{t+\Delta t}\underset{\sim}{\ddot{u}}\right]\Delta t \qquad (5.57)$$

and

$${}^{t+\Delta t}\underset{\sim}{u} = {}^{t}\underset{\sim}{u} + {}^{t}\underset{\sim}{\dot{u}}\ \Delta t + \left[\left(\frac{1}{2} - \alpha\right){}^{t}\underset{\sim}{\ddot{u}} + \alpha\ {}^{t+\Delta t}\underset{\sim}{\ddot{u}}\right]\Delta t^2\ . \qquad (5.58)$$

Equation (5.58) may be rearranged to yield

$${}^{t+\Delta t}\underset{\sim}{\ddot{u}} = \frac{\Delta\underset{\sim}{u} - {}^{t}\underset{\sim}{\dot{u}}\ \Delta t}{\alpha\Delta t^2} - \frac{\left(\frac{1}{2} - \alpha\right)}{\alpha}\ {}^{t}\underset{\sim}{\ddot{u}}\ . \qquad (5.59)$$

Substituting Eq. (5.59) into Eq. (5.57) yields

$${}^{t+\Delta t}\underset{\sim}{\dot{u}} = 1 - \frac{\delta}{\alpha}\ {}^{t}\underset{\sim}{\dot{u}} + \left(1 - \frac{\delta}{2\alpha}\right){}^{t}\underset{\sim}{\ddot{u}}\ \Delta t + \frac{\delta}{\alpha\Delta t}\ \Delta\underset{\sim}{u}\ . \qquad (5.60)$$

Combining Eqs. (5.55), (5.59), and (5.60), and rearranging terms yields

$$[K_{eff}]\{\Delta u\} = {}^{t+\Delta t}\{R_{eff}\} , \qquad (5.61a)$$

where

$$[K_{eff}] = \frac{1}{\alpha\Delta t^2} [M] + \frac{\delta}{\alpha\Delta t} [C] + [K_T] , \qquad (5.61b)$$

$$\begin{aligned} {}^{t+\Delta t}\{R_{eff}\} = {}& {}^{t+\Delta t}\{R\} + [M] \left\{ \frac{1}{\alpha\Delta t}\ {}^{t}\dot{\underset{\sim}{u}} + \left(\frac{1}{2\alpha} -1 \right) {}^{t}\ddot{\underset{\sim}{u}} \right\} \\ & + [C] \left\{ \left(\frac{\delta}{\alpha} -1 \right) {}^{t}\dot{\underset{\sim}{u}} + \left(\frac{\delta}{2\alpha} -1 \right) {}^{t}\ddot{\underset{\sim}{u}}\ \Delta t \right\} \\ & - {}^{t}\{F\} . \end{aligned} \qquad (5.61c)$$

For linear problems, it can be shown that the Newmark-β method is stable provided the parameters δ and α are chosen to satisfy

$$\delta \geq \frac{1}{2} , \qquad (5.62a)$$

$$\alpha \geq \frac{1}{4}(\delta + \frac{1}{2})^2 . \qquad (5.62b)$$

For nonlinear problems, it is, in general, not possible to establish the global stability of the Newmark-β method. Local stability can be established by using values for α and β which satisfy Eqs. (5.62a and b).

Bathe [58] indicates that global stability may be maintained by performing equilibrium iterations. For dynamic problems, the accelerations, velocities, and internal state variables must satisfy

$$^{t+\Delta t}\{R\} - [M]\,^{t+\Delta t}\{\ddot{u}\} - [C]\,^{t+\Delta t}\{\dot{u}\} - \,^{t+\Delta t}F = 0\ . \quad (5.63)$$

If Eq. (5.63) is not satisfied, equilibrium does not exist, and the error in Eq. (5.63) represents the unbalanced load required to bring the solution into equilibrium;

$$^{t+\Delta t}\{R\} - [M]\,^{i}\{\ddot{u}\} - [C]\,^{i}\{\dot{u}\} - \,^{i}\{F\} = \,^{i}\{R_{unb}\}\ . \quad (5.64)$$

For each iteration after the first, it is necessary to evaluate the unbalanced load from Eq. (5.64). The displacement increment required to correct the unbalance is obtained from

$$^{i}[K_{eff}]\,^{i}\{\Delta u\} = \,^{i}\{R_{unb}\}. \quad (5.65)$$

The corrected displacement increment for the current load increment is given by

$$\Delta \underset{\sim}{u} = \,^{i-1}\Delta \underset{\sim}{u} + \,^{i}\Delta \underset{\sim}{u}\ . \quad (5.66)$$

The velocities and accelerations for the i^{th} iteration are given by Eqs. (5.59) and (5.60). In general, equilibrium iterations are performed until the Euclidean norm of the unbalanced load vector is reduced to within a specified tolerance.

5.5. Components of the Tangential Stiffness Matrix

In the preceding section, the equations necessary for the numerical solution of the implicit incremental equations of motion were presented. to utilize the implicit technique, it is necessary to evaluate the tangential stiffness matrix defined in Eq. (5.49) by

$$\frac{\partial}{\partial \underset{\sim}{u}}\ {}^{1}(\delta \dot{W}_I - \delta \dot{W}_E) d\underset{\sim}{u} = d^{1}(\delta \dot{W}_E - \delta \dot{W}_I) \ , \tag{5.67a}$$

or

$$\int_{{}^{1}B_o} d\tilde{T}^{\alpha\beta}\ \delta\dot{E}_{\alpha\beta}\ d^{1}B_o + \int_{{}^{1}B_o} \tilde{T}^{\alpha\beta}\ d(\delta\dot{E}_{\alpha\beta}) d^{1}B_o$$

$$- \int_{{}^{1}B_o} d^{1}f^{\alpha}\ \delta v_{\alpha}\ d^{1}B_o - \int_{\partial^{1}B_o} d^{1}t^{\alpha}\ \delta v_{\alpha}\ d(\partial^{1}B_o) \ . \tag{5.67b}$$

To evaluate Eq. (5.67b) it is necessary to have a constitutive equation relating the increment of the second Piola stress tensor and the increment in Green's strain; symbolically,

$$d\tilde{T}^{\alpha\beta} = C^{\alpha\beta\Gamma\phi}\ dE_{\Gamma\phi} \ . \tag{5.68}$$

Combining Eqs. (5.67b) and (5.68) yields the expression

$$\int_{{}^1B_o} C^{\alpha\beta\Gamma\phi}\, dE_{\Gamma\phi}\, \delta\dot{E}_{\alpha\beta}\, d^1B_o + \int_{{}^1B_o} \tilde{T}^{\alpha\beta}\, d(\delta\dot{E}_{\alpha\beta})\, d^1B_o$$

$$- \int_{{}^1B_o} d^1f^{\alpha}\, \delta V_{\alpha}\, d^1B_o - \int_{\partial^1B_o} d^1t^{\alpha}\, \delta V_{\alpha}\, d(\partial^1B_o) \ . \tag{5.69}$$

Green's strain tensor may be written as

$$E_{\alpha\beta} = \frac{1}{2}\left\{g_{ij}\, x^i{}_{,\alpha}\, x^j{}_{,\beta} - G_{\alpha\beta}\right\} , \tag{5.70}$$

where the current and reference configurations are described with respect to a common frame of reference. The rate of Green's strain may be written as

$$\dot{E}_{\alpha\beta} = \frac{1}{2}\left\{g_{ij}\, v^i|_{\alpha}\, x^j{}_{,\beta} + g_{ij}\, x^i{}_{,\alpha}\, v^j|_{\beta}\right\} \tag{5.71a}$$

$$= \frac{1}{2}\left\{v_i|_{\alpha}\, x^j{}_{,\beta} + v_i|_{\beta}\, x^i{}_{,\alpha}\right\} . \tag{5.71b}$$

The rate of Green's strain resulting from a virtual velocity, $\delta\underset{\sim}{v}$, can therefore be written as

$$\delta\dot{E}_{\alpha\beta} = \frac{1}{2}\left\{\delta v_j|_{\alpha}\, x^j{}_{,\beta} + \delta v_j|_{\beta}\, x^j{}_{,\alpha}\right\} . \tag{5.72}$$

Similarly, the increment in Green's strain is given by

$$dE_{\Gamma\phi} = \frac{1}{2}\left\{dx_m|_{\Gamma}\, x^m{}_{,\phi} + dx_n|_{\phi}\, x^n{}_{,\Gamma}\right\} . \tag{5.73}$$

In evaluating the second term in Eq. (5.69), the increment in the virtual rate of Green's strain is required and is given by

$$d(\delta\dot{E}_{\alpha\beta}) = \frac{1}{2}\left\{ \delta v_n|_{\alpha}\, dx^n{}_{,\beta} + \delta v_m|_{\beta}\, dx^m{}_{,\alpha} \right\} . \tag{5.74}$$

Note that the virtual velocity, δv, was chosen to have no temporal or quasi-static variation (i.e., $d(\delta v) = 0$).

The components of the deformation gradient may be related to the components of the displacement vector $\underset{\sim}{u}$ by the expression (see Section 6.7)

$$x^i{}_{,\beta} = \delta^i{}_{\beta} + u^i|_{\beta} . \tag{5.75}$$

Equation (5.75) is applicable to problems where the reference and spatial configurations are Cartesian; it is also applicable to problems where the reference and spatial configurations are cylindrical; however, for the cylindrical case the problem must also be axisymmetric. Substituting Eq. (5.75) into Eqs. (5.72), (5.73), and (5.74) yields

$$\delta\dot{E}_{\alpha\beta} = \frac{1}{2}\left\{\delta v_n|_{\alpha}(\delta^n{}_{\beta}+u^n|_{\beta})+\delta v_m|_{\beta}(\delta^m{}_{\alpha}+u^m|_{\alpha})\right\} , \tag{5.76}$$

$$dE_{\Gamma\phi} = \frac{1}{2}\left\{du_m|_{\Gamma}(\delta^m{}_{\phi}+u^m|_{\phi})+du_n|_{\phi}(\delta^n{}_{\Gamma}+u^n|_{\Gamma})\right\} , \tag{5.77}$$

$$d(\delta\dot{E}_{\alpha\beta}) = \frac{1}{2}\left\{v_n|_{\alpha}\, du^n|_{\beta}+\delta v_m|_{\beta}\, du^m|_{\alpha}\right\} . \tag{5.78}$$

The derivatives encountered in Eqs. (5.76), (5.77), and (5.78) may be evaluated using the following general relations:

$$v^i|_\alpha = v^i{}_{,\alpha} + v^k \, \Gamma^i_{\alpha k} \tag{5.79a}$$

and

$$v_i|_\alpha = v_{i,\alpha} - v_k \, \Gamma^k_{i\alpha} \; , \tag{5.79b}$$

where $\Gamma^i_{\alpha k}$ and $\Gamma^k_{i\alpha}$ are the appropriate Christoffel symbols. For Cartesian coordinates, $\Gamma^i_{\alpha k} = \Gamma^k_{i\alpha} = 0$. For cylindrical coordinates, the only nonzero Christoffel symbols are

$$\Gamma^2_{33} = -(x^2) \; , \; \Gamma^3_{23} = \Gamma^3_{32} = (\frac{1}{x^2}) \; , \tag{5.80}$$

where $x^1 = z$, $x^2 = r$, and $x^3 = \theta$ are the components associated with the cylindrical system.

Using the physical components of the virtual and differential strain rates, and carrying out the differentiation, one obtains for axisymmetric cylindrical coordinates

$$\delta\dot{E}_{11} = \delta v_{1,1} + \delta v_{n,1} \, u^n{}_{,1} \; , \tag{5.81a}$$

$$\delta\dot{E}_{22} = \delta v_{2,2} + \delta v_{n,2} \, u^n{}_{,2} \; , \tag{5.81b}$$

$$2(\delta\dot{E}_{12}) = \delta v_{2,1} + \delta v_{1,2} + \delta v_{n,1} \, u^n{}_{,2} + \delta v_{m,2} \, u^m{}_{,1} \; , \tag{5.81c}$$

$$\delta\dot{E}_{33} = \delta v_2/x^2 + \delta v_2\ u^2/(x^2)^2 \ , \tag{5.81d}$$

$$d(\delta\dot{E}_{11}) = \delta v_{m,1}\ du^m{}_{,1} \ , \tag{5.81e}$$

$$d(\delta\dot{E}_{22}) = \delta v_{m,2}\ du^m{}_{,2} \ , \tag{5.81f}$$

$$2d(\delta\dot{E}_{12}) = \delta v_{n,1}\ du^n{}_{,2} + \delta v_{m,2}\ du^m{}_{,1} \ , \tag{5.81g}$$

$$d(\delta\dot{E}_{33}) = \delta v_2\ du^2/(x^2)^2 \ , \tag{5.81h}$$

$$dE_{11} = du_{1,1} + du_{n,1}\ u^n{}_{,1} \ , \tag{5.81i}$$

$$dE_{22} = du_{2,2} + du_{n,2}\ u^n{}_{,2} \ , \tag{5.81j}$$

$$2dE_{12} = du_{2,1} + du_{1,2} + du_{n,1}\ u^n{}_{,2} + du_{m,2}\ u^m{}_{,1} \ , \tag{5.81k}$$

$$dE_{33} = du_2/x^2 + du_2\ u^2/(x^2)^2 \ . \tag{5.81ℓ}$$

Equations (5.81a) through (5.81ℓ) are sufficient to permit the evaluation of the first two terms of the tangential stiffness matrix. It can be verified that the first two terms of Eq. (5.69) can be written as

$$\left[[K_1] + [K_2({}^1\underset{\sim}{u})] + [K_3(\underset{\sim}{\tilde{T}})]\right]\{du\} \ , \tag{5.82}$$

where $[K_1]$ represents the standard finite element stiffness matrix; $[K_2({}^1u)]$ represents the modification to $[K_1]$ to account for the prior deformation; $[K_2({}^1\underset{\sim}{u})]$ is a function of the displacements at the beginning of the time increment. If an updated Lagrangian formulation is employed, the initial displacement matrix $[K_2(^1\underset{\sim}{u})]$ will be zero; $[K_3(\underset{\sim}{\tilde{T}})]$ represents the modification to $[K_1]$ associated with doing work on a stressed body; $[K_3(\underset{\sim}{\tilde{T}})]$ depends explicitly on the current stresses, and is referred to as the initial stress or geometric stiffness matrix; $[K_3(\underset{\sim}{\tilde{T}})]$ is routinely used to determine the "buckling" loads associated with a structure.

The remaining two terms in Eq. (5.69) represent corrections to the stiffness matrix to account for changes in the distributed body and surface loads resulting from the deformation. These terms can be used to represent non-conservative loads due to pressure, etc. These latter two terms are not significant to the current investigation, and the interested reader is referred to Hibbitt, Marcal, and Rice [27] for a more detailed treatment.

CHAPTER VI

FINITE ELEMENT AND GRAPHICS COMPUTER PROGRAMS

In the preceding chapters and sections, a theoretical framework necessary to solve problems in solid mechanics involving time-dependent plasticity has been presented. Detailed discussions were given concerning possible finite strain elastic-viscoplastic constitutive models, and methods for integrating both the equations of motion and the constitutive equations. The notation employed is compact and it may be difficult at times to discern how to get from the mathematics to a working computer program which solves the governing equations. The purpose of this chapter is to "fill in" some of the information necessary to implement the equations previously presented, and to describe the computer programs developed during the course of this investigation.

6.1. Computer Programs FINITE and GRAFIX

A new nonlinear static and dynamic finite element program called FINITE and associated interactive pre- and post-processing computer program, GRAFIX, were developed during this investigation. Both computer programs were developed from scratch, and involve approximately 10,000 lines of code. The programs are written in FORTRAN, and are currently operating on a VAX 11/780 computer. FINITE presently has two-dimensional and axisymmetric isoparametric continuum elements, and geometrically nonlinear truss, cable, and beam elements. The truss, cable, and beam elements were implemented at the author's employer's request so that FINITE could be used to solve problems encountered in the design of micro-wave antenna and transmission line towers. The two- dimensional elements can handle problems involving hyperelastic, hypoelastic, hyperelastic-viscoplastic, hypoelastic-viscoplastic, and updated hyperelastic-viscoplastic materials. The explicit integration portion of the program also has a combined hardening elastic-plastic material capability.

The program is written in such a manner that additional elements can be added simply by attaching additional element subroutines to the program. For example, three-dimensional continuum and plate/shell elements can be added with very little modification to the existing code. Similarly, different material constitutive models can be added with little modification to the existing code.

FINITE was designed to solve nonlinear problems, but will default to the simpler linear problem. Depending on the class of problem under consideration, either an updated Lagrangian or total Lagrangian formulation may be employed. During the course of the investigation, several problems not involving elastic-viscoplastic materials were solved and compared to published results to ascertain the correctness of the program. These problems involved such phenomena as the linear elastic buckling of beams, arches, and axisymmetric shells. An inherent feature of the finite element method is its ability to be implemented in a very general manner, enabling the same program to be used for many different geometries and materials simply by changing the input data.

FINITE was written to be used primarily as a research program, but great care was taken to make it as user friendly and as easy to use as possible. As a result, the program has many features which enable it to be used in a production mode. The most notable of these features is a comprehensive pre- and post-processing program called GRAFIX, which is directly compatible with FINITE. GRAFIX can be used to interactively generate and display the finite element model geometry. Portions or all of the model may be viewed graphically from any vantage point. The model may be modified or generated in more than one modeling session simply by saving the model previously generated. Files containing the node and element data for the model are compatible with FINITE. During execution of a problem, FINITE reads input data from files created by GRAFIX, and creates post-processing files containing node point displacements, and element Gauss point stresses. The post-processing files can then be read by GRAFIX and displayed in a variety of forms (i.e., displacement versus time, contour plots, distorted geometry plots, etc.). This is a very powerful capability, and eliminates almost all paper printout requirements. The contour plots contained in the Appendix were created using GRAFIX.

6.2. Command Interpreter

FINITE contains a front-end program which is used to input and generate geometry and material property data required by implicit and explicit time integration modules, as shown in Figure 6.1. Data necessary for the execution of FINITE is divided into DATA SETS. The DATA SETS read by the different portions of FINITE are contained within the blocks shown in Figure 6.1.

In general, the only interaction a user will have with FINITE is through the generation and input of the data necessary for the solution of a particular problem. In many cases, the volume of data will be quite substantial, thereby requiring an efficient mechanism for transmitting or communicating the data to the program. To minimize the effort required to define the data, FINITE employs a command interpreter. The command interpreter allows the use of alphabetic words or abbreviations to assist in the data input. The following items describe the essential features of the command interpreter:

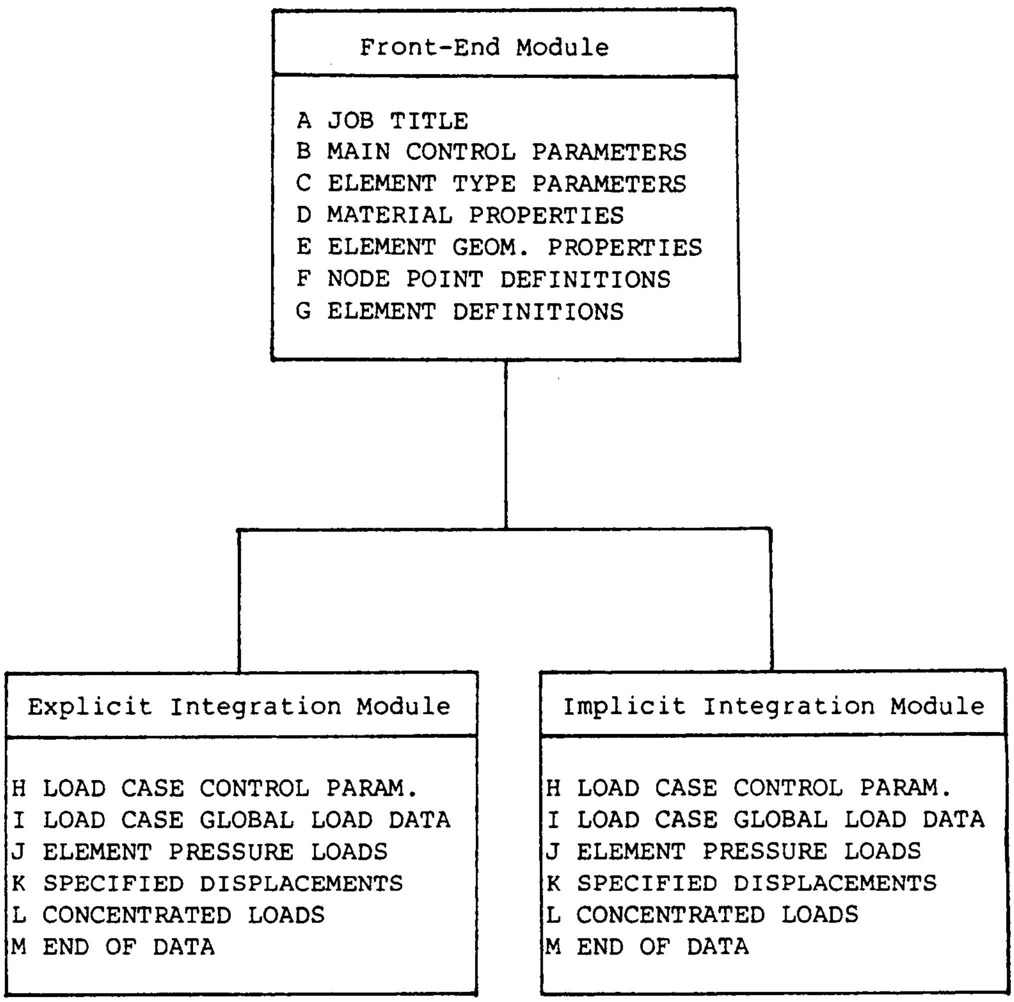

Figure 6.1. Modular Construction of Program FINITE.

1. Each line of input consists of a variable number of positional parameters (i.e., items which must be input sequentially). Parameters may be alphabetic words or numbers.
2. Each parameter on a line of input must be separated by either a comma or a blank space.
3. Many parameters have values to which they will default if no input is supplied. If no data are needed beyond a specific parameter, the data line may be terminated.
4. Parameters input in the form of alphabetic words or abbreviations may contain more than one character. For alphabetic words containing more than four characters, only the first four must be supplied.

Figure 6.2 shows the parameters input on FINITE's main control "card." To illustrate the versatility of the command interpreter, consider the following examples. Assume that a dynamic analysis of a linear elastic structure is to be performed, using a lumped mass matrix, no linear constraint equations are employed, and the implicit time integration module is to be used. The following are different ways of providing the same information:

1. DYNAMIC,NO,NO,NO,YES,LINEAR,IMPLICIT.
2. D,,,,YES,.
3. DYN,NO,,NO,YES,LINE,IMP.

IANAL, IMAT, ICONST, IGEOM, LMASS, ICLASS, INTYP

Parameter	Description	Acceptable Input	Default
IANAL	Type of Analysis	D, DYN, DYNAMIC, S, STAT, STATIC, blank	STATIC
IMAT	Nonlinear Material	YES, Y, NO, N, blank	NO
ICONST	Linear Constraint Equations	YES, Y, NO, N, blank	NO
IGEOM	Geometric Nonlinearities	YES, Y, NO, N, blank	NO
LMASS	Lumped Mass Matrix	YES, Y, NO, N, blank	NO
ICLASS	Analysis Procedure	LINE, LINEAR, U, UP, UPDA, UPDATED, T, TOT, TOTAL, blank	LINEAR
INTYP	Integration Procedure	I, IMPL, IMPLICIT E, EXPL, EXPLICIT	IMPLICIT

Figure 6.2. Main Control Card Parameters.

4. DYN NO NO NO YES LINEAR IMP.

5. D N N N Y L I.

Note that in Items 4 and 5, it was necessary to input an acceptable input for each parameter separated by a blank. Multiple blanks are interpreted as a single delimeter until the next alphanumeric character is encountered.

As a second example, assume that a static analysis with no nonlinearities or constraint equations is to be performed. The following are different ways of providing this information:

1. STATIC,NO,NO,NO,NO,LINEAR.

2. S.

3. "A COMPLETELY BLANK LINE OF INPUT."

4. STAT NO NO,NO YES.

5. STATIC NO NO NO.

6. S,,,,,LINEAR.

7. STAT,,,,,,, THIS IS AN EXAMPLE.

Note that in Item 4 both a comma and blank were used as a delimeter in the same line of input. Also, Item 7 has a comment positioned at the end of the line after all parameters have been accounted for by the use of sequential delimeters.

6.3. Load Case Control

The implcit time integration module of FINITE controls the problem execution during static, quasi-static and dynamic problems in which the tangent stiffness matrix is used. In the implicit time integration module, FINITE provides two options for the input of load and boundary condition information to the structure. In general, two basic types of loads and boundary conditions may be encountered:

1. Multiple loading conditions for a linear structure.
2. A single set of loads which must be applied sequentially.

Figure 6.3 shows the "Load Case Control Parameters" required as input by the implicit time integration module in FINITE. The KFORM parameter in Field One (Figure 6.3) controls the type of load case under consideration. Acceptable inputs for the KFORM parameter are:

1. NEW.
2. REFORM.
3. CONTINUE or CONT.
4. LOAD

A parameter input of NEW indicates that the loads and boundary conditions contained in this load case are not a continuation of the loads and boundary conditions from

KFORM, NINC, KFORMF, NITER, ITYP, IPRT, TIME, CONTL

Parameter	Description	Acceptable Input	Default
KFORM	Matrix Formation Control	NEW, REFORM, CONT, CONTINUE, LOAD	CONTINUE
NINC	Number of Load Increments	positive integer, blank	1
KFORMF	Matrix Formation Frequency	positive integer, blank	0
NITER	Number of Equilibrium Iterations	positive integer, blank	1
ITYP	Equilibrium Iteration Type	NEWT, NEWTON, MODI, MODIFIED, blank	MODIFIED
IPRT	Printout Frequency for Load Increments	positive integer, blank	0
TIME	Time at End of Load Case	positive real number, blank	0.0
CONTL	Iteration Convergence Tolerance	positive real number, blank	0.01

Figure 6.3. Load Case Control Parameters.

the previous load case. A parameter value of NEW is usually input for the first load case in a problem.

A parameter input of REFORM indicates that the system matrix should be reformed at the beginning of this load case. In addition, the loads and boundary conditions are a continuation of those from the previous load case.

A parameter input of CONTINUE or CONT indicates that the system matrix should not be reformed at the beginning of this load step. However, the loads and boundary conditions are a continuation of those from the previous load step. A parameter input of CONTINUE is normally used during a "constant tangent matrix" solution sequence (Section 5.4).

A parameter input of LOAD indicates that a new set of loads is being supplied, and that the previous system matrix is to be used. A parameter value of LOAD is usually used with linear problems having multiple loading conditions.

Within each load case, the loads may be applied in several increments. The number of increments per load case is controlled by the NINC parameter in Field Two (Figure 6.3). Due to cost, accuracy, or other constraints, it may not be desirable to reform the system matrices at the beginning of each load increment. Therefore, the KFORMF parameter in Field Three (Figure 6.3) allows a matrix reform frequency to be specified. The value of the KFORMF parameter indicates how often the matrices are to be reformed and factored. For example, if KFORMF equals 2, the system matrices will be reformed and factored every other load increment during the current load case.

The maximum number of iterations to be performed at the end of each load increment during the current load case is controlled by the NITER parameter. If the solution has not converged after NITER iterations, the program execution will continue to the next load increment using the information available from the last equilibrium iteration. The proper selection of the number of equilibrium iterations to be performed is usually based on experience gained from solving a particular class of problems.

The parameter ITYP controls the type of equilibrium iteraton to be performed at the end of each load increment. Two options are available:

1. Full Newton iterations.
2. Modified Newton iterations.

A full Newton iteration involves reforming the system equations at the beginning of each equilibrium iteration, and is obtained by an input of NEWTON or NEWT for parameter ITYP. A modified Newton iteration is obtained by specifying MODI or MODIFIED for parameter ITYP. If a divergent solution is encountered during a solution using modified Newton iterations, the program will automatically switch to a full Newton iteration. If a divergent solution is encountered after NITER iterations, the problem is terminated.

Figure 6.4 shows a basic flow chart for the implicit time integration module in FINITE. The explicit time integration module does not use the parameters discussed above since a tangent matrix is not used. The only parameters in Figure 6.3 which are used by the explicit time integration module are IPRT (printout frequency for load increments) and TIME (time at end of load case); all remaining parameters are ignored. To switch from one integration module to the other, only the INTYP parameter (Figure 6.2, page 127) on the main control card must be changed. A basic flow chart of the explicit time integration module is shown in Figure 6.5.

6.4. Two-Dimensional Element Geometry and Interpolation Functions

A typical two-dimensional or axisymmetric element is shown in Figure 6.6. The element is defined by eight points called nodes whose coordinates completely define the boundary of the element. The node point coordinates are defined with respect to a reference Cartesian or cylindrical coordinate system; this element is called a physical element. Also shown in Figure 6.6 is a square element defined by eight node points defined with respect to a ξ,η-coordinate system; this element is called a parametric element. To

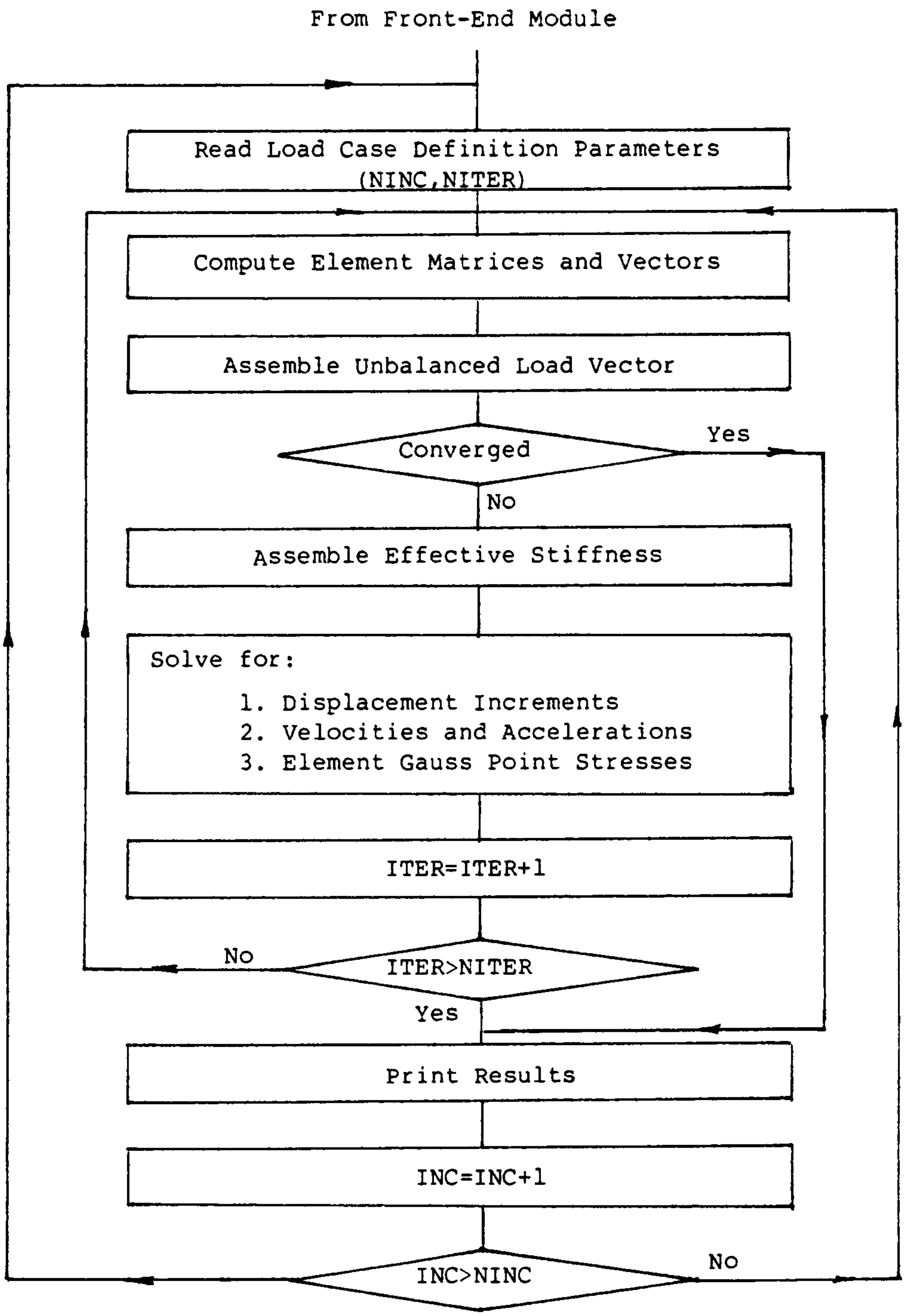

Figure 6.4. Flow Chart for Implicit Integration Module.

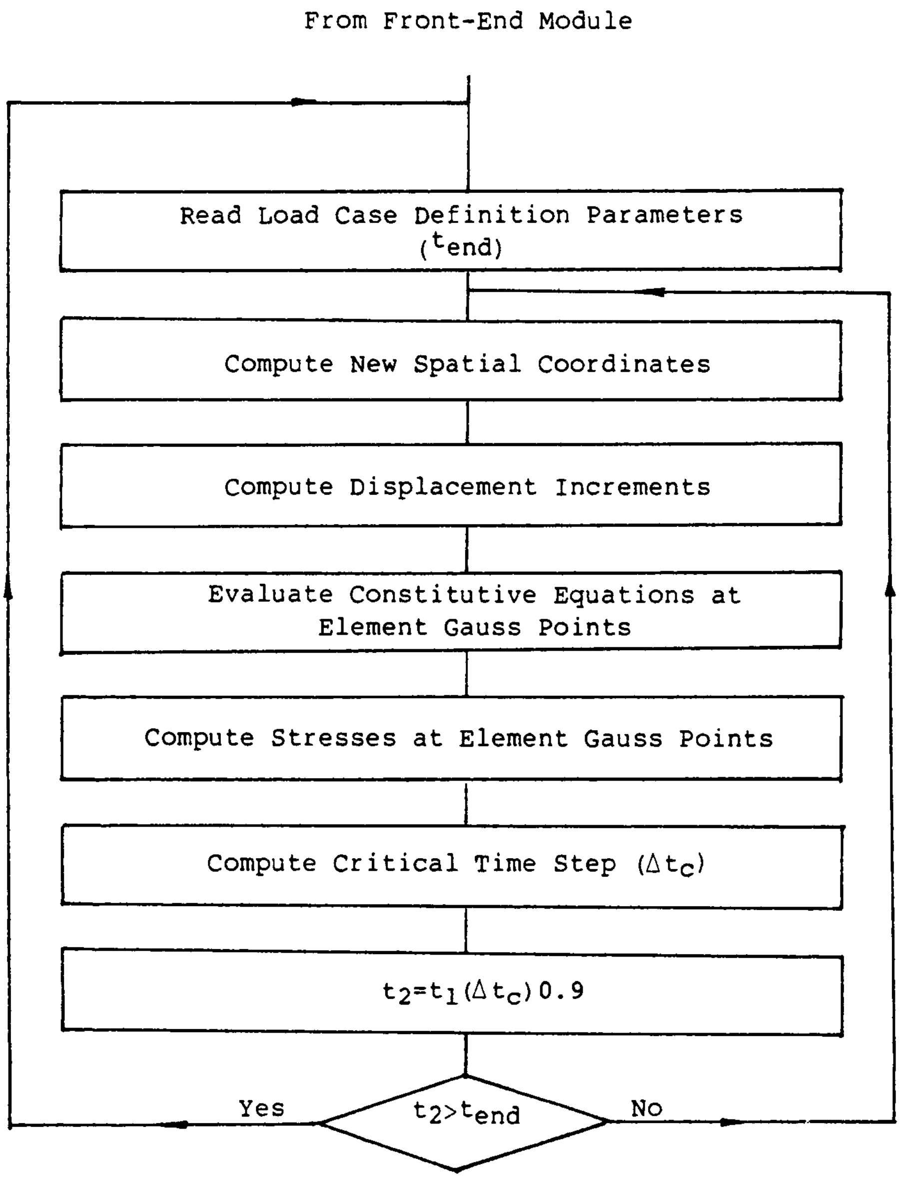

Figure 6.5. Flow Chart for Explicit Integration Module.

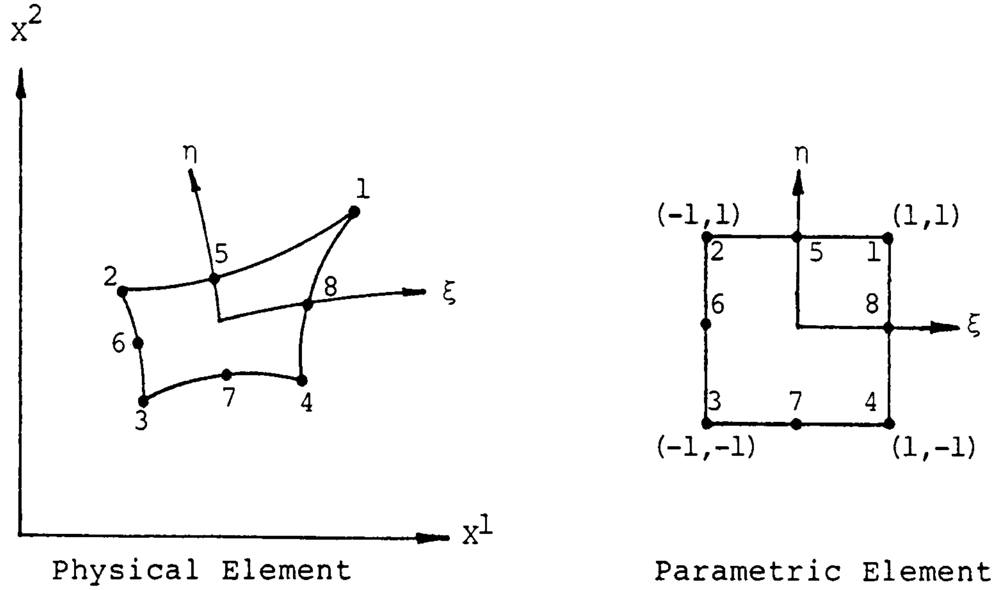

Figure 6.6. Two-Dimensional Iso-parametric Finite Element Geometry and Node Identification Numbers.

numerically integrate the governing integral equations presented in Chapter V, it is desirable to transform or map the geometry and equations for the physical element into the parametric element. This is accomplished by the use of interpolating polynomials or functions.

The serendipity interpolation functions (Bathe [39], page 200) for the parametric element are given by,

$$\begin{aligned}
h_5 &= \frac{1}{2}(1-\xi^2)(1+\eta) \\
h_6 &= \frac{1}{2}(1-\eta^2)(1-\xi) \\
h_7 &= \frac{1}{2}(1-\xi^2)(1-\eta) \\
h_8 &= \frac{1}{2}(1-\eta^2)(1+\xi) \\
h_1 &= \frac{1}{4}(1+\xi)(1+\eta) - \frac{1}{2}h_5 - \frac{1}{2}h_8 \\
h_2 &= \frac{1}{4}(1-\xi)(1+\eta) - \frac{1}{2}h_5 - \frac{1}{2}h_6 \\
h_3 &= \frac{1}{4}(1-\xi)(1-\eta) - \frac{1}{2}h_6 - \frac{1}{2}h_7 \\
h_4 &= \frac{1}{4}(1+\xi)(1-\eta) - \frac{1}{2}h_7 - \frac{1}{2}h_8 \ .
\end{aligned} \tag{6.1}$$

Equations (6.1) can be used to relate points in the parametric element to the corresponding point in the physical element through the equations,

$$X^1 = h_i \overline{X}_i^1$$
$$X^2 = h_i \overline{X}_i^2 \ , \qquad (6.2)$$

where the bar indicates that the quantity belongs to a node point, and the subscript i identifies the node point. The same interpolation functions can be used to describe the variation of any other variable within the physical element if the node point values of the variable are known. For example, if the node point temperatures are known, the temperature at any other point can be estimated from

$$T = h_i \overline{T}_i \ , \qquad (6.3)$$

where T is temperature in the physical element corresponding to the parametric point ξ,η at which the interpolation functions are evaluated.

The interpolation functions described by Eqs. (6.1) allow a quadratic variation for the dependent variable along the element boundary. A variety of different elements can be obtained by leaving out particular nodes in the element description. Figure 6.7 shows several possible "degenerate" elements which can be obtained. Note that if the mid-side nodes are not specified, a linear quadrilateral element is obtained.

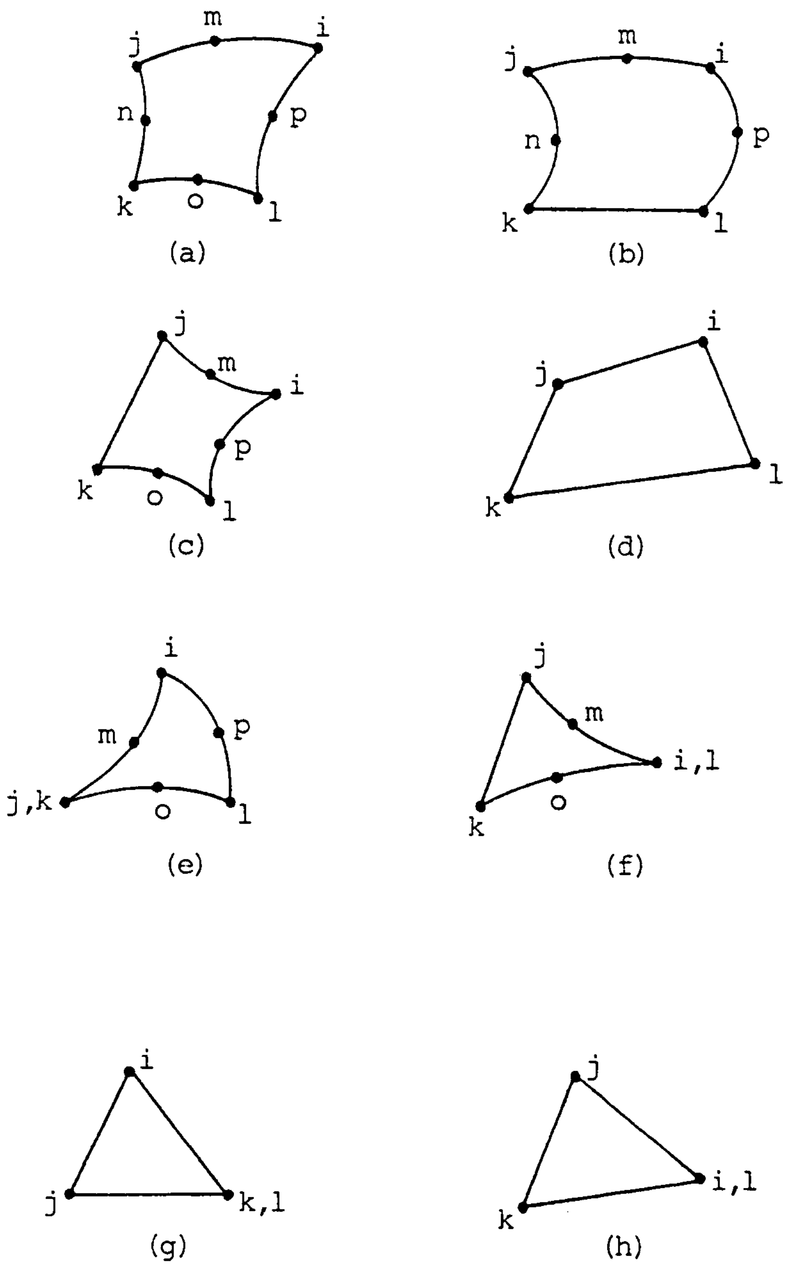

Figure 6.7. Degenerate Two-Dimensional Iso-parametric Element Geometries.

The displacement field in the physical element can be described in matrix form as

$$\begin{Bmatrix} u^1 \\ u^2 \end{Bmatrix} = \begin{bmatrix} h_1 & 0 & h_2 & 0 & h_3 & 0 & h_4 & 0 & h_5 & 0 & h_6 & 0 & h_7 & 0 & h_8 & 0 \\ 0 & h_1 & 0 & h_2 & 0 & h_3 & 0 & h_4 & 0 & h_5 & 0 & h_6 & 0 & h_7 & 0 & h_8 \end{bmatrix} \begin{Bmatrix} \bar{u}_1^1 \\ \bar{u}_1^2 \\ \bar{u}_2^1 \\ \bar{u}_2^2 \\ \bar{u}_3^1 \\ \bar{u}_3^2 \\ \bar{u}_4^1 \\ \bar{u}_4^2 \\ \vdots \\ \bar{u}_8^1 \\ \bar{u}_8^2 \end{Bmatrix}, \quad (6.4)$$

where the variables in the column vector on the right-hand side of the equation have the following superscript and subscript convention. The superscript identifies the displacement component, and the subscript defines the element node number where the displacement occurs. A much more compact way of writing Eq. (6.4) is

$$u^i = N^i_{\beta}\, \bar{u}^{\beta} \dagger \qquad i = 1,2$$
$$\beta = 1,16 \, . \qquad (6.5)$$

Since the same interpolation functions are used to describe both the geometry of the physical element (Eq. (6.2)) and the variation of the dependent variables within the physical element (Eqs. (6.3) and (6.4)), this element is called an iso-parametric element. It is possible to use different combinations of interpolation functions to obtain sub-parametric and super-parametric element descriptions; however, the iso-parametric formulation was used exclusively during this investigation.

6.5. Derivatives of the Interpolation Functions with Respect to the Parametric Coordinates

Throughout the iso-parametric element formulation it is necessary to compute the derivaties of the interpolation functions with respect to the parametric coordinates. In FINITE, the values of these derivatives are computed at Gauss Quadrature points and stored in a 2x8 matrix, P. The first row of the matrix contains the values of the derivatives of the eight interpolation functions with respect to the ξ-coordinate, the second row contains the values of the

---

†The interpolation functions are not tensor quantities; however, it is convenient to retain the inner product subscript convention.

derivatives of the eight interpolation functions with respect to η. Each column corresponds to a particular interpolation function. Since these derivatives are used in subsequent sections, they will be presented now.

$$
\begin{aligned}
P(1,5) &= \frac{\partial h_5}{\partial \xi} = -\ \xi(1+\eta) \\
P(1,6) &= \frac{\partial h_6}{\partial \xi} = -\ \tfrac{1}{2}(1-\eta^2) \\
P(1,7) &= \frac{\partial h_7}{\partial \xi} = -\ \xi(1-\eta) \\
P(1,8) &= \frac{\partial h_8}{\partial \xi} = \ \ \tfrac{1}{2}(1-\eta^2) \\
P(1,1) &= \frac{\partial h_1}{\partial \xi} = \ \ \tfrac{1}{4}(1-\eta) - \tfrac{1}{2}P(1,5) - \tfrac{1}{2}P(1,8) \\
P(1,2) &= \frac{\partial h_2}{\partial \xi} = -\ \tfrac{1}{4}(1+\eta) - \tfrac{1}{2}P(1,5) - \tfrac{1}{2}P(1,6) \\
P(1,3) &= \frac{\partial h_3}{\partial \xi} = -\ \tfrac{1}{4}(1-\eta) - \tfrac{1}{2}P(1,6) - \tfrac{1}{2}P(1,7) \\
P(1,4) &= \frac{\partial h_4}{\partial \xi} = \ \ \tfrac{1}{4}(1-\eta) - \tfrac{1}{2}P(1,7) - \tfrac{1}{2}P(1,8) \\
P(2,5) &= \frac{\partial h_5}{\partial \eta} = \ \ \tfrac{1}{2}(1-\xi^2) \\
P(2,6) &= \frac{\partial h_6}{\partial \eta} = -\ \eta(1-\xi) \\
P(2,7) &= \frac{\partial h_7}{\partial \eta} = -\ \tfrac{1}{2}(1-\xi^2) \\
P(2,8) &= \frac{\partial h_8}{\partial \eta} = -\ \eta(1+\xi)
\end{aligned}
\tag{6.6}
$$

$$P(2,1) = \frac{\partial h_1}{\partial \eta} = \frac{1}{4}(1+\xi) - \frac{1}{2}P(2,5) - \frac{1}{2}P(2,8)$$

$$P(2,2) = \frac{\partial h_2}{\partial \eta} = \frac{1}{4}(1-\xi) - \frac{1}{2}P(2,5) - \frac{1}{2}P(2,6)$$

$$P(2,3) = \frac{\partial h_3}{\partial \eta} = -\frac{1}{4}(1-\xi) - \frac{1}{2}P(2,6) - \frac{1}{2}P(2,7)$$

$$P(2,4) = \frac{\partial h_4}{\partial \eta} = -\frac{1}{4}(1+\xi) - \frac{1}{2}P(2,7) - \frac{1}{2}P(2,8) \; .$$

6.6. Derivatives with Respect to the Reference Configuration

Derivatives with respect to the reference configuration will be used in subsequent sections, and are given here for completeness. Through application of the chain rule for partial derivatives, the derivative of a variable with respect to the parametric coordinates may be written as

$$\frac{\partial}{\partial \xi} = \frac{\partial}{\partial X^1}\frac{\partial X^1}{\partial \xi} + \frac{\partial}{\partial X^2}\frac{\partial X^2}{\partial \xi} \tag{6.7}$$

and

$$\frac{\partial}{\partial \eta} = \frac{\partial}{\partial X^1}\frac{\partial X^1}{\partial \eta} + \frac{\partial}{\partial X^2}\frac{\partial X^2}{\partial \eta} \; . \tag{6.8}$$

Writing Eqs. (6.7) and (6.8) in matrix notation yields

$$\begin{Bmatrix} \dfrac{\partial}{\partial\xi} \\ \\ \dfrac{\partial}{\partial\eta} \end{Bmatrix} = \begin{bmatrix} \dfrac{\partial x^1}{\partial\xi} & \dfrac{\partial x^2}{\partial\xi} \\ \\ \dfrac{\partial x^1}{\partial\eta} & \dfrac{\partial x^2}{\partial\eta} \end{bmatrix} \begin{Bmatrix} \dfrac{\partial}{\partial x^1} \\ \\ \dfrac{\partial}{\partial x^2} \end{Bmatrix} . \tag{6.9}$$

The matrix of derivatives in Eq. (6.9) can be computed using Eqs. (6.2) and (6.6); that is,

$$\frac{\partial x^1}{\partial\xi} = \frac{\partial h_i}{\partial\xi}\,\bar{x}_i^1 , \tag{6.10}$$

$$\frac{\partial x^2}{\partial\xi} = \frac{\partial h_i}{\partial\xi}\,\bar{x}_i^2 , \tag{6.11}$$

$$\frac{\partial x^1}{\partial\eta} = \frac{\partial h_i}{\partial\eta}\,\bar{x}_i^1 , \tag{6.12}$$

$$\frac{\partial x^2}{\partial\eta} = \frac{\partial h_i}{\partial\eta}\,\bar{x}_i^2 . \tag{6.13}$$

For a single valued transformation, the matrix of derivatives will possess an inverse, and Eq. (6.9) can alternatively be written as

$$\begin{Bmatrix} \dfrac{\partial}{\partial x^1} \\ \\ \dfrac{\partial}{\partial x^2} \end{Bmatrix} = \begin{bmatrix} \dfrac{\partial\xi}{\partial x^1} & \dfrac{\partial\eta}{\partial x^1} \\ \\ \dfrac{\partial\xi}{\partial x^2} & \dfrac{\partial\eta}{\partial x^2} \end{bmatrix} \begin{Bmatrix} \dfrac{\partial}{\partial\xi} \\ \\ \dfrac{\partial}{\partial\eta} \end{Bmatrix} . \tag{6.14}$$

6.7. Deformation Gradient

The deformation gradient previously defined in Eq. (3.9) as

$$F^i_{\ \alpha} = x^i_{\ ,\alpha} \tag{6.15}$$

is used in FINITE to compute the components of the Cauchy stress tensor when the second Piola stress tensor components are known. In the discussion in Chapter III, no mention was given concerning displacements; all deformation-related quantities were written in terms of the deformation functions, χ, defined in Eq. (3.1). In this section, an expression for the deformation gradient in terms of the gradients of a displacement vector will be developed.

Let the position vector (defined with respect to a global Cartesian system) locating a particle with curvilinear coordinates X^α in the reference configuration be defined as $\underset{\sim}{R}$. Similarly, define a position vector at the same particle in the spatial configuration as $\underset{\sim}{r}$. The covariant base vectors of the reference and spatial curvilinear coordinate systems are defined as

$$\underset{\sim}{G}_\alpha = \frac{\partial \underset{\sim}{R}}{\partial X^\alpha} , \tag{6.16}$$

and

$$\underset{\sim}{g}_i = \frac{\partial \underset{\sim}{r}}{\partial x^i} \; . \tag{6.17}$$

Introduce a displacement vector, $\underset{\sim}{u}$, which relates the reference and spatial position vectors through the vector equation,

$$\underset{\sim}{r} = \underset{\sim}{R} + \underset{\sim}{u} \; . \tag{6.18}$$

The partial derivatives of Eq. (6.18) with respect to the reference system curvilinear coordinates can be written as

$$\frac{\partial \underset{\sim}{r}}{\partial X^\beta} = \frac{\partial \underset{\sim}{R}}{\partial X^\beta} + \frac{\partial \underset{\sim}{u}}{\partial X^\beta} \; , \tag{6.19}$$

or

$$\frac{\partial \underset{\sim}{r}}{\partial x^i} \frac{\partial x^i}{\partial X^\beta} = (\delta^\alpha{}_\beta + u^\alpha|_\beta) \underset{\sim}{G}_\alpha = \underset{\sim}{g}_i \frac{\partial x^i}{\partial X^\beta} \tag{6.20}$$

If the right-hand side of Eq. (6.20) is shifted to the base vectors of the reference configuration, Eq. (6.20) may be written as

$$\frac{\partial x^i}{\partial X^\beta} g_i{}^\alpha \underset{\sim}{G}_\alpha = (\delta^\alpha{}_\beta + u^\alpha|_\beta) \underset{\sim}{G}_\alpha \; , \tag{6.21}$$

where the "shifter," $g_i{}^\alpha$, is defined as

$$g_i{}^\alpha = \underset{\sim}{g}_i \cdot \underset{\sim}{G}^\alpha \; . \tag{6.22}$$

The components of Eq. (6.21) are given by

$$\frac{\partial x^i}{\partial X^\beta}\, g_i{}^\alpha = (\delta^\alpha{}_\beta + u^\alpha|_\beta) \;. \tag{6.23}$$

When the reference and spatial coordinate systems are Cartesian, the shifter is given by

$$g_i{}^\alpha = \delta_i{}^\alpha \;, \tag{6.24}$$

and Eq. (6.23) reduces to

$$\frac{\partial x^i}{\partial X^\beta} = \delta^i{}_\beta + u^i{}_{,\beta} \;. \tag{6.25}$$

When the reference and spatial coordinate systems are cylindrical, the shifter is more complicated than Eq. (6.24), and in general can be evaluated from Eq. (6.22). However, for the special case of axisymmetric analyses, parallel transport can be used since the displacement vector does not depend on the θ-direction, and the deformation gradient is given by

$$x^i{}_{,\alpha} = \delta^i{}_\alpha + u^i{}_{,\alpha} + u^k\, \Gamma^i{}_{\alpha k} \;. \tag{6.26}$$

For two-dimensional problems in Cartesian coordinates, the components of the deformation gradient written in matrix form are

$$[F] = \begin{bmatrix} 1+u^1{}_{,1} & u^1{}_{,2} & 0 \\ u^2{}_{,1} & 1+u^2{}_{,2} & 0 \\ 0 & 0 & 1 \end{bmatrix} . \tag{6.27}$$

For axisymmetric problems in cylindrical coordinates, the components of the deformation gradient written in matrix form are

$$[F] = \begin{bmatrix} 1+u^1{}_{,1} & u^1{}_{,2} & 0 \\ u^2{}_{,1} & 1+u^2{}_{,2} & 0 \\ 0 & 0 & 1+\frac{u^2}{X^2} \end{bmatrix} . \tag{6.28}$$

The displacement derivatives are given by

$$u^i{}_{,\alpha} = N^i{}_{\beta,\alpha}\, \bar{u}^\beta , \tag{6.29}$$

where $N^i{}_\beta$ are components of the matrix of interpolation functions given in Eq. (6.4), and $\bar{u}^\beta$ are the node point displacements.

6.8. Strain Increment-Displacement Matrix

As pointed out in Section 5.5, the implicit integration of the governing incremental equations of motion requires the formation of a tangential stiffness matrix. To evaluate the tangential stiffness matrix it is necessary to establish a matrix which relates the increment in Green's strain to the displacement increments. The increments in the components of Green's strain tensor are related to the displacement increments through Eqs. (5.81i through 5.81ℓ) which are repeated here for completeness:

$$dE_{11} = du_{1,1} + du_{n,1}\, u^{n}{}_{,1} \;, \qquad (6.30a)$$

$$dE_{22} = du_{2,2} + du_{n,2}\, u^{n}{}_{,2} \;, \qquad (6.30b)$$

$$2dE_{12} = du_{2,1} + du_{1,2} + du_{n,1}\, u^{n}{}_{,2} + du_{m,2}\, u^{m}{}_{,1} \;, \qquad (6.30c)$$

$$dE_{33} = du_{2}/x^{2} + du_{2}\, u^{2}/(x^{2})^{2} \;. \qquad (6.30d)$$

In Eq. (6.30d), the coordinate x^2 is the radius in a cylindrical coordinate system. For plane strain computations, $dE_{33} = 0$. For two-dimensional and axisymmetric problems there are only two displacement components, and the dummy indices m and n take on values from 1 to 2.

It will be convenient to write Eqs. (6.30a through 6.30d) in the following matrix form:

$$\{dE\} = [\,[B_0] + [B_1]\,]\,\{d\bar{u}\} \;, \qquad (6.31)$$

where

$$\{dE\}^T = [\, dE_{11} \,,\, dE_{22} \,,\, 2dE_{12} \,,\, dE_{33} \,] \;, \qquad (6.32)$$

$$\begin{aligned}\{d\bar{u}\}^T = [\, & d\bar{u}^1_1 \,,\, d\bar{u}^2_1 \,,\, d\bar{u}^1_2 \,,\, d\bar{u}^2_2 \,,\, d\bar{u}^1_3 \,,\, d\bar{u}^2_3 \,, \\ & d\bar{u}^1_4 \,,\, d\bar{u}^2_4 \,,\, d\bar{u}^1_5 \,,\, d\bar{u}^2_5 \,,\, d\bar{u}^1_6 \,,\, d\bar{u}^2_6 \,, \\ & d\bar{u}^1_7 \,,\, d\bar{u}^2_7 \,,\, d\bar{u}^1_8 \,,\, d\bar{u}^2_8 \,] \;. \end{aligned} \qquad (6.33)$$

The matrix $[B_0]$ contains terms not depending explicitly on the current displacements, and the matrix $[B_1]$ contains all terms depending explicitly on the current displacements. Recall that the superscript appearing on the components of $\{d\bar{u}\}$ identifies the displacement increment component, and the subscript identifies the node number associated with the displacement increment.

The displacement increments and displacements within a finite element can be written in terms of the node point values using the interpolation function matrix defined by Eqs. (6.4) and (6.5); that is,

$$du_i = N_{i\beta}\, d\bar{u}^{\beta} \quad i = 1,2 \;,\; \beta = 1,16 \tag{6.34}$$

and

$$u^i = N^i{}_{\beta}\, \bar{u}^{\beta} \quad i = 1,2 \;,\; \beta = 1,16 \;. \tag{6.35}$$

Differentiating Eq. (6.34) with respect to the reference configuration coordinates yields

$$du_{i,j} = N_{i\beta,j}\, d\bar{u}^{\beta} \;, \tag{6.36}$$

where the derivatives of the interpolation functions are obtained by using Eqs. (6.6) and (6.14). For example,

$$\frac{\partial h_1}{\partial X^1} = \frac{\partial h_1}{\partial \xi}\frac{\partial \xi}{\partial X^1} + \frac{\partial h_1}{\partial \eta}\frac{\partial \eta}{\partial X^1} \;. \tag{6.37}$$

The matrix $[B_0]$ is seen to have the following components for axisymmetric cylindrical coordinates:

$$[B_0] = \left[\begin{array}{cccccccc} h_{1,1} & 0 & h_{2,1} & 0 & h_{3,1} & 0 & h_{4,1} & 0 \\ 0 & h_{1,2} & 0 & h_{2,2} & 0 & h_{3,2} & 0 & h_{4,2} \\ h_{1,2} & h_{1,1} & h_{2,2} & h_{2,1} & h_{3,2} & h_{3,1} & h_{4,2} & h_{4,1} \\ 0 & \frac{h_1}{x^2} & 0 & \frac{h_2}{x^2} & 0 & \frac{h_3}{x^2} & 0 & \frac{h_4}{x^2} \end{array}\right. \tag{6.38}$$

$$\left.\begin{array}{cccccccc} h_{5,1} & 0 & h_{6,1} & 0 & h_{7,1} & 0 & h_{8,1} & 0 \\ 0 & h_{5,2} & 0 & h_{6,2} & 0 & h_{7,2} & 0 & h_{8,2} \\ h_{5,2} & h_{5,1} & h_{6,2} & h_{6,1} & h_{7,2} & h_{7,1} & h_{8,2} & h_{8,1} \\ 0 & \frac{h_5}{x^2} & 0 & \frac{h_6}{x^2} & 0 & \frac{h_7}{x^2} & 0 & \frac{h_8}{x^2} \end{array}\right]$$

Consider the term $du_{n,1}\ u^n{}_{,1}$ appearing in Eq. (6.30a). This term can be written as

$$du_{n,1}\ u^n{}_{,1} = du_{1,1}\ u^1{}_{,1} + du_{2,1}\ u^2{}_{,1} \tag{6.39a}$$

$$= N_{1\beta,1}\ d\bar{u}^\beta\ u^1{}_{,1} + N_{2\beta,1}\ d\bar{u}^\beta\ u^2{}_{,1} \tag{6.39b}$$

$$= \{ N_{1\beta,1}\ u^1{}_{,1} + N_{2\beta,1}\ u^2{}_{,1} \}\ d\bar{u}^\beta\ . \tag{6.39c}$$

In Eq. (6.39c) the term $u^1{}_{,1}$ is given by

$$u^1{}_{,1} = N_{1\alpha,1}\ \bar{u}^\alpha\ , \tag{6.40}$$

and similarly, $u^2{}_{,1}$ is given by

$$u^2{}_{,1} = N_{2\alpha,1}\,\overline{u}^{\alpha} \; . \tag{6.41}$$

Similar expressions can be obtained for displacement dependent terms in Eqs. (6.30b) to (6.30d), and the components of the matrix $[B_1]$ are given as, for axisymmetric cylindrical coordinates,

$$\underset{4\times16}{[B_1]} = \left[\begin{matrix} h_{1,1}\,u^1{}_{,1} & h_{1,1}\,u^2{}_{,1} & h_{2,1}\,u^1{}_{,1} & h_{2,1}\,u^2{}_{,1} & \cdots \\ h_{1,2}\,u^1{}_{,2} & h_{1,2}\,u^2{}_{,2} & h_{2,2}\,u^1{}_{,2} & h_{2,2}\,u^2{}_{,2} & \cdots \\ \begin{pmatrix} h_{1,1}\,u^1{}_{,2} + \\ h_{1,2}\,u^1{}_{,1} \end{pmatrix} & \begin{pmatrix} h_{1,1}\,u^2{}_{,2} + \\ h_{1,2}\,u^2{}_{,1} \end{pmatrix} & \begin{pmatrix} h_{2,1}\,u^1{}_{,2} + \\ h_{2,2}\,u^1{}_{,1} \end{pmatrix} & \begin{pmatrix} h_{2,1}\,u^2{}_{,2} + \\ h_{2,2}\,u^2{}_{,1} \end{pmatrix} & \cdots \\ 0 & \dfrac{h_1\,u^2}{(X^2)^2} & 0 & \dfrac{h_2\,u^2}{(X^2)^2} & \cdots \end{matrix}\right.$$

$$\left.\begin{matrix} h_{8,1}\,u^1{}_{,1} & h_{8,1}\,u^2{}_{,1} \\ h_{8,2}\,u^1{}_{,2} & h_{8,2}\,u^2{}_{,2} \\ \begin{pmatrix} h_{8,1}\,u^1{}_{,2} + \\ h_{8,2}\,u^1{}_{,1} \end{pmatrix} & \begin{pmatrix} h_{8,1}\,u^2{}_{,2} + \\ h_{8,2}\,u^2{}_{,1} \end{pmatrix} \\ 0 & \dfrac{h_8\,u^2}{(X^2)^2} \end{matrix}\right] \; . \tag{6.42}$$

It is important to recognize that for an updated Lagrangian analysis, the reference configuration is the current configuration, and the matrix $[B_1]$ is zero. Also, the matrix $[B_0]$ is the infinitesimal strain-displacement matrix used in linear finite element programs. That is,

Linear Small Strain Analysis:

$$\{\varepsilon\} = [B_0]\{\bar{u}\} \ , \tag{6.43}$$

where $\{\varepsilon\}^T = \{\varepsilon_{11}, \varepsilon_{22}, 2\varepsilon_{12}, \varepsilon_{33}\}$ is a row vector containing the components of the infinitesimal strain tensor,

Updated Lagrangian Analysis:

$$\{dE\} = [B_0]\{d\bar{u}\} \ , \tag{6.44}$$

Total Lagrangian Analysis:

$$\{dE\} = [\ [B_0] + [B_1]\ ]\{d\bar{u}\} \ . \tag{6.45}$$

A comparison of Eqs. (5.81a,b,c,d) with Eqs. (6.30a,b,c,d) reveals that the matrices $[B_0]$ and $[B_1]$ also relate the virtual rate of Green's strain to the node point velocities. That is,

$$\{\delta\dot{E}\} = [\ [B_0] + [B_1]\ ]\{\delta\bar{v}\} \ , \tag{6.46}$$

where $\{\delta\bar{v}\}$ are the virtual node point velocities. Equation (6.46) appears in both the implicit integration of the incremental equations of motion (Eq. (5.67b)) and the explicit integration of the equations of motion (Eq. (5.28)).

A convenient way of writing Eq. (6.46) is,

$$\delta \dot{E}_{\alpha\beta} = L^{\phi}_{\alpha\beta} \; \delta \overline{v}_{\phi} \; ,$$

where $L^{\phi}_{\alpha\beta}$ represents the combination of the $[B_0]$ and $[B_1]$ matrices; that is,

$$[B] = [B_0] + [B_1] \; . \tag{6.47}$$

The $\alpha\beta$ subscripts identify the component of the virtual rate of Green's strain tensor, which is related to a particular row of the [B] matrix. The dummy index ϕ identifies a particular column in the [B] matrix.

6.9. Elastic Stress-Strain Matrix

In subsequent sections, a matrix containing the material constants for an isotropic elastic material will be used to relate conjugate stress and strain measures. The material constants are written in terms of Young's modulus, E, and Poisson's ratio, ν. For axisymmetric and plane strain conditions the material matrix is given by

$$[C] = \begin{bmatrix} A & B & 0 & B \\ B & A & 0 & B \\ 0 & 0 & D & 0 \\ B & B & 0 & A \end{bmatrix} , \tag{6.48}$$

where,

$$A = E(1-\nu)/(1+\nu)(1-2\nu)$$

$$B = E\nu/(1+\nu)(1-2\nu)$$

$$D = E/2(1+\nu) \ .$$

The corresponding stress and strain vectors for infinitesimal strain theory are

$$\begin{Bmatrix} \sigma_{11} \\ \sigma_{22} \\ \sigma_{12} \\ \sigma_{33} \end{Bmatrix} \quad \text{and} \quad \begin{Bmatrix} \varepsilon_{11} \\ \varepsilon_{22} \\ 2\varepsilon_{12} \\ \varepsilon_{33} \end{Bmatrix} . \tag{6.49}$$

Note that for plain strain, $\varepsilon_{33} = \phi$.

The same material constants are used to define a linear hyperelastic material,

$$\{\tilde{T}\} = [C]\{E\} , \tag{6.50}$$

and a linear hypoelastic material,

$$\{\overset{\nabla}{\sigma}\} = [C]\{d\} . \tag{6.51}$$

In the above equations, $\{\tilde{T}\}$ is the vector of second Piola stress components, $\{E\}$ is the vector of Green's strain components, $\{\overset{\nabla}{\sigma}\}$ is the vector containing components of the Jaumann derivative of the Cauchy stress, and $\{d\}$ is the vector of rate of deformation components.

6.10. Constitutive Equations

Figure 6.8 shows the elastic-viscoplastic constitutive equations implemented during this investigation. These implementations were controlled by the method used to solve the governing equations of motion (i.e., implicit or explicit), and the choice of the reference configuration (updated or total Lagrangian). In this section each of the six constitutive equations shown in Figure 6.8 will be presented in detail for the axisymmetric cylindrical coordinate case. Beside the title of each subsection, the type of integration method used for the equations of motion and for the constitutive equations, respectively, will be given in parentheses.

6.10.1. Hypoelastic-Viscoplastic (Implicit, Explicit)

This constitutive equation is given by Eq. (4.28) and is repeated here for completeness:

$$\dot{\tilde{T}}^{ij} = \{ B^{ijkl} - g^{ik}\,\tau^{lj} - g^{jk}\,\tau^{li} \} D_{kl}$$

$$- B^{ijkl}\,\gamma\langle\Phi(F)\rangle \frac{\partial f(\underset{\sim}{\tau})}{\partial \tau^{kl}} \; . \qquad (6.52)$$

Implicit Integration of Equations of Motion

Updated Lagrangian formulation

- Hypoelastic-viscoplastic (explicit integration)
- Updated hyperelastic-viscoplastic (explicit integration)

Total Lagrangian formulation

- Hyperelastic-viscoplastic (explicit integration)

Explicit Integration of Equations of Motion

Updated Lagrangian formulation

- Hypoelastic-viscoplastic (implicit integration)
- Updated hyperelastic-viscoplastic (implicit integration)

Figure 6.8. Relationship between Constitutive Equations and Analysis Formulations.

Equation (6.52) was implemented using an updated Lagrangian formulation in which all quantities are referenced to the current configuration. Multiplying the constitutive equation by Δt, yields an incremental form given by

$$\Delta\tilde{T}^{ij} = \{B^{ijkl} - g^{ik}\tau^{lj} - g^{jk}\tau^{li}\}\,\Delta\varepsilon_{kl}$$

$$- B^{ijkl}\,\gamma\langle\Phi(F)\rangle\,\frac{\partial f(\tau)}{\partial\tau^{kl}}\,\Delta t\ , \tag{6.53}$$

where

$$\Delta\varepsilon_{kl} = \frac{1}{2}\left(\frac{\partial\Delta u_k}{\partial x^l} + \frac{\partial\Delta u_l}{\partial x^k}\right) . \tag{6.54}$$

Using matrix notation, Eq. (6.53) can be written as

$$\{\Delta\tilde{T}\} = [A]\{\Delta\varepsilon\} - \{\Delta\tilde{T}^{(vp)}\}\ , \tag{6.55}$$

where

$$\{\Delta\tilde{T}\}^T = [\,\Delta\tilde{T}^{11},\Delta\tilde{T}^{22},\Delta\tilde{T}^{12},\Delta\tilde{T}^{33}\,]\ , \tag{6.56}$$

$$\{\Delta\varepsilon\}^T = [\,\Delta\varepsilon_{11},\Delta\varepsilon_{22},2\Delta\varepsilon_{12},\Delta\varepsilon_{33}\,]\ , \tag{6.57}$$

$$\{\Delta\tilde{T}^{(vp)}\} = [\,\Delta\tilde{T}^{11(vp)},\Delta\tilde{T}^{22(vp)},\Delta\tilde{T}^{12(vp)},\Delta\tilde{T}^{33(vp)}\,]\ . \tag{6.58}$$

The matrix [A] is given by

$$[A] = [D] - [C]\ , \tag{6.59}$$

where

$$[C] = \begin{bmatrix} 2\tau^{11} & 0 & \tau^{21} & 0 \\ 0 & 2\tau^{22} & \tau^{21} & 0 \\ \tau^{21} & \tau^{21} & (\tau^{11}+\tau^{22})/2 & 0 \\ 0 & 0 & 0 & 2\tau^{33} \end{bmatrix} , \tag{6.60}$$

and [D] is the matrix of elastic coefficients.

The components of $\{\Delta\tilde{T}^{(vp)}\}$ are obtained from

$$\{\Delta\tilde{T}^{(vp)}\} = [D]\{\Delta\varepsilon^{(vp)}\} , \tag{6.61}$$

where

$$\{\Delta\varepsilon^{(vp)}\}^T = [\Delta\varepsilon_{11}^{(vp)}, \Delta\varepsilon_{22}^{(vp)} \quad \Delta\varepsilon_{12}^{(vp)} \quad \Delta\varepsilon_{33}^{(vp)}] . \tag{6.62}$$

For a power law overstress function, the visco-plastic strain increments are obtained from

$$\Delta\varepsilon_{kl}^{(vp)} = \gamma\langle(F)^n\rangle \frac{3}{2} \frac{\tau'_{kl}}{\sqrt{3J_2}} \Delta t , \tag{6.63}$$

where n is the power law exponent,

$$F = \frac{\sqrt{3J_2}}{\phi({}^t\bar{\varepsilon}^{(vp)})} - 1 \tag{6.64}$$

is the overstress function, and τ'_{kl} are the deviatoric components of the Kirchhoff stress tensor; J_2 is the second invariant of the deviatoric Kirchhoff stress tensor, and

$\phi({}^{t}\varepsilon^{(vp)})$ is the value of the stress-strain curve evaluated at the current value of the integral of the equivalent viscoplastic strain rate. The equivalent viscoplastic strain increment is computed using the following relationship,

$$\Delta\bar{\varepsilon}^{(vp)} = \left\{ \frac{2}{9}\left[\left(\Delta\varepsilon_{11}^{(vp)} - \Delta\varepsilon_{22}^{(vp)}\right)^2 + \left(\Delta\varepsilon_{22}^{(vp)} - \Delta\varepsilon_{33}^{(vp)}\right)^2 + \left(\Delta\varepsilon_{33}^{(vp)} - \Delta\varepsilon_{11}^{(vp)}\right)^2\right] + \frac{4}{3}\left[\left(\Delta\varepsilon_{12}^{(vp)}\right)^2\right]\right\}^{1/2} . \tag{6.65}$$

The integral of the equivalent viscoplastic strain rate is computed using the recursive relationship

$$^{t+\Delta t}\bar{\varepsilon}^{(vp)} = {}^{t}\bar{\varepsilon}^{(vp)} + \Delta\bar{\varepsilon}^{(vp)} . \tag{6.66}$$

The incremental strains in Eq. (6.55) can be related to the finite element incremental node point displacements through the $[B_0]$ matrix presented in Section 6.6; that is,

$$\{\Delta\varepsilon\} = [B_0]\{\Delta\bar{u}\} . \tag{6.67}$$

Substituting Eqs. (6.67) and (6.61) into (6.55) yields the equation

$$\{\Delta\tilde{T}\} = [A][B_0]\{\Delta\bar{u}\} - [D]\{\Delta\varepsilon^{(vp)}\} . \tag{6.68}$$

Equation (6.68) is used to assemble the tangential stiffness matrix for the element, with the incremental node point displacements as the unknown variables. The term $[D]\{\Delta\varepsilon^{(vp)}\}$ contributes to the element unbalanced load vector, and serves as a correction term when computing the incremental stresses.

The second Piola stress components at time t+Δt are obtained by adding the Truesdell stress increments to the second Piola stress components at time t;

$$ {}^{t+\Delta t}_{t}\{\tilde{T}\} = {}^{t}_{t}\{\tilde{T}\} + {}^{t}_{t}\{\Delta\tilde{T}\} \ . \tag{6.69}$$

The left superscript identifies the time at which the variable is known, and the left subscript identifies the configuration to which the variable is referenced. The components of the Kirchhoff stress tensor at time t+Δt are obtained from

$$ {}^{t+\Delta t}\underset{\sim}{\tau} = {}^{t+\Delta t}_{t}\underset{\sim}{G} \; {}^{t+\Delta t}_{t}\underset{\sim}{\tilde{T}} \; {}^{t+\Delta t}_{t}\underset{\sim}{G}^{T} \quad , \tag{6.70}$$

where ${}^{t+\Delta t}_{t}\underset{\sim}{G}$ is the deformation gradient at time t+Δt, referenced to the geometric configuration at time t.

Note that two different stress quantities are used; the constitutive equation is a function of the Kirchhoff stress, and the incremental Lagrangian equations of motion require the increment in the second Piola stress.

6.10.2. Updated Hyperelastic-Viscoplastic (Implicit, Explicit)

This constitutive equation is discussed in Section 4.3, and is written in compact form in Eqs. (4.34) to (4.37). Similar to the development in the previous section, the rate equations are cast into incremental form

$$\Delta\tilde{T}^{ij} = C^{ijkl} \left(\Delta\varepsilon_{kl} - \Delta\varepsilon_{kl}^{(vp)} \right) , \tag{6.71}$$

where

$$\Delta\varepsilon_{kl}^{(vp)} = \gamma \langle \Phi(F) \rangle \frac{\partial f}{\partial \sigma^{kl}} \Delta t , \tag{6.72}$$

and all quantities are referenced to the current configuration.

Using matrix notation, Eq. (6.71) can be written as

$$\{\Delta\tilde{T}\} = [C]\{\Delta\varepsilon\} - \{\Delta\tilde{T}^{(vp)}\} , \tag{6.73}$$

where

$$\{\Delta\tilde{T}\}^T = [\, \Delta\tilde{T}^{11}, \Delta\tilde{T}^{22}, \Delta\tilde{T}^{12}, \Delta\tilde{T}^{33} \,] , \tag{6.74}$$

$$\{\Delta\varepsilon\}^T = [\, \Delta\varepsilon_{11}, \Delta\varepsilon_{22}, 2\Delta\varepsilon_{12}, \Delta\varepsilon_{33} \,] , \tag{6.75}$$

$$\{\Delta\tilde{T}^{(vp)}\} = [\, \Delta\tilde{T}^{11(vp)},\ T^{22(vp)}, \Delta\tilde{T}^{12(vp)}, \Delta\tilde{T}^{33(vp)} \,] , \tag{6.76}$$

and [C] is the matrix of elastic coefficients.

The components of $\{\Delta\tilde{T}^{(vp)}\}$ are given by

$$\{\Delta\tilde{T}^{(vp)}\} = [C]\{\Delta\varepsilon^{(vp)}\} \quad , \tag{6.77}$$

where

$$\{\Delta\varepsilon^{(vp)}\}^T = [\,\Delta\varepsilon_{11}^{(vp)}, \Delta\varepsilon_{22}^{(vp)}, 2\Delta\varepsilon_{12}^{(vp)}, \Delta\varepsilon_{33}^{(vp)}\,] \ . \tag{6.78}$$

For a power law overstress function, the viscoplastic strain increments are obtained from

$$\Delta\varepsilon_{kl}^{(vp)} = \gamma\langle(F)^n\rangle \, \frac{3}{2} \, \frac{\sigma'_{kl}}{\sqrt{3J_2}} \, \Delta t \quad , \tag{6.79}$$

where n is the power law exponent,

$$F = \frac{\sqrt{3J_2}}{\phi({}^t\bar{\varepsilon}^{(vp)})} - 1 \tag{6.80}$$

is the overstress function, and σ'_{kl} are the deviatoric components of the Cauchy stress tensor; J_2 is the second invariant of the deviatoric Cauchy stress tensor, and $\phi({}^t\bar{\varepsilon}^{(vp)})$ is the value of the stress-strain curve evaluated at the current value of the equivalent viscoplastic strain integral. The equivalent viscoplastic strain integral is computed using Eqs. (6.65) and (6.66).

Using Eqs. (6.67) and (6.77), the constitutive equation, Eq. (6.71), can be written as

$$\{\Delta\tilde{T}\} = [C][B_0]\{\Delta\bar{u}\} - [C]\{\Delta\varepsilon^{(vp)}\} \ . \tag{6.81}$$

This equation is used to assemble the tangential stiffness matrix for the element, with the incremental node point displacements as the unknown variables. The term $[C]\{\Delta\varepsilon^{(vp)}\}$ contributes to the element unbalanced load vector, and serves as a correction term when computing the incremental stresses.

The second Piola stresses at time $t+\Delta t$ are obtained by adding the stress increments to the second Piola stresses at time t;

$$ {}^{t+\Delta t}_{t}\{\tilde{T}\} = {}^{t}_{t}\{\tilde{T}\} + \{\Delta\tilde{T}\} \; . \tag{6.82} $$

The components of the Cauchy stress at time $t+\Delta t$ are obtained from

$$ {}^{t+\Delta t}\underset{\sim}{\sigma} = \frac{{}^{t+\Delta t}\rho}{{}^{t}\rho} \; {}^{t+\Delta t}_{t}\underset{\sim}{G} \; {}^{t+\Delta t}_{t}\underset{\sim}{T} \; {}^{t+\Delta t}_{t}\underset{\sim}{G}^{T} \; , \tag{6.83} $$

where ${}^{t+\Delta t}_{t}\underset{\sim}{G}$ is the deformation gradient relating the configuration at time $t+\Delta t$ to the configuration at time t.

6.10.3. Hyperelastic-Viscoplastic (Implicit, Explicit)

This constitutive equation is similar to the updated-hyperelastic viscoplastic constitutive equation, except that it uses a total Lagrangian formulation in which the reference configuration is not updated. The incremental form of the constitutive equation is given by

$$\Delta\left({}_{t_0}^{t}\tilde{T}^{\alpha\beta}\right) = D^{\alpha\beta kl}\left(\Delta\left({}_{t_0}^{t}E_{kl}\right) - \Delta\left({}_{t_0}^{t}E_{kl}^{(vp)}\right)\right) , \qquad (6.84)$$

where

$$\Delta\left({}_{t_0}^{t}E_{kl}^{(vp)}\right) = \gamma < \Phi(F) > \frac{\partial f}{\partial\, {}_{t_0}^{t}\tilde{T}^{kl}} \Delta t \ . \qquad (6.85)$$

In matrix notation, Eq. (6.84) can be written as

$$\{\Delta\tilde{T}\} = [D]\{\Delta E\} - \{\Delta\tilde{T}^{(vp)}\} , \qquad (6.86)$$

where

$$\{\Delta\tilde{T}\}^T = [\ \Delta\tilde{T}^{11}, \Delta\tilde{T}^{22}, \Delta\tilde{T}^{12}, \Delta\tilde{T}^{33}\ ] , \qquad (6.87)$$

$$\{\Delta T\}^T = [\ \Delta E_{11}, \Delta E_{22}, 2\Delta E_{12}, \Delta E_{33}\ ] , \qquad (6.88)$$

$$\{\Delta\tilde{T}^{(vp)}\} = [\ \Delta\tilde{T}^{11(vp)}, \Delta\tilde{T}^{22(vp)},$$

$$\Delta\tilde{T}^{12(vp)}, \Delta\tilde{T}^{33(vp)}\ ] , \qquad (6.89)$$

and [D] is the matrix of elastic coefficients; all quantities are evaluated at time t, and referenced to the original onfiguration at t_0.

The components of $\{\Delta\tilde{T}^{(vp)}\}$ are given by

$$\{\Delta\tilde{T}^{(vp)}\} = [D]\{\Delta E^{(vp)}\} , \qquad (6.90)$$

where

$$\{\Delta E^{(vp)}\}^T = [\ \Delta E_{11}^{(vp)}, \Delta E_{22}^{(vp)}, 2\Delta E_{12}^{(vp)}, \Delta E_{33}^{(vp)}\ ] . \qquad (6.91)$$

For a power law overstress function, the viscoplastic strain increments are obtained from

$$\Delta E_{kl}^{(vp)} = \gamma\langle(F)^n\rangle \frac{3}{2} \frac{\tilde{T}'_{kl}}{\sqrt{3J_2}} \Delta t , \qquad (6.92)$$

where n is the power law exponent,

$$F = \frac{\sqrt{3J_2}}{\phi({}^t\bar{E}^{(vp)})} -1 \qquad (6.93)$$

is the overstress function, and $\tilde{T}'_{kl}$ are the deviatoric components of the second Piola stress tensor; J_2 is the second invariant of the deviatoric second Piola stress tensor, and $\phi({}^tE^{vp})$ is the value of the nominal stress-strain curve evaluated at the current value of the equivalent viscoplastic strain integral. The equivalent viscoplastic strain integral is computed using equations similar to Eqs. (6.65) and (6.66).

Using Eqs. (6.45) and (6.90), the constitutive equation can be written as

$$\{\Delta\tilde{T}\} = [D][B]\{\Delta\bar{u}\} - [D]\{\Delta E^{(vp)}\} , \qquad (6.94)$$

which is used to assemble the tangential stiffness matrix for the element, with the incremental node point displacements as the unknown variables. The term [D] $\{E^{(vp)}\}$ contributes to the element unbalanced load vector, and serves as a correction term when computing the incremental stresses.

The second Piola stresses at time t+Δt are obtained by adding the stress increments to the second Piola stresses at time t;

$$ {}^{t+\Delta t}_{t_0}\{\tilde{T}\} = {}^{t}_{t_0}\{\tilde{T}\} + {}^{t}_{t_0}\{\Delta\tilde{T}\} \ . \qquad (6.95) $$

Note that for this analysis method, it is not necessary to transform the second Piola stresses to a different configuration, since both the constitutive equations and the incremental equations of motion use the same stress tensor.

6.10.4. Hypoelastic-Viscoplastic (Explicit, Implicit)

This constitutive equation was discussed in Section 5.1, and is given by Eq. (5.12). It represents an implicit integration of the hypoelastic-viscoplastic constitutive equation, and was used in conjunction with the explicit integration of the equations of motion using an updated Lagrangian formulation, with all variables referenced to the current configuration. For completeness, Eq. (5.12) is repeated below:

$$ \dot{\sigma}^{mn} = K^{mn}{}_{ij} \, C^{ijkl}\left(D_{kl} - {}^{t}D^{(vp)}_{kl}\right) + g^{mk} \, \omega_{kl} \, \sigma^{ln} + g^{nk} \, \omega_{kl} \, \sigma^{lm} \ . \qquad (6.96) $$

For a power law overstress function the partial derivative in Eq. (5.12) was given in Eq. (5.15) as

$$\frac{\partial\, {}^{t}D^{(vp)}_{rs}}{\partial \sigma^{mn}} = \frac{3}{4J_2}\,\gamma F^{b}\left\{ \frac{b}{F\phi({}^{t}\bar{\varepsilon}^{(vp)})} - \frac{1}{\sqrt{3J_2}} \right\} \sigma'_{rs}\, \sigma'_{mn}$$

$$+ \gamma F^{b}\, \frac{3}{2}\, \frac{1}{\sqrt{3J_2}} \left(\delta_{rm}\, \delta_{sn} - \frac{1}{3}\, \delta_{rs}\, \delta_{mn} \right) , \qquad (6.97)$$

where b is the power law exponent, F is the overstress defined by

$$F = \frac{\sqrt{3J_2}}{\phi({}^{t}\bar{\varepsilon}^{(vp)})} - 1 , \qquad (6.98)$$

$\phi(\bar{\varepsilon}^{(vp)})$ is the value of the static stress-strain curve evaluated at the current value of the equivalent visco-plastic strain, ${}^{t}\bar{\varepsilon}^{(vp)}$; J_2 is the second invariant of the deviatoric Cauchy stress; and $\underset{\sim}{\sigma}'$ is the deviatoric Cauchy stress tensor.

It can be shown that Eq. (5.12) with (5.15) can be written in incremental matrix form as

$$\{\Delta\sigma\} = [H]^{-1}\, [C]\, \left(\{\Delta\varepsilon\} - \{\Delta\varepsilon^{(vp)}\} \right) + [S]\{\sigma\} , \qquad (6.99)$$

where

$$\{\Delta\sigma\}^T = [\Delta\sigma^{11}, \Delta\sigma^{22}, \Delta\sigma^{12}, \Delta\sigma^{33}] \;, \qquad (6.100)$$

$$\{\Delta\varepsilon\}^T = [\Delta\varepsilon_{11}, \Delta\varepsilon_{22}, 2\Delta\varepsilon_{12}, \Delta\varepsilon_{33}], \qquad (6.101)$$

$$\{\Delta\varepsilon^{(vp)}\}^T = [\Delta\varepsilon_{11}^{(vp)}, \Delta\varepsilon_{22}^{(vp)}, 2\Delta\varepsilon_{12}^{(vp)}, \Delta\varepsilon_{33}^{(vp)}], \qquad (6.102)$$

$$\{\varepsilon\}^T = [\sigma^{11}, \sigma^{22}, \sigma^{12}, \sigma^{33}] \;; \qquad (6.103)$$

[C] is the matrix of elastic coefficients, and

$$[S] = \begin{bmatrix} 0 & 0 & 2\Delta\omega_{12} & 0 \\ 0 & 0 & 2\Delta\omega_{21} & 0 \\ \Delta\omega_{12} & \Delta\omega_{21} & 0 & 0 \\ 0 & 0 & 0 & 0 \end{bmatrix} \;, \qquad (6.104)$$

where $\Delta\omega_{12}$ and $\Delta\omega_{21}$ are components of the incremental spin tensor, $\Delta\omega_{12} = \dot{\omega}_{12}\,\Delta t$. The matrix [H] is computed from the equation

$$[H] = [I] + A_1\,[C]\,[A_2\,[M] + A_3\,[P]\,) \;, \qquad (6.105)$$

where A_1, A_2, and A_3 are constants defined as

$$A_1 = \frac{\Delta t}{2} \;, \qquad (6.106)$$

$$A_2 = \frac{3}{4J_2}\,\gamma F^b \left\{ \frac{b}{F\phi(\,{}^t\bar{\varepsilon}^{(vp)}\,)} - \frac{1}{\sqrt{3J_2}} \right\} \;, \qquad (6.107)$$

$$A_3 = \frac{3\,F^b}{2\sqrt{3J_2}} \;. \qquad (6.108)$$

The matrix [M] is defined as

$$[M] = \{\dot{\sigma}'\}\{\dot{\sigma}'\}^T , \tag{6.109}$$

where

$$\{\dot{\sigma}'\}^T = [\dot{\sigma}'_{11}, \dot{\sigma}'_{22}, 2\dot{\sigma}'_{12}, \dot{\sigma}'_{33}] . \tag{6.110}$$

The matrix [P] is defined as

$$[P] = \begin{bmatrix} \frac{2}{3} & -\frac{1}{3} & 0 & -\frac{1}{3} \\ -\frac{1}{3} & \frac{2}{3} & 0 & -\frac{1}{3} \\ 0 & 0 & 2 & 0 \\ -\frac{1}{3} & -\frac{1}{3} & 0 & \frac{2}{3} \end{bmatrix} . \tag{6.111}$$

The components of $\{\Delta\varepsilon\}$ are related to the incremental finite element node point displacements by Eq. (6.44); that is,

$$\{\Delta\varepsilon\} = [B_0]\{\Delta\bar{u}\} . \tag{6.112}$$

The components of $\{\Delta\varepsilon^{vp)}\}$ are obtained from

$$\{\Delta\varepsilon^{(vp)}\} = \gamma F^n \frac{3}{2} \frac{t}{\sqrt{3J_2}} \{\sigma'\} . \tag{6.113}$$

The incremental spin $\Delta\omega_{12} = -\Delta\omega_{21}$ is obtained by the following relationship:

$$\Delta\omega_{12} = \frac{\partial h_i}{\partial X^2} \Delta u_i^1 - \frac{\partial h_i}{\partial X^1} \Delta\bar{u}_i^2 , \tag{6.114}$$

where the superscript on the terms $\Delta\bar{u}^1$ and $\Delta\bar{u}^2$ denotes the displacement component, and the subscript identifies the finite element node number. For an eight-noded isoparametric element, i = 1,8.

The components of the Cauchy stress at time t+Δt are obtained from the equation

$$ {}^{t+\Delta t}\underset{\sim}{\sigma} = {}^{t}\underset{\sim}{\sigma} + \Delta {}^{t}\underset{\sim}{\sigma} \ . \qquad (6.115) $$

Note that this constitutive equation uses the same stress tensor that is required by the updated Lagrangian statement of the equations of motion.

6.10.5. Updated Hyperelastic-Viscoplastic (Explicit, Implicit)

The implementation of a hyperelastic-viscoplastic material description in which the constitutive equation is integrated using the implicit midpoint interval technique discussed in Section 5.1, follows closely the development in the preceding section. The incremental constitutive equation is given by

$$ \{\Delta\tilde{T}\} = [H]^{-1}\,[C]\,(\,\{\Delta\varepsilon\} - \{\Delta\varepsilon^{(vp)}\}) \ , \qquad (6.116) $$

where

$$ \{\Delta\tilde{T}\} = [\ \Delta\tilde{T}_{11}, \Delta\tilde{T}_{22}, \Delta\tilde{T}_{12}, \Delta\tilde{T}_{33}\ ] \qquad (6.117) $$

is the vector containing the components of the Truesdell stress increment. (Recall that the Truesdell stress increment is the change in the second Piola stress referenced to the updated or current geometry.) The remaining terms in Eq. (6.116) are defined in Section 6.10.4.

Once the node point displacement increments are obtained through an explicit integration of the equations of motion, the second Piola stress increments are obtained from Eq. (6.116). The second Piola stress at time t+Δt referenced to the configuration at time t is obtained as

$$ {}^{t+\Delta t}_{t}\tilde{\underset{\sim}{T}} = {}^{t}_{t}\tilde{\underset{\sim}{T}} + {}^{t}_{t}\Delta\tilde{\underset{\sim}{T}} \;, \tag{6.118} $$

where the left superscript identifies the time at which the quantity is known, and the left subscript identifies the time associated with the configuration to which the quantity is referenced. For example, ${}^{t+\Delta t}_{t}\tilde{\underset{\sim}{T}}$ denotes the second Piola stress at time t+Δt referenced to the geometric configuration at time t. Also, note the following relationship between the second Piola stress at time t, referenced to the geometric configuration at time t, and the Cauchy stress;

$$ {}^{t}_{t}\tilde{\underset{\sim}{T}} = {}^{t}\underset{\sim}{\sigma} \;. \tag{6.119} $$

No subscript is used with the Cauchy stress since by definition it is always referenced to the current configuration.

Equation (6.83) is used to compute the Cauchy stress at time $t+\Delta t$; that is,

$$
{}^{t+\Delta t}\sigma = \frac{{}^{t+\Delta t}\rho}{{}^{t}\rho}\; {}^{t+\Delta t}_{\ t}\underset{\sim}{G}\; {}^{t+\Delta t}_{\ t}\underset{\sim}{\tilde{T}}\; {}^{t+\Delta t}_{\ t}\underset{\sim}{G}^{T} , \qquad (6.120)
$$

where ${}^{t+\Delta t}_{\ t}\underset{\sim}{G}$ (with transpose ${}^{t+\Delta t}_{\ t}\underset{\sim}{G}^{T}$) is the deformation gradient at time $t+\Delta t$ referenced to the configuration at time t. The deformation gradient is computed by the procedures discussed in Section 6.7.

6.11. Numerical Integration of Element Volume Integrals

The governing finite element equations obtained from the rate form of the principle of virtual work (Eq. (5.56) for the implicit time integration procedure, and Eq. (5.31) for the explicit time integration procedure) require the evaluation of several volume integrals. It has become standard practice to perform these integrations using some form of Newton-Cotes integration or Gaussian Quadrature.

All numerical integration schemes require a certain number of function evaluation operations and corresponding weighting factors. For Gaussian Quadrature, the integral over the area of the parametric element is evaluated using the following equation:

$$\int_{-1}^{1}\int_{-1}^{1} f(\xi,\eta)\,d\xi\,d\eta = \sum_{j=1}^{n}\sum_{k=1}^{n} \omega_j\,\omega_k\,f(\xi_j,\eta_k) \ , \qquad (6.121)$$

where n represents the number of sampling points or function evaluation points in the element, ω_j and ω_k are appropriate weighting factors corresponding to the sampling points ξ_j and η_k. Equation (6.121) basically requires the integrand to be evaluated at n^2 predetermined values of ξ and η, called sampling points. Each function evaluation is then multiplied by appropriate weighting factors, and summed. An excellent discussion of Gaussian Quadrature and other integration techniques is given by Bathe [39].

To use Eq. (6.121), the volume integrals for the physical element must be transformed to the parametric element. For two-dimensional elements the thickness is constant, and it suffices to integrate only over the planar element area and multiply by the thickness to obtain the volume integral. For axisymmetric elements, the integrand will involve a factor of $2\pi r$; that is,

$$\int_{vol} F(r,z)r\,dr\,dz\,d\theta = 2\pi\int_{area} r\,F(r,z)\,dr\,dz \ . \qquad (6.122)$$

The right-hand side of Eq. (6.122) therefore involves only an area integration. By using Eq. (6.14), all derivatives in the integrand can be written in terms of the parametric coordinates. For more detailed treatments, the reader is referred to Bathe [39] and Zienkiewicz [59].

Subroutines in finite element programs using iso-parametric elements are therefore primarily concerned with evaluating the value of the integrand at the n^2 sampling points. The actual summation and weighting of the integrand evaluations requires only a few programming steps. FINITE provides the user with the option of using from 1 to 16 Quadrature points. Since integrand evaluations are performed at different locations in the element, it is possible to have the material at a different condition at each point. For example, it is possible to have an element which is deforming plastically at some sampling points in the element and be deforming elastically at the remaining sampling points. This is one of the powerful features inherent in the numerical integration of iso-parametric element equations.

6.12. Implicit Updated Lagrangian Analysis

This section summarizes the operations involved during an analysis which solves the incremental equations of motion using an implicit updated Lagrangian formulation.

1. Evaluate constitutive equation

$$ {}_t^t\{\Delta T\} = [D]\,{}_t^t\{\Delta E\} - [A]\,{}_t^t\{\Delta E^{(vp)}\} \ . $$

2. Strain increment-displacement increment matrix

$$ {}_t^t\{\Delta E\} = {}_t^t[B]\,{}_t^t\{\Delta \bar{u}\} \ . $$

3. Form element tangential stiffness matrix and residual load vector

$$ {}_t^t[K_T]_e = \int {}_t^t[B]^T [D]\,{}_t^t[B]\,dvol + \int {}_t^t\tilde{T}^{\alpha\beta}\, d(\delta\dot{E}_{\alpha\beta})\,dvol $$

$$ {}_t^t\{F\}_e = \int {}_t^t[B]^T \left({}_t^t\{\tilde{T}\} + [D]\,{}_t^t\{\Delta E^{(vp)}\}\right)dvol \ . $$

4. Form system matrices

$$ {}_t^t[K_{eff}] = \frac{1}{\alpha\Delta t^2}[M] + \frac{\delta}{\alpha\Delta t}[C] + [K_T] $$

$$ {}^{t+\Delta t}\{R_{eff}\} = {}^{t+\Delta t}\{R\} + [M]\left\{\frac{1}{\alpha\Delta t}\,{}^t\dot{\underset{\sim}{u}} + \left(\frac{1}{2\alpha} - 1\right){}^t\ddot{u}\right\} $$

$$ + [C]\left\{\left(\frac{\delta}{\alpha} - 1\right){}^t\dot{\underset{\sim}{u}} + \left(\frac{\delta}{2\alpha} - 1\right){}^t\ddot{\underset{\sim}{u}}\,\Delta t\right\} - {}_t^t\{F\} $$

5. Solve for incremental displacements

$$ {}^{t}_{t}[K_{eff}]\{\Delta\bar{u}\} = {}^{t+\Delta t}_{t}\{R_{eff}\} . $$

6. Compute element stress increments

$$ {}^{t}_{t}\{\Delta\tilde{T}\} = [D]\,{}^{t}_{t}[B]\{\Delta\bar{u}\} - [A]\,{}^{t}_{t}\{\Delta E^{(vp)}\} . $$

7. Compute total stress

$$ {}^{t+\Delta t}_{t}\{\tilde{T}\} = {}^{t}_{t}\{\tilde{T}\} + {}^{t}_{t}\{\Delta\tilde{T}\} . $$

8. Update geometry

$$ {}^{t+\Delta t}\{x\} = {}^{t}\{X\} + {}^{t}_{t}\{\Delta\bar{u}\} . $$

9. Compute deformation gradient

$$ {}^{t+\Delta t}_{t}[G] = [({}^{t+\Delta t}x, {}^{t}X)] . $$

10. Update stresses to current configuration

$$ {}^{t+\Delta t}_{t}\underset{\sim}{\tilde{T}} = \frac{{}^{t+\Delta t}\rho}{{}^{t}\rho}\,{}^{t+\Delta t}_{t}\underset{\sim}{G}\,{}^{t+\Delta t}_{t}\underset{\sim}{\tilde{T}}\,{}^{t+\Delta t}_{t}\underset{\sim}{G}^{T} . $$

11. Go to Step 1 to start next time step.

6.13. Implicit Total Lagrangian Analysis

This section summarizes the operations involved during an analysis which solves the incremental equations of motion using a total Lagrangian formulation.

1. Evaluate constitutive equation

$$ {}^{t}_{t_o}\{\Delta T\} = [D]\,{}^{t}_{t_o}\{\Delta E\} - [D]\,{}^{t}_{t_o}\{\Delta E^{(vp)}\} \ . $$

2. Strain increment-displacement increment matrix

$$ {}^{t}_{t_o}\{\Delta E\} = {}^{t}_{t_o}[B]\{\Delta \bar{u}\} \ . $$

3. Form element tangential stiffness matrix and load vector

$$ {}^{t}_{t_o}[K_T]_e = \int {}^{t}_{t_o}[B]^T[D]\,{}^{t}_{t_o}[B]\,dvol + \int {}^{t}_{t_o}\tilde{T}^{\alpha\beta}\ d(\delta \dot{E}_{\alpha\beta})\,dvol \ . $$

$$ {}^{t}_{t_o}\{F\}_e = \int {}^{t}_{t_o}[B]^T({}^{t}_{t_o}\{\tilde{T}\} + [D]\,{}^{t}_{t_o}\{\Delta E^{(vp)}\})\,dvol \ . $$

4. Form system matrices

$$ {}^{t}_{t_o}[K_{eff}] = \frac{1}{\alpha \Delta t^2}[M] + \frac{\delta}{\alpha \Delta t}[C] + {}^{t}_{t_o}[K_T] \ . $$

$$ {}^{t+\Delta t}_{t_o}\{R_{eff}\} = {}^{t+\Delta t}\{R\} + [M]\{\frac{1}{\alpha\Delta t}\ {}^{t}\dot{\underset{\sim}{u}} + (\frac{1}{2\alpha} - 1)\ {}^{t}\ddot{\underset{\sim}{u}}\} $$

$$ + [C]\{(\frac{\delta}{\alpha} - 1)\ {}^{t}\dot{\underset{\sim}{u}} + (\frac{\delta}{2\alpha} - 1)\{{}^{t}\ddot{\underset{\sim}{u}}\Delta t\} - {}^{t}_{t_o}\{F\} \ . $$

5. Solve for incremental displacements

$$ {}^{t}_{t_o}[K_{eff}]\{\Delta\bar{u}\} = {}^{t+\Delta t}_{t_o}\{R_{eff}\} \ . $$

6. Compute element stress increments

$$ {}^{t}_{t_o}\{\Delta\tilde{T}\} = [D]{}^{t}_{t_o}[B]\{\Delta\bar{u}\} - [D]{}^{t}_{t_o}\{\Delta E^{(vp)}\} \ . $$

7. Compute total stress

$$ {}^{t+\Delta t}_{t_o}\{\tilde{T}\} = {}^{t}_{t_o}\{\tilde{T}\} + {}^{t}_{t_o}\{\Delta\tilde{T}\} \ . $$

8. Go to Step 1 to start next time step.

6.14. Explicit Updated Lagrangian Analysis

This section summarizes the operations involved during an analysis which solves the equations of motion using an explicit updated Lagrangian formulation.

1. Compute strain increment-displacement matrix

$$ {}_t^t\{\Delta E\} = {}_t^t[B]\{\Delta\bar{u}\} \ . $$

2. Compute element internal force vector

$$ {}_t^t\{I\}_e = \int {}_t^t[B]\,{}_t^t\{\tilde{T}\}dvol \ . $$

3. Form system mass, $\{M\}$, external force, $\{E\}$, and internal force, $\{I\}$, vectors.

4. Compute displacements at $t+\Delta t_2$

$$ {}^{t+\Delta t_2}\{\bar{u}\} = {}^t\{\bar{x}\} + \frac{\Delta t_2}{\Delta t_1}\,[{}^t\{\bar{x}\} - {}^{t-\Delta t_1}\{\bar{x}\}] $$

$$ + \frac{1}{2}(\Delta t_2 + \Delta t_1)\Delta t_2\{M\}^{-1}({}_t^t\{E\} - {}_t^t\{I\}) . $$

5. Compute displacement increments

$$ {}^t\{\Delta\bar{u}\} = {}^{t+\Delta t_2}\{\bar{x}\} - {}^t\{\bar{x}\} \ . $$

6. Evaluate constitutive equation

$$ {}_t^t\{\Delta T\} = [D]\,{}_t^t\{\Delta E\} - [A]\,{}_t^t\{\Delta E^{(vp)}\} \ . $$

7. Compute stress increments

$$ {}_{t}^{t}\{\Delta\tilde{T}\} = [D]\,{}_{t}^{t}[B]\{\Delta\bar{u}\} - [A]\,{}_{t}^{t}\{\Delta E^{(vp)}\} \;. $$

8. Obtain total stresses

$$ {}_{t}^{t+\Delta t}{}^{2}\{\tilde{T}\} = {}_{t}^{t}\{\tilde{T}\} + {}_{t}^{t}\{\Delta\tilde{T}\} \;. $$

9. Update geometry

$$ {}^{t+\Delta t}{}^{2}\{\bar{x}\} = {}^{t}\{\bar{X}\} + {}^{t}\{\Delta\bar{u}\} \;. $$

10. Compute deformation gradient

$$ {}_{t}^{t+\Delta t}{}^{2}[G] = [\,(\,{}^{t+\Delta t}{}^{2}\bar{x},{}^{t}\bar{X}\,)\,] \;. $$

11. Update stresses to current configuration

$$ {}_{t}^{t+\Delta t}{}^{2}\underset{\sim}{\tilde{T}} = \frac{{}^{t+\Delta t}\rho}{{}^{t}\rho}\;{}_{t}^{t+\Delta t}{}^{2}\underset{\sim}{G}\;{}_{t}^{t+\Delta t}{}^{2}\underset{\sim}{\tilde{T}}\;{}_{t}^{t+\Delta t}{}^{2}\underset{\sim}{G}^{T} \;. $$

Depending on the particular constitutive law, this operation may not be required.

12. Go to Step 1 to start next time step.

CHAPTER VII

NUMERICAL EXAMPLES

Much of the experimental data used to develop constitutive descriptions are limited to small strains and are usually uniaxial in nature. Therefore, the extension of these theories to finite strain environments relies heavily on mathematics and invariance principles. To compound the problem, the macroscopic quantities, such as displacements and force, are often the only quantities which can be obtained from experiments involving severe environments. Therefore, numerical calculations which relate these macroscopic quantities to constitutive variables are important.

In this chapter, numerical examples are presented which enable different aspects of the constitutive equations and solution techniques presented in the preceding chapters to be evaluated. The first problem is frequently referred to as Taylor's cylinder and involves a right circular cylinder impacting on a rigid wall. The second problem is a cantilevered beam subjected to a triangular pulse. The basic reason for choosing these two problems is to compare the finite-strain, elastic-viscoplastic constitutive equations presented in Chapter IV. Both problems involve dynamic plasticity at finite strain.

7.1. Taylor's Cylinder

Taylor's cylinder problem involves a right circular cylinder impacting a rigid wall as illustrated in Figure 7.1. The problem was first presented by G. Taylor [60] as a method for determining the dynamic yield stress of metals. Taylor presented a simplistic one-dimensional wave propagation analysis to determine the final shape of the cylinder and a procedure for determining the dynamic yield stress of the material. The following excerpts from Taylor's paper provide an interesting insight into the problem as Taylor envisioned it:

> When a cylindrical projectile strikes perpendicularly on a flat rigid target, the stress at the impact end immediately rises to the elastic limit, and an elastic compression wave travels toward the rear end. The stress in this wave is equal to the elastic limit. If the material is one in which the stress rises when the strain exceeds that corresponding with the elastic limit, the elastic wave is followed by a plastic one. On reaching the rear end of the projectile, the elastic wave is reflected as a wave of tension which is superposed on the compression wave. . . . The reflected wave runs forward along the projectile until it meets the front of the plastic wave advancing from the front of the target plate. In this plastic wave, the stress will not rise appreciably above the yield stress at any point close to the plastic-elastic boundary, but the velocity may be nearly zero, or, at any rate, will be very different from that in the rear part where plastic flow has not taken place. At the moment when the reflected wave has just reached the plastic boundary, the part of the specimen which lies behind this is stress-free, and is moving as a rigid body. . . . To obtain a simplified picture of the phenomenon to serve as a framework for thinking about the motion, the simplest possible assumption about the plastic-strain relationship was made, namely, that the

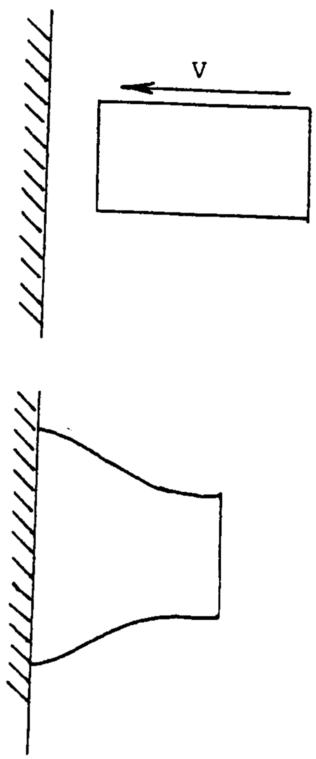

Figure 7.1. Taylor's Cylinder Problem.

stress in the part of the projectile where the material is yielding is constant and equal to the yield stress S. Further, the radial inertia is neglected, so that the stress can be considered as constant over any cross-section.

Taylor's analysis is based on an incompressible, rigid, perfectly plastic material constitutive equation. The computed shape of a projectile for several impact velocities and stages of deformation is shown in Figure 7.2.

Presented simultaneously with Taylor's theoretical considerations, were Whiffin's [61] results of experiments for various metallic materials. Figure 7.3 shows the correlation between Tayor's theoretical model and Whiffin's experimental results for mild steel. Figure 7.4 shows the profiles of several test cylinders for various impact velocities. It is interesting to note how well Taylor's theory computed the final length of the test specimens, even though the theoretical shape (radial distortion) does not agree well with the experimental specimens for impact velocities above 810 ft/sec.

Lee and Tupper [62] presented a modification to Taylor's theory by considering an elastic-plastic material constitutive equation, and used the specific example of a nickel-chrome steel cylinder. This example was chosen since the material did not exhibit a significant amount of strain rate sensitivity.

Raftopoulos and Davids [63] considered the effects of different material constitutive equations on the profiles

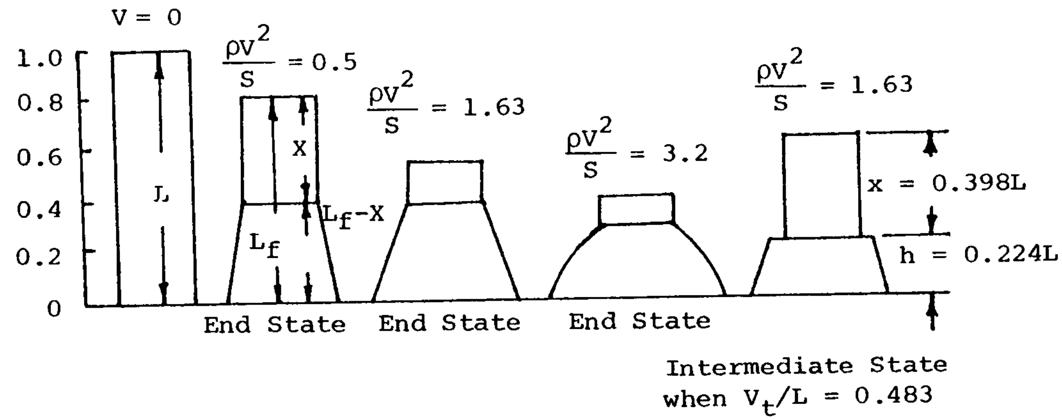

Figure 7.2. Taylor's Computed Projectile Profiles [60].

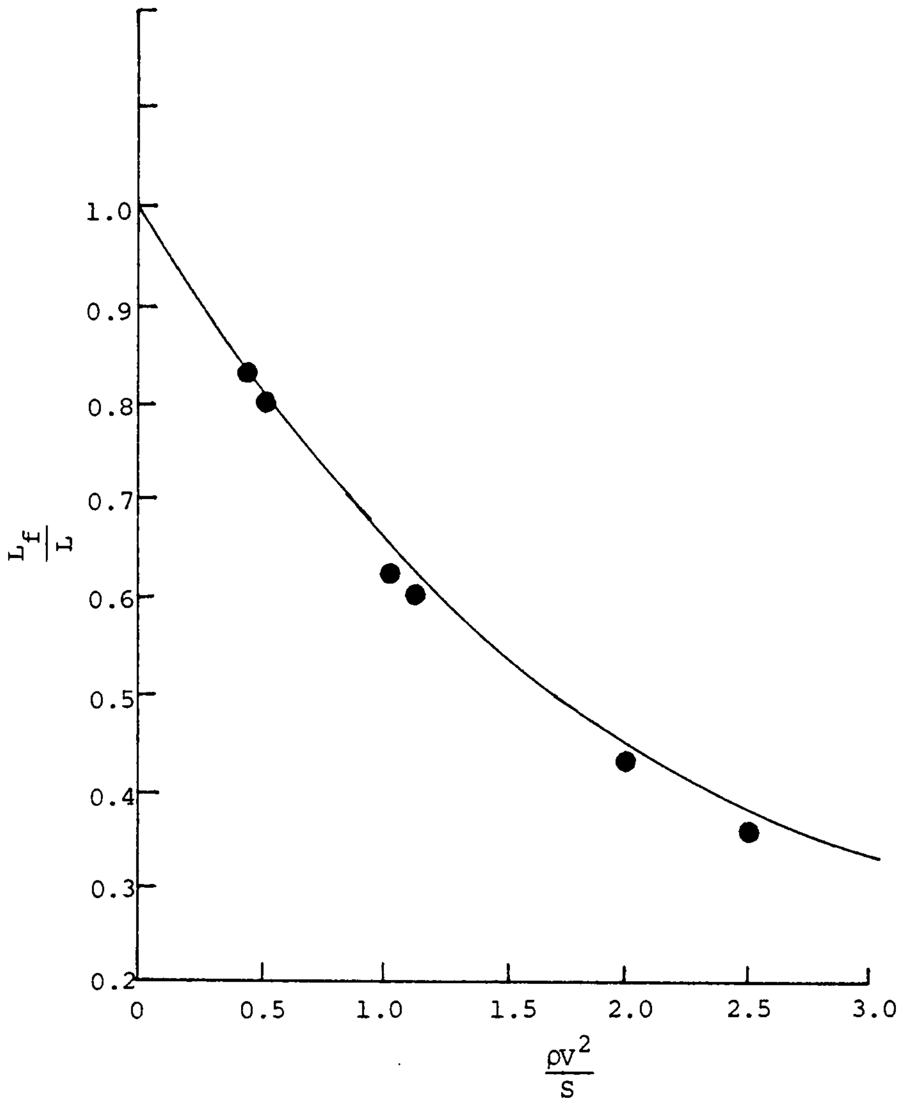

Figure 7.3. Comparison of Taylor's Theory with Whiffin's Experimental Data [60].

Figure 7.4. Profiles of Impacted Cylinders [60].

and final length of the cylinders. In particular, the following constitutive descriptions were considered: (1) rigid, perfectly plastic; (2) elastic, perfectly plastic; (3) rigid, linear work-hardening; (4) elastic, linear work- hardening; and (5) Malvern's one-dimensional stress-strain relation. Raftopoulos and Davids concluded that the assumption of one-dimensional motion in plastic impact can give satisfactory agreement with actual profiles, provided a "certain" amount of work-hardening is accounted for.

Wilkins and Guinan [64] performed a detailed study of the Taylor's cylinder problem using the finite-difference computer program HEMP. The calculations used equation-of- state data obtained from Hugoniot shock wave experiments and ultrasonic measurements. The dynamic yield stresses for the materials under consideration were obtained by a trial- and-error method, in which the yield stress was modified until the experimental and analytical data agreed. Based on these computations, Wilkins and Guinan concluded that at large strains, there is a limiting strain rate above which strain rate effects are insignificant. The effects of mass loss and target flexibility have been considered by Recht [65].

Fukuoka and Toda [66] computed the response of a mild steel cylinder described by an elastic-viscoplastic constitutive equation of the Perzyna type. The governing equations were integrated using the method of characteristics approach. The boundaries of the elastic and viscoplastic regimes are shown in Figure 7.5 for three instances in time following the impact.

Recently, Argyris [46] presented the results of computations performed using an explicit finite element computer program for the nickel-chrome steel cylinder studied by Lee. Excellent agreement between the computed and experimental profiles was obtained. Recall that the nickel-chrome steel material exhibits no significant strain rate sensitivity.

In the current investigation, the Taylor's cylinder problem is considered for an aluminum alloy (6061-T6) which exhibits a moderate amount of strain rate sensitivity. In particular, comparisons are made between the numerical results obtained using the various finite strain, elastic-viscoplastic constitutive equations presented in Chapter IV.

7.2. Dynamic Material Properties for 6061-T6 Aluminum

The mechanical properties of 6061-T6 aluminum at high strain rates have been studied by Hoge [11]. Representative stress-strain curves at various strain rates and temperatures are shown in Figure 2.3, page 12. The static stress- strain curve used in this analysis is shown in Figure 7.6. The updated Lagrangian-based constitutive

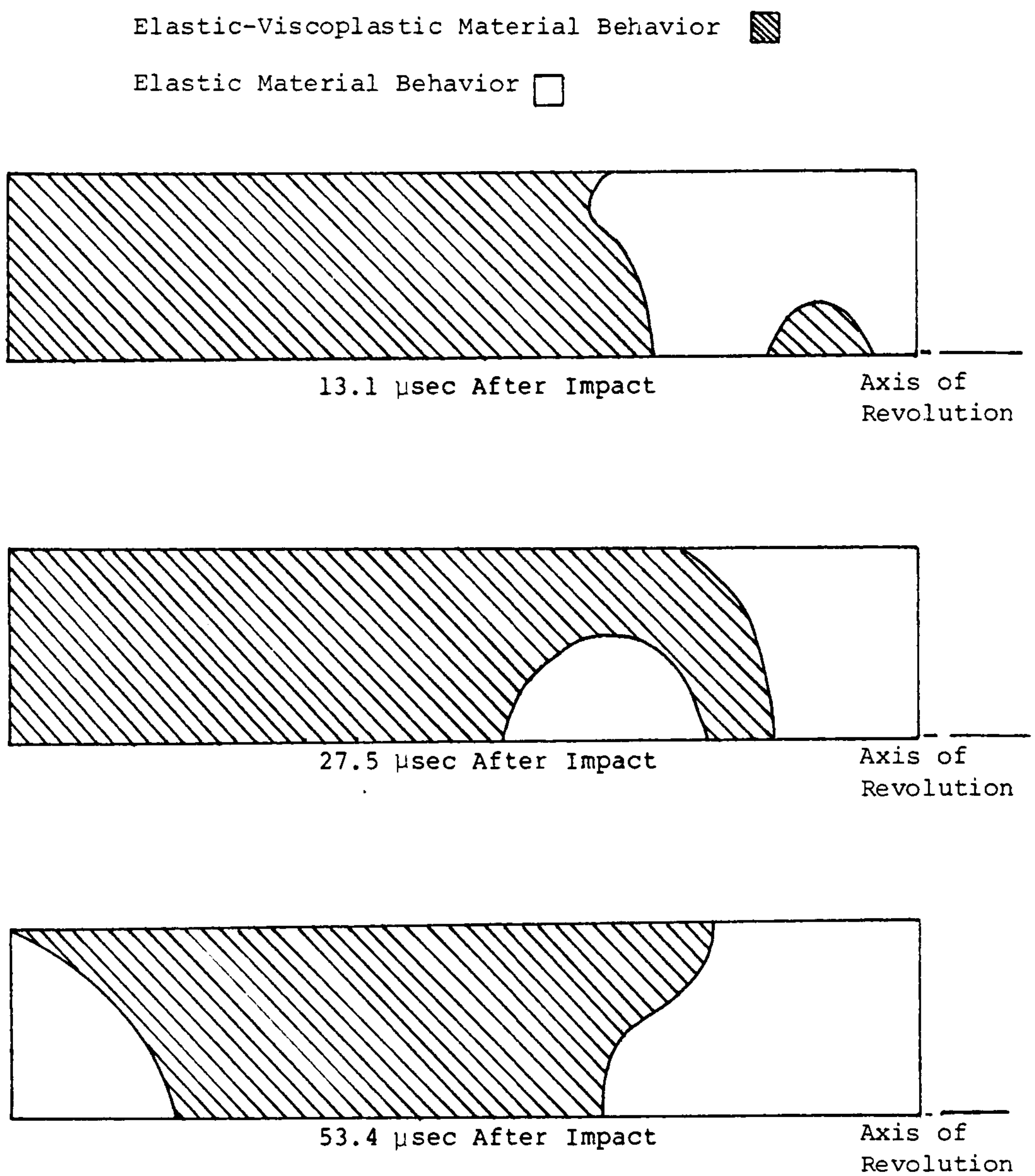

Figure 7.5. Viscoplastic Zones Computed by Fukuoka and Toda [66].

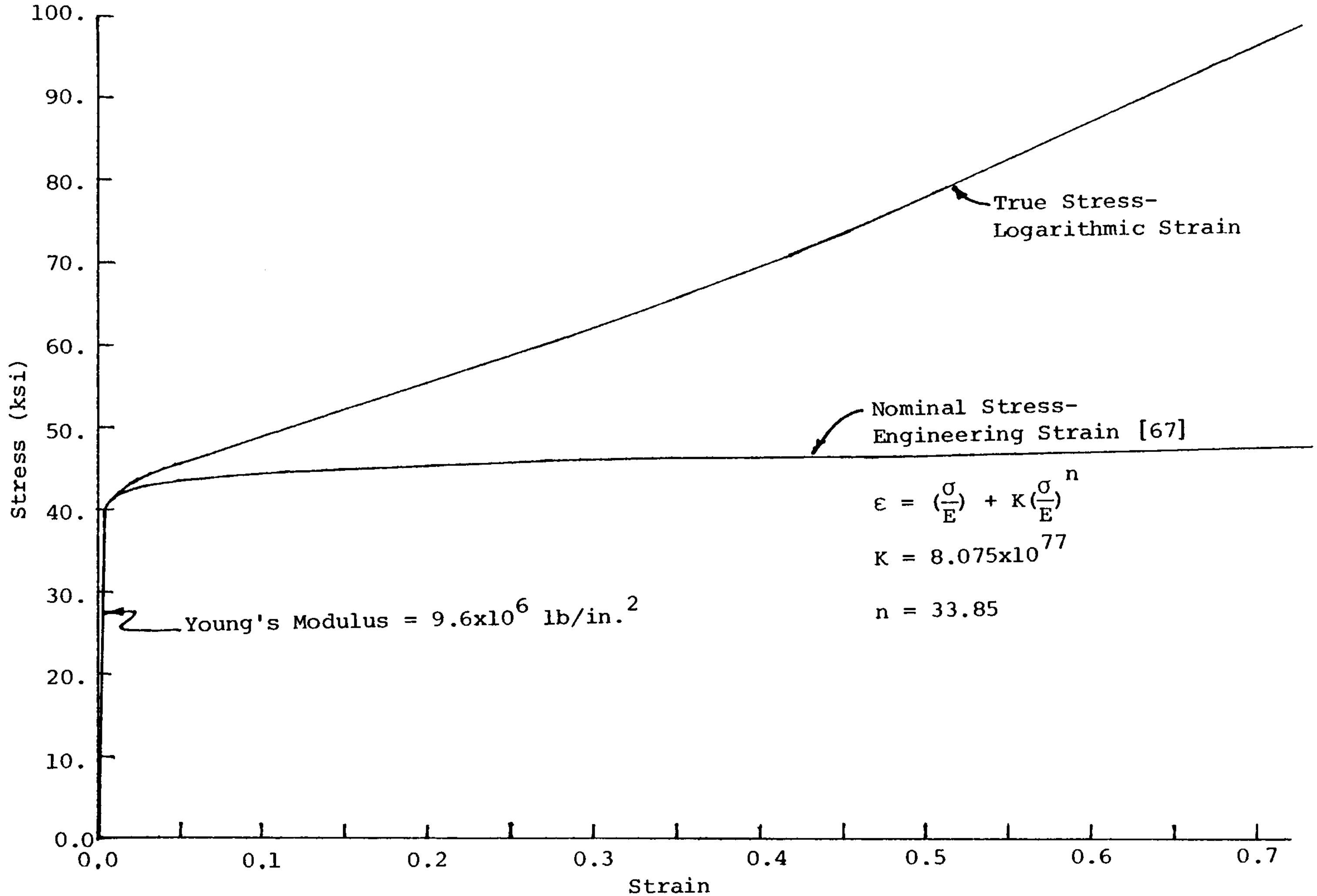

Figure 7.6. Static Stress-Strain Curves for 6061-T6 Aluminum.

equations employed the true stress-logarithmic strain curve, and the total Lagrangian-based constitutive equations utilized the engineering stress-engineering strain curve. The curves shown in Figure 7.6 are based on tension tests.

The dynamic yield stress as a function of strain rate is shown in Figures 7.7 and 7.8. The curve in Figure 7.7 was presented by Parkes [68], and represents an average curve for aluminum which is based upon available literature data for various alloys. The data in Figure 7.8 were presented by Hoge [11] for aluminum alloy 6061-T6. Most of the computations were performed using a uniaxial Perzyna-type flow rate given by

$$\dot{\varepsilon}^{(P)} = 6{,}500 \left(\frac{\sqrt{3J_2}}{\phi(\overline{\varepsilon})} - 1 \right)^4 . \tag{7.1}$$

The above equation is consistent with the expression given in Figure 7.7, but also scales the subsequent yield surfaces by the same amount as the initial yield stress.

A review of the computational results presented in later sections revealed that computations performed using Eq. (7.1) did not agree well with experimental data. To obtain satisfactory agreement, it was necessary to increase the strain rate sensitivity parameter in Eq. (7.1) from 6,500 to 650,000. At the same time that this activity was underway, the experimental data of Hoge (Figure 7.8) was

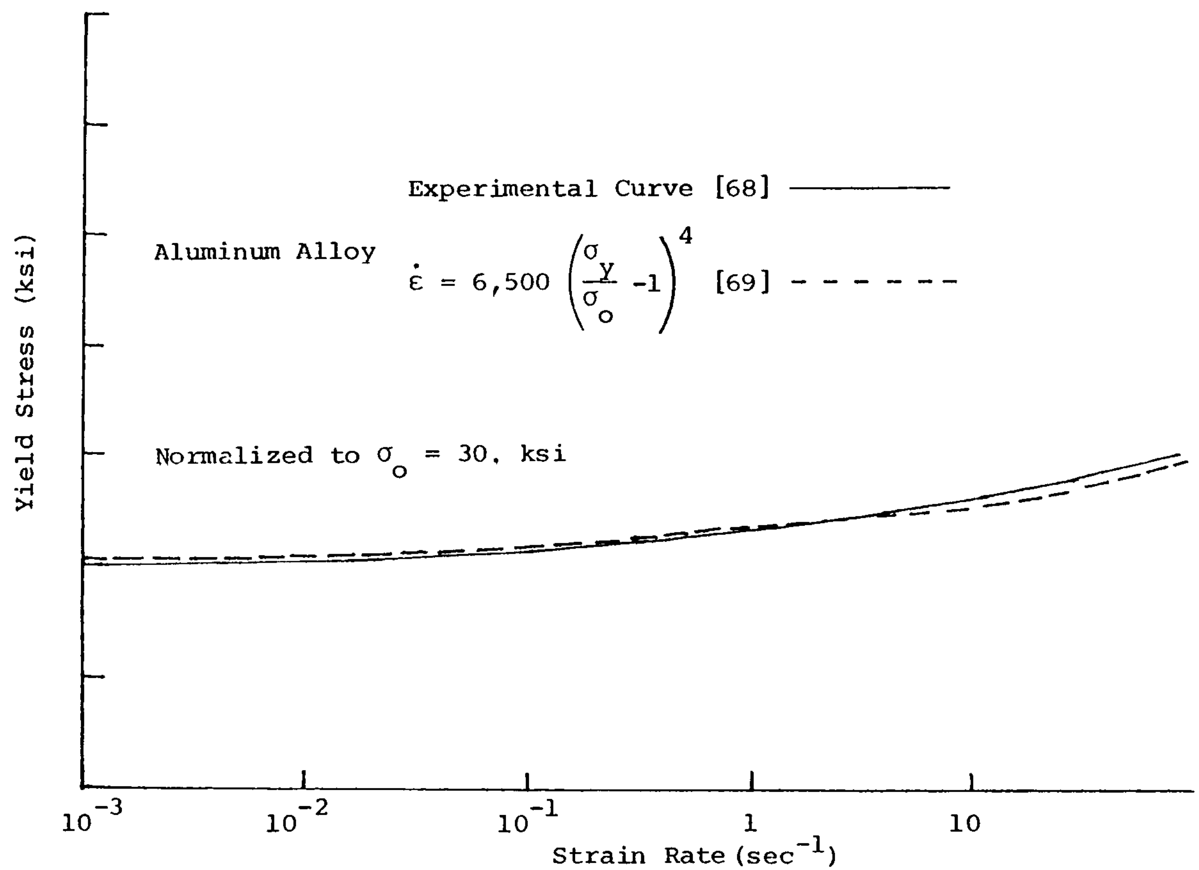

Figure 7.7. Dynamic Yield Stress versus Strain Rate.

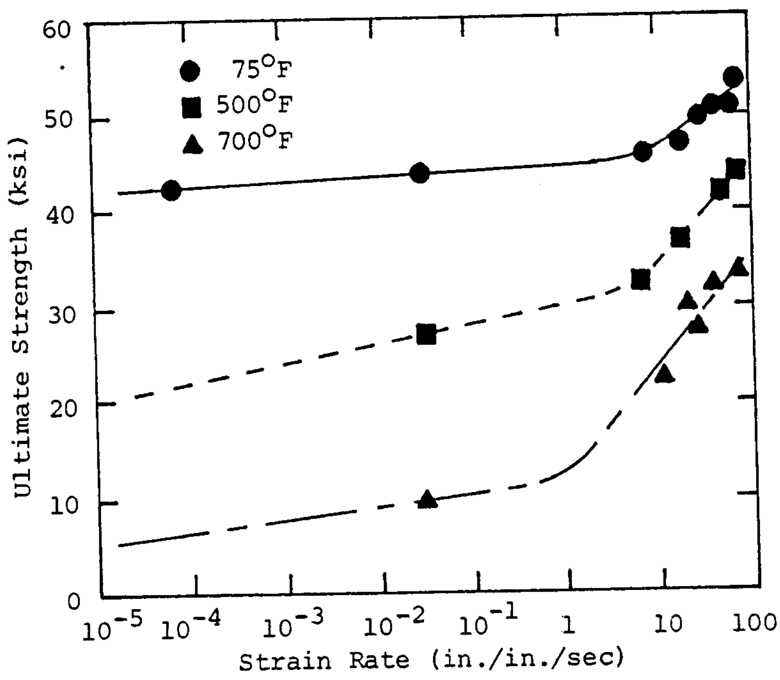

Figure 7.8. Effect of the Logarithm of Strain Rate on the Tensile Strength of 6061-T6 Aluminum [11].

found. Based on Hoge's data, a suitable uniaxial flow rule was found to be

$$\dot{\varepsilon}^{(vp)} = \exp\left(\frac{\frac{\sqrt{3J_2}}{2} - \phi(\bar{\varepsilon})}{2,388}\right) . \qquad (7.2)$$

Equation (7.2) was implemented during this investigation. However, very few numerical results were obtained because of problems encountered in computing the function $y = e^x$ when x is a large number. The VAX 11/780 computer used in this study was not capable of evaluating the function $y = e^x$ for a value of x greater than 88. Time did not permit the development of a special algorithm to circumvent the problem. However, for the strain rates involved, Eq. (7.2) agrees well with Eq. (7.1) when a strain rate sensitivity parameter of 650,000 sec^{-1} is used in Eq. (7.1).

In all the constitutive equations, the material bulk modulus was considered to be constant. Therefore, it was necessary to consider impact velocities small enough to ensure that a more complicated equation of state was not required. For higher impact velocities, and corresponding hydrostatic pressures, a suitable equation of state for aluminum is given by Wilkins [70].

7.3 Numerical Results for Taylor's Cylinder

The dimensions of the impact cylinder and the axisymmetric finite element mesh used in these analyses are shown in Figure 7.9. The cylinder has the same dimensions as the cylinder utilized by Lee [62] and Argyris [46].

The centerline displacement of the free end of the cylinder is shown as a function of time for various impact velocities and constitutive descriptions in Figure 7.10. Curves 5, 6, and 7 of Figure 7.10 were computed using an updated hyperelastic-viscoplastic constitutive description, with impact velocities of 8,000., 6,000., and 4,000. in./sec, respectively. For an impact velocity of 8,000. in./sec, the ratio of the impact velocity to the bar wave speed for the material is 0.04. Since an updated Lagrangian-type formulation was used, the true stress-logarithmic strain curve in Figure 7.6, page 192, was used. A strain rate sensitivity parameter of 6,500. sec^{-1} was used in all three computations. A comparison of curves 5, 6, and 7 shows the effect of increasing the impact velocity, which will be discussed in more detail later in this section.

Curve 5 also presents the results for a hypoelastic-viscoplastic formulation. The computed results for both the updated hyperelastic-viscoplastic and hypoelastic-viscoplastic constitutive formulations were nearly identical, and are shown as a single curve. Curve 4 was computed using a hyperelastic-viscoplastic constitutive formulation. Since the kinetic and kinematic variables used in the hyperelastic-viscoplastic constitutive equations are referenced to the original configuration, the

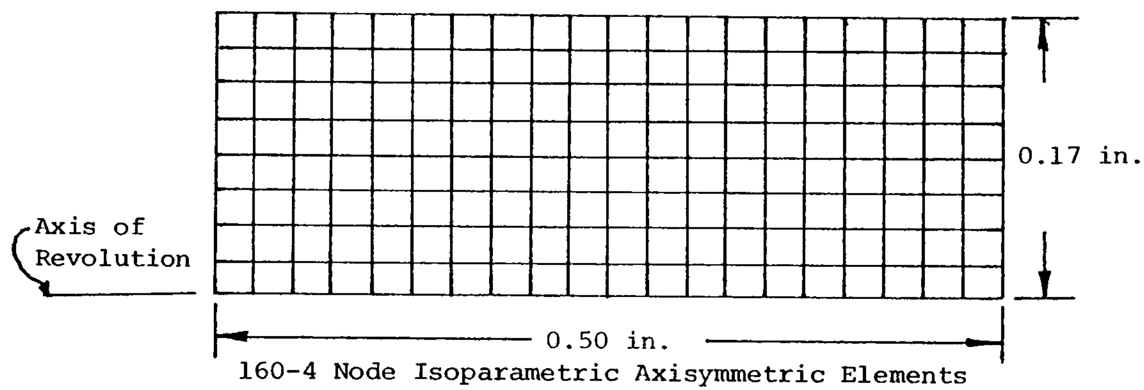

Figure 7.9. Finite Element Mesh Used in Computations for Taylor's Cylinder Problem.

Figure 7.10. Centerline Displacement at Free End of Cylinder for Various Impact Velocities and Constitutive Descriptions.

1. Hypoelastic-plastic, impact velocity = 8,000. in./sec.

2. Updated hyperelastic-viscoplastic,
impact velocity = 8,000. in./sec;
material viscosity = 650,000. sec^{-1}.

3. Hypoelastic-viscoplastic,
impact velocity = 8,000. in./sec;
material viscosity = 650,000. sec^{-1}.

4. Hyperelastic-viscoplastic,
impact velocity = 8,000. in./sec;
material viscosity = 6,500. sec^{-1}.

5. Updated hyperelastic-viscoplastic and
hypoelastic-viscoplastic,
impact velocity = 8,000. in./sec;
viscosity parameter = 6,500. sec^{-1}.

6. Updated hyperelastic-viscoplastic,
impact velocity = 6,000. in./sec;
material viscosity = 6,500. sec^{-1}.

7. Updated hyperelastic-viscoplastic,
impact velocity = 4,000. in./sec;
material viscosity = 6,500. sec^{-1}.

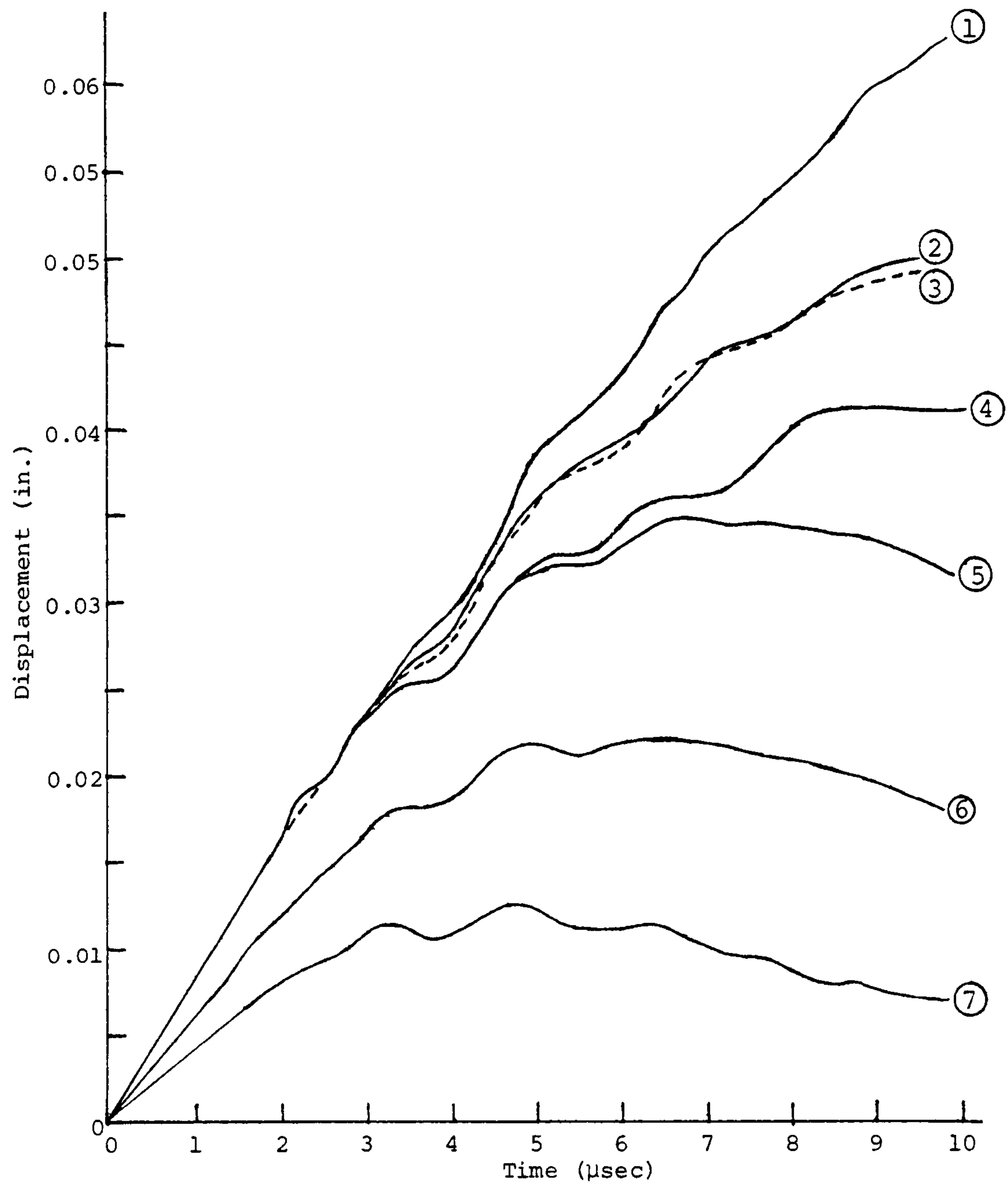
Displacement (in.)
0.06
0.05
0.05
0.04
0.03
0.02
0.01
0
Time (μsec)
0
1
2
3
4
5
6
7
8
9
10
1
2
3
4
5
6
7

Figure 7.10.

nominal stress-engineering strain curve in Figure 7.6, page 192, was used. Note that curve 4 obtains a significantly higher free end centerline displacement than does curve 5. Also, curves 4 and 5 were computed using the same impact velocity, strain rate sensitivity parameter, and power law exponents.

Based on curves 4 and 5, one can conclude that for the same impact velocity, strain rate sensitivity parameter, and power law exponent, the updated hyperelastic-viscoplastic and hypoelastic-viscoplastic constitutive equations yield similar numerical results for Taylor's cylinder problem. However, the numerical results obtained using a hyperelastic-viscoplastic constitutive equation may be significantly different. The difference may be accounted for by considering the increase in the area over which the Cauchy stress acts as the cylinder deforms. During deformation, the impact end of the cylinder expands radially, with a corresponding increase in cross-sectional area. Therefore, for a given force level acting on a cross-section of the cylinder, the Cauchy stress will be lower than the corresponding component of the second Piola stress which is based on the initial (smaller) cross-sectional area. Therefore, the overstress computed using the second Piola stress will be higher than the overstress computed using the Cauchy stress. Since the overstress will be higher for the second Piola stress, the corresponding viscoplastic strain rate will be higher, and result in more inelastic deformation.

To obtain similar results from the updated hyperelastic-viscoplastic/hypoelastic-viscoplastic formulations, it will be necessary to use a strain rate sensitivity parameter and power law exponent consistent with the continuum mechanics formulation used to perform the computations. For example, if a split Hopkinson bar experiment is used to obtain the dynamic yield stress data, the original cross-sectional area of the specimen is readily available. Therefore, split Hopkinson bar data based on the original cross-sectional area of the specimen must be converted to the instantaneous area for use with a hypoelastic-viscoplastic constitutive equation.

Curves 2 and 3 of Figure 7.10 provide another comparison of the updated hyperelastic-viscoplastic and hypoelastic-viscoplastic constitutive formulations. These curves again indicate that the two formulations yield similar results, which was pointed out earlier during the discussion concerning curve 5. Curves 2 and 3 are based on a strain rate sensitivity parameter of 650,000. sec^{-1}, while curve 5 is based on a strain rate sensitivity parameter of 6,500. sec^{-1}. Note that as the strain rate sensitivity parameter increases, the strain rate sensitivity of the material decreases. As seen in Figure 7.10, an increase in the strain rate sensitivity parameter from 6,500. sec^{-1}

to 650,000. sec^{-1}, moved curve 5 to curves 2 and 3, which approaches the inviscid plasticity results shown as curve 1.

The average dynamic yield stress on the impact face of the cylinder is shown in Figure 7.11, for an impact velocity of 8,000. in./sec. Figure 7.12 shows the results of these calculations compared to the experimental data of Whiffin. For an impact velocity of 8,000. in./sec, the final length of an experimentally impacted cylinder should be 0.45 in. for an initial length of 0.5 in. The final computed length using a strain rate parameter of 6,500. sec^{-1} was found to be 0.468 in., and the "average flow stress" in the cylinder was computed to be 92,000 psi. For a strain rate sensitivity parameter of 650,000. sec^{-1}, the computed final length and "average flow stress" were found to be 0.45 in. and 66,000. psi, respectively. It is seen from Figure 7.11 that the results obtained when a strain rate sensitivity parameter of 650,000. sec^{-1} was used, agree more closely with the experimental data.

Wilkins and Guinan concluded that the "average dynamic flow stress" for 6061-T6 aluminum was 60,900 psi. Therefore, these computations agree, at least in principle, with the computations of Wilkins and Guinan. However, a more thorough comparison reveals that the extent of the propagation of the inelastic wave is greater for the present computations than those presented by Wilkins and Guinan. Part of the difference may be associated with the

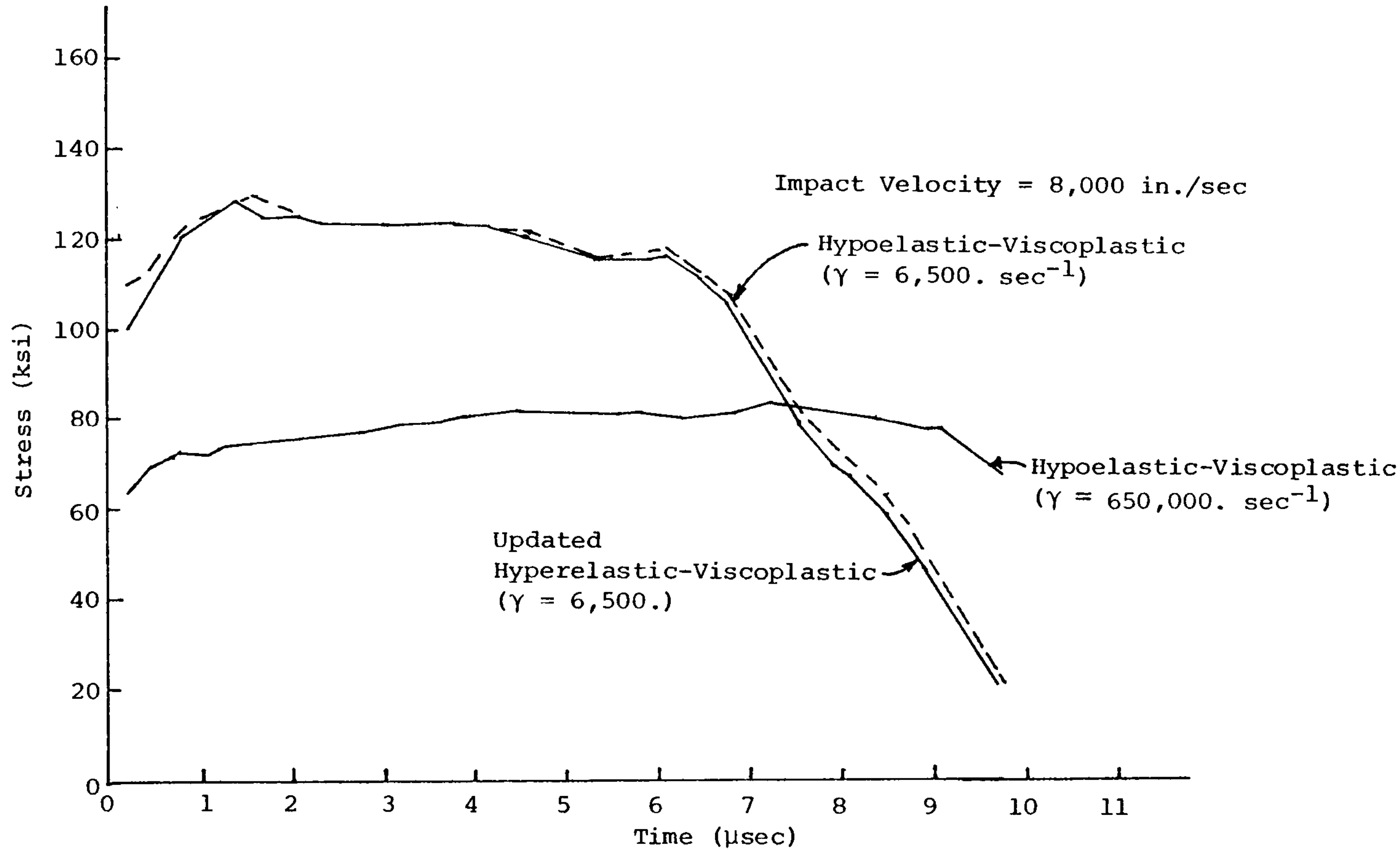

Figure 7.11. Average Dynamic Yield Stress on the Impact Face of the Cylinder.

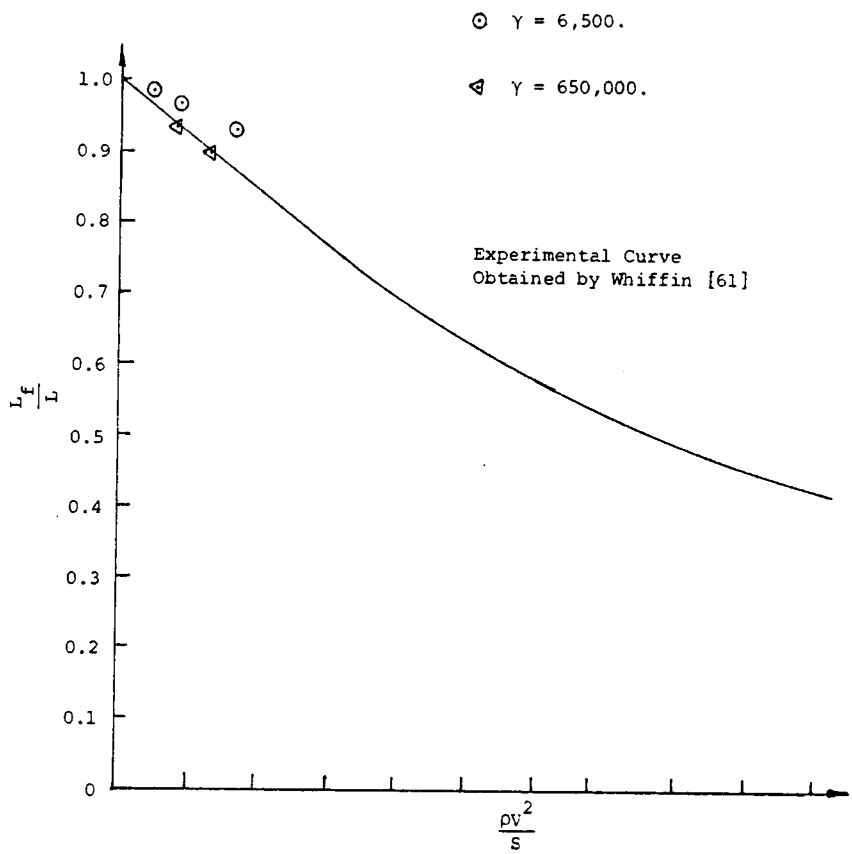

Figure 7.12. Comparison with Experimental Data of Whiffin.

different equations of state used to relate the hydrostatic pressure and density of the material.

Figures A.1 through A.34, in the Appendix, contain a sequence of yield surface and equivalent plastic strain contour plots for an impact velocity of 8,000. in./sec. A hypoelastic-viscoplastic constitutive description using a strain rate sensitivity parameter of 650,000. sec^{-1} was used in the computations from which the contour plots were obtained. It is interesting to watch the propagation of the elastic wave after impact, by successively leafing through the plots. It can also be seen that, in many regions, a very complex two-dimensional stress profile exists. A comparison of these contour plots with the results presented by Fukuoka and Toda (Figure 7.5, page 191) reveals the same characteristic shape for the viscoplastic region at various instances of time after impact.

Figure A.1 shows the yield function contours 0.148 sec after impact. The densely packed vertical contours represent the elastic wave front. Figures A.3, A.5, A.7, and A.9 show the elastic wave front as it progresses down the length of the cylinder. Note that the elastic wave front propagates basically as a planar wave in these figures. The contours to the left of the elastic wave front indicate that the inelastic deformation exhibits a moderate amount of two-dimensional variation.

Figures A.11, A.13, A.15, A.17, A.19, A.21, A.23, A.25, A.27, A.29, A.31, and A.33 show yield function contours after the elastic wave has reflected off the free-end of the cylinder. In these figures the yield functions display a significant amount of two-dimensional variation, and it is not always possible to see an elastic wave front. Figures A.2, A.4, A.6, A.8, A.10, A.12, A.14, A.16, A.18, A.20, A.22, A.24, A.26, A.28, A.30, A.32, and A.34 show the development and extent of the inelastic deformation. Note the one-dimensional character of the inelastic deformation.

The hyperelastic-viscoplastic computations were performed using the implicit time integration scheme presented in Chapter V. The hypoelastic-viscoplastic and updated hyperelastic-viscoplastic computations were performed using both the explicit and implicit time integration techniques. Computer CPU run times for the implicit integration scheme were typically two and one-half hours on a VAX 11/780. Equally important, the implicit algorithm had typical machine resident times of five hours. In one instance, a run was made which used approximately 11 hours of CPU time, and resided in the machine for approximately 26 hours. The explicit time integration scheme had typical CPU times of 40 minutes, and machine residency times of 42 minutes. The implicit procedure suffered from having to recompute and solve the system matrices at each time step, and also was very IO oriented.

As observed by other researchers, the explicit time integration procedure is far superior to the implicit algorithm for hyperbolic-type problems.

To obtain stable solutions using the explicit constitutive equation discussed in Section 5.1, it was necessary to use a time step of 2.0×10^{-8} sec. The implicit constitutive equation was stable when the time step was selected based on the amount of time required for an elastic wave to propagate across the minimum length of an element face. Therefore, the implicit constitutive equation imposed no additional time step restrictions on the explicit or implicit time integration procedures.

7.4 Cantilevered Beam Subjected to Triangular Impulse

Taylor's cylinder problem involves finite strains, with the rotations being of less importance. The second problem considered is a cantilevered beam subjected to a triangular impulse, and dominated by large rotations; the stretching components of the strain are considered infinitesimal. Figure 7.13 gives properties for a fictitious material used in the analysis, and shows the time history response of the cantilever tip. The results of this numerical experiment indicate that the three material descriptions yield almost identical results. The hypoelastic and updated hyperelastic-viscoplastic descriptions

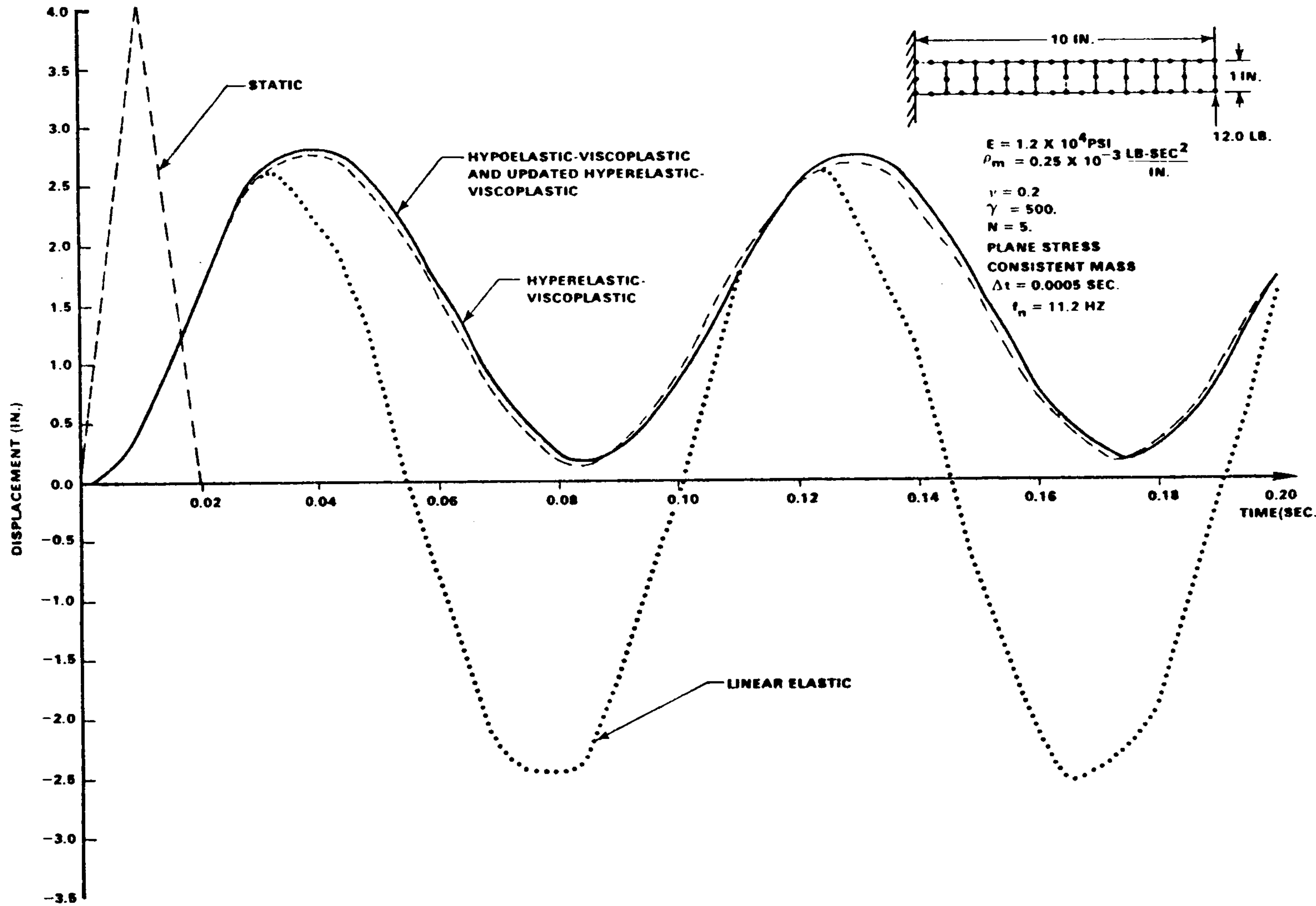

Figure 7.13. Response of an Elastic-Viscoplastic Cantilever Beam.

predicted a slightly larger permanent set than did the hyperelastic-viscoplastic material description. Therefore, it can be concluded that when the dilatational strains are infinitesimal, the same strain rate sensitivity parameter and power law exponent can be used with the three constitutive formulations without significantly influencing the computational results.

All three material descriptions were integrated using the explicit constitutive equations, in conjunction with the implicit time integration procedure. The solution was found too unstable for time steps greater than 5×10^{-4} sec. The CPU time required for this problem was approximately 40 minutes on a VAX 11/780.

CHAPTER VIII

SUMMARY

In the preceding chapters, the kinematic and kinetic variables used to describe finite deformation motion of solid continua were developed. Subsequently, several constitutive equations were presented which differed primarily in the choice of the kinematic and kinetic variables. Theoretical discussions were presented concerning the possible correctness of the various descriptions, and numerical computations were presented which compared the proposed constitutive descriptions. It was shown that the hyperelastic-viscoplastic, updated hyperelastic-viscoplastic and hypoelastic-viscoplastic (employing the Kirchhoff stress tensor) could be implemented effectively and efficiently using an implicit integration technique. The explicit time integration procedure was suitable to use with any of the constitutive descriptions, but due to the nature of the time step selection procedure, was more compatible with the updated Lagrangian procedures.

The implicit integration of the elastic-viscoplastic constitutive equations was found to be significantly better than explicit procedures, and required little additional numerical work. In addition, it was determined that the implicit integration of the constitutive equations was

suitable for use with either the implicit or explicit schemes used to integrate the equations of motion.

The hypoelastic and updated Lagrangian constitutive equations were found to yield almost identical results; the use of the Kirchhoff stress tensor versus the Cauchy stress tensor yielded very similar results. The hyperelastic-viscoplastic constitutive equations yielded significantly different results than the hypoelastic-viscoplastic or updated hyperelastic-viscoplastic constitutive equations employing the same strain rate sensitivity parameter and power law exponent when the dilatational strain components were finite. No significant difference in the results obtained using the three constitutive formulations was observed when the dilatational strain components were small. In addition, it was found that the Perzyna-type constitutive equations were fairly insensitive to the actual shape of the work-hardening portion of the static stress-strain curve.

The amount of strain rate sensitivity predicted by Eq. (7.1) for 6061-T6 aluminum was too large, and a much larger strain rate sensitivity parameter was required to obtain computational results which agreed with experimental data for Taylor's cylinder problem. The larger strain rate sensitivity parameter was shown to be consistent with experimental data of Hoge.

CHAPTER IX

CONCLUSIONS AND RECOMMENDATIONS

This chapter presents a list of conclusions drawn from this investigation, and recommendations for future research. The conclusions drawn are:

1. For a Perzyna power law viscoplastic strain rate evolution law, the three finite strain constitutive formulations may not yield comparable numerical results when the same strain rate sensitivity parameter and power law exponent are used by the three formulations.
2. The updated hyperelastic-viscoplastic and hypoelastic-viscoplastic constitutive formulations yielded nearly identical numerical results for both Taylor's cylinder problem and the impulsively loaded cantilever beam problem.
3. For Taylor's cylinder problem, the hyperelastic-viscoplastic constitutive formulation yielded significantly different numerical results than the updated hyperelastic-viscoplastic and hypoelastic-viscoplastic constitutive formulations. It was concluded that, when finite dilatational strains are present, it is necessary to use dynamic yield stress data consistent

with the continuum mechanics formulation used in the constitutive equations.

4. When the dilatational strains are small, all three constitutive formulations yield nearly identical numerical results, and the continuum mechanics interpretation of the dynamic yield stress data is not as important.
5. Implicit integration of the elastic-viscoplastic constitutive equations is far superior to the explicit integration method, and requires less total computational effort.
6. The three finite strain, elastic-viscoplastic constitutive formulations required approximately the same amount of computational effort.
7. The computed change in length of Taylor's cylinder agreed well with experimental data when a Perzyna overstress constitutive equation was used.
8. The elastic-viscoplastic constitutive equations using the implicit integration technique were much more stable than the hypoelastic-plastic constitutive equations. In addition, it was noted that an updated hyperelastic-plastic constitutive equation does not satisfy Prager's consistency relationship, and when large hydrostatic pressures are present it was difficult

to keep the computed stress state on the yield surface.

The recommendations for future research are:

1. The Taylor's cylinder problem involved large hydrostatic pressures which may invalidate the additive decomposition of the rate of deformation into elastic and viscoplastic components. More work should be done in developing an elastic-viscoplastic constitutive equation based on Lee's multiplicative decomposition of the deformation gradient.
2. The present constitutive equations use an isotropic hardening assumption. More work should be performed to determine how well they perform in reversed loading conditions.
3. The present constitutive equations use a constant elastic bulk modulus. More work should be performed to determine how to include a more general equation of state, and how the equation of state influences the results for Taylor's cylinder problem.
4. The hypoelastic-plastic constitutive equation was implemented using a tangent modulus-type approach. Since it is difficult to keep the computed stress state on the yield surface, it may be more desirable to step out elastically

into the stress space, and then return radially to the yield surface.

5. The current computer program is limited to two-dimensional problems. Three-dimensional elements should be added to permit more geometries and stress states to be represented.
6. Many finite strain dynamic plasticity problems involve the impact of one or more bodies. Impact logic should be added to the computer program to permit more problems to be studied.
7. A general procedure for converting the stress state at a variable number of Gauss integration points to a variable number of node point stress states is needed. This would greatly improve the post-processing of data obtained from isoparametric elements which can have a variable number of nodes on the element.

BIBLIOGRAPHY

BIBLIOGRAPHY

1. Malvern, L. E. "The Propagation of Longitudinal Waves in a Bar Exhibiting a Strain-Rate Effect," Journal of Applied Mechanics, 18:203-208, June 1951.

2. Hart, E. W., C. Y. Li, H. Yamada, and G. L. Wire. "Phenomenological Theory: A Guide to Constitutive Relations and Fundamental Deformation Properties," Constitutive Equations in Plasticity, A. S. Argon, editor. Cambridge: The MIT Press, 1975. Pp. 149-197.

3. Perzyna, P. "The Constitutive Equations for Rate-Sensitive Plastic Materials," Quarterly of Applied Mathematics, 20(No. 4):321-332, January 1963.

4. Bodner, S. R. "Constitutive Equations for Dynamic Material Behavior," Mechanical Behavior of Materials Under Dynamic Loads, U. S. Lindholm, editor. New York: Springer-Verlag, 1968. Pp. 176-190.

5. Lindholm, U. S. "Some Experiments in Dynamic Plasticity Under Combined Stress," Mechanical Behavior of Materials Under Dynamic Loads, U. S. Lindholm, editor. New York: Springer-Verlag, 1968. Pp. 77-95.

6. Sokolovsky, V. V. "The Propagation of Elastic-Viscous-Plastic Waves in Rods," Prinkladnaia Matematika I, Mekhanika, 12:161-280, May-June 1948.

7. Key, S. W., Z. E. Beisinger, and R. D. Krieg. "HONDO II: A Finite Element Computer Program for the Large Deformation Dynamic Response of Axisymmetric Solids," Sandia National Laboratories SAND 78-0422, Albuquerque, New Mexico, October 1978.

8. Johnson, G. R. "High Velocity Impact Calculations in Three Dimensions," Journal of Applied Mechanics, n.v.:95-100, March 1977.

9. Manjoine, M. J. "Influence of Rate of Strain and Temperature on Yield Stresses of Mild Steel," Journal of Applied Mechanics, 11(A):211-218, December 1944.

10. Lindholm, U. S. "High Strain Rate Tests," Techniques in Metals Research. Vol. 5, Part 1. R. F. Bunshah, editor. New York: Interscience, 1971. Pp. 199-271.

11. Hoge, K. G. "Influence of Strain Rate on Mechanical Properties of 6061-T6 Aluminum under Uniaxial and Biaxial States of Stress," Experimental Mechanics, 6:204-211, April 1966.

12. Rosen, A., and S. R. Bodner. "The Influence of Strain Rate and Strain Ageing on the Flow Stress of Commercially-Pure Aluminum," Journal of the Mechanics and Physics of Solids, 15:47-62, 1967.

13. Mukherjee, S. "Thermoviscoplastic Response of Cylindrical Structures Using a State-Variable Model," United States Department of Energy Report No. C00-2733-19. Prepared by Cornell University, Ithaca, New York, February 1979.

14. Key, S. W., J. H. Biffle, and R. D. Krieg. "A Study of the Computational and Theoretical Differences of Two Finite Strain Elastic-Plastic Constitutive Models," Formulations and Computational Algorithms in Finite Element Analysis, R. J. Bathe, J. T. Oden, and W. Wunderlich, editors. Cambridge: Massachusetts Institute of Technology, 1977. Pp. 321-352.

15. Malvern, L. E. Introduction to the Mechanics of a Continuous Medium. Englewood Cliffs, New Jersey: Prentice-Hall, 1969.

16. Hill, R. "Some Basic Principles in the Mechanics of Solids without a Natural Time," Journal of the Mechanics and Physics of Solids. Vol. 7. London: Pergamon Press, LTD., 1959. Pp. 209-225.

17. Truesdell, C. "Corrections and Additions to the Mechanical Foundations of Elasticity and Fluid Dynamics," Journal of Rational Mechanics and Analysis, 2:593-616, 1953.

18. Nemat-Nasser, S. "Continuum Bases for Consistent Numerical Formulations of Finite Strains in Elastic and Inelastic Structures," Finite Element Analysis of Transient Nonlinear Structural Behavior. New York: American Society of Mechanical Engineers, 1975. Pp. 85-90.

19. Washizu, K. Variational Methods in Elasticity and Plasticity. Second edition. New York: Pergamon Press, 1975.

20. Kanchi, M. B., O. C. Zienkiewicz, and D. R. J. Owen. "The Visco-Plastic Approach to Problems of Plasticity and Creep Involving Geometric Non-Linear Effects," International Journal for Numerical Methods in Engineering, 12(No. 1):169-181, January 1978.

21. Nagarajan, S., and E. P. Popov. "Nonlinear Elastic-Viscoplastic Analysis Using the Finite Element Method," Computational Methods in Nonlinear Mechanics, J. T. Oden et al., editors. Austin: The Texas Institute for Computational Mechanics, 1974. Pp. 979-988.

22. Green, A. E., and P. M. Nagdhi. "A General Theory of an Elastic-Plastic Continuum," Archives for Rational Mechanics and Analysis, 18:251-281, 1965.

23. Green, A. E., and P. M. Naghdi. "A Thermodynamic Development of Elastic-Plastic Continua," Irreversible Aspects of Continuum Mechanics. Berlin: Springer-Verlag, 1966. Pp. 117-131.

24. Hill, Rodney. The Mathematical Theory of Plasticity. Oxford, England: Clarendon Press, 1950.

25. Lee, E. H. "Some Comments on Elastic-Plastic Analysis," Stanford University Division of Applied Mechanics No. 80-5, Stanford, California, October 1980.

26. Hutchinson, J. W. "Finite Strain Analysis of Elastic-Plastic Solids and Structures," Numerical Solution of Nonlinear Structural Problems. R. F. Hartung, editor. New York: American Society of Mechanical Engineers, 1973. Pp. 17-29.

27. Hibbitt, H. D., P. V. Marcal, and J. R. Rice. "A Finite Element Formulation for Problems of Large Strain and Large Displacement," International Journal of Solids and Structures, 6:1069-1086, August 1970.

28. McMeeking, R. M., and J. R. Rice. "Finite-Element Formulations for Problems of Large Elastic-Plastic Deformation," International Journal of Solids and Structures, 11(No. 5):601-616, May 1975.

29. Lee, E. H. "Elastic-Plastic Deformation at Finite Strains," Journal of Applied Mechanics, 36:1-6, March 1969.

30. Bathe, K. J., H. Ozdemir, and E. L. Wilson. "Static and Dynamic Geometric and Material Nonlinear Analysis," University of California-Berkeley Report No. UC SESM 74-4, Berkeley, California, February 1974.

31. Howard, J. V., and S. L. Smith. "Recent Developments in Tensile Testing," Proceedings of the Royal Society, 107(A):113-125, January 1925.

32. Yaghmai, S. "Incremental Analysis of Large Deformation in Mechanics of Solids with Applications to Axisymmetric Shells of Revolution," University of California Structural Engineering Laboratory Report No. UC SESM 68-17, Berkeley, California, 1968.

33. Argyris, J. H., and M. Kleiber. "Incremental Formulation in Nonlinear Mechanics and Large Strain Elasto-Plasticity--Natural Approach, Part 1," Computer Methods in Applied Mechanics and Engineering, 11(No. 2):215-247, May 1977.

34. Lubarda, V. A., and E. H. Lee. "A Correct Definition of Elastic and Plastic Deformation and Its Computational Significance," Journal of Applied Mechanics, 48:35-40, March 1981.

35. Wang, Y. S. "A Simplified Theory of the Constitutive Equations of Metal Plasticity at Finite Deformation," Journal of Applied Mechanics, 40:941-947, December 1973.

36. Tanaka, M. "Elastoplastic Constitutive Laws Based on Combined Isotropic and Kinematic Hardening," Osaka [Japan] University Faculty of Engineering, Technology Reports, 25:101-115, March 1975.

37. Prager, W. "A New Method of Analyzing Stresses and Strains in Work-Hardening Plastic Solids," Journal of Applied Mechanics. 23:493-496, December 1956.

38. Ziegler, H. "A Modification of Prager's Hardening Rule," Quarterly of Applied Mathematics, 17(No. 1):55-65, April 1959.

39. Bathe, K. Finite Element Procedures in Engineering Analysis. Englewood Cliffs, New Jersey: Prentice-Hall, 1982.

40. Zienkiewicz, O. C., and I. C. Cormeau. "Visco-Plasticity-Plasticity and Creep in Elastic Solids--A Unified Numerical Solution Approach," International Journal for Numerical Methods in Engineering, 8(No. 4):821-845, April 1974.

41. Cormeau, I. C. "Numerical Stability in Quasi-Static Elasto/Visco-Plasticity," International Journal for Numerical Methods in Engineering, 9(No. 1):109-127, January 1975.

42. Hughes, T. J. R., and R. L. Taylor. "Unconditionally Stable Algorithms for Quasi-Static Elasto/Visco-Plastic Finite Element Analysis," Computers and Structures, 8(No. 2):169-173, April 1978.

43. Zienkiewicz, O. C. "Visco-Plasticity, Plasticity, Creep and Visco-Plastic Flow (Problems of Small, Large and Continuing Deformation)," Lecture Notes in Mathematics: 461 Computational Mechanics, J. T. Oden, editor. Berlin: Springer-Verlag, 1975. Pp. 297-328.

44. Argyris, J. H., L. E. Vaz, and K. J. William. "Improved Solution Methods for Inelastic Rate Problems," Computer Methods in Applied Mechanics and Engineering, 16(No. 2):231-277, November 1978.

45. Argyris, J. H., et al. "Finite Element Method--The Natural Approach," Computer Methods in Applied Mechanics and Engineering, 17/18:1-106, January 1979.

46. Argyris, J. H., J. St. Doltsinis, and K. J. William. "New Developments in the Inelastic Analysis of Quasistatic and Dynamic Problems," International Journal for Numerical Methods in Engineering, 14(No. 12):1813-1850, December 1979.

47. Key, Samuel W. "A Finite Element Procedure for the Large Deformation Dynamic Response of Axisymmetric Solids," Computer Methods in Applied Mechanics and Engineering, 4(No. 2):195-218, September, 1974.

48. Belytschko, T., N. Holmes, and R. Mullen. "Explicit Integration-Stability, Solution Properties, Cost," Finite Element Analysis of Transient Nonlinear Structural Behavior, T. Belytschko, J. R. Osias, and P. V. Marcal, editors. New York: American Society of Mechanical Engineers, 1975. Pp. 1-21.

49. Bathe, K. J. "Finite Element Formulation, Modeling, and Solution of Nonlinear Dynamic Problems," Numerical Methods for Partial Differential Equations, Seymour Porter, editor. New York: Academic Press, 1979. Pp. 1-40.

50. Bertholf, L. D., and S. E. Benzley. "TOODY II, A Computer Program for Two-Dimensional Wave Propagation," Sandia Laboratories SC-RR-68-41, Albuquerque, New Mexico, November 1968.

51. Richtmeyer, R. D., and K. W. Morton. Difference Methods for Initial-Value Problems. Second edition. New York: John Wiley and Sons, 1967.

52. Zukas, Jonas A. "Numerical Simulation of Impact Phenomena," Impact Dynamics, J. A. Zukas, T. Nicholas, H. F. Swift, L. B. Greszczuk, and D. R. Curran, editors. New York: John Wiley and Sons, 1982. Pp. 367-417.

53. Wilkins, M. L. "Use of Artificial Viscosity in Multidimensional Fluid Dynamic Calculations," Journal of Computational Physics, 36(No. 3):281-303, July 1980.

54. Turner, M. J., E. H. Dill, H. C. Martin, and R. Melosh. "Large Deflections of Structures Subjected to Heating and External Loads," Journal of Aerospace Sciences, 27(No. 2):97-106, February 1960.

55. Haisler, W. E. "Development and Evaluation of Solution Procedures for Nonlinear Structural Analysis." Ph.D. dissertation, Texas A&M University, College Station, 1970.

56. Hofmeister, Lawrence D., Gilbert A. Greenbaum, and David A. Evensen. "Large Strain, Elasto-Plastic Finite Element Analysis," AIAA Journal, 9(No. 7):1248-1254, July 1971.

57. Newmark, N. M. "A Method of Computation for Structural Dynamics," American Society of Civil Engineers, Journal of Engineering Mechanics Division, 85:67-94, 1959.

58. Bathe, K. J. "Assessment of Current Finite Element Analysis of Nonlinear Problems in Solid Mechanics," Proceedings of the Third Symposium on the Numerical Solution of Partial Differential Equations. New York: Academic Press, Inc., 1976. Pp. 117-164.

59. Zienkiewicz, O. C. The Finite Element Method. Third edition. London: McGraw-Hill Book Company, 1977.

60. Taylor, G. I. "The Use of Flat-Ended Projectiles for Determining Dynamic Yield Stress, I. Theoretical Considerations," Proceedings of the Royal Society, 194(A):289-299, November 1948.

61. Whiffin, A. C. "The Use of Flat-Ended Projectiles for Determining Dynamic Yield Stress, II. Tests on Various Metallic Materials," Proceedings of the Royal Society, 194(A):300-322, November 1948.

62. Lee, E. H., and S. J. Tupper. "Analysis of Plastic Deformation in a Steel Cylinder Striking a Rigid Target," Journal of Applied Mechanics, 21:63-70, March 1954.

63. Raftopoulos, Demetrios, and Norman Davids. "Elasto-plastic Impact on Rigid Targets," AIAA Journal, 5(No. 12):2254-2260, December 1967.

64. Wilkins, M. L., and M. W. Guinan. "Impact of Cylinders on a Rigid Boundary," Journal of Applied Physics, 44(No. 3):1200-1206, March 1973.

65. Recht, Rodney F. "Taylor Ballistic Impact Modelling Applied to Deformation and Mass Loss Determinations," International Journal of Engineering Science, 16(No. 10):809-817, October 1978.

66. Fukuoka, H., and H. Toda. "High Velocity Impact of Mild Steel Cylinder," High Velocity Deformation of Solids. K. Kawata and J. Shiori, editors. Berlin: Springer-Verlag, 1978. Pp. 397-402.

67. Ng, D. H. Y., M. Delich, and L. H. N. Lee. "Yielding of 6061-T6 Aluminum Tubings under Dynamic Biaxial Loadings," Experimental Mechanics, 19:200-206, June 1979.

68. Parkes, E. W. "The Permanent Deformation of a Cantilever Struck Transversely at Its Tip," Proceedings of the Royal Society, 228(A-1173):462-476, March 1955.

69. Bodner, S. R., and P. S. Symonds. "Experimental and Theoretical Investigation of the Plastic Deformation of Cantilever Beams Subjected to Impulsive Loading," Journal of Applied Mechanics, 29:719-728, December 1962.

70. Wilkins, Mark L. "Calculation of Elastic-Plastic Flow," Methods in Computational Physics, Fundamental Methods in Hydrodynamics. Vol. 3. Berni Alder, Sidney Fernbach, and Manuel Rotenberg, editors. New York: Academic Press, 1964. Pp. 211-263.

APPENDIX

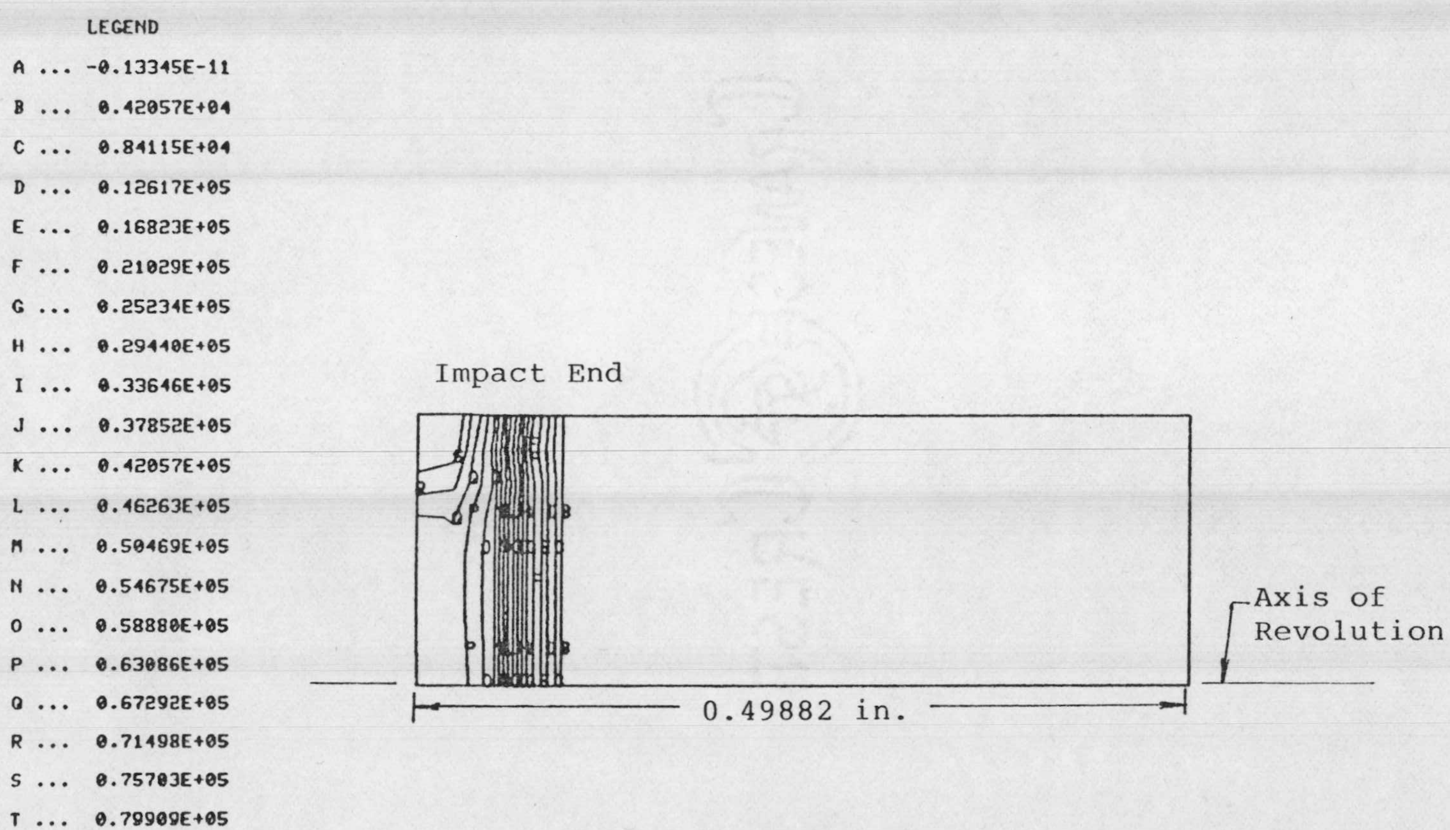

Figure A.1. Equivalent Stress 0.148 μsec After Impact.

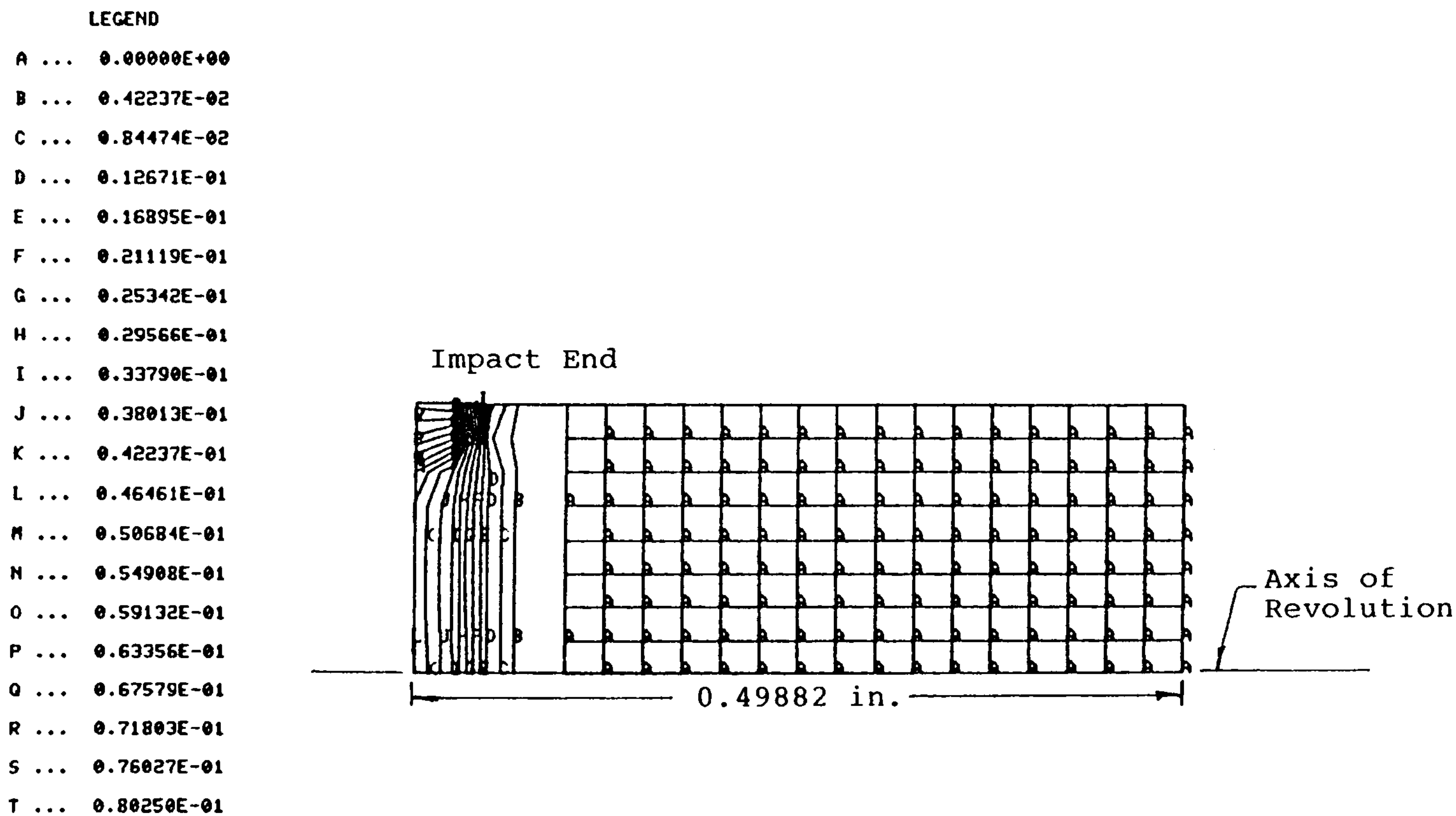

Figure A.2. Equivalent Plastic Strain 0.148 μsec After Impact.

LEGEND

A ... -0.20546E-11
B ... 0.40908E+04
C ... 0.81815E+04
D ... 0.12272E+05
E ... 0.16363E+05
F ... 0.20454E+05
G ... 0.24545E+05
H ... 0.28635E+05
I ... 0.32726E+05
J ... 0.36817E+05
K ... 0.40908E+05
L ... 0.44999E+05
M ... 0.49089E+05
N ... 0.53180E+05
O ... 0.57271E+05
P ... 0.61362E+05
Q ... 0.65452E+05
R ... 0.69543E+05
S ... 0.73634E+05
T ... 0.77725E+05

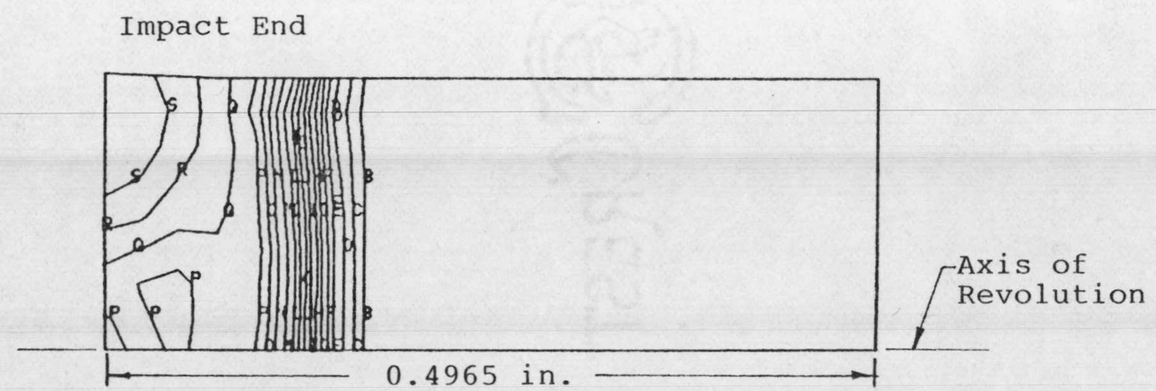

Figure A.3. Equivalent Stress 0.443 μsec After Impact.

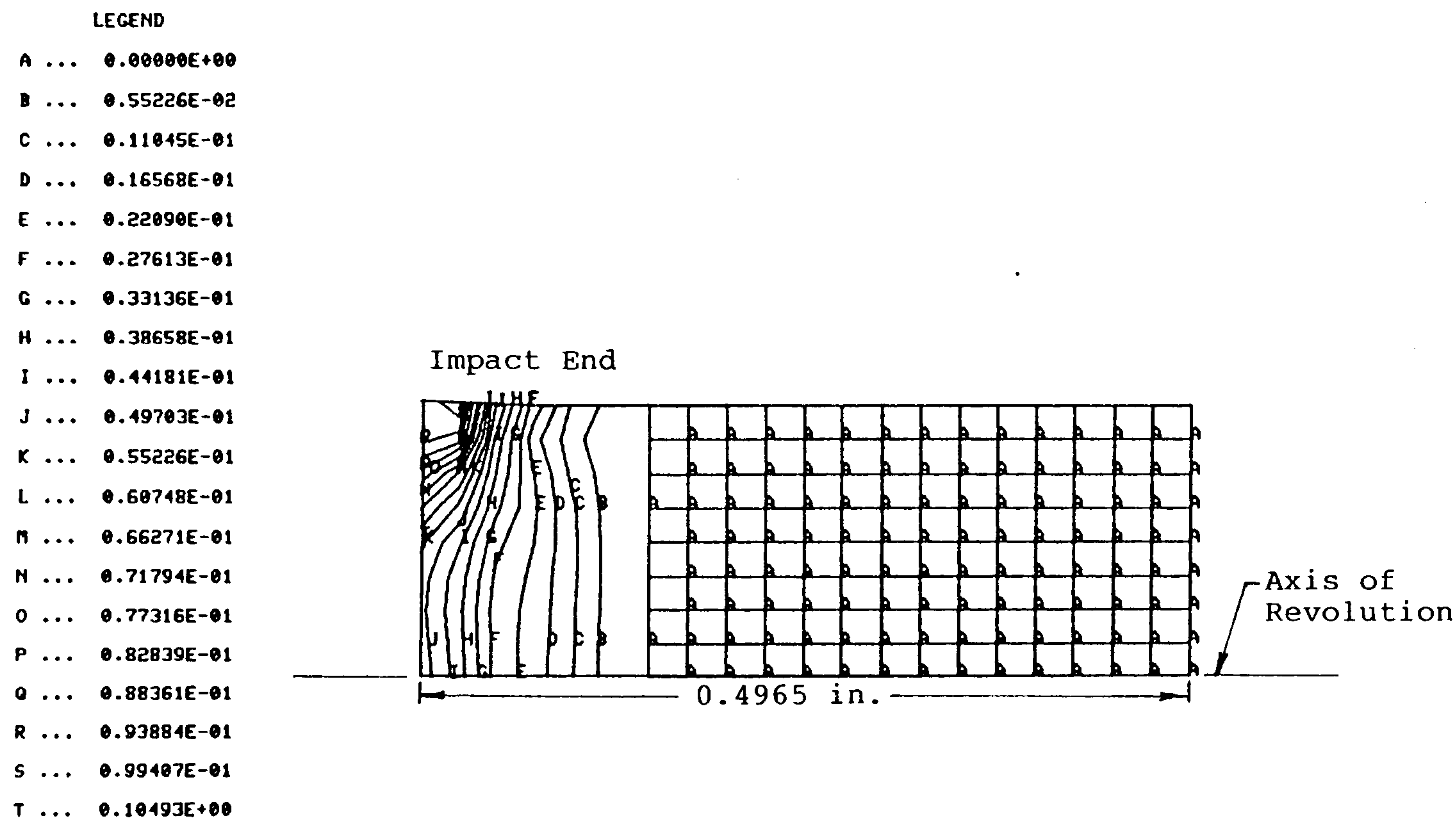

Figure A.4. Equivalent Plastic Strain 0.443 μsec After Impact.

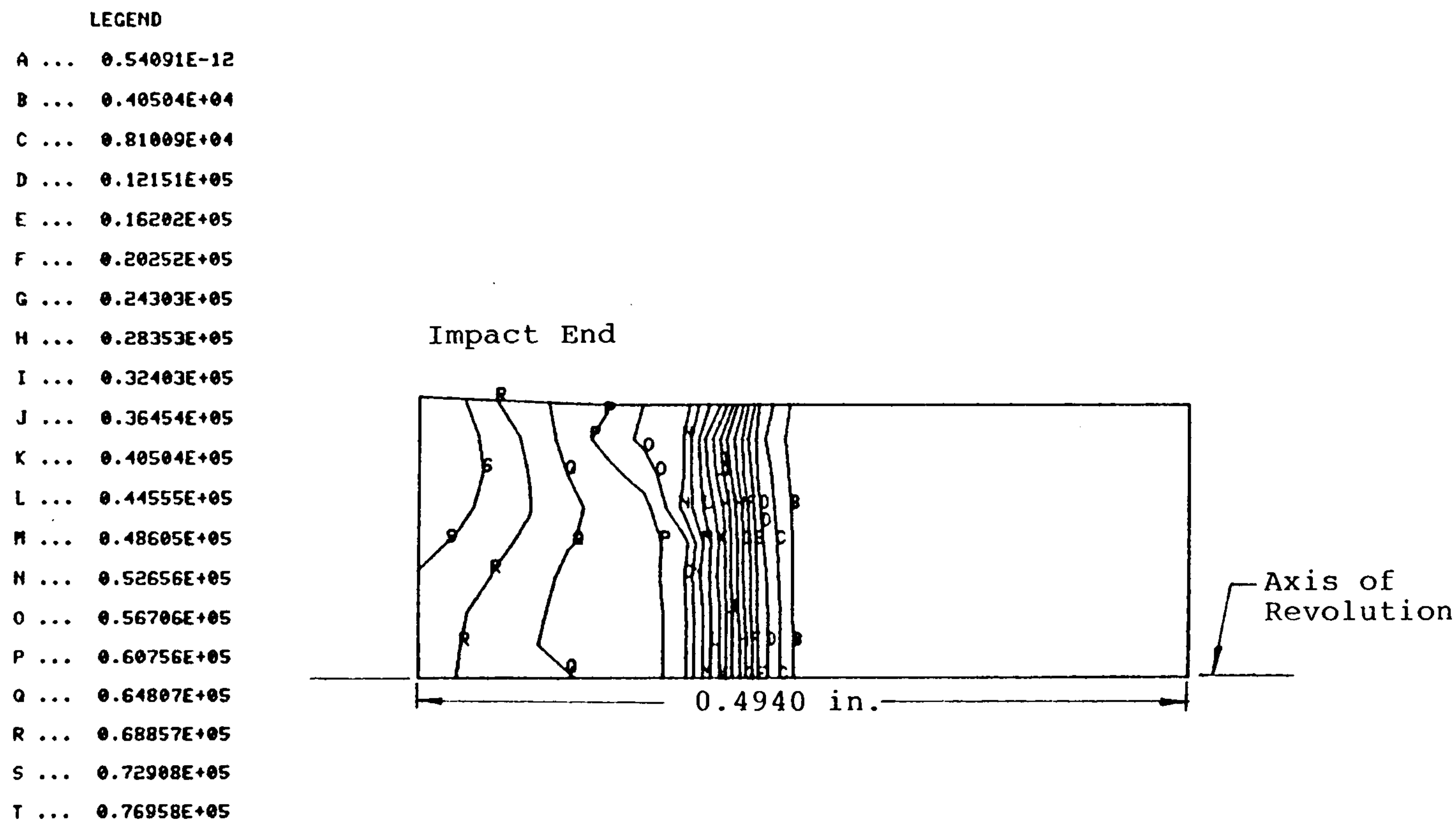

Figure A.5. Equivalent Stress 0.749 μsec After Impact.

LEGEND

A ... 0.00000E+00
B ... 0.60644E-02
C ... 0.12129E-01
D ... 0.18193E-01
E ... 0.24258E-01
F ... 0.30322E-01
G ... 0.36386E-01
H ... 0.42451E-01
I ... 0.48515E-01
J ... 0.54580E-01
K ... 0.60644E-01
L ... 0.66708E-01
M ... 0.72773E-01
N ... 0.78837E-01
O ... 0.84902E-01
P ... 0.90966E-01
Q ... 0.97030E-01
R ... 0.10309E+00
S ... 0.10916E+00
T ... 0.11522E+00

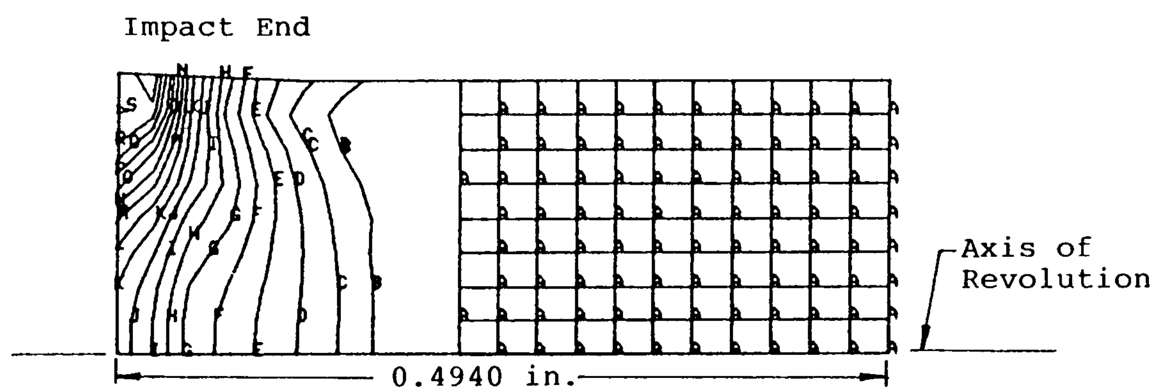

Figure A.6. Equivalent Plastic Strain 0.749 μsec After Impact.

LEGEND

A ...	0.80868E-13
B ...	0.40480E+04
C ...	0.80961E+04
D ...	0.12144E+05
E ...	0.16192E+05
F ...	0.20240E+05
G ...	0.24288E+05
H ...	0.28336E+05
I ...	0.32384E+05
J ...	0.36432E+05
K ...	0.40480E+05
L ...	0.44528E+05
M ...	0.48576E+05
N ...	0.52624E+05
O ...	0.56672E+05
P ...	0.60720E+05
Q ...	0.64769E+05
R ...	0.68817E+05
S ...	0.72865E+05
T ...	0.76913E+05

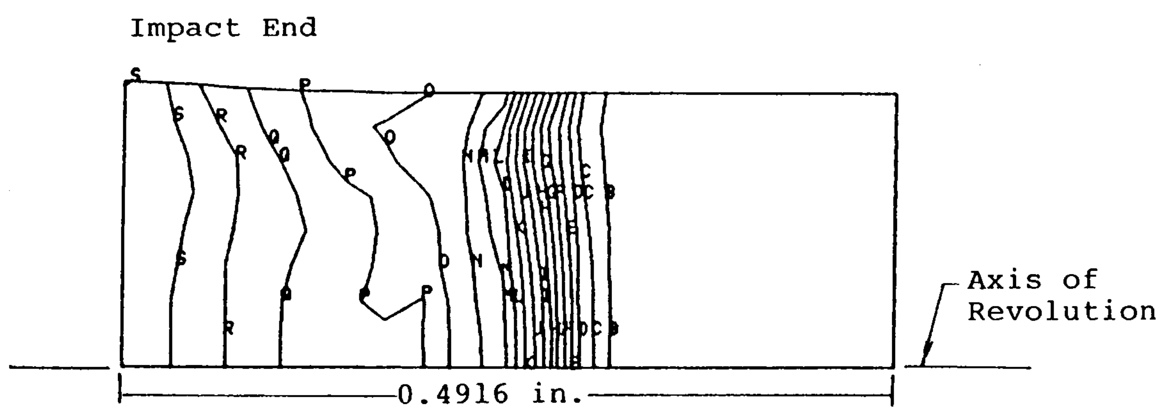

Figure A.7. Equivalent Stress 1.06 μsec After Impact.

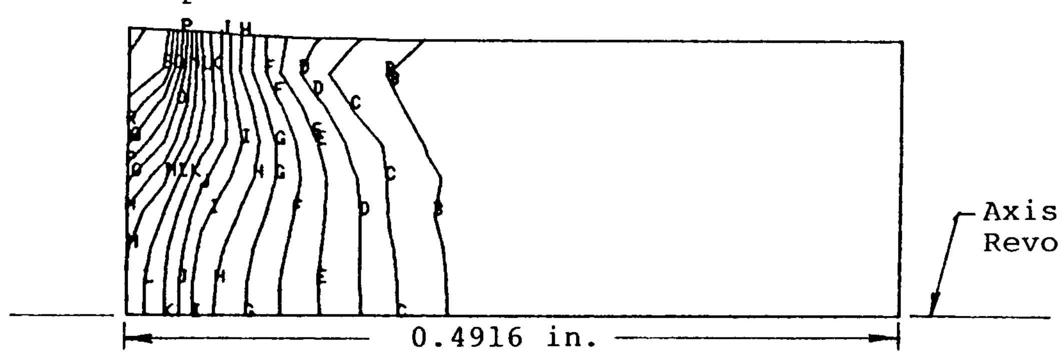

Figure A.8. Equivalent Plastic Strain 1.06 μsec After Impact.

LEGEND

A ...	0.36723E+01
B ...	0.41659E+04
C ...	0.83282E+04
D ...	0.12490E+05
E ...	0.16653E+05
F ...	0.20815E+05
G ...	0.24977E+05
H ...	0.29140E+05
I ...	0.33302E+05
J ...	0.37464E+05
K ...	0.41626E+05
L ...	0.45789E+05
M ...	0.49951E+05
N ...	0.54113E+05
O ...	0.58275E+05
P ...	0.62438E+05
Q ...	0.66600E+05
R ...	0.70762E+05
S ...	0.74924E+05
T ...	0.79087E+05

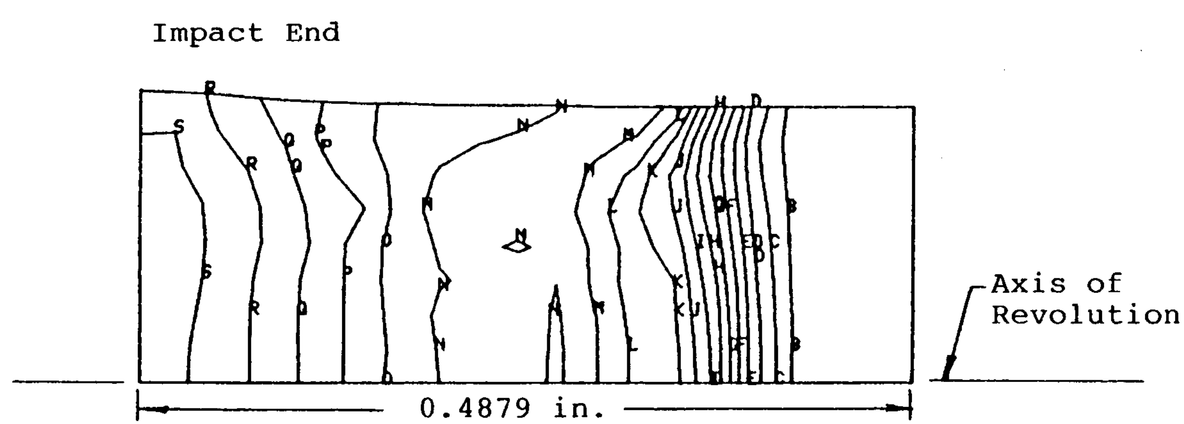

Figure A.9. Equivalent Stress 1.51 μsec After Impact.

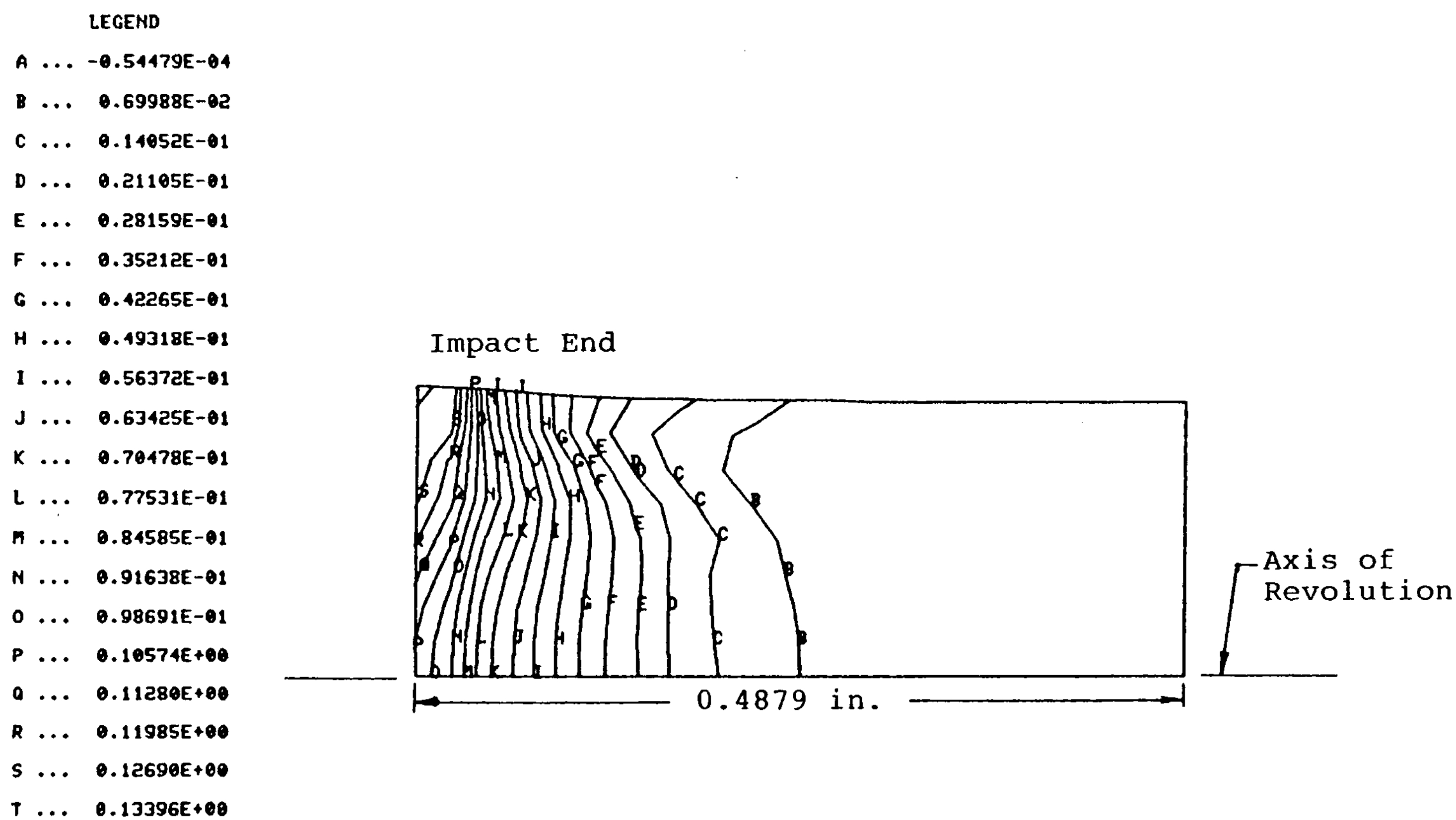

Figure A.10. Equivalent Plastic Strain 1.51 μsec After Impact.

LEGEND

A ... 0.43373E+04
B ... 0.83560E+04
C ... 0.12375E+05
D ... 0.16393E+05
E ... 0.20412E+05
F ... 0.24431E+05
G ... 0.28449E+05
H ... 0.32468E+05
I ... 0.36486E+05
J ... 0.40505E+05
K ... 0.44524E+05
L ... 0.48542E+05
M ... 0.52561E+05
N ... 0.56580E+05
O ... 0.60598E+05
P ... 0.64617E+05
Q ... 0.68635E+05
R ... 0.72654E+05
S ... 0.76673E+05
T ... 0.80691E+05

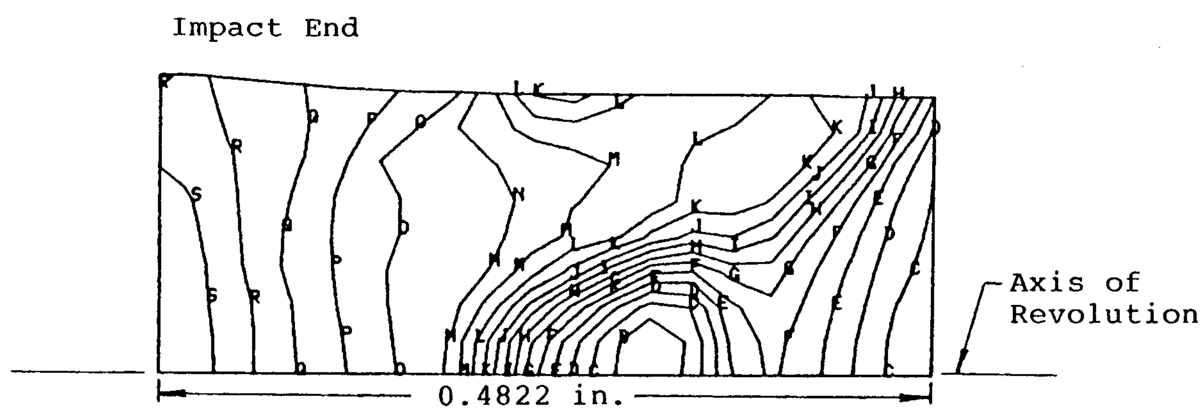

Figure A.11. Equivalent Stress 2.29 μsec After Impact.

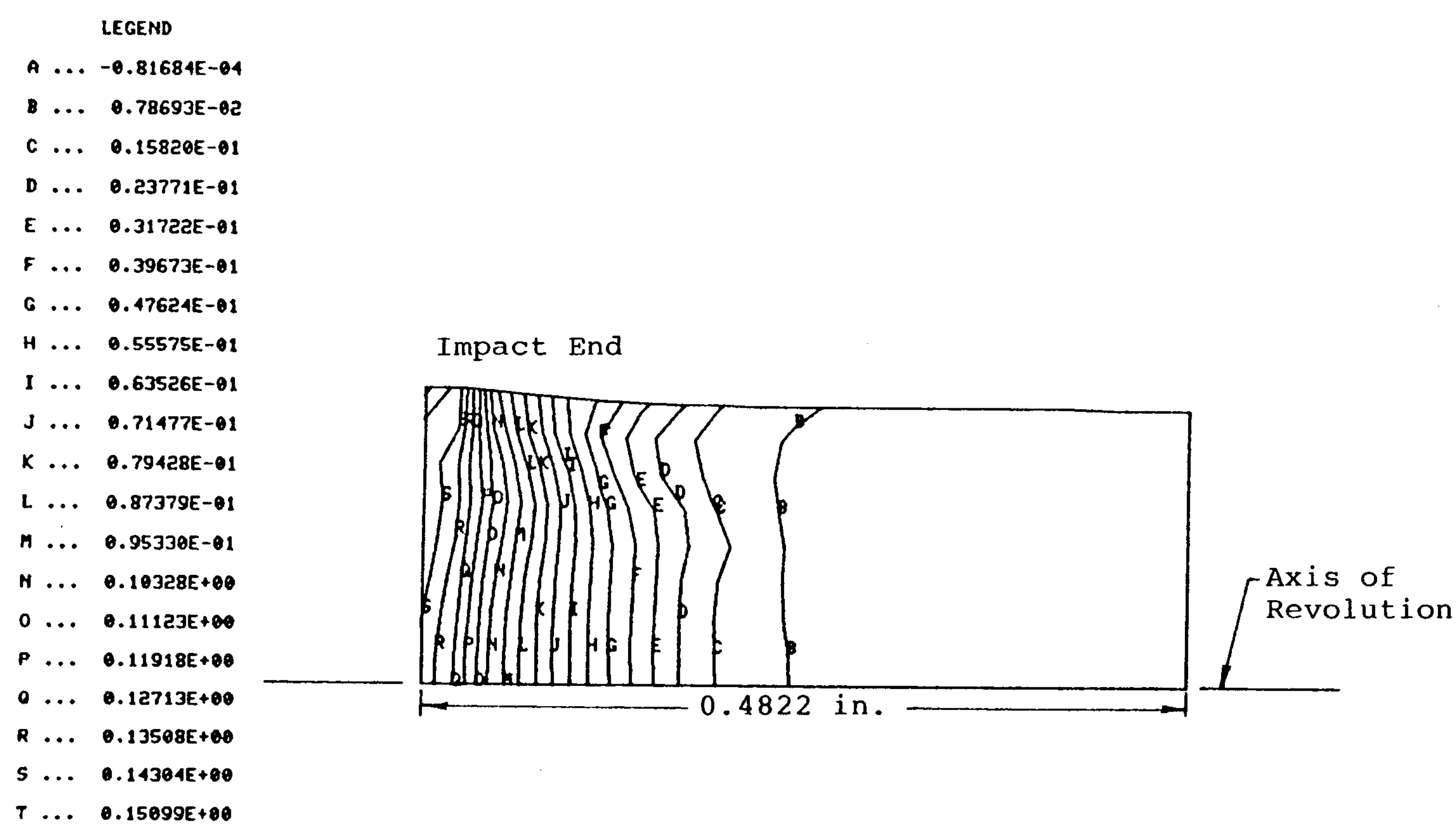

Figure A.12. Equivalent Plastic Strain 2.29 μsec After Impact.

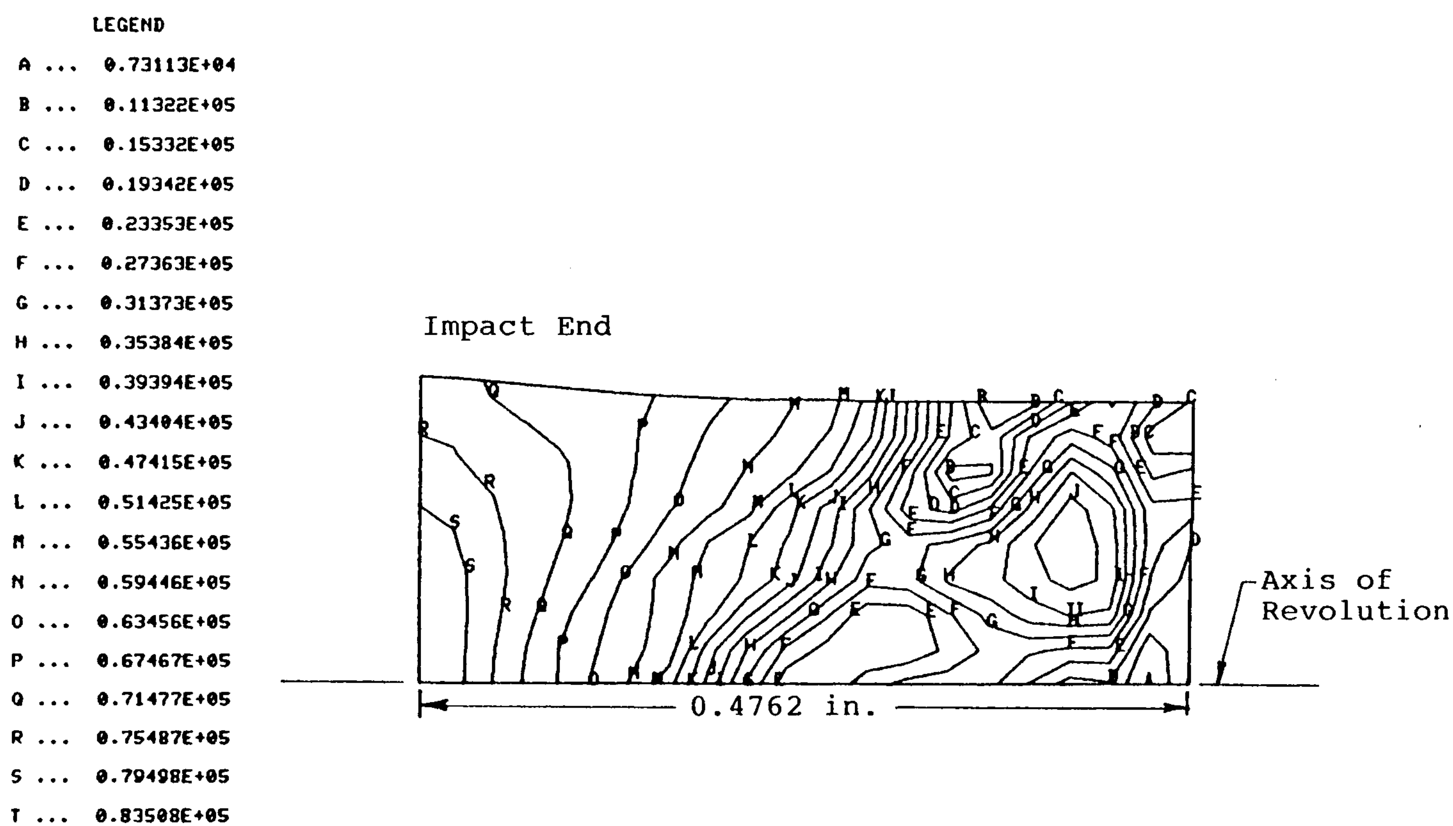

Figure A.13. Equivalent Stress 3.06 μsec After Impact.

LEGEND

A ... 0.00000E+00
B ... 0.94125E-02
C ... 0.18825E-01
D ... 0.28238E-01
E ... 0.37650E-01
F ... 0.47063E-01
G ... 0.56475E-01
H ... 0.65888E-01
I ... 0.75300E-01
J ... 0.84713E-01
K ... 0.94125E-01
L ... 0.10354E+00
M ... 0.11295E+00
N ... 0.12236E+00
O ... 0.13178E+00
P ... 0.14119E+00
Q ... 0.15060E+00
R ... 0.16001E+00
S ... 0.16943E+00
T ... 0.17884E+00

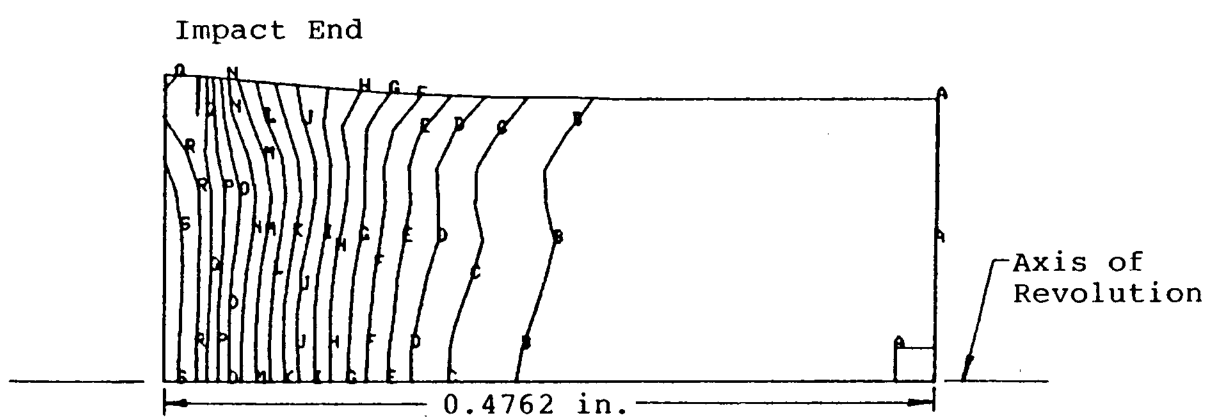

Figure A.14. Equivalent Plastic Strain 3.06 μsec After Impact.

LEGEND

A ... 0.51382E+04
B ... 0.95555E+04
C ... 0.13973E+05
D ... 0.18390E+05
E ... 0.22807E+05
F ... 0.27224E+05
G ... 0.31642E+05
H ... 0.36059E+05
I ... 0.40476E+05
J ... 0.44893E+05
K ... 0.49311E+05
L ... 0.53728E+05
M ... 0.58145E+05
N ... 0.62562E+05
O ... 0.66980E+05
P ... 0.71397E+05
Q ... 0.75814E+05
R ... 0.80231E+05
S ... 0.84648E+05
T ... 0.89066E+05

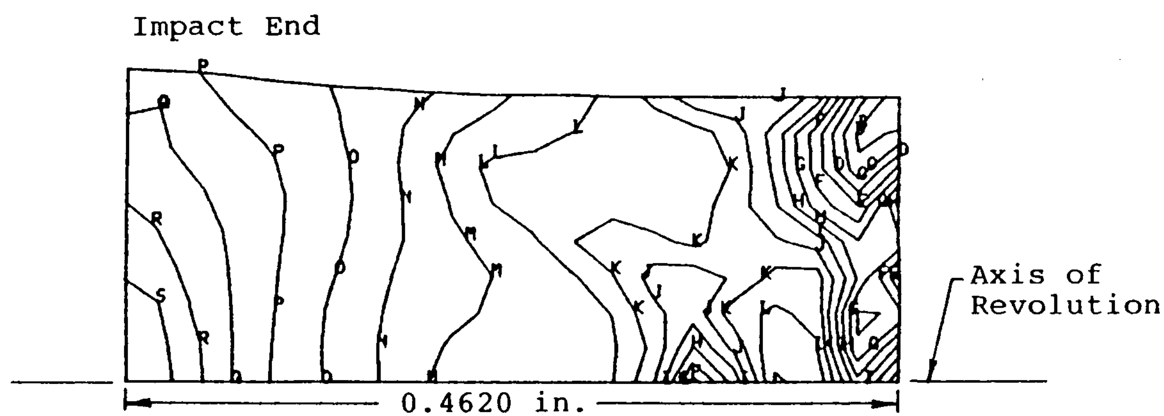

Figure A.15. Equivalent Stress 3.80 μsec After Impact.

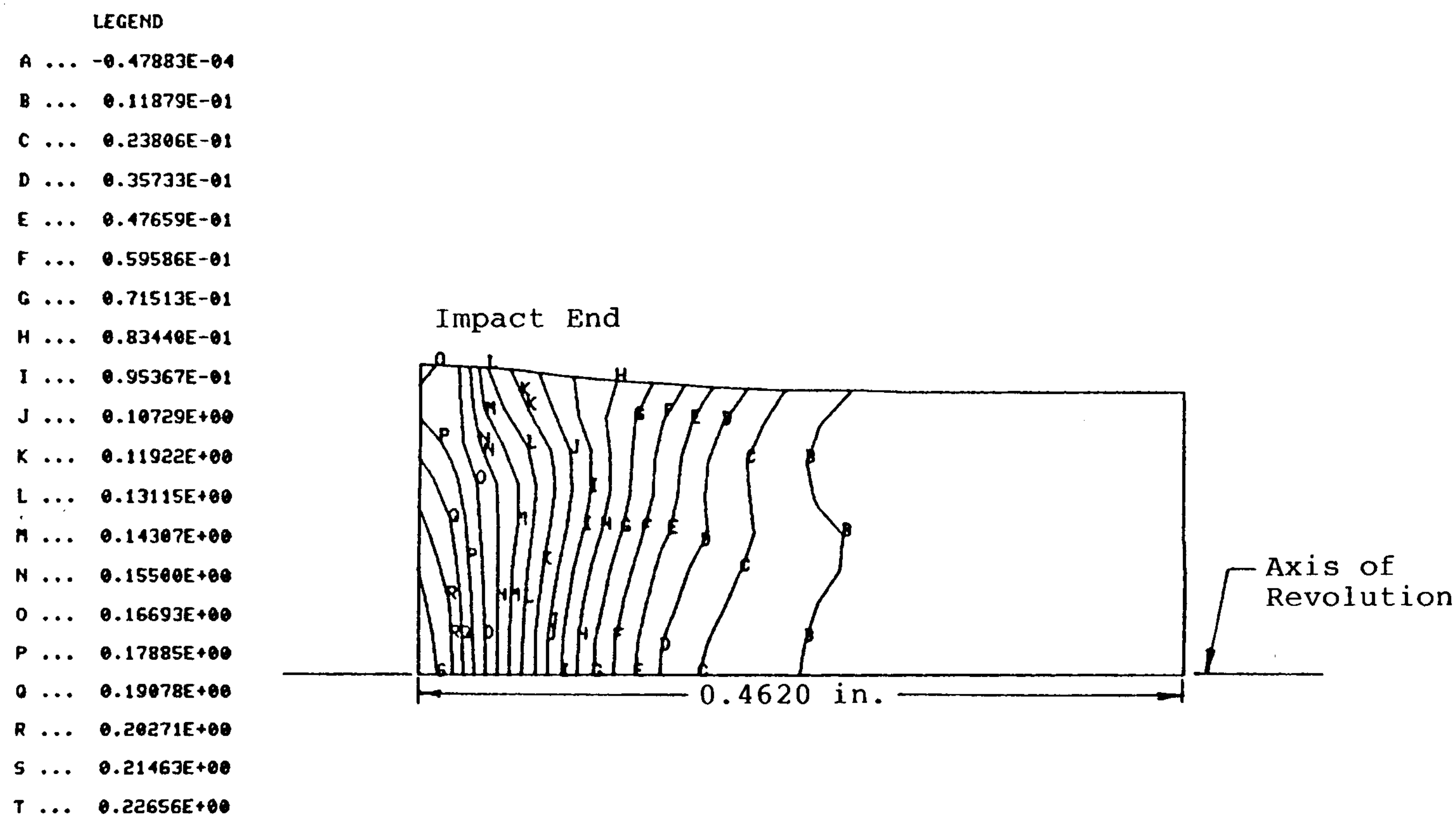

Figure A.16. Equivalent Plastic Strain 3.80 μsec After Impact.

LEGEND

A ...	0.13371E+05
B ...	0.17311E+05
C ...	0.21251E+05
D ...	0.25191E+05
E ...	0.29132E+05
F ...	0.33072E+05
G ...	0.37012E+05
H ...	0.40952E+05
I ...	0.44893E+05
J ...	0.48833E+05
K ...	0.52773E+05
L ...	0.56713E+05
M ...	0.60654E+05
N ...	0.64594E+05
O ...	0.68534E+05
P ...	0.72474E+05
Q ...	0.76415E+05
R ...	0.80355E+05
S ...	0.84295E+05
T ...	0.88235E+05

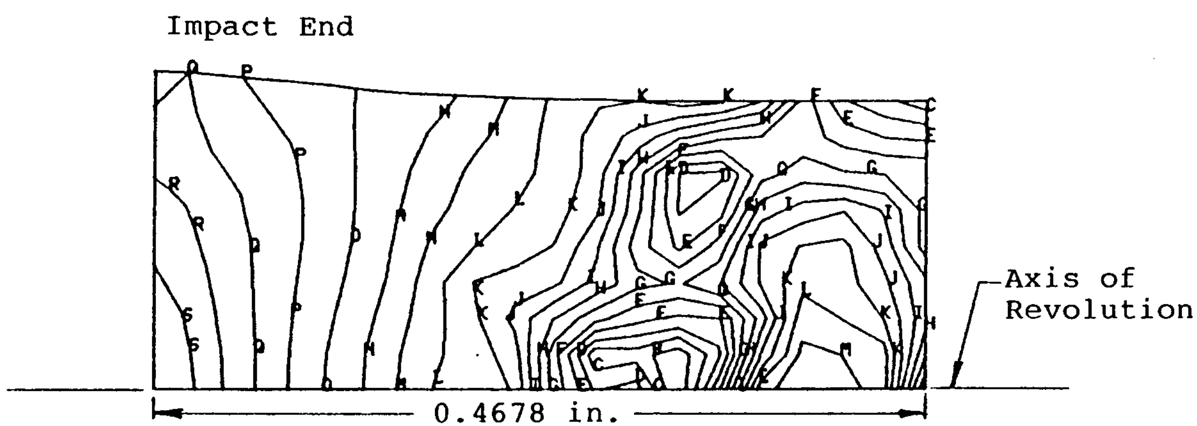

Figure A.17. Equivalent Stress 4.51 μsec After Impact.

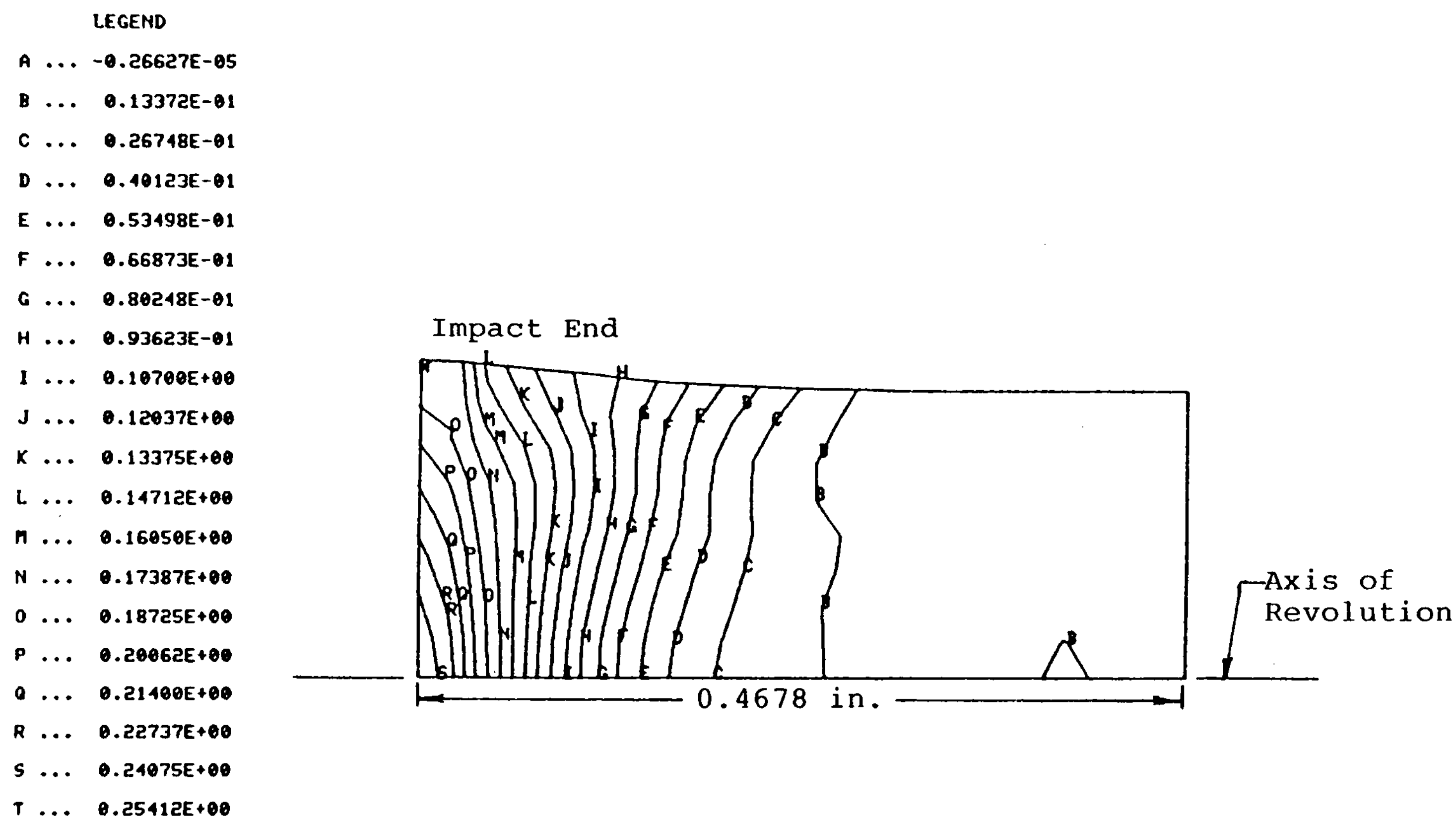

Figure A.18. Equivalent Plastic Strain 4.51 μsec After Impact.

LEGEND

A ...	0.58421E+04
B ...	0.10183E+05
C ...	0.14525E+05
D ...	0.18866E+05
E ...	0.23207E+05
F ...	0.27548E+05
G ...	0.31889E+05
H ...	0.36231E+05
I ...	0.40572E+05
J ...	0.44913E+05
K ...	0.49254E+05
L ...	0.53596E+05
M ...	0.57937E+05
N ...	0.62278E+05
O ...	0.66619E+05
P ...	0.70960E+05
Q ...	0.75302E+05
R ...	0.79643E+05
S ...	0.83984E+05
T ...	0.88325E+05

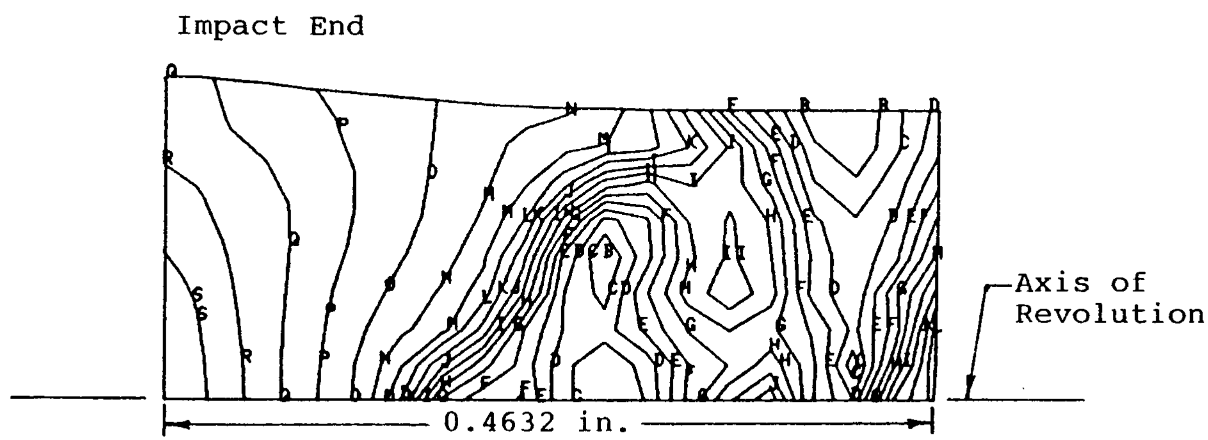

Figure A.19. Equivalent Stress 5.20 μsec After Impact.

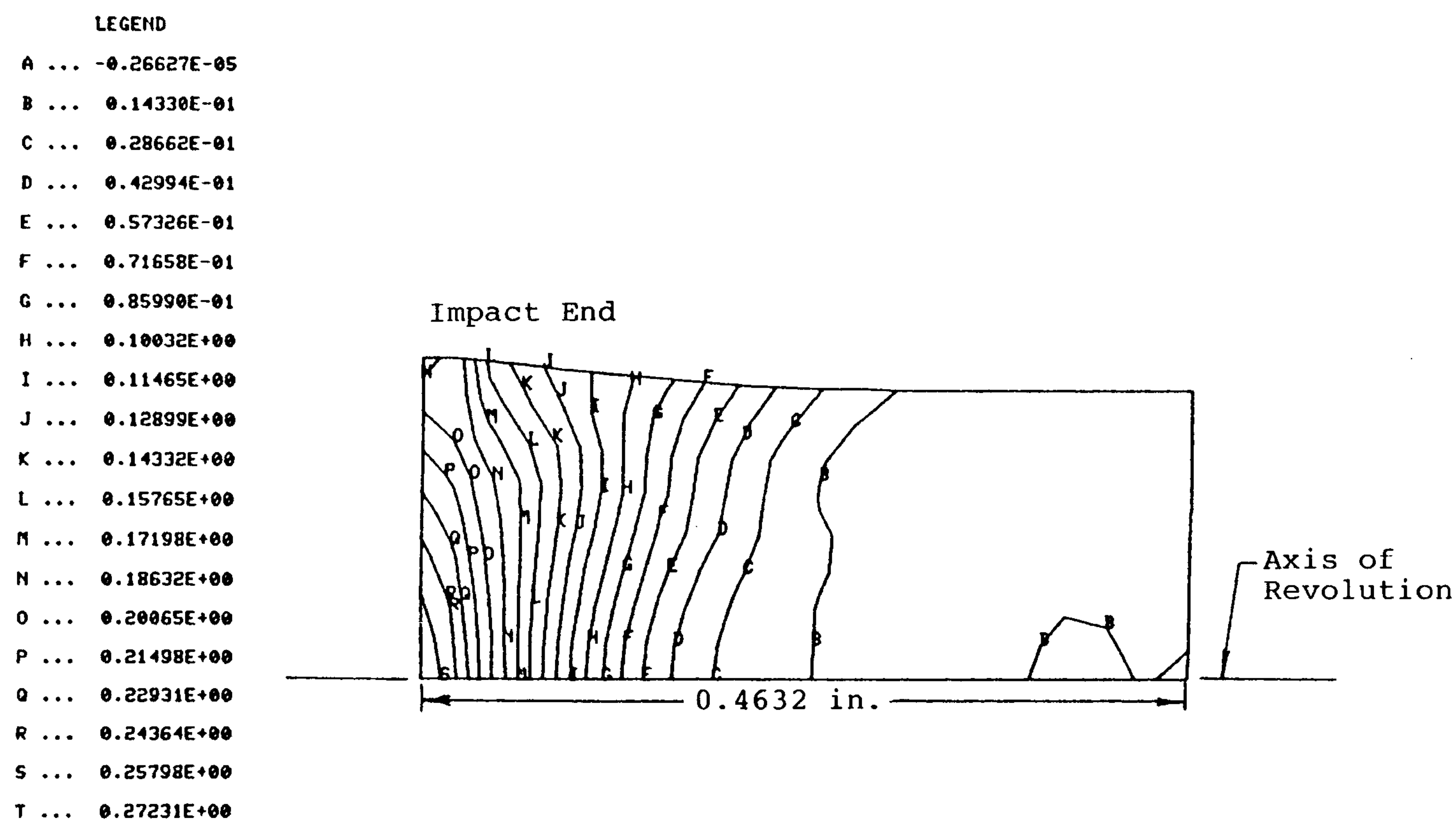

Figure A.20. Equivalent Plastic Strain 5.20 μsec After Impact.

LEGEND

A ...	0.73149E+04
B ...	0.11730E+05
C ...	0.16146E+05
D ...	0.20562E+05
E ...	0.24977E+05
F ...	0.29393E+05
G ...	0.33808E+05
H ...	0.38224E+05
I ...	0.42639E+05
J ...	0.47055E+05
K ...	0.51470E+05
L ...	0.55886E+05
M ...	0.60301E+05
N ...	0.64717E+05
O ...	0.69132E+05
P ...	0.73548E+05
Q ...	0.77963E+05
R ...	0.82379E+05
S ...	0.86794E+05
T ...	0.91210E+05

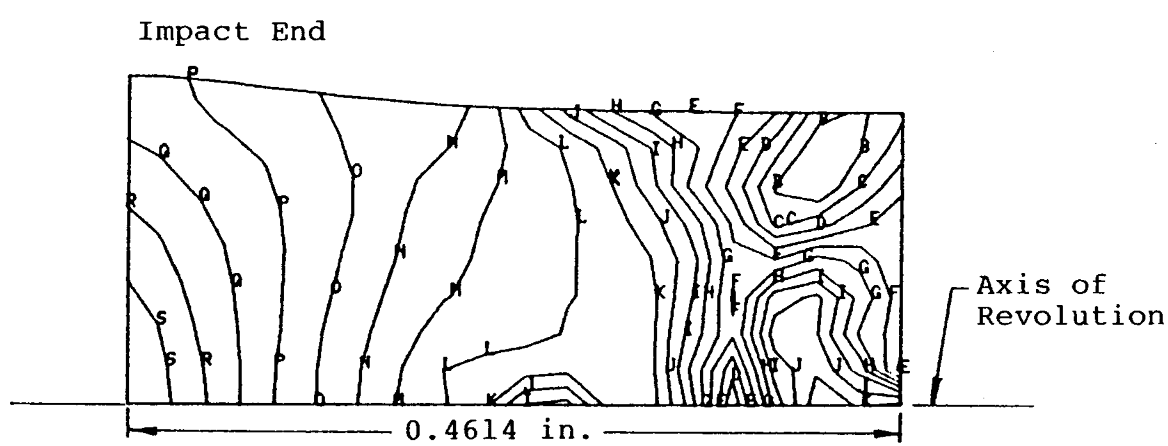

Figure A.21. Equivalent Stress 5.87 μsec After Impact.

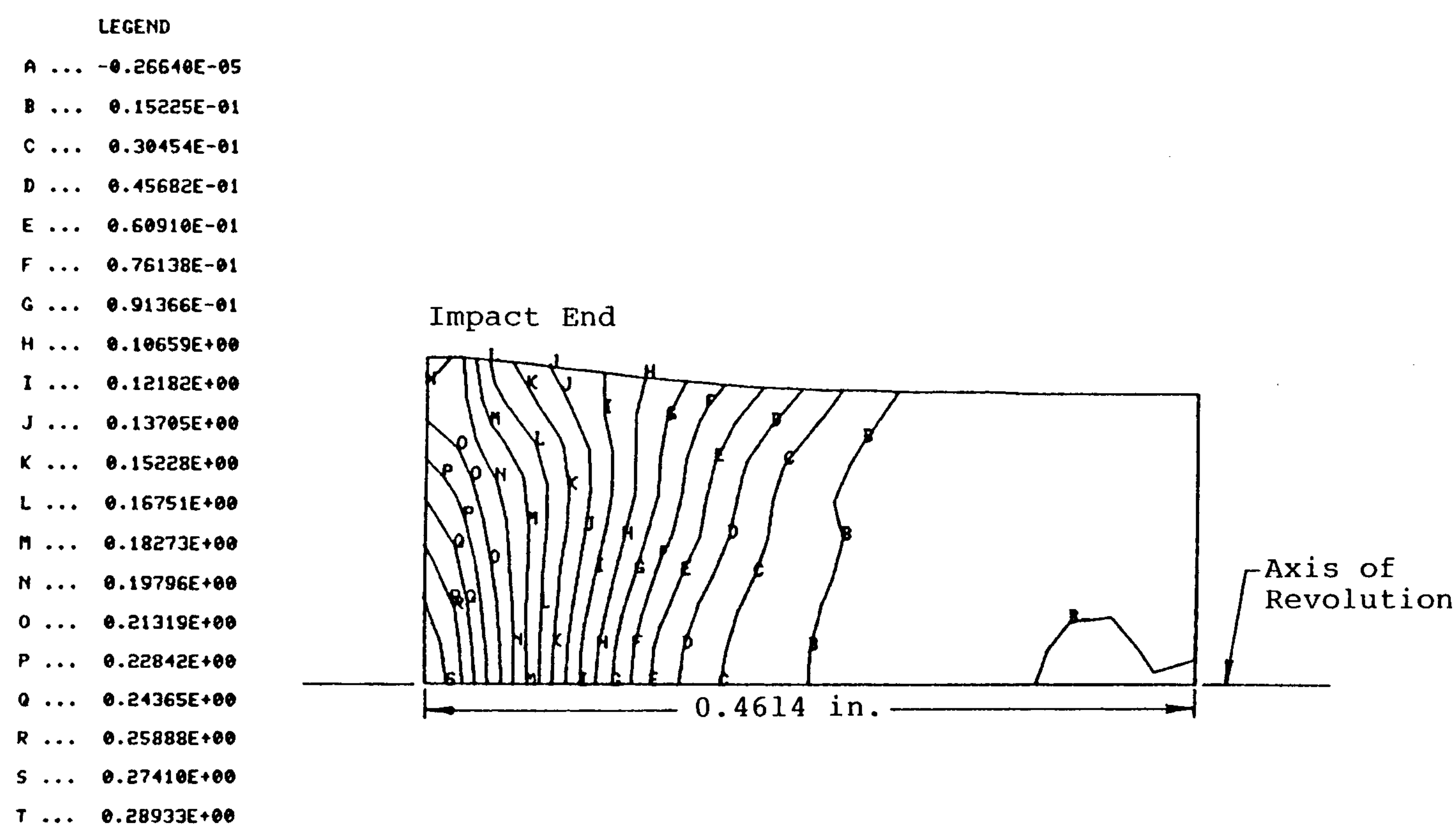

Figure A.22. Equivalent Plastic Strain 5.87 μsec After Impact.

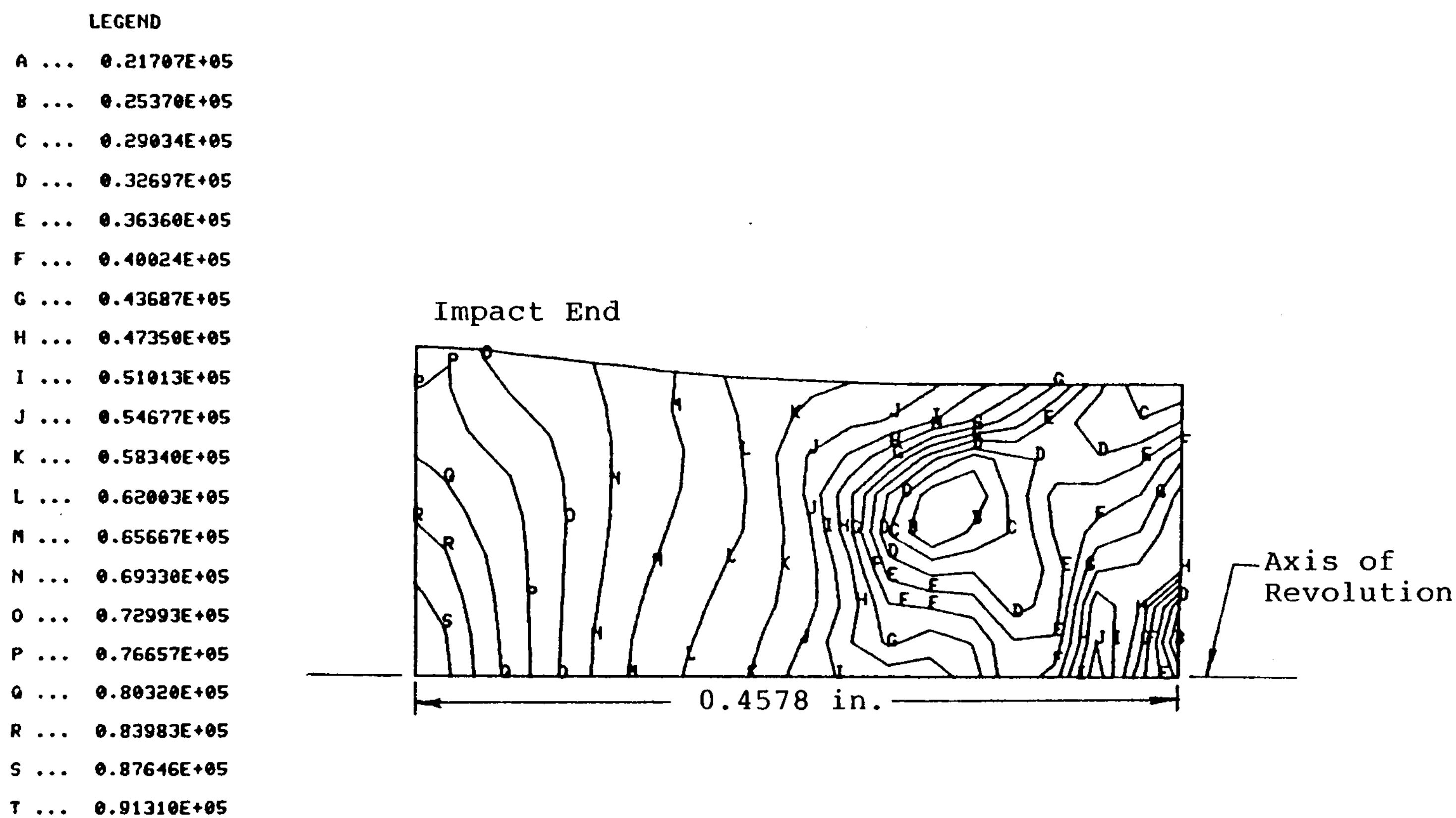

Figure A.23. Equivalent Stress 6.54 μsec After Impact.

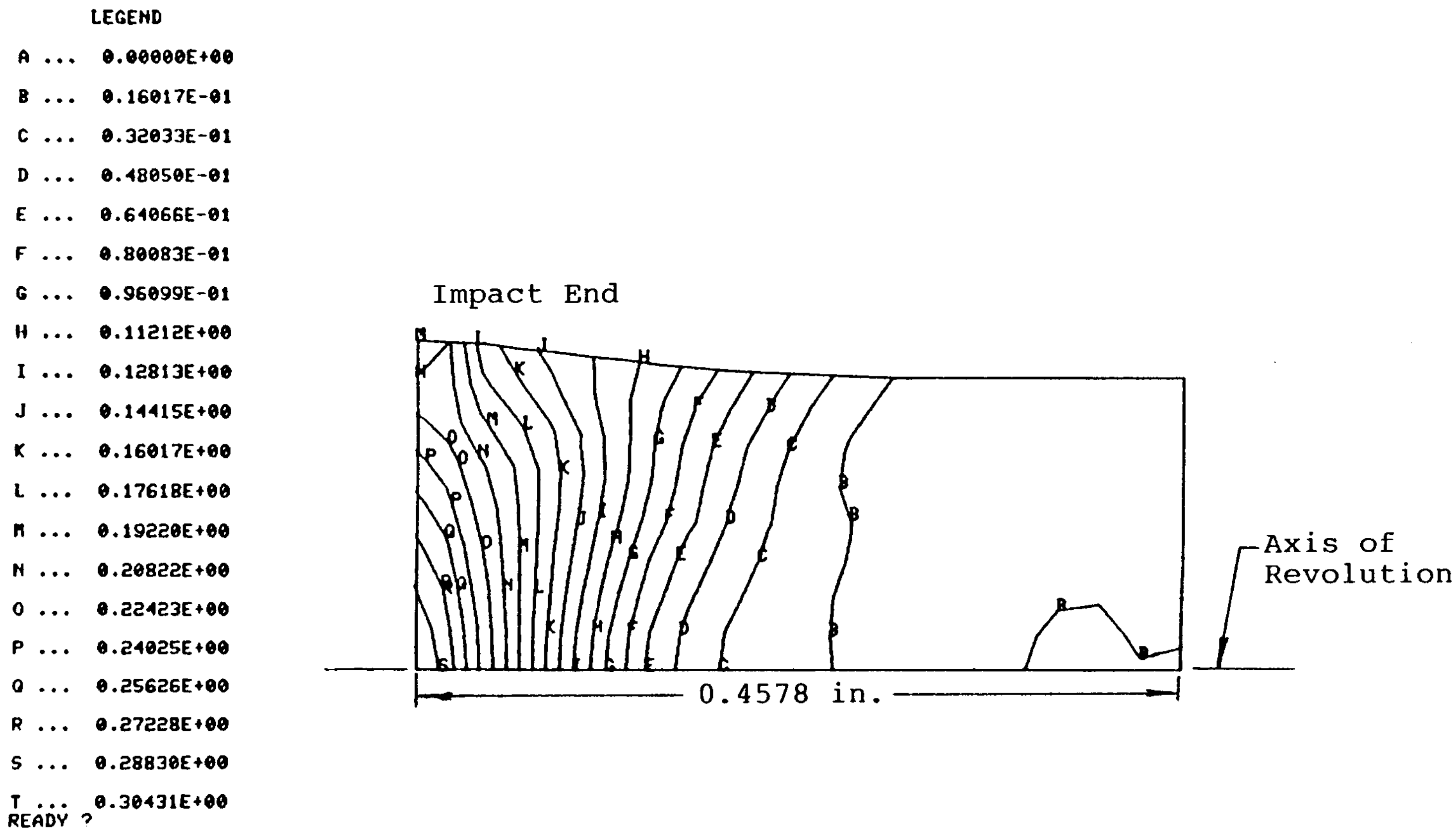

Figure A.24. Equivalent Plastic Strain 6.54 μsec After Impact.

LEGEND

A ... -0.31006E+03
B ... 0.43558E+04
C ... 0.90216E+04
D ... 0.13687E+05
E ... 0.18353E+05
F ... 0.23019E+05
G ... 0.27685E+05
H ... 0.32351E+05
I ... 0.37017E+05
J ... 0.41682E+05
K ... 0.46348E+05
L ... 0.51014E+05
M ... 0.55680E+05
N ... 0.60346E+05
O ... 0.65012E+05
P ... 0.69677E+05
Q ... 0.74343E+05
R ... 0.79009E+05
S ... 0.83675E+05
T ... 0.88341E+05

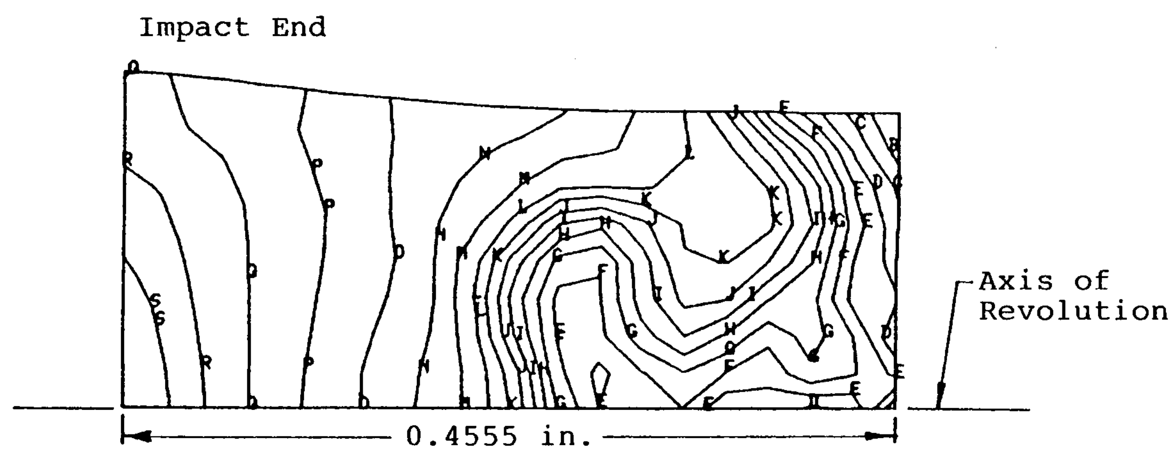

Figure A.25. Equivalent Stress 7.19 μsec After Impact.

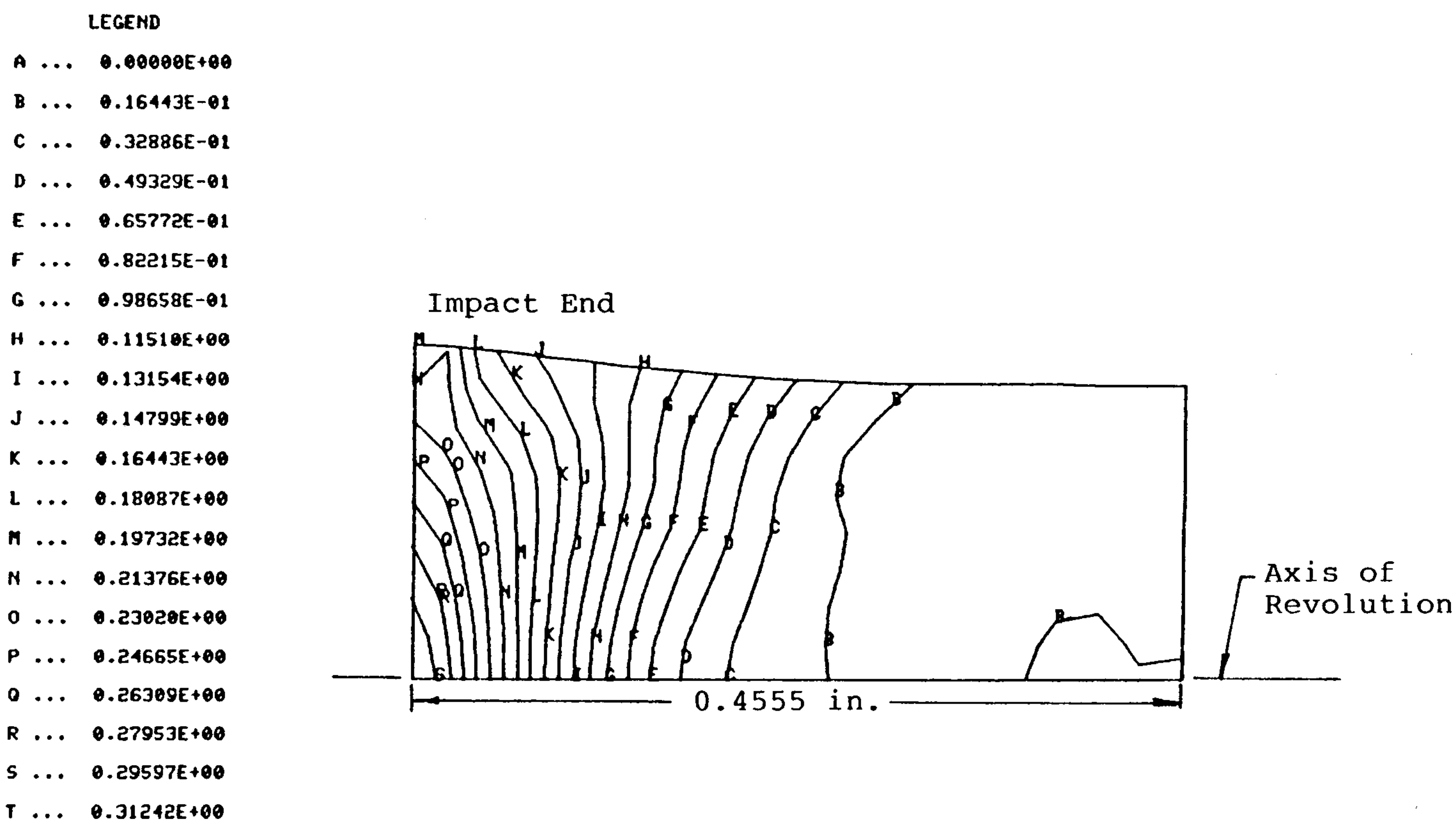

Figure A.26. Equivalent Plastic Strain 7.19 μsec After Impact.

LEGEND

A ...	0.91028E+04
B ...	0.13230E+05
C ...	0.17357E+05
D ...	0.21483E+05
E ...	0.25610E+05
F ...	0.29737E+05
G ...	0.33864E+05
H ...	0.37991E+05
I ...	0.42118E+05
J ...	0.46245E+05
K ...	0.50372E+05
L ...	0.54498E+05
M ...	0.58625E+05
N ...	0.62752E+05
O ...	0.66879E+05
P ...	0.71006E+05
Q ...	0.75133E+05
R ...	0.79260E+05
S ...	0.83387E+05
T ...	0.87513E+05

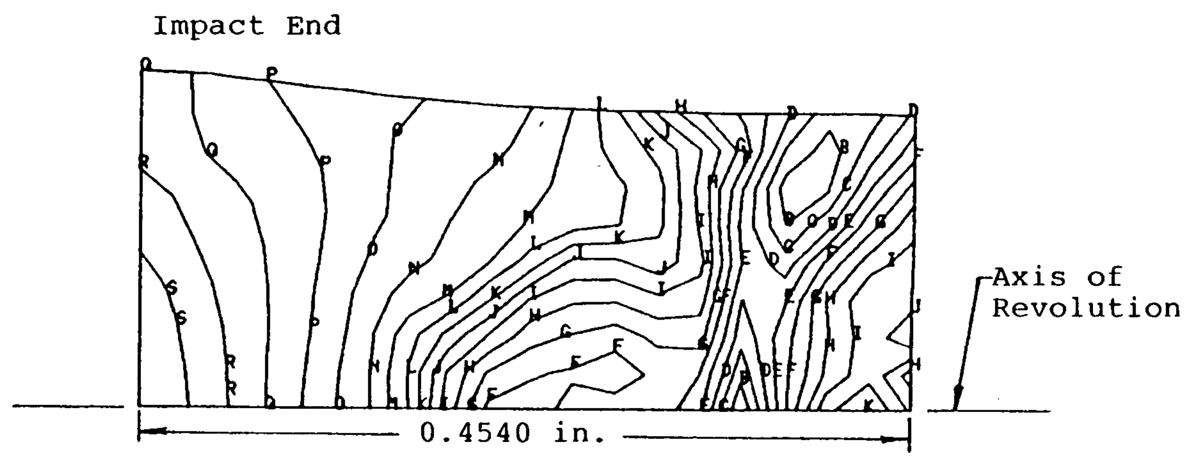

Figure A.27. Equivalent Stress 7.83 μsec After Impact.

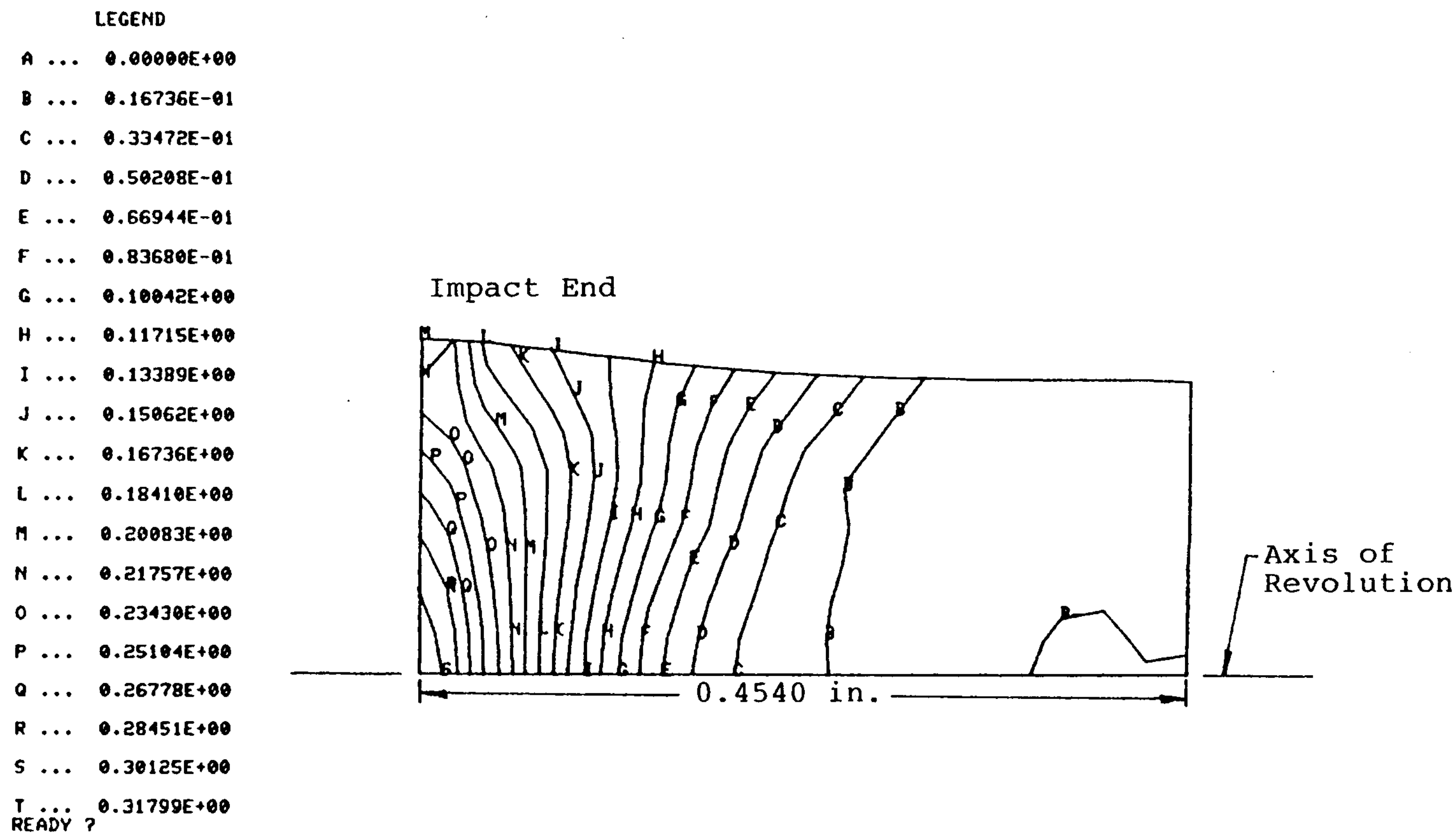

Figure A.28. Equivalent Plastic Strain 7.83 μsec After Impact.

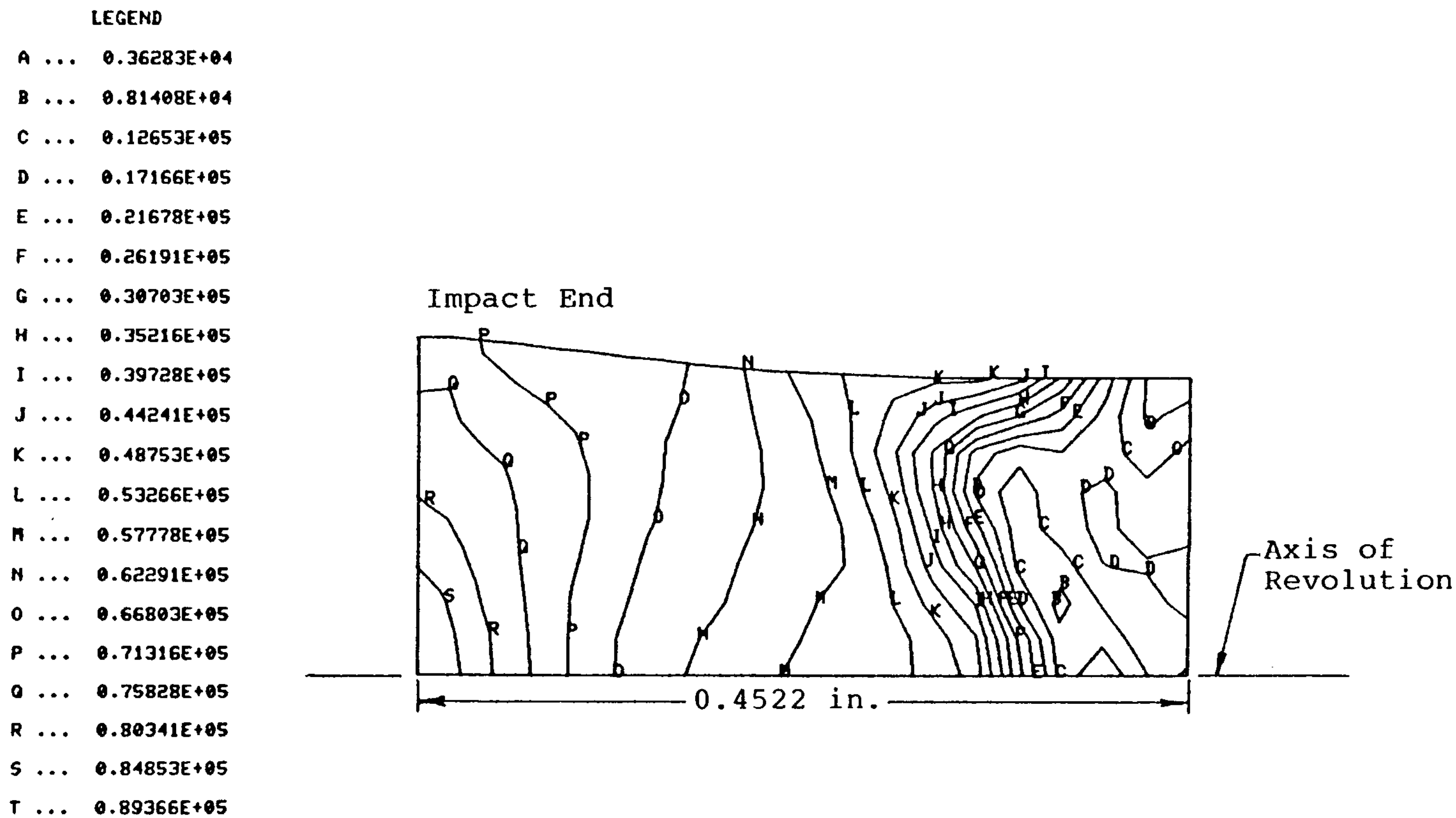

Figure A.29. Equivalent Stress 8.48 μsec After Impact.

LEGEND

A ... 0.00000E+00
B ... 0.17063E-01
C ... 0.34125E-01
D ... 0.51188E-01
E ... 0.68250E-01
F ... 0.85313E-01
G ... 0.10238E+00
H ... 0.11944E+00
I ... 0.13650E+00
J ... 0.15356E+00
K ... 0.17063E+00
L ... 0.18769E+00
M ... 0.20475E+00
N ... 0.22181E+00
O ... 0.23888E+00
P ... 0.25594E+00
Q ... 0.27300E+00
R ... 0.29006E+00
S ... 0.30713E+00
T ... 0.32419E+00

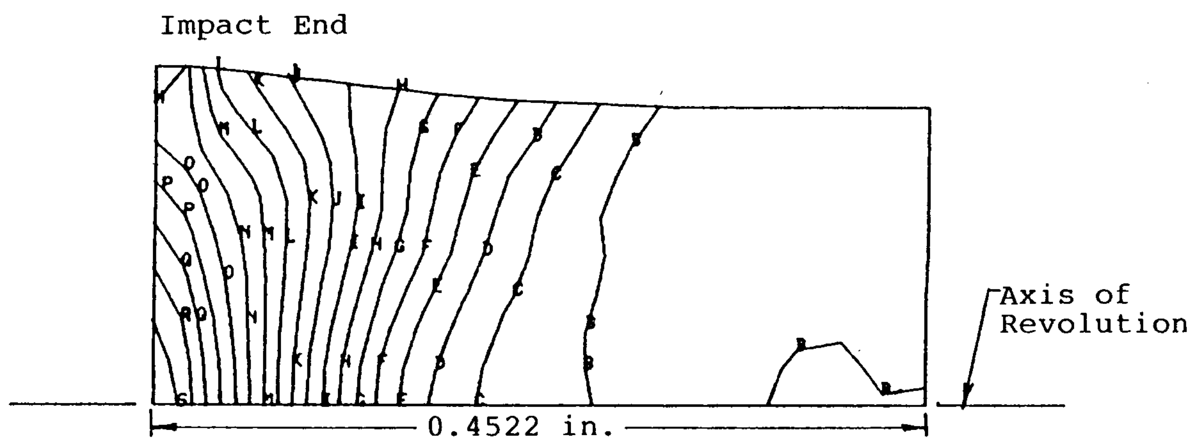

Figure A.30. Equivalent Plastic Strain 8.48 μsec After Impact.

LEGEND

A ... 0.59831E+04
B ... 0.10037E+05
C ... 0.14091E+05
D ... 0.18145E+05
E ... 0.22199E+05
F ... 0.26253E+05
G ... 0.30307E+05
H ... 0.34361E+05
I ... 0.38415E+05
J ... 0.42470E+05
K ... 0.46524E+05
L ... 0.50578E+05
M ... 0.54632E+05
N ... 0.58686E+05
O ... 0.62740E+05
P ... 0.66794E+05
Q ... 0.70848E+05
R ... 0.74902E+05
S ... 0.78956E+05
T ... 0.83010E+05

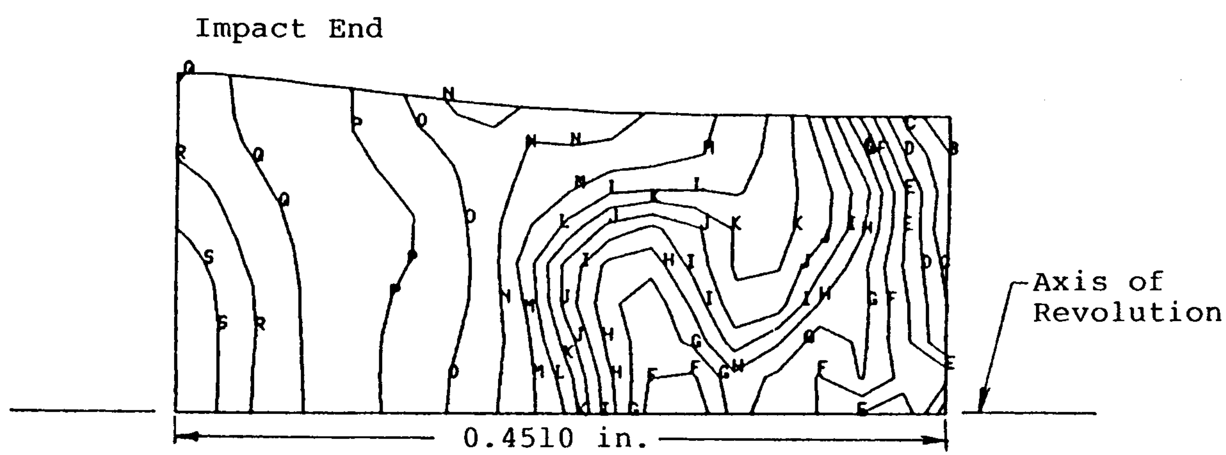

Figure A.31. Equivalent Stress 9.11 μsec After Impact.

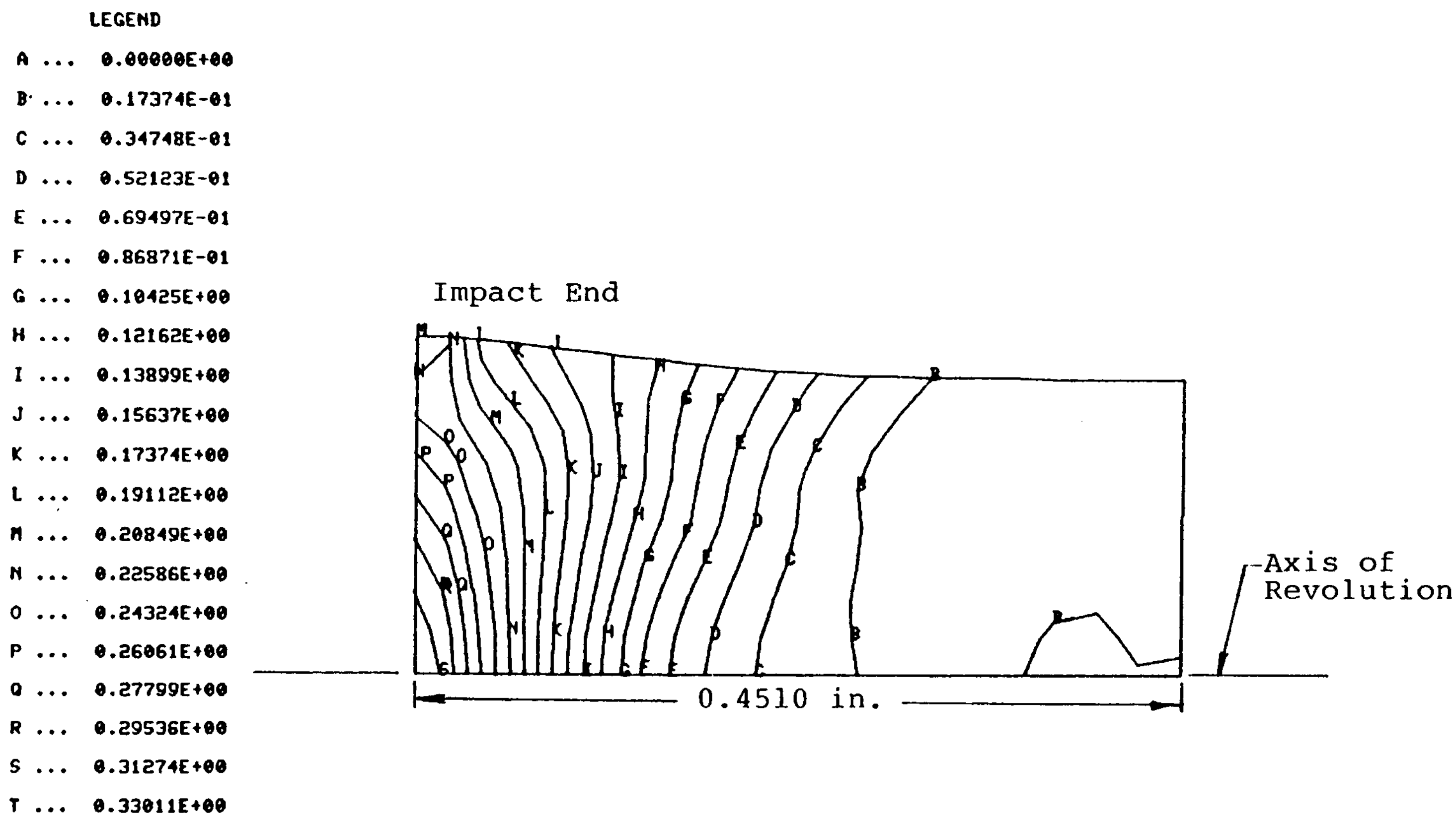

Figure A.32. Equivalent Plastic Strain 9.11 μsec After Impact.

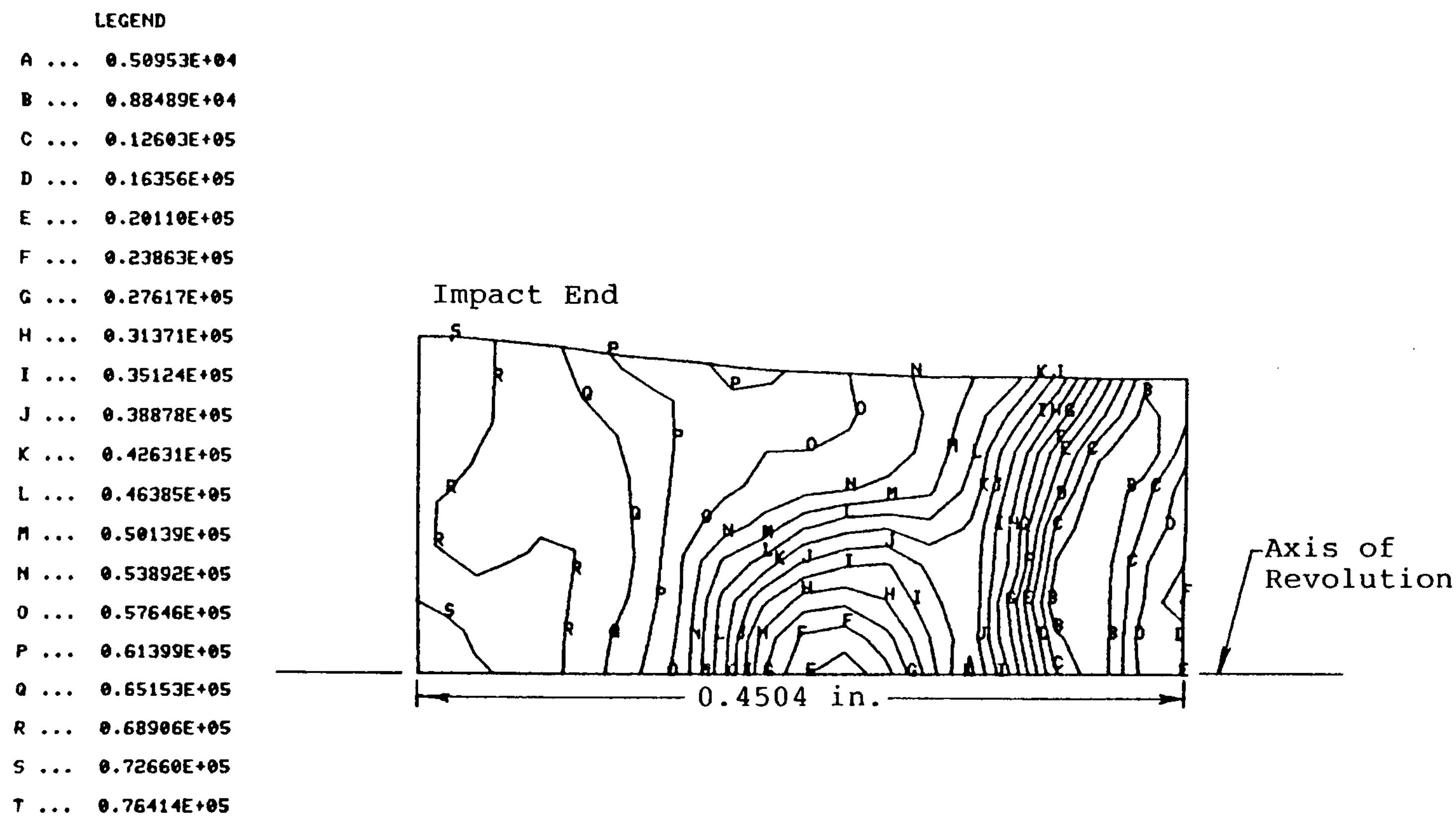

Figure A.33. Equivalent Stress 9.75 μsec After Impact.

LEGEND

A ...	0.00000E+00
B ...	0.17390E-01
C ...	0.34779E-01
D ...	0.52169E-01
E ...	0.69559E-01
F ...	0.86949E-01
G ...	0.10434E+00
H ...	0.12173E+00
I ...	0.13912E+00
J ...	0.15651E+00
K ...	0.17390E+00
L ...	0.19129E+00
M ...	0.20868E+00
N ...	0.22607E+00
O ...	0.24346E+00
P ...	0.26085E+00
Q ...	0.27824E+00
R ...	0.29563E+00
S ...	0.31301E+00
T ...	0.33040E+00

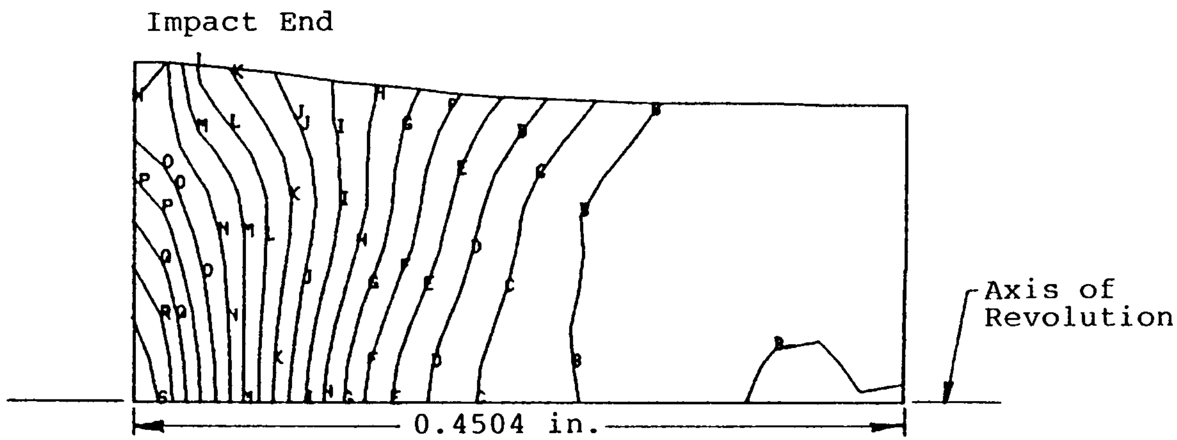

Figure A.34. Equivalent Plastic Strain 9.75 μsec After Impact.

VITA

Robert Allen LeMaster was born in Troy, Ohio, on September 18, 1953. He graduated from Miami East High School in Casstown, Ohio, in June 1971. The following September he entered Mt. Vernon Nazarene College at Mt. Vernon, Ohio. In June 1973 he transferred to Akron University at Akron, Ohio, where he received a Bachelor of Science degree in Mechanical Engineering, cum laude. After graduation from Akron University, he was employed by Hissong Consultants in Mt. Vernon, Ohio. In September 1977 he accepted a teaching-research assistantship at Ohio State University in Columbus, Ohio. He received a Master of Science degree in Engineering Mechanics in August 1978, at which time he accepted employment with Sverdrup Technology, Inc., in Tullahoma, Tennessee.

In September 1977 he began part-time graduate study at The University of Tennessee Space Institute in Tullahoma, Tennessee. He received the Doctor of Philosophy degree with a major in Engineering Science and Mechanics in June 1983.

The author is a member of Tau Beta Pi, Phi Kappa Phi, and the American Society of Mechanical Engineers. Mr. LeMaster will continue to be employed by Sverdrup Technology, Inc.

He is married to the former Debbie Hinton of Westerville, Ohio, and has one son, Michael.